The University of Sheffield

Department of Geography

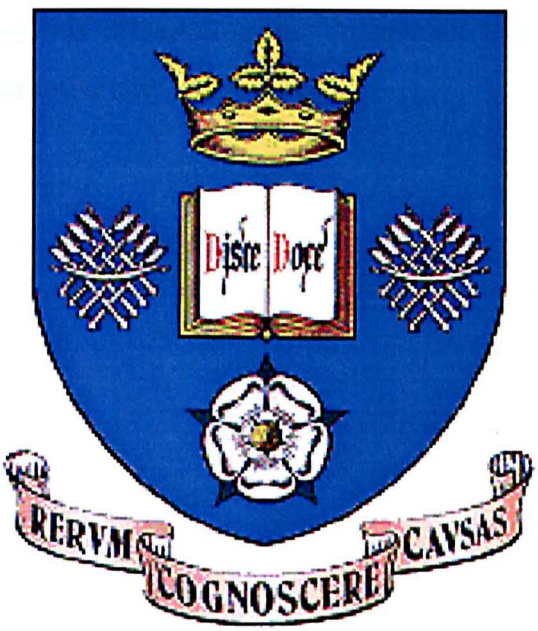

Flow Separation in Meander Bends

A thesis submitted for the fulfilment of the requirements of a doctorate in philosophy degree

By

Daniel R. Parsons

NOVEMBER 2002

Declaration

I herby declare that this dissertation entitled '*Flow separation in meander bends*' is entirely my own work. I have recognised all sources of information and the ideas of others throughout the thesis. Sections that have involved collaboration with others are also wholly acknowledged.

Furthermore, no part of this dissertation has already or will be submitted for any other degree at any other university.

Dan Parsons

30th October 2002

Acknowledgements

This is a tied PhD studentship and was funded by a Natural Environment Research Council grant (GR3/9715) awarded to Prof. S. N. Lane (Leeds) and Prof. R. I. Ferguson (Sheffield) titled *'Application of large eddy simulation for understanding natural river flows.'*

I want to thank my primary supervisor Rob Ferguson for giving me the opportunity to carry out this work and the unwavering support and immense encouragement he has afforded me. I would also like to thank my second supervisor Stuart Lane for his enthusiasm and assistance throughout the project. During the three years, Richard Hardy has proved to be an invaluable source of knowledge, a good friend and great source of beer.

I am grateful to the farmer, Mr Williams, for access to the field site and also acknowledge the fieldwork assistance and company of the following: Ben Surridge, Barry Hankin, Amy Smith, Dave Mould, and Cate Tully. I would also like to thank Louise Sime for her help in the field and for numerous, rambling, discussions about rivers and Matlab. I also extend thanks to all the other PhD students and the staff at Sheffield Geography department, notably Andy Hodson, Giles Wiggs, Andy Baird, Brian Gravey and Paul Dunlop. I would also like to thank Dave Maddison, Jill Ulmanus and Paul Bentley for their technical assistance and organisation. I also thank Simon Tait for discussion on PIV use and his assistance in constructing the field wading rod in the Civil Engineering workshop. I am also grateful to Jim Best and Mark Franklin for allowing me to take advantage of the PIV system in their sedimentology laboratory in Leeds. Mark Lawless helped me enormously with the laboratory experiment and has provided much entertainment on many nights out up in Leeds.

Finally, I would like to thank my parents for giving me the opportunities that have resulted in this PhD and Kristina, my girlfriend, for her patience and understanding at several junctures throughout the three years.

Abstract

Most investigations of river meanders have concentrated on classical bends that have a helical flow structure through the pool, which is carried through into the entrance of the next bend. However, it is known that flow separation can occur at the outer bank before the bend apex or at the inner bank after the apex and that this results in the breakdown of the classical flow model. Although some of the controls and the implications of flow separation are now known, the frequency of occurrence, three-dimensional (3-D) flow structure, sediment dynamics, controls on separation presence, and full geomorphological implications are poorly understood.

This thesis uses a combination of fieldwork and 3-D numerical flow modelling (computational fluid dynamics, CFD) to investigate meander bends where flow separation and recirculation zones are present. An initial reconnaissance survey of over 600 bends revealed that flow separation is common, being present in approximately 50% of bends. The survey also identified high bend angles of turn and the high angles of flow impingement onto the outer bank as important controls on the presence of separation. Investigations in a 22 bend sub-set indicated that expansions in channel width, breaks in bank-line curvature and the angle of inflow, as governed by upstream planform, were important in generating flow separation.

Detailed fieldwork combined with validated and verified time-averaged CFD modelling in three bends with separation zones enabled identification and examination of the 3-D flow fields. The simulations reveal that the flow structure in bends with separation differs considerably from the classical flow model, with the helical motion found in classical bends being very intense in the bend entrance but dissipating at or just after the bend apex. The turbulent flow structures produced by the shear layer between the downstream and recirculating flow are also investigated in the field bends and attempts at modelling transient flow structures with large eddy simulation (LES) in a simple open channel flow expansion are detailed.

The geomorphological, sedimentological, and ecological implications of both the time-averaged and the transient flow structures within the bends are examined and discussed.

Dissemination

Papers:

Hardy R, Lane SN, Ferguson R, Parsons DR. in press. Assessing the credibility of a series of computational fluid dynamic simulations of open channel flow. *Hydrological Processes.*

Parsons DR. in press. Discussion of 'Three Dimensional Numerical Study of Flows in Open-Channel Junctions.' *Journal of Hydraulic Engineering – ASCE.*

Lane SN, Hardy RJ, Keylock CJ, Elliott L, Ingham DB, Ferguson RI, Parsons DR. submitted. The implications of complex river bed structure for numerical modelling and the identification of channel-scale flow structures. *Hydrological Processes.*

Ferguson RI, Parsons DR, Lane SN, Hardy RJ. in prep. Combined field and CFD investigation of mean flow structure in high-curvature meander bends: 1. Inner-bank separation at normal discharges. To be submitted to *Water Resources Research.*

Parsons DR, Ferguson RI, Lane SN, Hardy RJ. in prep. Combined field and CFD investigation of mean flow structure in high-curvature meander bends: 2. Survival of inner-bank separation at bankfull discharge. To be submitted to *Water Resources Research.*

Parsons DR, Ferguson RI, Lane SN, Hardy RJ. in prep. Combined field and CFD investigation of mean flow structure in high-curvature meander bends: 3. Separation at the outer bank. To be submitted to *Water Resources Research.*

Parsons DR, Ferguson RI, Lane SN, and Hardy RJ. in prep. Flow separation in meander bends: an investigation of frequency and controls. To be submitted to *Earth Surface Processes and Landforms.*

Parsons DR, Ferguson RI, Hardy RJ, Lawless M, Lane SN, Best, J. in prep. Large-eddy simulation of shear layer dynamics at an open channel flow expansion: validation and sensitivity. To be submitted to *Hydrological Processes.*

Parsons DR. Hardy RJ, Ferguson RI, Lane SN. in prep. Topographic representation in three-dimensional numerical flow modelling. To be submitted to *Earth Surface Processes and Landforms.*

Presentations:

Parsons DR, Ferguson RI, Lane SN, Hardy RJ. 2000. Flow separation in meander bends. Oral paper presented to the ***British Geomorphological Research Group*** Postgraduate Conference, University of Glasgow, April 2000

Lane SN, Bradbrook KF, Biron PM, Caudwell SWB, Ferguson RI, Hardy RJ, Keylock CJ, Hardy RJ, Parsons DR, Richards KS, Roy AG. 2000. Understanding form-process linkages in river channel confluences using a CFD approach. Oral paper presented to the ***British Geomorphological Research Group*** Annual Conference, University of Sheffield, September 2000

Parsons DR, Ferguson RI, Lane SN, Hardy RJ. 2001. Flow separation in meander bends: a statistical investigation of frequency and controls. Oral paper presented to the ***British Geomorphological Research Group*** Postgraduate Conference, University of Portsmouth, April 2001

Hardy RJ, Lane SN, Ferguson RI, Parsons DR. 2001. Development of a grid convergence index for verification of models of open channel flow. Oral paper presented to the ***American Geophysical Union***, Spring Meeting, Boston, May 2001

Parsons DR, Ferguson RI, Lane SN, Hardy RJ. 2001. Numerical modelling of flow separation in meander bends. Oral paper presented to the ***American Geophysical Union***, Spring Meeting, Boston, May 2001

Parsons DR, Ferguson RI, Lane SN, Hardy RJ. 2001. CFD modelling of flow separation in meander bends. Poster presented to the ***British Geomorphological Research Group*** Annual Conference, University of Nottingham, September 2001

Parsons DR, Ferguson RI, Lane SN, Hardy RJ. 2002. Topographic representation in numerical flow modelling. Oral paper presented to the ***British Geomorphological Research Group*** Postgraduate Symposium, University of Leeds, April 2002

Parsons DR, Ferguson RI, Lane SN, Hardy RJ. 2002. Flow separation in meander bends and the formation of bed sediment patches. Oral paper presented to the ***British Hydrological Society*** River-bed patches symposium, Loughborough University, May 2002.

Parsons DR, Ferguson RI, Lane SN, Hardy RJ. 2002. Flow structure in bends with separation at the inner bank and the persistence of separation at high flow. Oral paper presented to the ***British Geomorphological Research Group*** meeting, Leeds University, September 2002.

Contents

CHAPTER THREE - Mid-Level Field Study

CHAPTER FOUR - Numerical Modelling of Flow

CHAPTER FIVE - Time-averaged Flow Structures in Bends with Separation

CHAPTER SIX - Transient Flow Structures in Bends with Separation

CHAPTER SEVEN - Summary, Conclusions and Further Research

Chapter 1
Introduction and Background

1.1 FOREWORD

The flow structure in meander bends has been of interest to geomorphologists, sedimentologists, and engineers for many years. This is because of important, but complex, interactions between the flow structure and the distribution of boundary shear stress, the flux, transport, and size sorting of sediments, and hence the controls on channel morphology.

There is now a good understanding of form and process in classical meander bends with a regular geometry (*see* Dietrich, 1987). However, in some sharper bends, flow separation is known to occur through eddying in a horizontal plane and slowly re-circulating flow at either the outer bank before the bend apex or at the inner bank after the apex. The presence of flow separation radically alters the processes occurring in bends, although the nature of these alterations are poorly understood.

This thesis will investigate the nature of the flow in meander bends where flow separation and re-circulation zones are present. The project comprises a general reconnaissance field survey of many meanders, more detailed investigations in a subset of bends, followed by intensive field studies and numerical flow modelling (Computational Fluid Dynamics, CFD) in specific case-study bends that have large separation zones.

This chapter initially places this thesis into context by reviewing research approaches within fluvial geomorphology (1.2) before providing a firm background to what is currently known about form and flow processes in meander bends (1.3). The chapter then briefly introduces the use of the numerical flow modelling (CFD) applied in this thesis and outlines the recent developments that are significant to application of CFD to river channels (1.4). The research questions that are raised in the background literature and approaches to the numerical modelling are then outlined, along with

the full aims and specific objectives of this study (1.5). The chapter finishes with a brief introduction to the structure of the thesis (1.6).

1.2 APPROACHES TO FLUVIAL GEOMORPHOLOGY

Geomorphology was dominated by the Davisian approaches which concentrated on the history of landforms, until Strahler (1950, 1952) argued for a dynamic systems approach for the discipline, based upon scientific relationships which should be produced from the combination of empirical research, where experimentation provided observations for analysis, and rational research that involves construction of mathematical models from *'total experiences'*. Strahler (1952) argued that with increased understanding the empirical and the rational would converge on reality (Lane and Richards, 1997).

The response to this in fluvial geomorphology was largely empirical, involving derivation of functional relationships between morphological parameters and controlling variables (*e.g.* Leopold and Maddock, 1953; Leopold and Wolman, 1960; Dury, 1955). Typically, these involved large-*n* studies (Richards, 1996), where specific features of many individual forms were 'measured'. Schumm and Lichty (1965) introduced the concept of scale into these empirical relationships highlighting that the relationship between morphological parameters and controlling variables would alter as the scale of inquiry, in both time and space, is changed. For example, as the scale of inquiry moves from the reach scale or short timescales to larger space or longer timescales then the channel morphology transforms from being a dependent to an independent variable. Thus, in situations where processes are acting at scales shorter than those of interest, these smaller scale processes can be 'relaxed' and parameterised at the larger scales (Church and Mark, 1980).

The main problems with empirical approaches is that rather than establishing how channel form and change are a direct result of river channel processes, they involve inferences from separate variations of 'process' and 'form' in both time and space (Lane and Richards, 1997). Simpson (1963) argues that the historical circumstances in which a process acts must be considered: empirical relationships between process and form are clouded by the fact that each event is based within a different set of *conditional* circumstances. A full explanation of events can only be achieved by

combination of an evaluation of historical properties with the appropriate *immanent* processes causing any change (Simpson, 1963). Thus, explanations based only on empirical relationships can lack any physical meaning and cannot explicitly reveal what the formative mechanisms are. Moreover, feedback and an interrelationship between from and process (Figure 1.1; 1.2) and non-linear behaviour within systems (*e.g.* Phillips, 1992) means that separating the dependent and independent variables through time and space scales becomes even more complex. This is because any form produced is not just a function of external controls but is also a result of internal dynamics. Thus, small-scale short-term events can be propagated and result in an effect on long-term large-scale system evolution (Lane and Richards, 1997). The reach-scale conceptual model proposed for rivers by Ashworth and Ferguson (1986) (Figure 1.1) highlights these relationships and that feedback is inherent within the system.

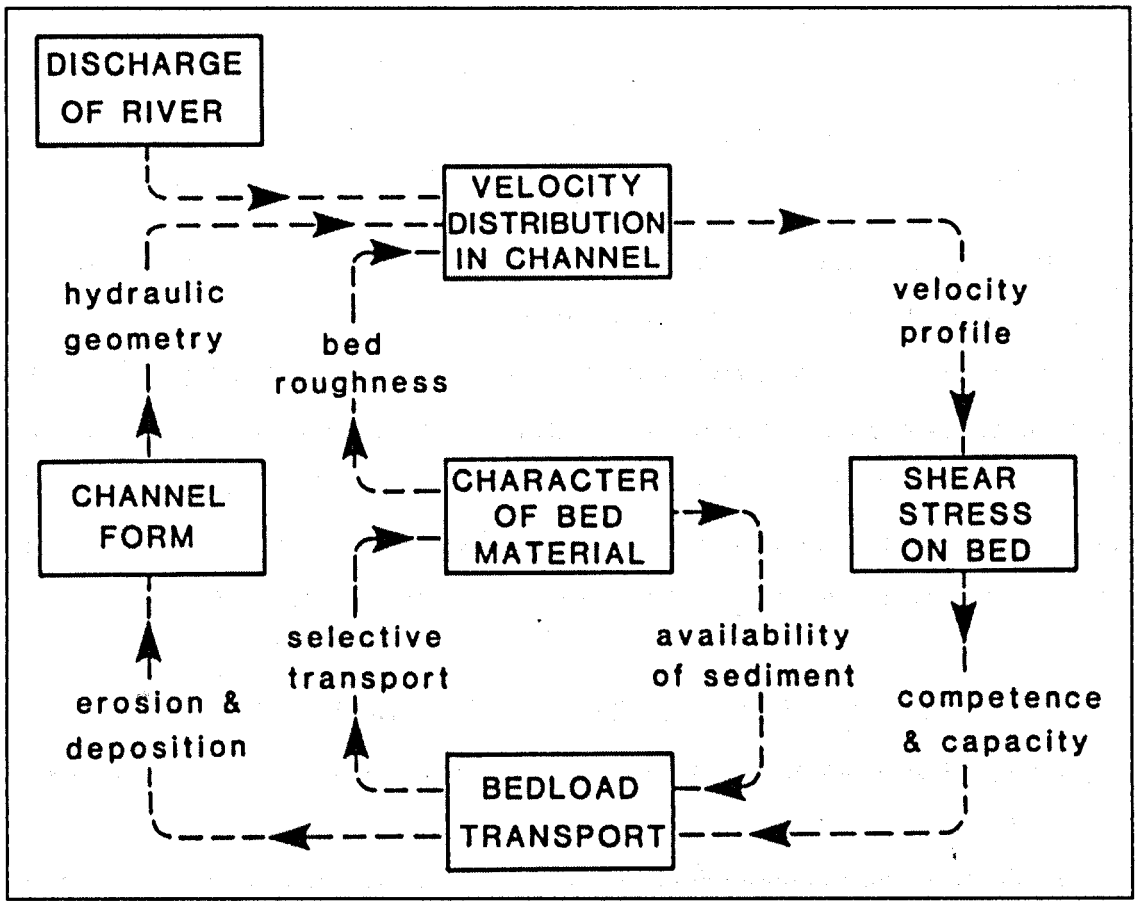

Figure 1.1: Conceptual model of form-process linkages in river channels (adapted from Ashworth and Ferguson, 1986)

An understanding of form and change in form requires a detailed consideration of the processes and the linkages between the variables highlighted in Figure 1.1. Thus, recent research in fluvial geomorphology has begun to examine how river channel form changes through time in response of temporal and spatial variations in the governing processes and how these processes change in response to temporal and spatial variations in form. This has generally led to case-study research that examines changes in form as controlling variables change and how 'morphological conditioning' of form, or a rivers history (Schumm, 1977), impinges on process and thus future form (Figure 1.2). This movement to more detailed case-study research, from large-*n* to small-*n* study (Richards, 1996), has also seen a reduction in the scales at which inquiry is made. Small reaches of river channels are investigated in very high detail to study the physical processes and to investigate the nature of feedback between form and process. This movement has led towards a more process-based understanding of the interaction between form and process in river channels (*e.g.* Dietrich and Smith, 1983; Carson and Lapointe, 1983; Ashworth and Ferguson, 1986; Biron *et al.*, 1993a; Ashmore *et al.*, 1992; Lane *et al.*, 1995; Rhoads and Kenworthy, 1995; Hodskinson and Ferguson, 1998; De Serres *et al.*, 1999; Bradbrook *et al.*, 2000a,b).

However, Lane and Richards (1997) note that this increased use of small-scale intensive case-study research raises a number of philosophical and methodological issues. The main issue they raise concerns the drawing of general conclusions on long-term large-scale fluvial system change from small-*n* case-study research. They also question whether the main problem facing fluvial geomorphology is now a lack of knowledge about how the *conditional* circumstances wherein *immanent* processes operate, influence and modify the mode in which the *immanent* processes act (Simpson, 1963). Nonetheless, case study research allows theoretical generalization about process of channel change that is conditioned and modified by the boundary conditions applied (Richards, 1996). This moves focus away from developing general laws towards accounting for the uniqueness of the events produced by their operation within *conditional* circumstances. Generalization becomes concerned with increasing understanding of the processes involved in maintaining recursive system behaviour (Richards, 1996; Lane and Richards, 1997). This type of intensive study provides a framework in which to explore the dynamic behaviour of specific

landforms and processes through time. This is clearly the goal of geomorphology (Richards, 1996).

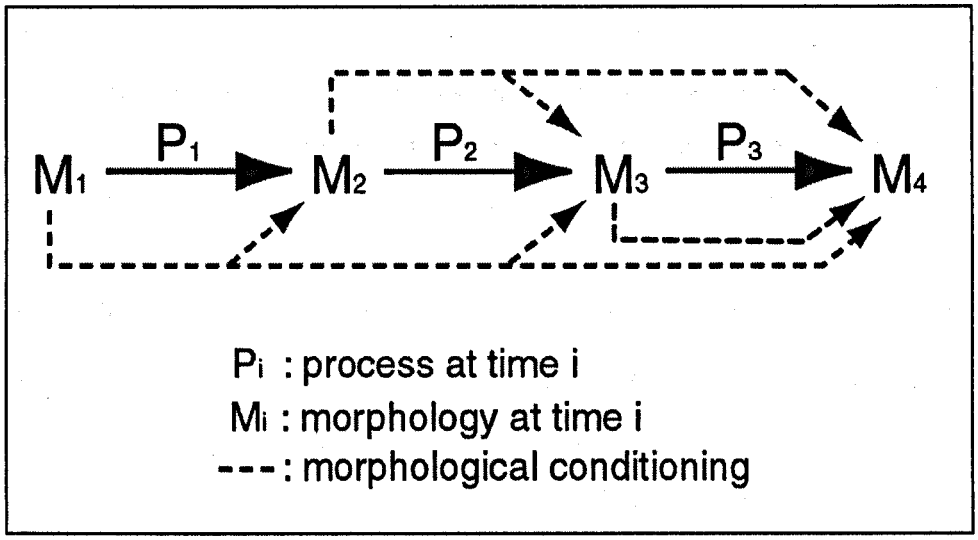

Figure 1.2: Form-process feedback and effect of morphological conditioning on process and future form (adapted from Lane, 1998b).

Nevertheless, difficulties have been encountered in the process of generalisation based upon small-*n* studies. For example, there has been great debate over the controls on flow structure generation at river channel confluences (*e.g.* Rhoads and Kenworthy, 1995; McLelland *et al.*, 1996; De Serres *et al.*, 1998). These difficulties have primarily been because generalisations have been based upon separate field case-study observations, where different conditions and different measuring techniques have been applied. Laboratory experimentation has been employed in an attempt to constrain or to highlight variables that might control flow structure generation with some success (*e.g.* Best and Roy, 1991; Biron *et al.*, 1996). More recently numerical flow modelling has been applied to investigate some of the issues raised using both field and laboratory methods (*e.g.* Bradbrook *et al.*, 1998; 2000a; 2001). This numerical modelling approach, when combined with field and laboratory experiments, has begun to answer some of the questions regarding controlling variables in flow structure generation at river channel confluences (Bradbrook *et al.*, 1998; 2001; Lane *et al.*, 2000) and the controls on the formation of outer bank separation in meander bends (Hodskinson and Ferguson, 1998). Thus, ideally case-study research should be performed using a combination of

complementary approaches, including field case studies, laboratory experimentation, and numerical modelling.

The focus on the success of small-*n* case-study research should not however distract from the need of large-*n* study. Indeed, large-*n* studies provide the context for the small-*n* generalizations and avoid discrepancies between causes because of the characteristics of a case. Large-*n* studies also indicate the frequency of occurrence of the forms and processes, generate the research questions that lead to more intensive investigations and also provide a means to sample the small-*n* from the large-*n* (Richards, 1996).

Therefore, in the examination of flow-form feedback in meander bends with separation zones, this thesis applies the full range of methodological and philosophical approaches discussed above. Initially, large-*n* studies are performed on full river reaches progressing through to intensive small-*n* field case studies of individual bends and laboratory experimentation, which are combined with the powerful tool of numerical flow modelling.

1.3 BACKGROUND: RIVER CHANNEL BENDS

1.3.1 River meander form

River channel meanders are ubiquitous geomorphological features in many landscapes and as such, they have received much scientific attention and investigation over the years. It is now known that there is a continuum of river channel patterns from straight through meandering to braided and anasotomosing (Leopold and Wolman, 1957; Ferguson, 1987). Meandering occurs where there is a balance between stream power and bank erodability and sediment transport. In an attempt to investigate and explain the meandering process, many have attempted to characterise meander trains through measurement of geometric properties such as wavelength, curvature and amplitude (Hickin and Nanson, 1975) and through analysis of direction change series (*e.g.* Ferguson, 1976). Most natural meandering rivers do not exhibit an entirely regular pattern and it is now recognised that although meanders do show some degree of regularity, variations in a number of important variables such as floodplain typography, local geology and sedimentology, inhibit what is essentially a regular process (Ferguson, 1973; 1976; 1979).

The planform of classical type meander bends comprises a variation in radius of curvature (R_c) from a minimum at the bend apices to infinity at the crossovers between bends. This variation is often asymmetric with a reduction in R_c to a minimum occurring more rapidly in the upper portion of the bend before the apex, followed by a gentler rise in R_c to the bend exit (Carson and Lapointe, 1983; Dietrich, 1987). In association with the downstream variation in R_c, channel cross-sections vary continuously through the bend (Dietrich and Smith, 1983; Ikeda, 1984) and are also usually asymmetric. The channel is typically deepest against the outer concave bank near the zone of minimum R_c (Figure 1.3). The channel section shallows towards the inner convex bank where a point-bar is often present. The maximum depth of the pool near the concave bank has been found to vary inversely with the ratio of R_c to local channel width (Leliavsky, 1955; Thorne, 1989) although bank strength also plays a part (*e.g.* Friedkin, 1945; Thorne, 1982). Between successive bends, the cross sections are close to a uniform depth and begin to take the asymmetric pattern on approach to the bend entrance. Downstream of the bend apex, the pool shoals and the point-bar drops rapidly into the talweg of the channel (Dietrich and Smith, 1983; Dietrich, 1987) where the point-bar face tends to cut obliquely across the channel in the downstream direction (Figure 1.3).

This planform shape and the associated bar/pool topography are viewed as the classical picture of meander bend form and is well documented in the literature (*e.g.* Friedkin, 1945; Leopold and Wolman, 1960, Ackers and Charlton, 1970; Bluck, 1971; Dietrich and Smith, 1983; Markham and Thorne, 1992). However, there are many subtle variations from this classical picture. In many circumstances, channel width has been found to increase to a maximum at the bend apex (*e.g.* Dietrich and Smith, 1983; Carson, 1986; Markham and Thorne, 1992), although other studies document it remaining constant throughout the bend (De Vriend and Geldof, 1983). Some meanders can become distorted due to a number of erosion resistant floodplain features, which can produce irregular bend planforms that depart from the classical case (Lewin and Brindle, 1977). Moreover, compound meander forms with two or more zones of low radius and two or more pools in one bend have also been documented (Brice, 1974; Hooke and Harvey, 1983; Parker *et al.*, 1983; Thompson, 1986). Meanders that have very high amplitudes have also been observed (Whiting and Dietrich, 1993a; 1993b). The width (W) to depth (D) ratio in bends has been

found to influence point-bar form (Onishi, 1972; Dietrich, 1987; Markham and Thorne, 1992). In wide shallow channels the bar top is flat in the zone of minimum radius and in such situations the point bar can extend across the full channel width. However, as the width:depth ratio (wd_r) decreases point-bar development is suppressed and small steep sided forced bars are produced by channel curvature (Ferguson, 1981; Hasegawa and Yamaoka, 1984; Ikeda, 1985; Dietrich, 1987).

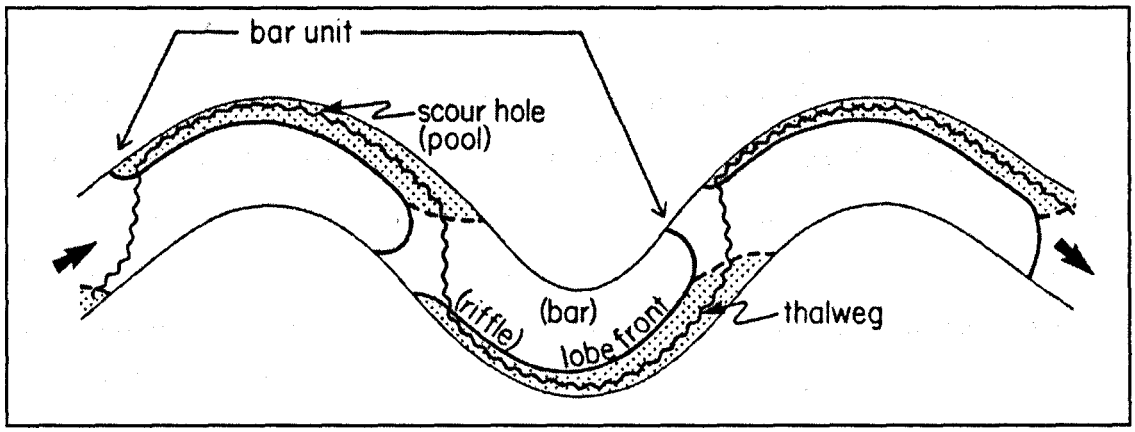

Figure 1.3: River meander form (from Dietrich, 1987)

This description of what is currently known about classical meander bend morphology provides the setting for the following discussions of the distribution of flow, shear stress, and sediment transport in bends.

1.3.2 Flow structure and shear stress distributions in meander bends

Flow fields in meander bends are controlled by the resultant of forces arising from continuous, and related, variations in channel curvature and bed topography. The flow response to channel form determines the distribution of boundary shear stress through the bend, which in turn controls sediment transport and thus channel form.

1.3.2.1 Curvature effects

Water flow in bends is heavily influenced by planform curvature, with the streamline of maximum velocity displaced towards the outer bank of each bend in the zone of greatest curvature and crossing the centreline between bends (Wilson, 1973; Hey and Thorne, 1975; Dietrich and Smith, 1983; Dietrich, 1987). The channel curvature

induces an outward acting centrifugal force that acts throughout the water column. The effects of this are reduced at the bed due to friction, which results in a net outwards transfer of water at the surface. This creates a water surface topography characterised by super-elevation at the outer bank and depression at the inner bank creating a cross-stream water surface slope that is superimposed on the downstream surface slope (Bridge and Jarvis, 1976; 1982). The cross-stream water surface slope produces an inwardly acting pressure gradient force. These two forces oppose each other, with the outwardly acting centrifugal force dominating in the upper part of the velocity profile where velocity is greater than the depth averaged velocity and the inwardly acting pressure gradient force dominating in the lower potion of the velocity profile where velocities are below the depth averaged. These forces therefore result in a secondary circulation superimposed on the primary downstream flow, where water at the surface moves rapidly towards the outer bank where it down-wells and water at the bed moves more slowly towards the inner bank (Figure 1.4) (Thompson, 1896; Einstein and Shen, 1964; Wilson, 1973; Hey and Thorne, 1975; Thompson, 1986; Dietrich, 1987).

There are three main definitions of this secondary circulation based on different methods of rotation. There is some debate over which is the most appropriate definition in given circumstances (*see* Lane *et al.*, 1999b; Rhoades and Kenworthy, 1999). However defined, these secondary currents are usually weaker than the primary flow, although they do have a significant influence on the distributions of velocity, boundary shear stress, and channel morphology. Interaction between the primary and secondary flows results in a helical or spiral motion of the flow through the bend (Figure 1.4) that is replaced by one of opposite vorticity in the next bend (Dietrich, 1987). The flow distribution through a bend is thus highly asymmetrical with maximum flow asymmetry developing downstream of the bend apex, due to the distance required for flow adjustment to the imposed curvature (Jackson, 1975; Furbish, 1988; 1991). As radii of curvature increase at the bend exit, the forces producing helical flow reduce and the secondary circulation and the flow asymmetry begins to decline (De Vriend and Geldof, 1983).

The strength of the helical circulation in bends increases with curvature, velocity, degree of super-elevation, and depth of the pool. This is because each of these factors will increase the magnitude of the centrifugal acceleration and thus the

pressure gradient force (Dietrich, 1987). There is therefore a positive feedback relationship between channel form and flow processes, whereby deeper sharper bends have higher secondary circulation velocities which helps maintain them as deeper and sharper. This produces a co-variation of channel morphology in both the cross-section and the planform directions of the channel. The relationship between discharge and strength of secondary circulation therefore depends on the relative variation in the above factors, especially velocity and curvature, in individual bends (Hooke, 1975; Bathurst *et al.*, 1979; Markham and Thorne, 1992). As a result, the strength of secondary circulation is often at a maximum at intermediate stages. As stage increases, primary currents dominate due to the main flow following a straighter path and shoaling over the point bar (Dietrich and Smith, 1983).

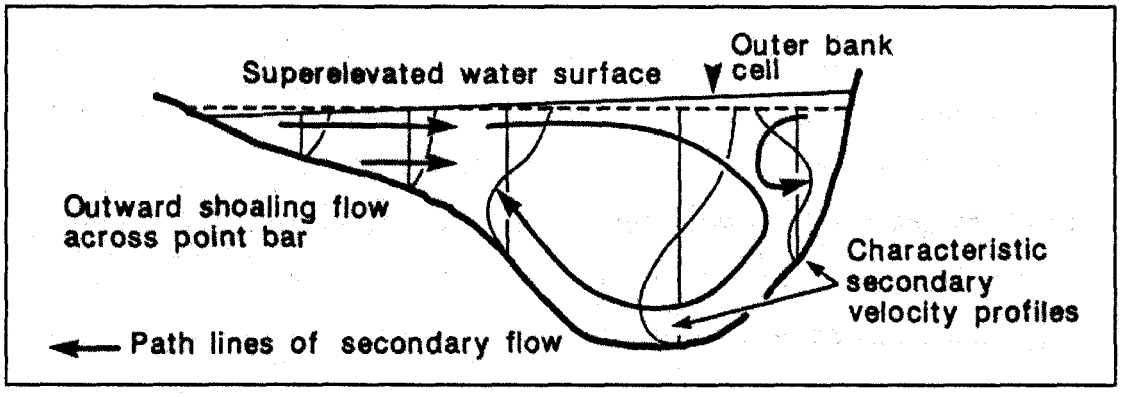

Figure 1.4: Secondary flow at a classical river bend apex illustrating the main skew-induced main secondary circulation cell, the shoaling over the point bar and the small outer bank roughness cell (from Markham and Thorne, 1992).

A smaller secondary circulation cell of reverse rotation is often present close to the outer bank (Hey and Thorne, 1975; Bridge and Jarvis, 1976; Bathurst *et al.*, 1977; 1979; Dietrich and Smith, 1983; Thorne *et al.*, 1985; Markham and Thorne, 1992; Blanckaert and Graf, 2001) (Figure 1.4). The cell is usually confined to a small region close to the outer bank (Markham and Thorne, 1992) and is highly turbulent (Blanckaert and Graf, 2001). Bathurst *et al.* (1977) found that this small outer bank cell is present in single bends, countering earlier arguments that it was a relict cell from upstream. It is therefore thought to be caused by the complex interaction of the main secondary circulation cell with the outer bank and flow stagnation and thus may

be related to boundary roughness effects in particular. The development of the cell seems sensitive to both the character of the outer bank: being stronger where the bank is rough (Hey and Thorne, 1975) and steep (Bathurst *et al.*, 1977). It is also sensitive to flow stage and has been found to be of greatest magnitude at intermediate to higher flow stages (Bathurst *et al.*, 1977; Markham and Thorne, 1992). More importantly, if it is boundary roughness driven, the cell is almost certainly non-persistent and thus intermittent in nature. Indeed, two different types of secondary circulation can be envisaged: persistent curvature induced circulation and a non-persistent (intermittent) turbulence driven secondary circulation. If non-persistent secondary circulation is averaged through time, it resembles persistent circulation and thus the two types may become indistinct (Lane *et al.*, 2000). There is thus a possibility that the cell is a result of the averaging process applied in previous studies, rather than a coherent flow structure in nature.

The main curvature induced secondary circulation cell and smaller outer-bank cell combine to drive the maximum primary flow filament below the water surface and closer to the outer bank at the bend apex through to the bend exit. This produces a region of high shear stress in the region of strong downwelling where the two cells combine (Bathurst *et al.*, 1977; Markham and Thorne, 1992). However, the crossover between bends introduces a spatial lag such that the maximum near-bank velocity and shear stress is often displaced past the bend apex (Furbish, 1991). The nature of the change in vorticity between bends and the inheritance of flow structure from one bend to the next is a complicated issue that has to date been somewhat avoided. Nevertheless, it is known that the spatial lag and suppression of the core of velocity below the surface combine to produce a higher than expected shear stress on the lower sections of the outer bank (*e.g.* Bathurst *et al.*, 1979) just downstream of the bend apex (Hooke, 1975; Dietrich, 1987; Furbish, 1988). Maximum bed shear stress follows the zone of highest velocity through the bend, moving from the inner bank at bend entry to near the outer bank at the bend exit. Velocities are low near the inner bank through the bend, especially downstream of the apex, and as a result, shear stress values are generally much lower over and around the point-bar region. Figure 1.5 illustrates the classical pattern of shear stress in meander bends. With an increase in discharge, the crossing of high velocity tends to occur later through the

bend due to inertial effect of the flow. This causes maximum shear to be concentrated even further downstream on the outer bank close to the bend exit.

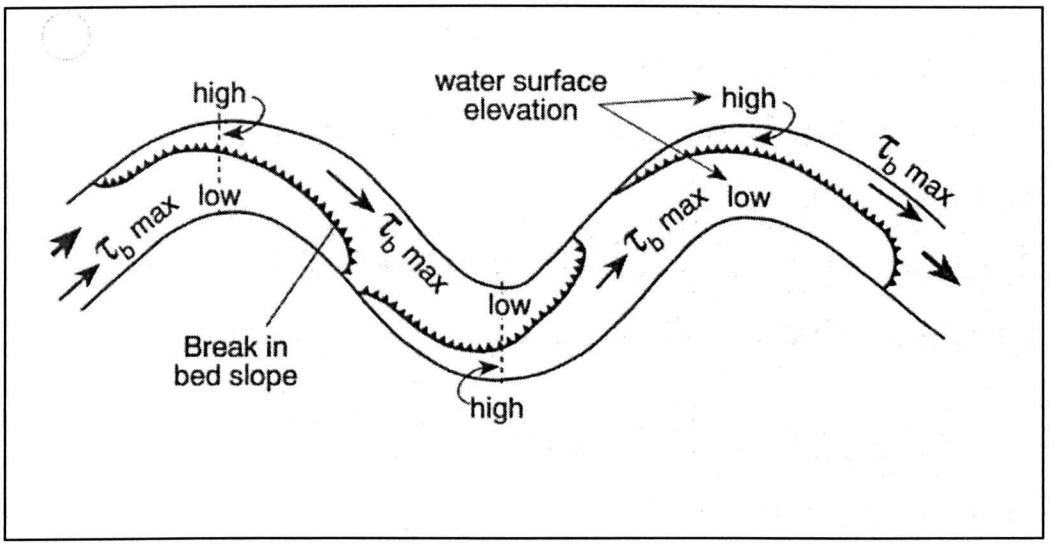

Figure 1.5: Shear stress distribution in a classical meander bend (after Dietrich and Whiting, 1989)

1.3.2.2 Bed topography effects

Although curvature of the channel has a significant impact on the flow distribution through a bend, the bed topography and cross section shape also heavily influence this distribution.

In bends with a well-developed point bar pool topography, the flow structure through the bend can be dramatically altered. Before the bend apex near the inner bank, the rapidly changing bed topography can produce a shoaling effect that drives flow into the pool. The forced movement of this flow around the point-bar that is produced by this shoaling effect has been termed 'downstream convective accelerations' (*e.g.* Dietrich and Smith, 198), which have the effect of reducing the downstream water surface slope near the inner bank, resulting in a reduction of the cross-stream surface slope and the pressure gradient term throughout the bend (Smith and McLean, 1984). Thus, flow across the point-bar area can become outwardly directed throughout the vertical and the helical motion is restricted to the central pool areas of the bend (Bridge and Jarvis, 1982; Dietrich and Smith, 1983; Smith and McLean, 1984;Yamaoka and Hasegawa, 1984). Although there may still be a deviation in the direction of flow from the bed to the surface due to curvature-driven pressure

gradient effects (Figure 1.6), this deviation is mediated by the shoaling effect of the bar and the flow is still outwardly directed throughout the depth. Past the bend apex, in the downstream part of the bend the shallowing pool and the deepening point bar results in flow being inwardly directed throughout the vertical (Figure 1.6). As well as affecting the secondary circulation, this topographic steering also forces the zone of high velocity to move more rapidly across the channel. This produces an equally rapid shifting of the zone of maximum boundary shear stress towards the outer bank earlier than expected in a bend. Dietrich and Smith (1983) demonstrates that it is the changing bed topography that produces this flow pattern rather than the influence of flow patterns generalised in the upstream bend.

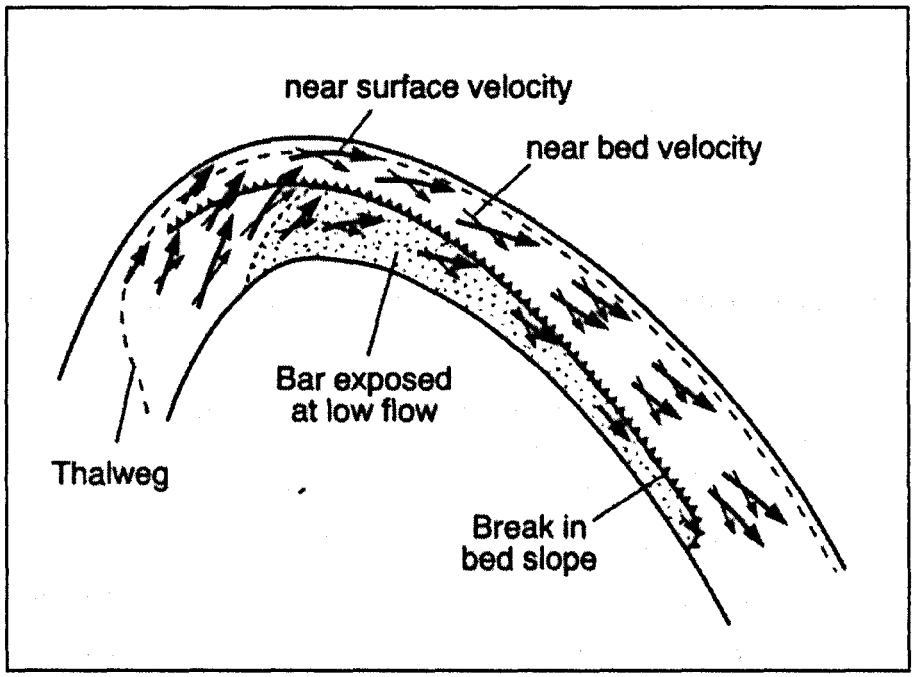

Figure 1.6: Flow field in an asymmetric bend with a well-developed point bar (after Dietrich, 1987)

The cross sectional shape and width:depth ratio (wd_r) ratio can have a significant effect on this observed flow structure. Where the wd_r is large (>10), point bar development is extensive, shoaling is common, and the full flow depth over the point bar is outwardly directed (Dietrich and Smith, 1983). However, when the ratio is low (<10), channels tend to be deep and narrow, shoaling is uncommon and all near-bed flow is inwardly directed (Markham and Thorne, 1992).

Thorne *et al.* (1985) found that this type of flow structure is very sensitive to flow stage, being present at low and intermediate stages but an inwardly directed near bed flow structure developing over the point bar as stage increased. However, Thorne *et al.* (1985) also state that this relationship will be mediated by how the wd_r varies with flow stage in different channels. In channels where width is almost constant with stage, helical flow will expand to the full channel width. In bends where width increases rapidly with flow stage, outward flow across it would persist. Thus, it is clearly a function of the relationship between point-bar form and the depth and velocity distributions across the point bar area as stage changes. Whiting (1997) confirms this through analysis of the change in flow force balance with changes in discharge.

1.3.3 Sediment transport, erosion and channel change

1.3.3.1 At the channel bed

As discussed above, flow structures in bends produced by a combination of curvature and topographic forcing result in a cross-stream skewed boundary shear stress pattern with a distinct zone of maximum shear stress. In the downstream direction, this shifts back and forth across the channel (Figure 1.5).

Although the movement of suspended load through bends is controlled by the flow direction throughout the velocity profile, transport directions of bed sediment are governed by the force balance of the near-bed fluid velocity vectors and the cross-stream and downstream channel slope (Engelund, 1974; Bridge, 1977; 1984; Hasegawa and Yamaoka, 1984; Dietrich and Smith, 1984; Allen, 1985; Odgaard, 1986a,b; Nelson and Smith, 1989a,b; Ikeda, 1989). In sand bedded streams, this non-uniform shear stress pattern produces a skewing of dune crests through the bend (Dietrich, 1987) with dunes becoming orientated towards the inside of bends and migrating up the point bar face (Kisling-Moller, 1992). The skewing of the dunes also results in secondary bedform migration in the main dune troughs towards the inner bank area (Dietrich, 1987). In bends with gravel-bed rivers with heterogeneous sediments the shear stress pattern results in pronounced sorting of bed materials such that the coarsest particles tend to be near the outside of bends and the bed material fines inside up the point-bar face (Jackson, 1976; Bridge and Jarvis, 1976; Van

Alphen *et al.*, 1984; Ikeda, 1989). This cross-stream sorting becomes more pronounced between the bend apex and the bend exit, such that point bars often have gravel heads but sandy tails (*e.g.* Bluck, 1971).

The paths of sediment movement through bends and the controls were investigated by Dietrich and Smith (1984). They found that coarse sediment moves from near the inner bank at the bend entrance into the pool near the bend exit; finer sediments move from near the outer bank at entry onto the point bar near the innerbank close to the bend exit (Figure 1.7). Indeed, tracer studies have confirmed that finer sediments are moved up the point-bar face and deposited on the point-bar head (Thorne and Lewin, 1979). The location of maximum sediment transport through the bend therefore occurs through the centre of the channel, where the balance of shear stress and sediment size is more favourable to entrainment and movement (Dietrich and Whiting, 1989).

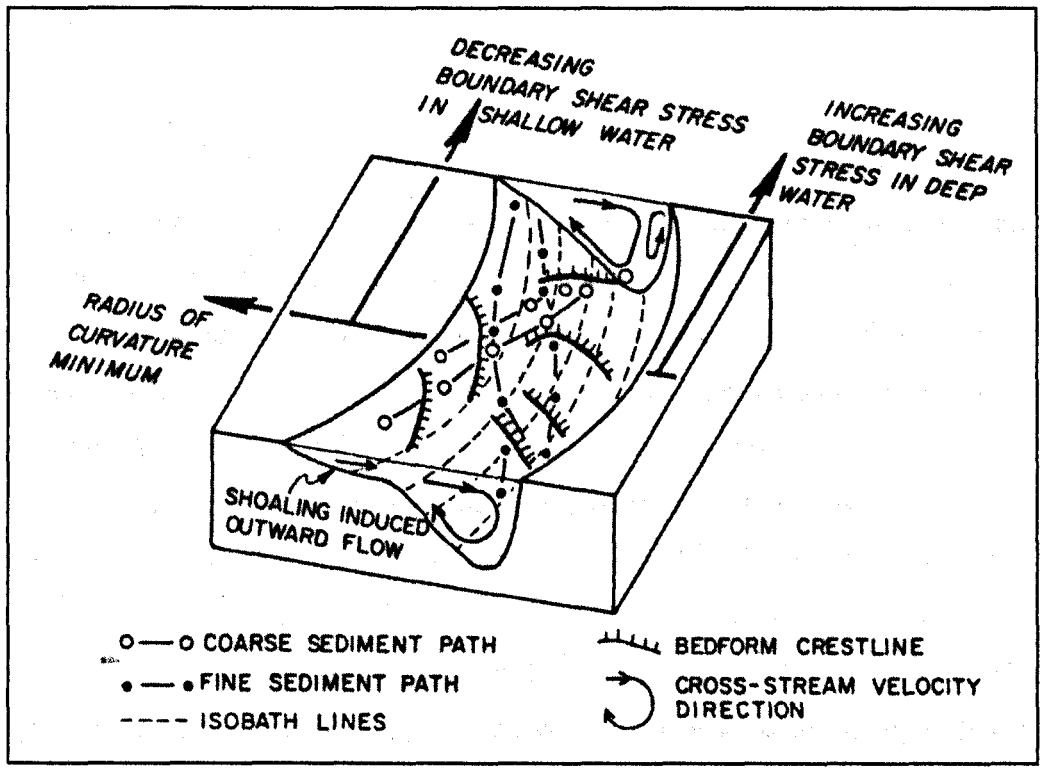

Figure 1.7: Particle sorting through a classical bend (Dietrich and Smith, 1984)

When combined with fine overbank deposits, this fining of sediment sizes up the point bar results in the distinctive fining upwards sedimentology often found in

floodplains (Allen, 1985). However, in rivers with high wd_r, the sorting up the point bar face is often absent (Dietrich, 1987). Consideration of the force balance reveals that the component of cross-stream slope is small and results in insufficient drag on the larger particles.

The systematic variations in shear stress and sediment size can be viewed as a stabilizing mechanism of bends as they mediate bed load transport and erosion. Stable bed morphology in a bend is produced when bed shear is balanced by sediment transport. Thus, increasing shear stress is balanced by converging sediment transport (Dietrich and Smith, 1984; Dietrich *et al.*, 1984). If stage falls, an increase in shoaling over the point bar increases erosion of the bar head and results in filling of the pool. An increase in stage reduces shoaling across the point bar and flow will become directed inwards over the bar as the pressure gradient term begins to increase. The result is scour in the pool and deposition up the point bar. This adjustment of bedforms to flow stage tends to be much slower in gravel bed rivers than sand bedded rivers.

1.3.3.2 At the channel banks

The presence of helical flow through bends and the resultant shear stress pattern discussed above produces erosion and bed scour at the outer bank downstream of the apex and deposition across the inner bank point bar. For a migrating meander to be in an *equilibrium* condition, deposition at the inner bank must balance the erosion of the outer bank (Thorne and Welford, 1994). On average, this is the case, maintaining a constant width. Scouring at the bed and erosion mid-way down the outer bank typically result in migration through undercutting and banktop block failures of the overlying cohesive sediments (Hooke, 1995). This pattern of erosion results in an outward and downvalley shift in the bend (Odgaard, 1987; Furbish, 1988; Hooke, 1997), which becomes more asymmetrical in transverse section, with deposition occurring across the point-bar region. The increases in curvature and depth produced by this process accentuate the helical flow structure, creating a positive feedback loop between form and process. This provides a physical basis for the observed tendency for bend migration rates to increase as the ratio of radius of curvature (R) to

channel width (W) decreases (Figure 1.8; Hickin and Nanson, 1975; Chen and Shen, 1984; Hooke, 1987; Biedenharn *et al.*, 1989; Furbish, 1988; 1991).

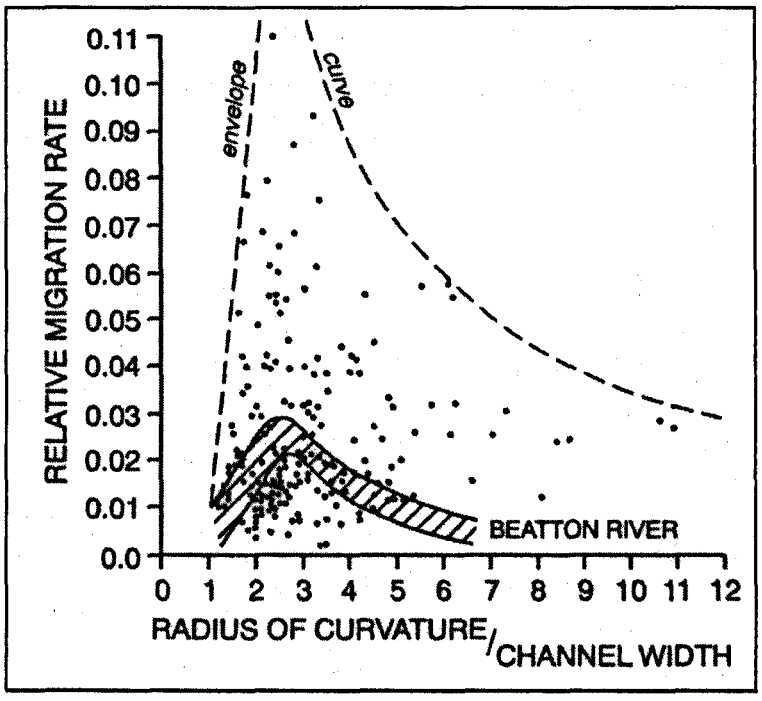

Figure 1.8: Relationship of migration rate to bend curvature for data from Nanson and Hickin (1975) and Hooke (1987).

This classical picture of how meander bends grow is complicated by several inter-related factors. First, local rates of bank retreat depend not just on the curvature-induced flow structure but also on bank strength as affected by height, stratigraphy, sediment properties, and vegetation. As mentioned above, spatial variations in these will distort the regularity of the meander train (Ferguson, 1976; 1979). This opens the way for the second factor, which is that the flow structure in one bend depends partly on that in the channel immediately upstream. Thus, in anything other than a perfectly regular meander train, the flow structure in bends of a given radius can differ according to the curvature of the upstream bend and the flow structure it therefore inherits (Jackson, 1975). Variation in flow asymmetry and helical flow through individual bends can lead to differing rates of bank migration in separate parts of the bend and result in the planform of bends becoming highly asymmetric (Carson and Lapointe, 1983; Lapointe and Carson, 1986). These factors lead to a diversity of rates and directions of migration as demonstrated theoretically by Furbish (1991) and numerically in the simulations of Sun *et al.* (1996).

Finally, bend tightness exerts an important control over observed flow structure. As mentioned above (1.3.2.1) as curvature of bends increases, the depth of the pool, degree of super-elevation, and the strength of secondary circulation all increase. In very sharp bends, with a bend curvature (R_c/w) below about 2, the classical helical flow structure model of curvature induced persistent secondary circulation breaks down through flow separation (1.3.4).

1.3.4 Flow separation in meander bends

Flow separation occurs through eddying and slowly recirculating flow at either the outer bank before the bend apex or at the inner bank after the apex (Figure 1.9) (Bagnold, 1960; Ippen and Drinker, 1962; Carey, 1969; Leeder and Bridges, 1975; Hickin, 1977; 1978, 1979; Woodyer *et al.*, 1979; Andrle, 1994). Some bends have also been noted as having separation at both banks (Markham and Thorne, 1992; Andrle, 1994). The presence of flow separation radically alters the processes occurring in bends. This section reviews the current understanding of the form, flow, and sediment processes in bends with separation zones.

1.3.4.1 Outer bank separation

Flow separation is thought to develop at the outer bank due to an upstream acting pressure gradient produced by the main filament of flow striking the outer bank at a high angle (Ippen and Drinker, 1962; Markham and Thorne, 1992; Andrle, 1994; Burge and Smith, 1999). As a result of the pressure gradient force, the main flow stagnates and divides with a proportion forced upstream into a zone of re-circulation. Flow within the re-circulation zone is much slower than that in the main channel, although velocity in the separation zone is not uniform, with a zone of almost 'dead' flow in the centre of re-circulation and a narrow core of faster flow moving upstream along the outer bank (Hickin, 1986; Andrle, 1994) in a perched channel (Burge and Smith, 1999). The presence of the separation zone at the outer bank forces the fastest downstream current to shift to the inside of the bend. This radically alters the distribution of shear stress and thus the direction and rate of migration, with a tendency for erosion of the point bar and inner bank but deposition of a 'concave-bank bench' (Page and Nanson, 1982) near the outer bank. Development of a

concave bank bench proceeds from initial deposition through aggradation, colonisation, and incorporation into the floodplain (Page and Nanson, 1982). Migration of the convex bank allows abandonment and further bench development. The accretions of bench deposits can constitute over 25% of the floodplain (Hickin, 1986; Burge and Smith, 1999).

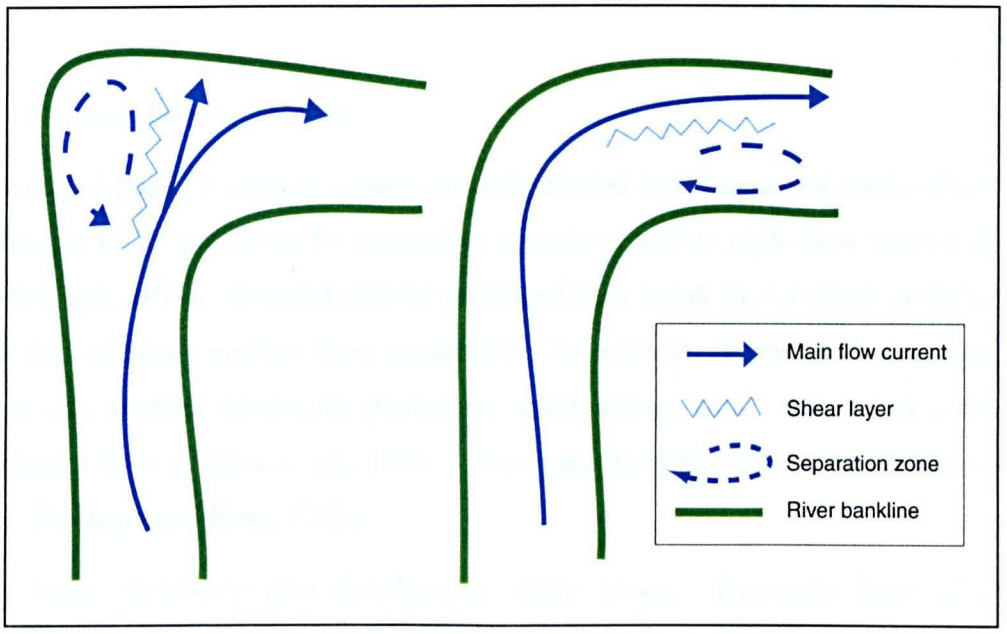

Figure 1.9: Idealised planform view of bends with outer bank (left) and inner bank (right) separation.

As mentioned previously, Hickin and Nanson (1975) found that apex migration rates tend to be greatest for R_c/w in the range 2 to 3, then decrease abruptly for $R_c/w < 2$. This was attributed to the onset of outer-bank flow separation. Outer-bank separation can also be associated with locally high channel width (Hickin, 1977; Page and Nanson, 1982; Andrle, 1994). Moreover, Lewin (1978) and Andrle (1994) suggest that it is inner bank erosion that leads to the widening that facilitates outer bank separation development and maintenance. Nevertheless, the nature and the direction(s) of cause-effect linkage are unclear.

In an attempt to begin to understand this cause-effect linkage, Hodskinson and Ferguson (1998) applied a validated numerical flow model (*see* Table 4.1) to a hypothetical channel and were able to demonstrate that both the radius of the outer bank and the width at the channel apex were significant in producing and controlling the size of separation at the outer bank. They also showed that the size of the

separation zone was very sensitive to the bend inflow as controlled by upstream planform: when the main flow current was skewed close to the inner bank, the outer-bank separation zone was very large; but when the inflow was skewed close to the outer-bank no separation zone was present. The removal of the point-bar was also shown to increase the size of the separation, attributed to removing the topographical barrier to the flow across the inner-bank apex area.

1.3.4.2 Inner bank separation

At the inner bank, a zone of separation can develop downstream of the bend apex. It is thought to be produced by excessive curvature and/or high flow inertia (Leeder and Bridges, 1975). It could also be produced by a break in curvature at the convex bank that creates a sudden flow expansion. As a result, the main flow is unable to follow the channel boundary, producing a separation zone, which has slowly re-circulating flow (Taylor *et al.*, 1971; Leeder and Bridges, 1975; Van Alphen *et al.*, 1984; Hattingh and Rust, 1993).

Inner bank separation also develops in sharp bends. Evidence from laboratory experiments, natural rivers, and tidal creeks suggests that inner-bank separation develops only when R_c/w falls below ~2 (Bagnold, 1960; Hickin and Nanson, 1975; Leeder and Bridges, 1975), which corresponds to a bend turning ~30° in a streamwise distance of one channel width. Resistance to flow has been found to be at a minimum before inner bank separation. However, as R_c/w falls below 2, resistance rises rapidly due to the increase in turbulence intensities as flow separation and shear between the main flow and reverse eddy develops (Begin, 1981). The creation of a separation zone at the inner bank reduces the effective channel width and this may accelerate bend growth by concentrating the fast flow towards the outer bank. It also promotes inner-bank deposition in the separation zone leading to point-bar growth.

1.3.4.3 Significance of separation zones

The presence of flow separation radically alters the flow distribution and shear stress patterns through the bend. As a result, the patterns of erosion, deposition, and channel migration observed in classical bends can be expected to alter (*e.g.* Hickin

and Nanson, 1975). Indeed, Reid (1984) discusses artificially inducing separation at the concave bank as a control on floodplain erosion. Flow separation in bends is important for reasons beyond its effects on the direction and rate of bank erosion and bend migration. Mean velocity and turbulence intensity tend to be low within separation zones, which therefore act as backwaters or 'dead zones' that trap fine sediment, nutrients, phytoplankton, and pollutants (Page and Nanson, 1982; Tipping *et al.* 1993). They thus form distinctive ecological habitats (*e.g.* Reynolds, 2000) and can act as refugia sites during high flow events. The limited mixing between dead zone and main flow also delays solute mixing and dispersion through river reaches (*e.g.* Guymer, 1998; Hankin *et al.*, 2001; Hankin *et al.*, 2002; Boxall *et al.*, 2002). Several authors have noted changes in the occurrence and extent of flow separation zones according to flow stage. The existence of separation at the inner bank has been reported as transient, appearing only over a narrow range of intermediate flows (Bridge and Jarvis, 1982). However, Markham and Thorne (1992) reported that outer-bank separation occurred at bankfull stage, but not at lower discharges. Although, Andrle (1994) found that this was not the case with outer-bank reverse flow in Mansfield Creek, which was found to be persistent at all flow levels.

A shear layer exists in the boundary between the main downstream flow and the slow moving fluid in the separation zone (Figure 1.9). This layer has been observed to periodically deform into a series of spiral vortices that advect into the separation zone (Leeder and Bridges, 1975; Hickin, 1978). Hickin (1978) visually observed these events, noting a period of several minutes and a length of around 30s. Hickin (1978) suggested that advection of the vortices by the helical motion of the main flow perhaps dominated in the intervening periods of relative quiescence. Shear layers are inherently unstable and these zones have recently been investigated in detail at river channel confluences. Several scales of variation have been identified (Biron *et al.*, 1993b). Such turbulent flow structures include the formation of Kelvin-Helmholtz instabilities in the shear layer (*e.g.* Best and Roy, 1991; Sukhodolov and Rhoads, 2001), longer-term shear layer migration (*e.g.* Biron *et al.*, 1993b), and periodic upwelling and downwelling at certain positions in the channel (*e.g.* Bradbrook *et al.*, 1998). They can be extremely significant in the dissipation of energy, the amount and timing of flow mixing between the main current and the dead zone (*e.g.* Guymer, 1998), flow structure generation, boundary shear stress and thus

sediment entrainment and transport. This shear layer has also been observed to control fine sediment movement into the dead zone, with vortices dissipating in the dead zone and depositing suspended load (*e.g.* Hickin, 1978; Tipping *et al.*, 1993). Intermittently, each of these processes could be several orders of magnitude greater than the predicted time-average means. Consequently, analysis of flow structures with time-averaged techniques can lead to inaccurate or incorrect interpretations and conclusions. For example, the interpretation of flow structures, such as secondary circulation cells, could be an artefact of averaging periodic or intermittent processes (*e.g.* Shi *et al.*, 1999; Lane *et al.*, 2000), and concentrations of a pollutant could periodically exceed the computed time average levels (Lane *et al.*, 1999c).

1.3.4.4 Separation in other situations

Expansion of open channel flow and the production of areas of dead or reverse flow with an associated shear layer occur in many other situations. For example, they occur in the lee of obstacles such as large gravel bars (Carling *et al.*, 1994), after channel constrictions (Schmidt, 1990; Rubin *et al.*, 1990; Kimura and Hosoda, 1997) or near artificial structures such as bridges or groynes. The insights gained from these studies may help to understand separation in meander bends. In expansion situations, re-circulation zones are present over the full range of flows, and although the main channel velocity increases with stage, velocity in the re-circulation zone remains low allowing deposition even at very high flows. Re-circulation zones downstream of obstructions have been modelled using both experimental (Schmidt *et al.*, 1993) and numerical (Kimura and Hosoda, 1997) methods. The point of reattachment can vary considerably through time even with steady flow rates. Flow velocity, the water surface in the dead zone (Kimura and Hosoda, 1997) and the size of separation zone therefore fluctuate intermittently (Rubin and McDonald, 1995). This intermittency has been attributed to the distortion and interference between shear layer near the reattachment point and the influence the pulses of flow created have on future flow variability when incorporated into the re-circulation zone.

1.3.4.5 Unresolved issues

Although the presence of separated flow and the associated depositional forms has repeatedly been noted in the literature (*e.g.* Carey, 1969; Leeder and Bridges, 1975; Woodyer *et al.*, 1979; Alford *et al.*, 1982; Reid, 1984; Rohrer, 1984; Hickin, 1986; Markham and Thorne, 1992; Andrle, 1994; Hodskinson and Ferguson, 1998), few of these studies discussed the frequency of these phenomena or their distribution along study reaches. As a result, it is unknown how widespread bend flow separation is, and what the relative frequencies of inner- and outer-bank separation are. Also, discussion of the causes of separation has mostly been based on looking at the characteristics of bends with separation, without checking that they differ significantly from the characteristics of bends with the 'classical' flow structure and no separation. Much of the literature emphasises R_c/w as the key control but it is apparent that separation may depend on more than just the curvature of the bend of interest. The rate of change of curvature through the bend may be a more pertinent variable. The upstream planform may also be relevant via the orientation of the incoming maximum-velocity streamline. Locally resistant banks could also play a part, through their effect on bank curvature and the possibility of 'overtaking' of one bend by another. The size and height of the point bar through topographic steering and the 'blocking' of opportunity for the main flow to move inside could also be a factor.

Quantitative investigations of flow separation in bends are even scarcer. Rozovskii's (1957) measurements of flow structure in a 180° bend revealed inner-bank separation but he did not discuss it in detail. Hickin (1978) noted flow separation in some of the series of bends in which he made velocity measurements, and although his discussion is more concerned with the classical helical flow structure, he does mention that the secondary circulation in the main part of the bend was more intense than expected. This pattern of low secondary circulation in the separated flow zone and increased intensity in the main flow was also discussed by Markham and Thorne (1992) who attribute it to the curvature of the flow around the dead zone. Andrle (1994) discusses the flow structure in a bend with outer bank separation, but the sparse measurements do not reveal the full three-dimensional picture. As mentioned above, Hodskinson (1996) and Hodskinson and Ferguson (1998) investigated some of the controls on the formation of outer bank separation in 3-D computational flow

simulations for ideal bends. Nevertheless, they did not explicitly deal with the three-dimensional flow structure. The shear stress patterns that the flow structures produced are also poorly understood. Furthermore, although the shear layer has proven significant in other fluvial situations, no studies have investigated the shape and nature of shear layer periodicity in meander bends with flow separation.

1.3.4.6 Summary

Despite the fact that the development of recirculating flows in sharp meander bends can significantly alter bend processes, these bends have had very little attention. The conditions conducive to the onset of separation are still unclear as is the nature of the three-dimensional flow structure and the resultant shear stress patterns, sediment transport and channel change. The time-averaged shape and dynamics of the shear layer are unknown. How the flow patterns change with flow stage is also unclear.

1.4 MODELLING BEND FLOW

1.4.1 Introduction

There is a long history of modelling in the study of open channel flow processes, which has contributed significantly to the understanding of meander bend dynamics (1.2). The last ten years have seen a proliferation in the application of numerical flow models in fluvial geomorphology and hydrology (*see* Bates and Lane, 1998 and papers within). Recent enhancements to computational fluid dynamic (CFD) models have seen their utilization in the fields of river mechanics, fluvial geomorphology, and engineering hydraulics to enhance understanding of the interaction between river channel boundaries and the associated flow fields. Application of three-dimensional CFD modelling approaches has enabled an improved simulation of important flow processes, providing prediction fields that enhance insight and understanding, where field and laboratory measurements can rarely provide a sufficient process representation. Their application has been especially valuable in areas of complex flow structure such as braided river reaches (Lane *et al.*, 1995; Lane and Richards, 1998; Nicolas and Sambrook Smith, 1999), confluence zones (Bradbrook *et al.*, 1998; 2000a; Lane *et al.*, 2000), and areas of flow separation (Hodskinson, 1996;

Hodskinson and Ferguson, 1998). The use of CFD has proliferated as it can overcome some of the methodological and practical limitations of more traditional field and laboratory based approaches.

This section highlights the limitations associated with monitoring flow structures using field and laboratory approaches (1.4.2) before a discussion of how the recent research in applying CFD to open channels overcomes some of these limitations (1.4.3). The section then addresses some of the key issues and assumptions involved in using CFD for modelling open channel flow (1.4.4). The full background and details of CFD and its application to natural river channels is presented in Chapter 4.

1.4.2 Limitations of field and laboratory approaches

To quantify the flow velocity and understand the factors controlling flow structure in open channels there is a need to measure simultaneously all three components of velocity at many points within the flow under a large number of situations with varied boundary conditions. Methodological limitations in measurement techniques have precluded this in both field and laboratory studies.

Many of the studies upon which current understanding of bend flow is based have quantified flow structure using instruments that measure components of velocity in two-dimensions. In the case of electromagnetic current meters (ECM), the third dimension is often obtained using one of two main methods: (1) through inference based upon different treatments mass continuity leading to application of one of several rotation methods (*e.g.* Bhowmik, 1982; Rozovskii, 1957; Bathurst *et al.*, 1977; Paice, 1990); or (2) through measurement of all three dimensions by rotating the sampling direction of the instrument and measuring in two orientations consecutively (Markham and Thorne, 1992; McLelland *et al.*, 1996). However, both methods are prone to error. For example, Lane *et al.* (1999b; 2000) demonstrates that the rotation methods applied by many workers will inevitability identify secondary circulation and that this may be misleading. McLelland *et al.* (1996) note that measuring two orientations consecutively is prone to both positioning and longer term averaging errors. To overcome some of these problems, recent developments in field measurement instruments have enabled the use of three dimensional acoustic Doppler velocimeters (ADV) (*e.g.* Lane *et al.*, 1998) and acoustic Doppler current

profilers (ADCP), which provide three dimensional velocity measurements at a point and through a profile respectively. Improvements have also been made in instruments applied in laboratory flumes, with laser Doppler anemometry (LDA) and particle image velocimetery (PIV) providing 3D measurements through profiles and 2D instantaneous velocity maps respectively.

Although the recent development of these instruments has significantly improved measurements, to date no measurement instrument can provide instantaneous, three-dimensional measurements, simultaneously at a large enough number of points over a large enough spatial scale. Thus, at-a-point measurements have to be made and the time required to obtain velocity measurements of sufficient density and quality is very large. Further practical problems may arise in field studies when a constant discharge is required during the measurement period. Inference of flow structure from point samples is difficult, especially if features of the flow field are unsteady. Indeed, longer term fluctuations in the flow field which occur near regions of shear, for example in the mixing layer at separation zones or in the roughness induced outer bank cell, can introduce significant errors in velocity measurements and make interpretation of coherent flow structures very difficult. This is because averaged time velocity vector maps can include both persistent secondary circulation and non-persistent events (Lane *et al.*, 1999b; 2000). Thus, the nature of the interaction of these non-persistent flow features and persistent secondary circulation remains un-quantified and unclear.

Even with the limitations in the methodology outlined above, measurements of flow velocity in field studies have allowed assessment of the flow structures that develop under one set of boundary conditions and provide the context within which controls on this flow structure can be inferred. This has contributed significantly to current understanding of flow in natural channels. However, studying the effect of variations in boundary conditions is precluded by the time limitations in all field studies and practical limitations in finding suitable comparable sites in the field. Bradbrook *et al.* (1998) cite this problem as the main cause of the different inferences of flow structure controls at open channel confluences. Laboratory studies have introduced control into the experimental design, often based on simplified representation of field sites. However, the amount of variations in boundary conditions that can be performed remains relatively low. Thus, a complete

understanding of flow structures in open channels is limited by both shortcomings in measurement techniques and methodological difficulties.

1.4.3 Application of CFD to natural channels

Numerical flow modelling (CFD) is an alternative technique that has seen recent application in understanding open channel flow. It can overcome some of the difficulties associated with field and laboratory approaches, and the use of numerical models alongside field and laboratory studies can significantly enhance understanding. Indeed, CFD is a complementary technique that relies heavily on empirical data from either the field or the laboratory to provide both boundary conditions and validation data. CFD provides spatially rich three-dimensional velocity and turbulence prediction fields that are unobtainable through any other method. It can also provide information on pressure gradients, free surface elevations, and bed shear stresses, which are difficult to assess in the laboratory and field. Moreover, once a model is suitably validated, it allows ready alteration of boundary conditions in order to investigate cause-effect and feedback relationships (Figure 1.1; 1.2) within the system being investigated.

Although CFD overcomes some of the issues related to both the field and laboratory based approaches discussed above, the application to natural rivers channels of a numerical code that was developed for general engineering application results in a number of specific methodological issues and assumptions that have to be considered. Indeed, each application of a generic numerical flow model has to be suitably verified and validated: the correct solution of the appropriate equations must be obtained and the correct parameters and boundary conditions must be used to solve the equations (Lane and Richards, 2001). The degree to which each application is both verified and validated should be assessed and is improved through careful consideration of numerical grid used, the type of turbulence closure employed, and the correct definition of the boundary conditions.

CFD involves solving the Navier-Stokes equations by discretisation of the domain under consideration into a numerical grid. The solution obtained will be dependent on the grid design applied, although this dependence is reduced as grid cell size is reduced. However, as grid cell size reduces, the computing resources required

increase dramatically and a balance is therefore required between grid resolution and computing resources. In all situations, excluding straight flume applications, this grid must be deformed to fit the irregular channel boundary and consideration must be given to the amount of topographic representation that is incorporated within the grid. However, the sensitivity of model predictions to amount of topographic representation included within the numerical grid remains un-quantified.

Direct numerical simulation of the Navier Stokes equations is not possible for high Reynolds number flows with current computing power and a turbulence model is therefore required to close the Navier-Stokes equations. The type of turbulence closure applied can dramatically affect the predictions obtained. Most applications of CFD to open channels have employed two-equation turbulence models based on Reynolds averaging techniques that produce a time-averaged simulation (Hodskinson and Ferguson, 1998; Bradbrook *et al.*, 1998; 2000a). However, in flows with a large amount of shear, such as meander bends with flow separation zones, a wide range of turbulence scales are produced and as a result time-averaged modelling techniques will not fully capture the processes occurring within the system. Therefore, more recent applications of CFD to open channels have begun to explore the potential of transient turbulence models, more specifically Large Eddy Simulation (LES), to model this large-scale turbulence (Bradbrook *et al.*, 2000b). Although LES has demonstrated its ability to model some aspects of large-scale turbulent structure, its full potential and issues of sensitivity have not been assessed.

Once the numerical grid has been constructed, boundary conditions have to be specified for the channel bed and banks, the inflow cross-section, the outflow cross-section and the free surface. At the channel boundary, a roughness height has to be specified. This can be problematic as it must incorporate both the grain roughness and the form roughness not represented in the numerical grid. Indeed, several applications of CFD to natural channels have experienced problems with roughness specification (Hodskinson, 1996; Hodskinson and Ferguson, 1998; Lane *et al.*, 1999a) and very little is known about the sensitivity of model predictions to the relationship between the topographic representation included in the grid, grid distortion effects and the roughness parameter. Most models have also specified a constant roughness height over the whole channel boundary, and the effect of spatially variable roughness has not been assessed.

As meander bends are known to have large areas of superelevated flow and zones of depression some representation of the free surface may be required. Bradbrook *et al.* (1998) used a free surface model based on a porosity approximation that accounts for the effect of the free surface on a symmetry plane. The sensitivity of model predictions to the free surface representation must also be assessed. The upstream inflow into the model domain must be prescribed and this can be problematic in field situations where the full inflow distribution is difficult to quantify, which may impair predictions. The outflow to the model sets the free surface level and the pressure distribution within the model is set relative to that at the outflow section. Many of these methodological issues and assumptions, that remain un-quantified, are subject to examination and form specific thesis objectives alongside the substantive application of the model.

Although the application of CFD to open channel flow has a number of methodological issues, some of which remain un-investigated and un-quantified, its ability to produce three-dimensional predictions of the complete flow field have proven very useful. However, the application of CFD to open channel flow relies heavily upon both field and laboratory measurements. For example, boundary conditions are set using empirical measurements, or theoretical reasoning based upon field and laboratory experimentation and model validation is also based upon empirical measurements. The performance of the model is therefore closely intertwined with the ability to predict correctly the situation under investigation. Thus, understanding improves through an approach that applies a range of techniques, which minimises the individual effect of each of the methodological and practical issues associated with each approach.

1.5 RESEARCH QUESTIONS, AIMS AND OBJECTIVES

1.5.1 Research questions

Consideration of the previous work and background information on the numerical modelling outlined above generates a number of research questions that require investigation.

- How common is flow separation in meander bends?

- What factors control the occurrence of flow separation? How is it related to bend tightness, and what effect do other geometric factors seem to have?
- What is the relative frequency of inner and outer bank separation and what features seem to control whether separation is present at the inner bank or outer bank?
- What is the time-averaged flow structure in meander bends with 1) inner bank separation 2) outer bank separation?
- What is the 3D time-averaged shape of the shear zone, which direction does the shear zone skew?
- How does flow structure alter with stage? Does the occurrence or extent of separation change with flow stage?
- Does the separation shear zone have quasi-periodic flow structures? If so what are they and what effects do they seem to have? Does flow stage seem to alter any periodicities?
- How well can flow separation in natural meander bends be modelled by (a) time-average and (b) LES techniques? Do LES and time-average techniques provide similar results?
- To what extent does LES provide reliable information on spatio-temporal evolution of flow structures, especially in the shear zone areas?

1.5.2 Research aims and objectives

The primary aim of this thesis is:

> *To investigate the frequency and nature of flow in meander bends where flow separation and re-circulation zones are present, and ascertain the relative importance of different controls on flow structure generation and assess the geomorphological significance.*

Thus, this thesis will attempt to answer the above research questions and address the aim through several research objectives, which employs three distinct levels of field investigation, laboratory experimentation and the application of a CFD flow-modelling package. The specific objectives are:

1. Ascertain the frequency of occurrence of flow separation in river meanders.
2. Identify factors responsible for the formation of separation zones.
3. Quantify the three-dimensional flow structure in meander bends with separated flow and evaluate the ability of the numerical model in simulating the observed flow structures.
4. Assess the ability of LES in modelling periodic aspects of the flow field.
5. Explore flow structures generated by different combinations of boundary conditions and flow stages, and consider the geomorphological implications of the modelling results.

1.6 THESIS STRUCTURE

The aims and objectives outlined above were tackled through a programme of research that ranged from a general field reconnaissance survey to detailed case study investigations. This programme of research is reported in the following six chapters.

Chapter 2 discusses the use of a visual reconnaissance survey of over 600 bends to ascertain the frequency of occurrence of flow separation in two lowland rivers. Additionally, relatively simple field measurements were taken and were used in an attempt to predict the presence or absence of flow separation in bends.

Chapter 3 reports on detailed fieldwork that was performed in fewer bends (twenty-two) in a study that included flow measurements and surveying. This level of investigation provides a more process-based examination of the factors responsible for the existence of separated flow within bends.

Chapter 4 describes the numerical flow model (PHOENICS), which is used extensively in the following chapters. It introduces the mathematical background to the basic equations that are used and how they are solved, the grid generation methods, and the turbulence closure techniques. The chapter also covers boundary condition specification for the bed, banks, free surface, incoming flow and outlet pressure distributions. The chapter fully evaluates the assumptions and simplifications that are introduced in each stage of model development and

application. The chapter also considers some of the philosophical and methodological issues of model verification and validation.

Chapter 5 discusses the time-averaged flow structures at three natural bends: two with inner bank separation and one with a large outer bank separation. The chapter examines the similarities and differences between more classical bends and bends with regions of separated flow. It also examines the similarities and differences in the flow structure between bends with separation at opposite banks. The influence of flow stage is examined by modelling one bend at near bank-full flow. The geomorphological implications of the findings are considered and discussed.

In Chapter 6, the nature of transient flow within bends is investigated. Initially, 3D point velocity data gathered within the bends examined in chapter 5 are used to illustrate and examine the transient flow fields. The ability of the numerical model to reproduce the transient flow processes with a large eddy simulation (LES) turbulence scheme invoked is then examined.

Chapter 7 summarises the conclusions of the work and suggests further avenues for research based on the findings and conclusions of this thesis.

Chapter 2
Field Sites and Reconnaissance Survey

2.1 INTRODUCTION

This chapter details the use of an extensive reconnaissance visual survey of river channel bends to answer elements of research questions 1 to 3 (1.5.1). Thus, the reconnaissance survey considered the frequency of inner- and outer-bank separation occurrence and size, and applied statistical methods to explore the extent to which the presence, location, and size of separation zones can be predicted from readily observed channel properties. The nature of the survey is extensive, covering a very large number of bends in relatively little detail, in order to place into context the more detailed mid-level fieldwork (3.1) and flow modelling case study bends (5.1, 6.1). It also provided a systematic means of identifying bends that were good examples of more general cases. This visual survey builds on the work of Hodskinson (1997) who carried out a similar, less detailed and less extensive, survey of non-classical bends on four rivers, which included reaches of the Rivers Bollin and Dean.

The chapter begins by detailing the rivers and the reaches (2.2) used in the reconnaissance survey. The chapter then outlines the methods employed in the reconnaissance survey (2.3) and explains how each variable was measured. Section 2.4 presents the results of the survey in terms of the frequency and size of separation zones (2.4.1) and the possible factors that contribute to their occurrence (2.4.2 and 2.4.3). Section 2.5 draws the results together and considers the role of each factor in a more general context.

2.2 FIELD SITES

The reconnaissance survey was conducted along reaches of the River Bollin and its tributary the River Dean, in Cheshire, England. These small rivers rise on the

western side of the anticlinal Pennine Hills and flow in a north-westerly direction across the Weichselian glacial sediments of the Cheshire Plain eventually flowing into the Irish Sea after joining the larger River Mersey (Figure 2.1). The study reaches extend for a valley length of 11 km along the Bollin (UK Ordnance Survey grid reference SJ898777 to SJ858812 and SJ840820 to 825835) and 10.5 km along the Dean (SJ925777 to SJ875822) (see Figures 5.2 and 5.16 for photos of example bends along the reaches).

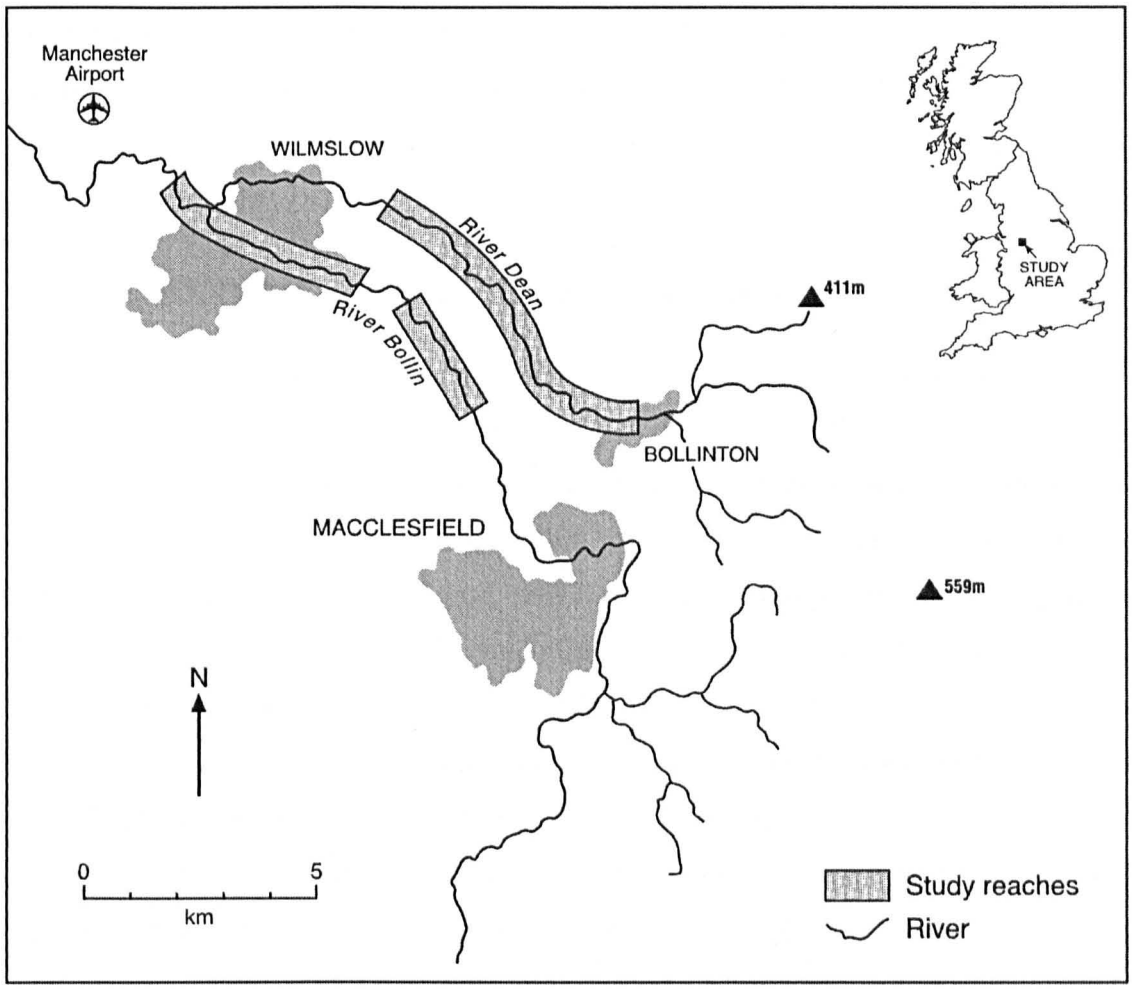

Figure 2.1: Location of study reaches

Both rivers are actively meandering and have predominantly gravel beds in the study reaches with well-developed pool-riffle morphology. The riverbanks have a high silt-clay content of at least 7% (Knighton, 1970), which forms tight cohesive banks. Riffle-surface D_{84} grain sizes are typically about 80 mm in the Bollin and 60 mm in the Dean. Both rivers have a mean gradient of 0.44 m/km (Knighton, 1970,

Hodskinson, 1997). The hydrological regime is flashy with flood events possible at any time of year, but associated in particular with autumn and winter frontal rainfall and summer convective storms. Along the study reaches, the bankfull discharge range between 5 to 10 m^3s^{-1} along the Bollin and between 2 and 3 m^3s^{-1} along the Dean, with bankfull widths of 7-9 m and 3-5 m respectively (Knighton, 1975). Both rivers occupy broad shallow troughs incised in glacial deposits (Hooke *et al.*, 1990) so their channels are locally confined by low valley terraces which restrict the otherwise freely meandering pattern. Most of the floodplain is used for pasture but there are often isolated trees or small stands along the banks, and large woody debris occasionally obstructs the flow. The survey was performed at intermediate to low stages in both rivers: about 0.7 m^3s^{-1} on the Dean and 2.1 m^3s^{-1} on the Bollin.

2.3 RECONNAISSANCE SURVEY METHODS

In order to provide a representative sample of bends for each river, a large number of bends were examined, 441 for the River Dean and 224 for the River Bollin. The philosophy behind the survey was that, although every river bend can be considered unique in detail, the processes responsible for bend evolution are the same for all bends (*e.g.* Markham and Thorne, 1992). Thus, attempts to produce general descriptions and/or models of bend flow, sediment transport processes, and geomorphic evolution should be confined to major features of bends rather than unique details. A checklist of such features was developed for this purpose, piloted on a short reach of the River Dean, and then modified before being used for the full survey (Figure 2.2). The checklist covered the presence/absence and size of inner- and outer-bank flow separation, together with a range of information on possible controlling factors. It required only visual inspection and a few simple measurements that could be made from the river bank. Subjective judgements were avoided as far as possible in designing the checklist, but to avoid any operator variance the entire survey was done by the author.

Bends were defined as any change in general bank line direction thus excluding straight sections from the analysis. The existence of significant flow separation at the inner, outer, or both banks was noted, and where separation occurred the proportion of the apex bankfull width (W) that it affected was estimated using

surface floats and string streamers for visualization (Figure 5.2). Separations smaller than W/8 were excluded as the pilot study suggested that they are generally caused by small, isolated bank irregularities and collapsed bank material rather than overall bend geometry. They are therefore considered as unique details of individual bends and not principal flow features caused by ubiquitous bend processes. Significant separations were classed as small (<W/4), medium (W/4 to W/2), or large (>W/2).

RIVER:
DATE:
FLOW-LEVEL:

Bend No.	Bank-full Inflow X-S		Separation		Bar		Angle of bend turn		Main L Flow	Bed Mat	Bank Veg	Notes
	Width	Depth	Type	Size	Type	Size	Dstm	Upst				

Figure 2.2 – The reconnaissance survey checklist form

The existence of any of three types of emergent bar (point, mid-channel, or concave-bank bench) was recorded and bar size relative to channel width was estimated using the same classes as for size of separation zone. The nature of the outer bank strength was recorded using two two-way classifications: whether the bank was low (cut into the floodplain) or high (cut into a terrace), and whether the top of the bank had only low vegetation (normally grass) or trees. For subsequent analysis this information was reduced to an ordinal scale of bank strength: 1 for low grassy banks, 2 for high grassy banks or low tree-covered banks, and 3 for high tree-covered banks. Notes were also made on several other factors including; bed material type, upstream

channel position, inflow characteristics, photograph number and bend identification number. The bend identification number increased in the downstream direction. Odd numbers were assigned to right handed bends and even numbers were assigned to left handed bends (increasing in the downstream direction). If two consecutive bends were orientated in the same direction or single meanders had more than one zone of increased curvature (Hooke and Harvey, 1983) they were annotated with a letter (*i.e.* 12a and 12b), thus allowing the identification of multi-headed and compound meander forms. Bend inflow bank-full width and depth were measured at selected bends along each main reach to check for any significant changes in river scale and character between reaches.

At each bend, two more quantitative measurements were made, one relating to bend planform and the other more to flow structure as affected by upstream planform. The planform variable generally discussed in relation to flow separation is radius of curvature (R) (*e.g.* Hickin and Nanson, 1975; Furbish, 1991), but this is far harder to define and measure in the field than is apparent from typical textbook diagrams. R is the inverse of the channel curvature $d\theta/ds$ (where θ is channel direction at centreline distance s). It varies continuously in any bend that is not an arc of a circle, and its local value can only reliably be estimated from values of $\Delta\theta/\Delta s$ over short segments. It is therefore quicker and easier to measure $\Delta\theta$ for the entire bend (*i.e.* the total angle of turn, denoted hereafter by ω), which is unambiguous and is known to have a strong inverse correlation with R/W for both natural bends and a range of idealised geometries (Ferguson, 1973; Hey, 1976). Estimates of ω were made from the difference between compass bearings along the banks at crossovers between successive bends (Figure 2.3). Repeat measurements of ω at a selection of bends showed repeatability to a standard deviation of $\pm 3°$, which is very small compared to typical angles of turn. The other measurement was of the angle at which the fastest current impinges on the outer bank. This is denoted hereafter by ϕ and was defined (Figure 2.3) as the difference between a bearing looking upstream along the outer bank at the zone of impingement and one looking upstream along the fastest current. Perfect potential flow in an isolated gentle bend would therefore have $\phi = 0$, but in a series of bends the delayed crossover from one bend to the next gives $\phi > 0$, and if either the inner or the outer bank is very sharply curved it is possible for ϕ to approach 90°: the current is locally perpendicular to the outer bank rather than

parallel with it. Estimation of ϕ is more subjective than ω, but repeat measurements for a selection of bends indicated that it is repeatable to a standard deviation of ±5° which is again small compared to the typical value of the angle.

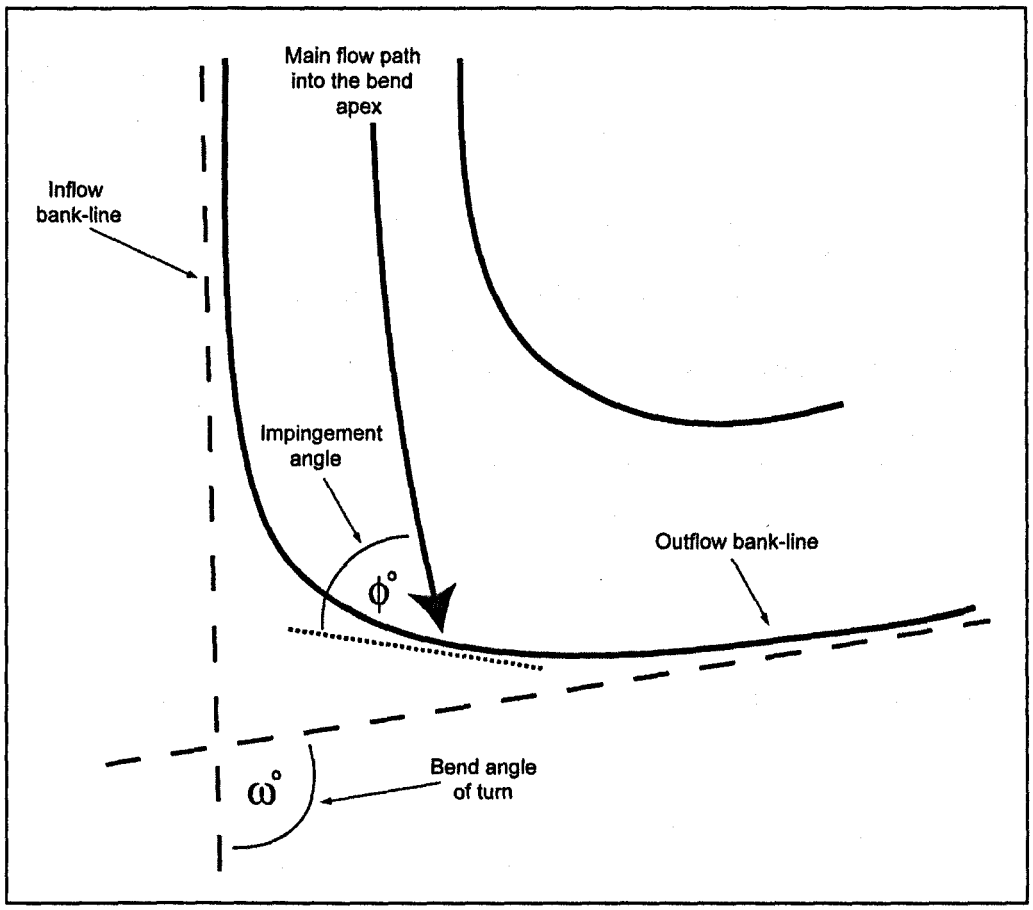

Figure 2.3: Definition sketch of bend angle of turn (ω) and flow impingement angle at outer bank (ϕ).

The survey was strictly a spatial sample and was only performed at normal, lower, flow stages. The survey does not explicitly examine the effect of stage on flow structure, but concentrates on the frequency of separation zones at normal flow and investigates those factors that lead to separation at this flow stage.

2.4 RESULTS

2.4.1 Frequency and size of separation

The proportion of bends exhibiting significant flow separation is summarised in Table 2.1 and illustrated in Figure 2.4. Almost half the bends along each river have a

significant zone of separation at one or both banks. Inner- and outer-bank separation are almost equally common overall, with frequencies of roughly 30%, but inner-bank separation is commoner than outer-bank separation along the Bollin and the reverse is true of the Dean. The difference between the rivers in this respect is not great in percentage terms, but is statistically significant because of the large sample sizes. Around 10% of bends in each river have separation zones on both sides.

Table 2.1: Frequencies of occurrence (%) of inner- and outer-bank flow separation in bends along the Rivers Bollin and Dean. Only separation zones wider than 1/8 of the apex banktop width are counted.

River	Number of bends	Percentage of bends with separation at stated bank					
		either	both	inner	outer	inner only	outer only
Bollin	224	50	9	35	24	26	14
Dean	411	48	13	28	33	16	20
combined	635	49	11	31	30	19	18

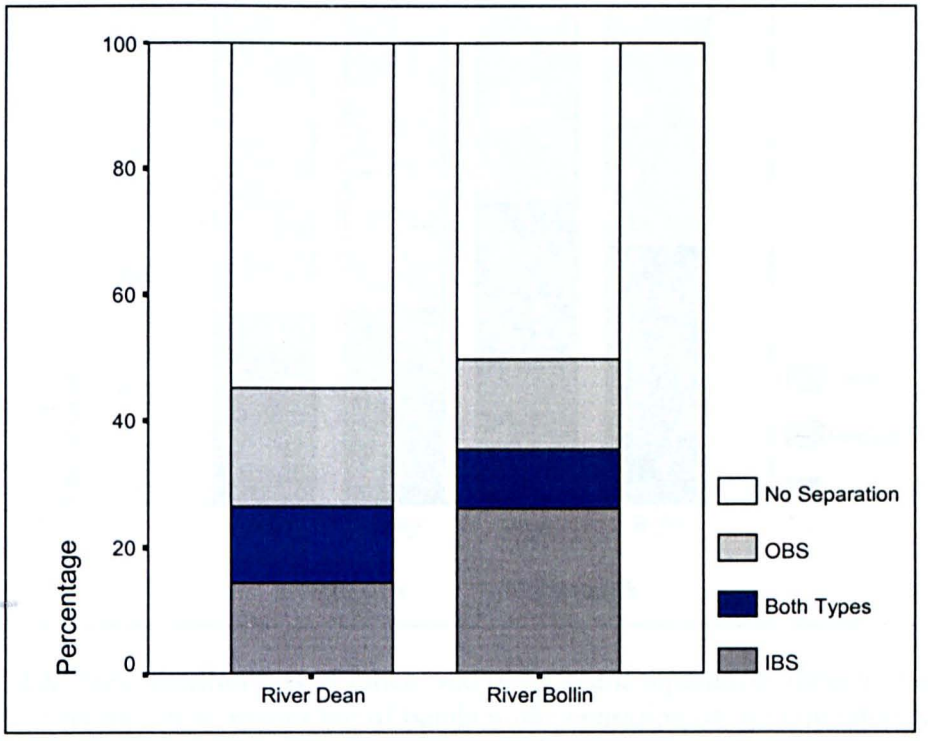

Figure 2.4: Frequency of flow separation at the inner and/or outer bank of bends along the study reaches. Separation is only counted if the zone of reverse flow extended more than one-eighth of the banktop width.

The size distributions of inner- and outer-bank separation zones are skewed for both types of separation and both rivers (Figure 2.5). Large separation zones (those extending over more than half the channel width) are relatively rare. For the River Dean, the decline in frequency with separation size is steeper for inner-bank separation than outer-bank separation. This results in a greater proportion of medium and large-scale outer-bank separations in contrast with the relatively smaller inner-bank separations. The overall trends of both inner-bank and outer-bank separation size frequency are similar in the River Bollin, but smaller separations were more common at the inner bank. This may reflect the intermediate to low flow at the time of the survey. At higher flows, shoaling over the point bar would perhaps wash out these smaller-scale inner-bank separation zones (Bridge and Jarvis, 1982; Dietrich and Smith, 1983).

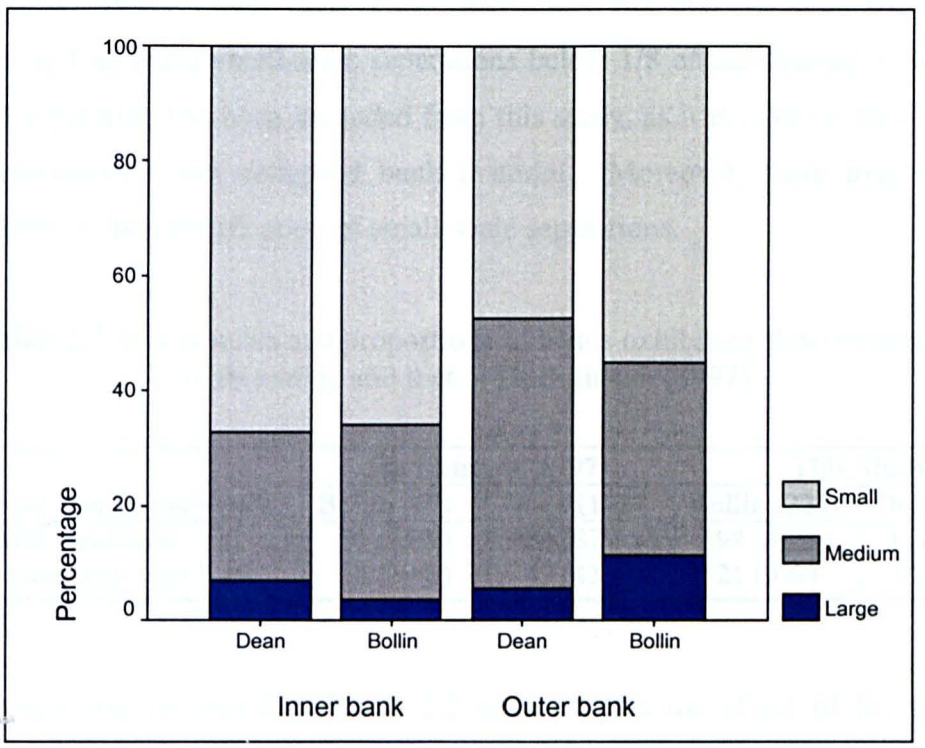

Figure 2.5: Size distributions of inner- and outer-bank separation zones in bends of the two rivers. Percentages are of bends with separation of the indicated type.

As mentioned above, this study builds upon a similar visual survey carried out by Hodskinson (1997) on reaches of four rivers. He recorded the frequency of a number of bend features, including the size and type of chutes and flow separation. The four rivers he investigated were the Rivers Bollin and Dean (67 and 102 bends), and the

Allt Dubhaig and River Truim (27 and 17 bends), two high gradient rivers in the Scottish Highlands. Hodskinson (1997) examined the differences between the occurrences of a range of bend features on each river. He found that although the Rivers Bollin and Dean exhibited similar flow features, there was a significant difference between the rivers in terms of the proportion of bends with regions of separated flow (Table 2.2). He also found greater differences between the two Cheshire Rivers and the two Highland rivers, the later exhibiting far less separation and multi-heading but many more chute cut-offs.

Hodskinson (1997) discovered that along the reaches he investigated, 75% of bends on the River Bollin and 87% of bends on the River Dean exhibited flow separation. He also found that along these two rivers the bends had reverse flow at the inner bank, outer bank and at both banks in proportions close to 1:1:2. The frequency of bends with separated flow in this present study is lower than that found by Hodskinson (1997) (Table 2.1, 2.2). However, his classification was slightly different and included small-scale separations below 1/8 of the channel width. This scale of separation has been excluded from this study, as it is likely to be caused by bank irregularities and collapsed bank material. Moreover, there may be more subjectivity in the identification of small-scale separations.

Table 2.2: Frequencies and proportions of bends exhibiting flow separation in this study and that of Hodskinson (1997).

	Hodskinson (1997)		This Study	
Rivers and number of bends	**Bollin (67)**	**Dean (102)**	**Bollin (224)**	**Dean (411)**
Bends with separation	50 (75%)	89 (87%)	**199 (45%)**	**111 (49%)**
At both inner and outer bank	20 (30%)	43 (43%)	**21 (9%)**	**52 (12%)**

The comparison presented in Table 2.2 demonstrates the effect of the sampling strategies employed in the two studies and the definition of 'significant' separation zone applied. Hodskinson also reports a much higher frequency of separation occurring at both banks simultaneously (Table 2.2). The existence of small-scale separation zones caused by irregularities at the opposite bank of a significant separation would be expected and can be explained. Large-scale flow separation at one bank reduces the effective channel width (*e.g.* Leeder and Bridges, 1975). This reduction results in the main filament of flow moving closer to the opposite bank.

Since the main flow is closer to the opposite bank, the velocity gradient in that region is higher, increasing the likelihood of small-scale flow separations at bank irregularities. This present study would not recognise these in the sample as they would be too small, but they would have been included by Hodskinson.

2.4.2 Relationship with angle of turn and impingement angle

As indicated above the bend angle of turn ω is a surrogate for mean curvature whereas the impingement angle ϕ is more influenced by upstream planform and local curvature at the apex. Thus, the two angles should not be strongly correlated, and Figure 2.6 confirms this.

Angles of turn range widely to a maximum of almost 180°, though the modal angle is less than 90°. Impingement angles do not generally exceed ω (although there are exceptions to this), nor do they exceed 90° in bends that turn through more than this angle. Otherwise, they are distributed fairly uniformly between 0° and these upper limits. When compared with bends that have separation, those with no separation generally have lower impingement angles and lower angles of turn (Figure 2.6). There is, however, no discernable difference between the inner and outer bank separation plots (Figure 2.6).

The average value of ω is higher for bends with flow separation at one or other bank (median ω >80°) than for bends without separation (median ω <60°), though there is considerable overlap in the distributions (Figure 2.7). In general ω increases with the size of the separation zone, though this trend is clearer for the Bollin than the Dean. Analysis of variance shows that the differences in each panel of Figure 2.7 are statistically significant at the 0.01 level, though post-hoc analysis between all individual variables discloses that most of the difference lies between the condition of no separation and separation of any size.

The equivalent plots of impingement angle by size of separation zone (Figure 2.8) also show a tendency for ϕ to increase with size of separation zone. These plots show even more scatter and overlap than in Figure 2.7, but the differences are again statistically significant.

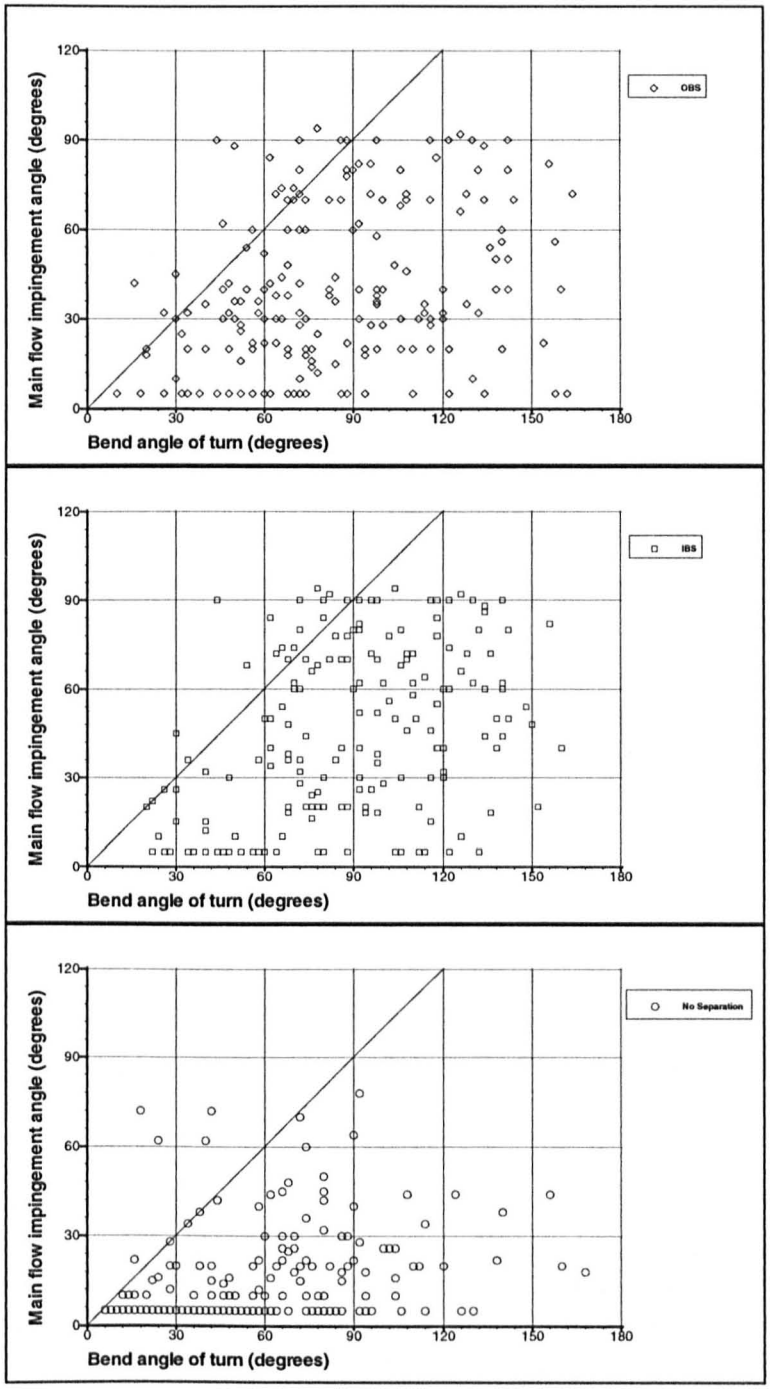

Figure 2.6: Scatter plots of impingement angle (ϕ) against angle of turn (ω) for all bends, plotted separately for outer bank separation (OBS), inner bank separation (IBS), and no separation. Reference lines are shown at 30°intervals for ω and ϕ, and where $\phi = \omega$.

2.4.3 Qualitative factors

Chi-square tests (Table 2.3) were initially performed to see if the presence or absence of flow separation is associated with any of the qualitative controlling factors recorded in the survey: presence and size of point bar, outer-bank strength, and

compound or multi-headed planform. Analysis for each factor was then carried out separately for inner and outer bank separation.

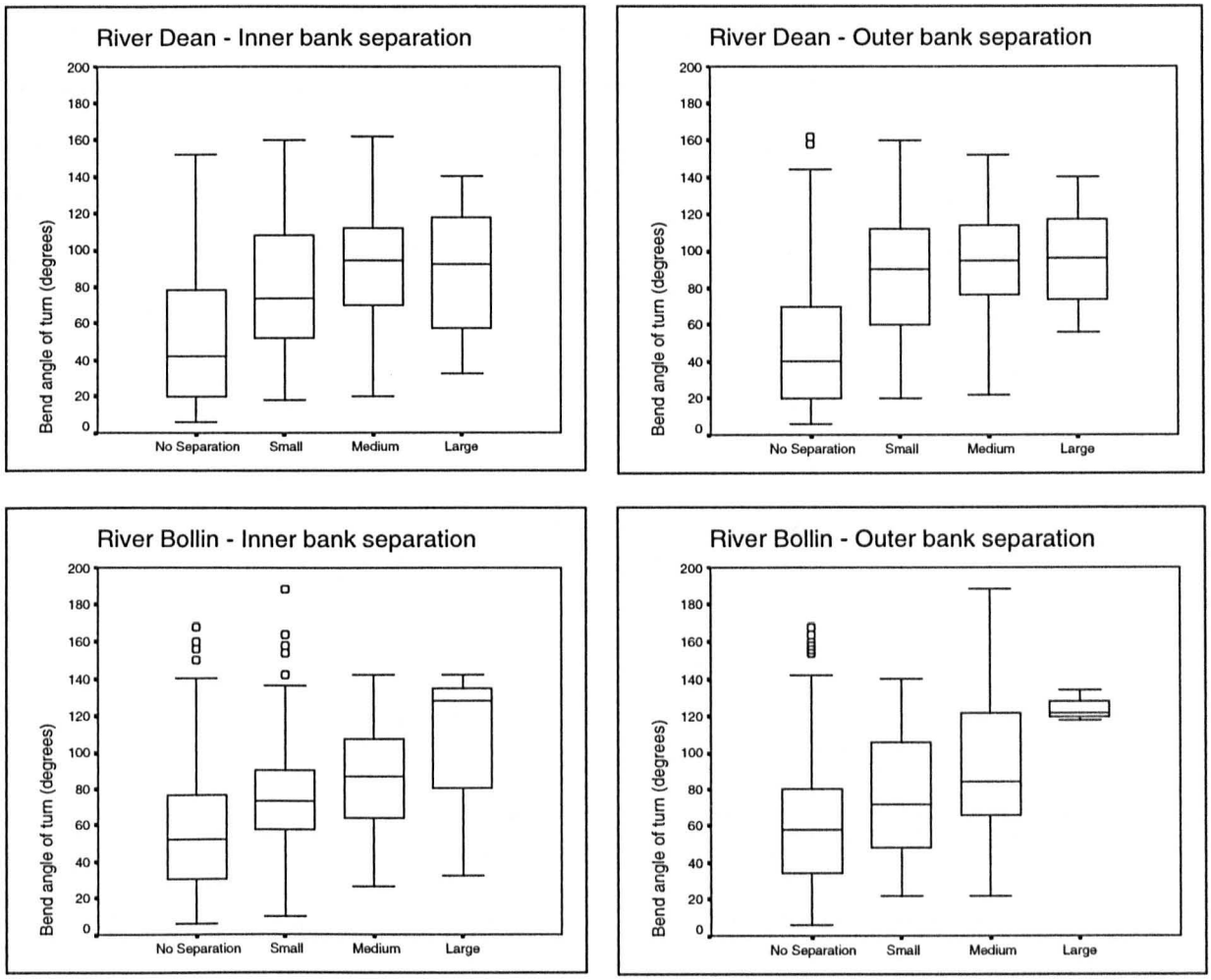

Figure 2.7: Box plots of angles of turn (ω) of bends with separation zones of different sizes, for the inner and outer bank cases on each of the two rivers. Each box is based on at least 25 bends except in the case of 'large' separations, for which the sample sizes range from 15 to 3.

Table 2.3: Chi-square *p*-values for the significance of association between qualitative channel properties and presence of separated flow.

Variable	River Dean			River Bollin		
	Inner	Outer	Either	Inner	Outer	Either
Point bar	0.000	0.317	0.000	0.000	0.773	0.000
Bank strength	0.115	0.000	0.000	0.118	0.019	0.010
Multi-heading	0.907	0.160	0.075	0.594	0.749	0.654

The association with point bar presence was significant for both rivers; flow separation is more likely where a point bar is present. The association between point-bar size and occurrence of separation was significant in the production of an inner bank separation, but was insignificant for outer bank separation (Table 2.3). Separation is also significantly more likely in bends with stronger outer banks (*i.e.* cut into a terrace and/or with tree roots), though when this analysis was done separately for inner- and outer-bank separation, the association with bank strength was only significant for outer-bank separation (Table 2.3). The presence or absence of separation was not associated to a significant degree with compound or multi-headed bends.

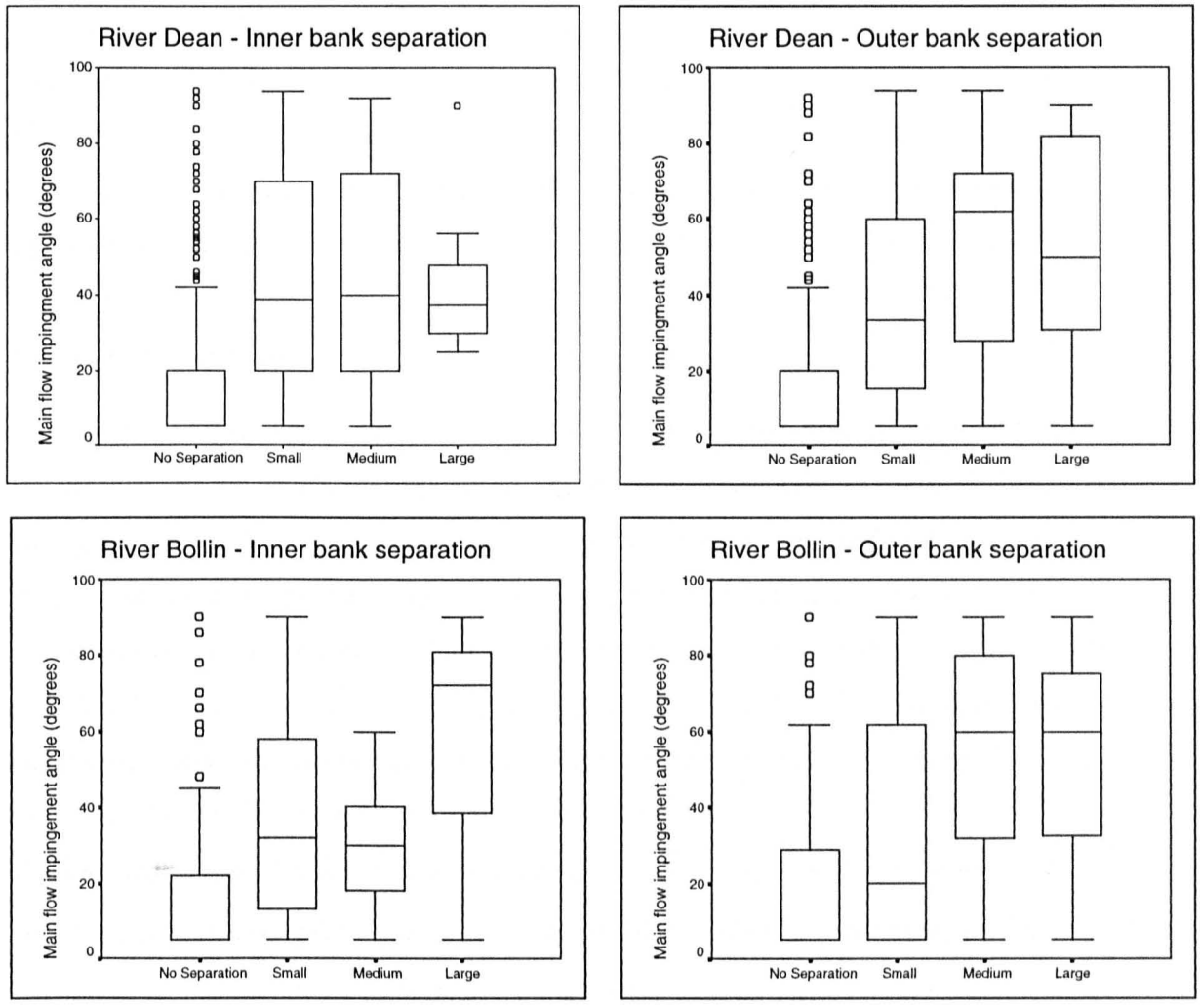

Figure 2.8: Box plots of impingement angles (ϕ) of bends with separation zones of different sizes for the inner and outer bank cases on each of the two rivers. Each box is based on at least 25 bends except in the case of 'large' separations, for which the sample sizes range from 15 to 3.

2.4.4 Predictive equations for occurrence of flow separation

The results summarised above indicate that most of the factors included in the survey are associated in some way with the occurrence, and in certain cases also size, of flow separation. However, the relative and combined effect of each variable is not shown by analyses of one factor at a time. Multivariate regression analyses were therefore performed to identify the interacting and combined effects of the factors and to obtain equations which predict the occurrence or size of inner- or outer-bank flow separation from simple bend properties.

If the interest is in predicting the occurrence of separation, the appropriate regression model uses the logit transformation $y = \ln (p/(1-p))$ where p is the probability of separation. The finite 0 to 1 range of p is thus mapped onto a symmetric infinite range of y, allowing the assumption of a normal distribution of errors around the regression. The independent variables are the five factors discussed above: bend angle of turn (ω), main flow impingement angle (ϕ), bank strength, occurrence/size of point bar, and multi-heading. The model was fitted by the method of maximum likelihood, in a forward stepwise procedure. Separate analyses were done initially for the two rivers, and for inner- and outer-bank separation.

In the River Dean, significant independent variables in the prediction of separation occurrence are, in order of importance, ϕ, ω, and outer-bank strength (Table 2.4). Multi-heading and point-bar existence/size were insignificant predictors (at the 0.05 level) and were excluded from the final model. All the independent factors are positively related to the production of separation. The regression model accurately predicts 83% of all cases, correctly forecasting 75% and 88% of separation zone occurrences and non-occurrences respectively. However, the variance explained by the independent variables is relatively low (pseudo $R^2 = 0.31$). In the River Bollin dataset, significant predictors are, in order of importance, ϕ, point-bar existence/size, outer-bank strength, and ω (Table 2.4). Multi-heading was an insignificant factor in the analysis. Once again, each of the independent factors is positively related to the production of separation. The regression model predicts 75% of all cases correctly, accurately forecasting 72% and 79% of separated flow occurrence and non-occurrence respectively. However, the variance explained in the dummy dependent variable is again generally low (pseudo $R^2 = 0.40$). Thus, the main factors favouring

separation in bends of the River Dean are high ϕ, ω, and outer-bank strength. Although ϕ remains highly significant in the River Bollin, bank strength and point-bar existence/size are more influential than ω.

Table 2.4: Summary of results of logit regression analysis to predict the presence (1) or absence (0) of flow separation at the inner bank, outer bank, or either bank in the two study rivers. Coefficients shown are log odds for continuous variables (impingement angle and angle of turn) and odds for the categorical variables. Significance levels are indicated by * ($p < 0.05$), ** ($p < 0.001$), or ns (not selected for final model using forward stepwise procedure with cut-off set at $p = 0.05$). Sample sizes are 224 for the Bollin and 411 for the Dean.

Predictor	River Dean			River Bollin		
	Inner	Outer	Either	Inner	Outer	Either
Impingement angle	0.0310**	0.0331**	0.6302**	0.0184*	0.0394**	0.0481**
Angle of turn	0.0132**	0.0204**	0.0248**	0.0100*	ns	0.009*
Bank strength (vs. weak)	-	-	-	-	-	-
medium	ns	1.680**	1.532	ns	ns	2.693*
strong	ns	4.255**	3.699**	ns	ns	3.723**
Point bar (vs. none)	-	-	-	-	-	-
small	2.964*	ns	ns	5.775**	ns	5.185**
medium	2.878	ns	ns	2.094	ns	1.631
large	2.000	ns	ns	1.796	ns	1.945
Multi-heading (vs. none)	-	-	-	-	-	-
multi-headed	ns	ns	ns	ns	ns	ns
Constant	-3.053	-3.570	-3.386	-2.354	-2.313	-0.867
% Predicted correctly:						
- Absence of separation	90	90	88	83	94	79
- Presence of separation	46	63	75	43	43	72
- Overall	79	82	83	69	82	75

Prediction of the size of separation strictly requires multinomial regression, which uses an extension of the logit-transformation principle. In the present application, this gave very similar results to a conventional ordinary-least-squares multiple regression; results from the latter are shown (Table 2.5). The occurrence and size of inner-bank separation in both rivers is positively influenced by ω, ϕ, and point-bar size in decreasing order of importance. However, the proportion of variance explained by this regression model is small in both rivers (Table 2.5). The occurrence and size of outer-bank separation is related to ϕ, outer-bank strength, and ω (in decreasing order of importance) for the Dean, and ϕ and outer-bank strength for the Bollin. Once more, all factors are positively related to the occurrence/size of

flow separation zone but only a small proportion of total variance is explained by the predictors.

Table 2.5: Best-fit coefficients in linear regression analyses to predict the size (0 to 3 for none, small, medium, large) of inner- and outer-bank separation zones in the two rivers. Significance of predictors is indicated by * ($p < 0.05$) ** ($p < 0.001$), or ns (not selected for final model using forward stepwise procedure with $p = 0.05$). Sample sizes are 224 for the Bollin and 411 for Dean.

Predictor	River Dean		River Bollin	
	Inner	Outer	Inner	Outer
Constant	-0.016	-0.116	0.017	-0.076
Angle of turn	0.0007**	0.0011**	0.0008*	ns
Impingement angle	0.0022**	0.0031**	0.0012*	0.0033**
Point-bar size	0.1762*	ns	0.0923*	ns
Bank strength	ns	0.0557**	ns	0.0462*
Multi-heading	ns	ns	ns	ns
R^2	0.23	0.36	0.11	0.25

In summary, for both rivers, the factors that seem to influence the occurrence and size of inner bank separation zone are increases in ω, ϕ, and point-bar prevalence and size. Factors that seem to influence the occurrence and size of outer-bank separation zone are increases in ϕ, outer-bank strength, and ω.

2.5 DISCUSSION

The angle of turn of a bend is a significant predictor in all but one of the regression models discussed above and was significant in both t-tests and analysis of variance tests. It is found to influence separation at both the inner and outer bank, although it is more significant in the production of inner-bank separation. A possible physical explanation for this finding stems from the superelevation of flow around a bend and the consequent occurrence of a zone of lower pressure at the inner bank, which is more likely to develop a zone of separated flow (Rozovskii, 1957). More generally, the potential for either type of flow separation would be expected to increase in bends with high angles of turn to the extent that these indicate high relative curvature (low R_c/w): the flow through the bend is less likely to be able to adjust its momentum to the imposed channel geometry. Both Leeder and Bridges (1975) and Rozovskii

(1957) found that bend tightness has a significant effect on the occurrence and size of inner bank flow separation: the tighter the bend the more probable the presence of separated flow. Other studies have linked outer-bank separation with bend curvature (Hickin and Nanson, 1975; Hickin, 1986).

The impingement angle ϕ of the fastest current on the outer bank also proves to be a significant factor in the generation of both types of flow separation, even when angle of turn is also in the regression model (Tables 2.4 and 2.5). It is consistently the most significant factor in explaining the occurrence of outer-bank separation. A possible physical explanation for this lies in the high dynamic pressure produced at the outer bank in a bend with high ϕ. This may force some of the flow upstream along the outer bank, possibly forming an embayment (Markham and Thorne, 1992). Although ϕ is most significant in relation to outer-bank separation, it is also the second most important factor in the regression models for inner-bank separation. The physical explanation here is that high outer-bank ϕ usually implies a strong cross-stream flow component and a high deviation angle between the main flow and the alignment of the inner bank at or just upstream of the apex. The more strongly the core filament of flow departs from the inner bank here, the more likely it is that flow separation will occur just downstream (Bagnold, 1960). Thus, the outer-bank flow impingement angle is not only directly relevant to separation at this bank, but also a proxy for conditions favouring inner-bank flow separation. Its significance in the analysis also indicates how important the nature of flow inheritance from upstream can be (*e.g.* Furbish, 1988).

The second most important factor in the regression analyses for predicting occurrence or size of outer-bank flow separation is the ordinal index of outer-bank strength. The important factors known to control river channel pattern are the bank strength in relation to the stream power, and the supply and transport of sediment from upstream, the bed and banks of the river. The balance of these factors and the resulting continuum of channel patterns have been examined and discussed extensively (*e.g.* Ferguson, 1987). Active meandering occurs where banks are sufficiently erodible to allow migration but not unconstrained widening, and the sediment input from upstream equals the output. In these active meandering reaches, local areas of increased bank strength, such as dense vegetation roots (especially trees), clay plugs (Fisk, 1944; Gagliano and Howard, 1983) and valley terraces

(Lewin and Brindle, 1977) frequently arise. If the present flow regime is ineffectual in eroding these features, confinement of individual bends can occur, resulting in distorted meanders, sharp bends, and the development and then maintenance of flow separation zones. It can thus be argued that actively meandering reaches, with irregular meanders, and the development and maintenance of separation zones are part of the continuum of river channel patterns (*e.g.* Ferguson, 1987).

The presence of multi-headed and compound meander planforms, where two zones of high curvature can develop in one bend (*see* Hooke and Harvey, 1983), was not found to be significant in predicting any type of flow separation. Multi-headed bends often occur where a migrating bend encounters a resistant floodplain feature such as a valley terrace (Lewin and Brindle, 1977), and this can lead to increased curvature and flow separation (Reid, 1984). However, in the present analysis such situations would involve high values of one, two or all three of impingement angle, angle of turn, and outer-bank strength so that multi-heading would not be independently significant. Moreover, two or more zones of increased curvature can occur without the formation of sharp bends (Hooke and Harvey, 1983).

The existence and size of any emergent point bar was found to be the third most significant factor in the production of inner-bank separation in both rivers. This probably relates again to the extent to which flow near the inner bank deviates from being parallel with the bank top and instead crosses towards the outer bank. An exposed point bar steers the entire flow towards the outer bank, creating a zone of low dynamic pressure in the flow expansion round the lee of the bar. The same is true, to at least some extent, for the submerged part of a point bar that again causes reduced pressure in its lee (Ippen and Drinker 1962). Whether the results would have been appreciably different had the survey been made at high stage is unclear. Dietrich and Smith (1983) and Dietrich (1987) argued that even in bankfull conditions, the topographic steering of the flow induced by the shoaling from upstream pool onto submerged point bar is generally sufficient that flow is outwardly directed through the flow depth across the inner bank region; this would seem to leave scope for lee separation to persist. However, this probably depends on the transverse angle of the bar surface: flat-topped bars with distal avalanche faces might retain lee eddies when steeper bars lose them.

Several authors have noted changes in the occurrence and extent of flow separation zones according to flow stage. For example, Bridge and Jarvis (1982) found that inner-bank separation in steep-sided intertidal creeks was transient and only occurred at a range of intermediate flows. Its disappearance at high tide is consistent with a reduction in topographic steering as just discussed. The likelihood of separation at lower tides is diminished as the main flow velocity is lower and the curvature of the bend can be reduced due to a greater decrease in width than in bend radius with stage. Markham and Thorne (1992) reported that outer-bank separation occurred at bankfull stage in a bend on the River Roding, but not at lower discharges. They identified alteration in the impingement angle as the likely explanation. As stage and velocity increase, the main flow encounters the bank at a higher angle, resulting in a greater portion of the incoming flow being forced to flow upstream. However, Andrle (1994) found that this was not the case with outer-bank reverse flow in Mansfield Creek, which was found to be persistent at all flow levels. The reconnaissance survey presented here was only carried out once, at intermediate to low flow, so conclusions cannot be drawn on the influence of stage on occurrence of flow separation. However, in one reach that was visited several times during the study period the main separation zones were still present and of a similar size at lower and moderately high flows. Section (6.2) details numerical flow modelling were the influence of flow stage on flow structures in case-study and idealized bends with separated flows is examined.

Although several of the predictors used in the regression models were highly significant, the variance that they collectively explained was generally low. This shows, not surprisingly, that the circumstances responsible for the occurrence of separated flow were not fully captured by the selection of simple observations that could be made from alongside the river. One obvious limitation is that bends with the same total angle of turn could have different mean dimensionless curvature R/W according to bend length and channel width. In any case, mean R/W is probably less relevant than maximum curvature, and this may need to be considered separately for each bank. Another limitation is the restriction to aspects of planform morphology, without consideration of pool depth, width/depth ratio, or point-bar slope, which would have required detailed within-channel surveying. The nature of the velocity field at the entrance to each bend is known to be relevant (Rozovskii, 1957;

Hodskinson and Ferguson, 1998) but was not measured except insofar as it is reflected in the impingement-angle measurement. Finally, the occurrence and size of flow separation probably depends to some extent on flow stage. For these reasons high R^2 values were not expected and it is somewhat surprising that the percentage of cases correctly predicted by the regression models is so high.

The process responsible for the evolution and formation of flow separation zones has been discussed by several workers. Markham and Thorne (1992) attempt a description of the evolutionary processes behind the formation of flow separation, whereby outer bank separation is created through the positive feedback between the impingement angle at the outer bank and the formation of an embayment. Reid (1984) describes the stalling of a meander loop against a resistant feature and the formation of a separation zone through a decrease in bend radius resulting in concave bank bench formation through deposition, followed by further migration, and the disappearance of the feature. Andrle (1994) discusses the formation of a large-scale outer bank separation zone and its abandonment through erosion across the inner bank over a period of a few months. Nevertheless, others (*e.g.* Page and Nanson, 1982; Hickin, 1986) have argued for the long-standing endurance of such features and that over long periods of time they contribute to the formation of large areas of the floodplain. Accounting for the differences in the sampling methodologies, the results obtained by Hodskinson (1997) and this study would suggest little change on the two rivers during the five years between the surveys. Nevertheless, it is expected that over such a large number of bends, any change in one bend's evolution would be cancelled out by changes in another and individual bends may have changed considerably during this period. Further research is required into the long-term development of bends with separated flow.

Each individual river reach reflects its own response to the overall regional characteristics, the imposed flow regime, sediment delivery, and resultant transport. The results of Hodskinson (1997) from two very different fluvial environments, suggest significant differences between the frequencies of bends exhibiting separated flow. Therefore, the results presented in this chapter are only applicable to relatively small lowland rivers similar to the two rivers examined. Nevertheless, the proportions of bends exhibiting separation zones in this visual survey and reported elsewhere in the literature indicate that these features are widespread and warrant

further, more detailed investigations of which processes seem to influence the generation and occurrence of flow separation.

There is also the obvious question of whether the predictors measured in the visual survey can properly be regarded as causes of separated flow, or rather as symptoms of its effects. Is the generally high angle of turn in bends with separated flow a result of the separation, rather than separation being forced by the angle? Does the impingement angle govern the volume of water forced upstream and thus the size of the separation zone, or does the area of separated flow determine the angle of main flow impingement? Is the size, and/or existence, of a point bar the result of deposition in an inner-bank separation zone, rather than the cause of the separation? These questions demonstrate the need for detailed process-response studies in these complicated bends, including comprehensive measurements of flow structure, shear stress distribution, and sediment pathways.

2.6 CHAPTER CONCLUSION

This chapter has demonstrated that flow separation is widespread in the two small lowland rivers investigated, with almost half of all bends exhibiting separation at one or both banks. In both rivers, the factors that seem to influence the occurrence and size of inner-bank separation zones are increases in bend angle of turn, main flow impingement angle and point-bar existence and size. Factors that seem to influence the occurrence and size of outer-bank separation are increases in main flow impingement angle, outer-bank strength, and bend angle of turn. Thus, there appear to be both commonalities and differences between inner-bank separation in an otherwise 'classical' bend, and outer-bank separation with an associated concave-bank bench.

Although the factors investigated are statistically significant, they only explain low amounts of variance, highlighting their inadequacy in the detail required for a full understanding of flow separation in bends. Moreover, several questions of cause-and-effect and possible stage dependence have been identified. Clearly, more detailed study of bends is required that includes factors such as width-depth ratio, rate of change of bend curvature, velocity distribution, and discharge. The next

chapter details a more intensive field study, where some of these factors are included in the measurement programme of 22 individual bends.

Chapter 3
Mid-Level Field Study

3.1 INTRODUCTION

The previous chapter used an extensive reconnaissance survey, to confirm that flow separation is common to meander bends in the two rivers investigated, and that broad controls on the frequency of inner and outer bank separation could be identified. However, although visually measured controls were significant in prediction of separation, the amount of explained variance was relatively low. This is perhaps not surprising given the simplistic approach required for an extensive survey. This chapter develops the reconnaissance survey by concentrating on more detailed field investigations in fewer bends. This more detailed approach includes topographic survey and flow measurements, permitting a more process-based analysis of the factors governing the presence of flow separation.

Initially, the methods applied in the field (3.2.1) and to analyse the data (3.2.2) are outlined. Results obtained are presented (3.3) in terms of the effect of topography (3.3.1) and flow field (3.3.2) on the occurrence of separation. Section 3.4 draws the results into a general discussion of the factors contributing to the formation of separation zones. The chapter ends with a summary (3.5) of the findings of this aspect of the research.

3.2 METHODS

3.2.1 Field methods

Topographic surveys and velocity measurements were taken in 22 of bends identified during the reconnaissance survey (2.2). A range of bends was chosen for analysis: 6 with inner-bank only, 2 with outer-bank only, 6 with no flow separation and 8 with both separation at both banks (Table 3.1). All bends studied for this aspect of enquiry were on reaches of the River Dean.

Table 3.1: Numbers of bends with inner- and outer-bank flow separation in the mid level study.

Number of bends	Number of bends with separation at						
	either bank	*both banks*	*inner bank*	*outer bank*	*inner only*	*outer only*	*no separation*
22	16	8	14	10	6	2	6

At each selected bend, a series of features were surveyed using a total station. Initially, both banklines were surveyed with an average 1 m spacing through the bends, with concentrations of points in areas of high bank curvature. Banklines were surveyed from crossover to crossover through the bend, providing data on the planform within which each bend was set. Through each bend a series of five cross sections were also surveyed. Sections were placed at the bend inflow, bend apex, and bend outflow, with the other two sections positioned between these (Figure 3.1). The arbitrariness in the placement of cross sections was minimised by positioning the apex section across the point of lowest radius at both banks, the bend inflow section across the riffle head before any bend curvature, and the outflow section after the bend curvature had reduced into the next riffle. Across each section, features such as bank top, water's edge and breaks in slope were surveyed and noted. The topographic survey thus provided information on the geometric properties of each bend for further analysis.

Figure 3.1: Photograph of methods used in surveying the channel cross sections with tapes placed across the channel.

At each of the five cross sections through the bend, low-density flow measurements were made using an Ott Current Meter (OCM). The OCM had a 30 mm propeller attached to a top-setting wading rod arrangement. Velocity was sampled for two minutes at each point, with the propeller aligned and oriented into the main flow direction. The position and alignment of the propeller in each section were estimated using a measuring tape placed across each section and taking compass bearings along both the section and along the flow direction as indicated by a flow streamer extending from the rear of the propeller (Figure 3.2). Measurements were taken at three positions across each section and at, 20, 40, and 80% of the flow depth in each vertical.

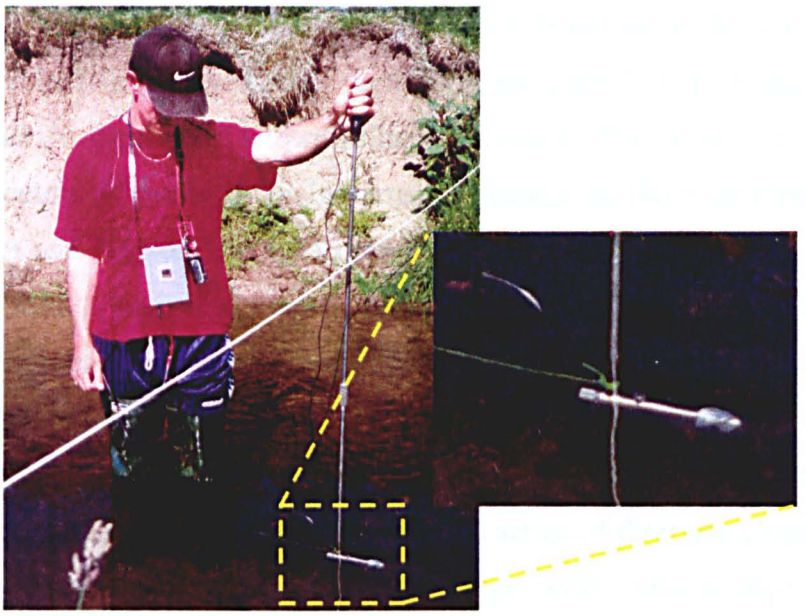

Figure 3.2: Photograph of methods applied using the Ott current meter to obtain low-density flow measurements.

If a separation zone was present within the bend at the flow stage investigated, the surface area of this zone was surveyed with the total station, using surface floats to define the extent of the zone where necessary.

3.2.2 Field data manipulation

As the reconnaissance survey suggested that there was a significant difference between bends with inner- and outer-bank separation, the study bends were divided into four classes: no separation, inner bank only, both (where outer bank size usually dominated) and outer bank only (Table 3.1).

The area of surface separated flow was determined by combining the bankline and separation zone surveys into a continuous series and calculating the area of the polygon formed. The area of separated flow was determined for each separation zone and this was normalised for each bend by dividing by the total water area from cross section 1 to 5.

An average radius of curvature (R_c) was calculated for each bend using both bankline surveys. The bankline distance (s) and the angle (θ) through which each bankline turned from the inflow section to the outflow section were calculated. As R_c is the inverse of channel curvature (θ/s), the average curvatures of both banks were used to provide an approximate channel centreline radius of curvature (*e.g.* Hickin, 1974). This radius of curvature was normalised for each bend using the average channel width (w) of the five surveyed cross sections of each bend. This produced the non-dimensional R_c/w parameter, known as bend curvature (B_c). However, although the overall curvature of bends is an important influence on flow structure (Bagnold, 1960; Hickin and Nanson, 1975; Furbish, 1988), it varies continuously in all bends that do not form a perfect arc of a circle (Figure 3.3). Indeed, individual breaks, peaks, or increases in curvature along either bank may be more important in forming separation zones. Thus, each bankline survey was transformed into a direction change series (Figure 3.3). This involves calculating the angle of turn per unit distance between each survey point, producing a series of direction change $\Delta\theta/\Delta s$ for each bank. Thus, peaks in the direction change series indicate rapid changes in bankline direction. As outer banks are longer than inner banks, bankline curvature series are plotted together against percentage bank distance. The maximum direction change for the inner (β_i) and outer (β_o) bank series of each bend was thus investigated as a possible cause of separation, especially in bends with low average curvature, where separation would not be expected.

The variations of width and depth through a bend have been suggested as significant controls on flow structures present within bends (*e.g.* Markham and Thorne, 1992). The bend average width-depth ratio (R_{wd}) was determined using the average of each of the five surveyed cross sections. The variability of width and depth through each bend was also calculated. A bend width ratio (R_w) was defined as the apex bend width divided by the bend inflow width and a bend depth ratio (R_d) was determined as the maximum pool scour depth at the apex divided by the mean inflow depth at

the upstream riffle. These two non-dimensional ratios thus provided indications of the degree to which the channel expands and the pool deepens into the apex of each bend. The gradient of the bed (B_g) from the riffle to the pool was also determined using the maximum channel depths at the inflow and apex, and calculating the angle of the slope.

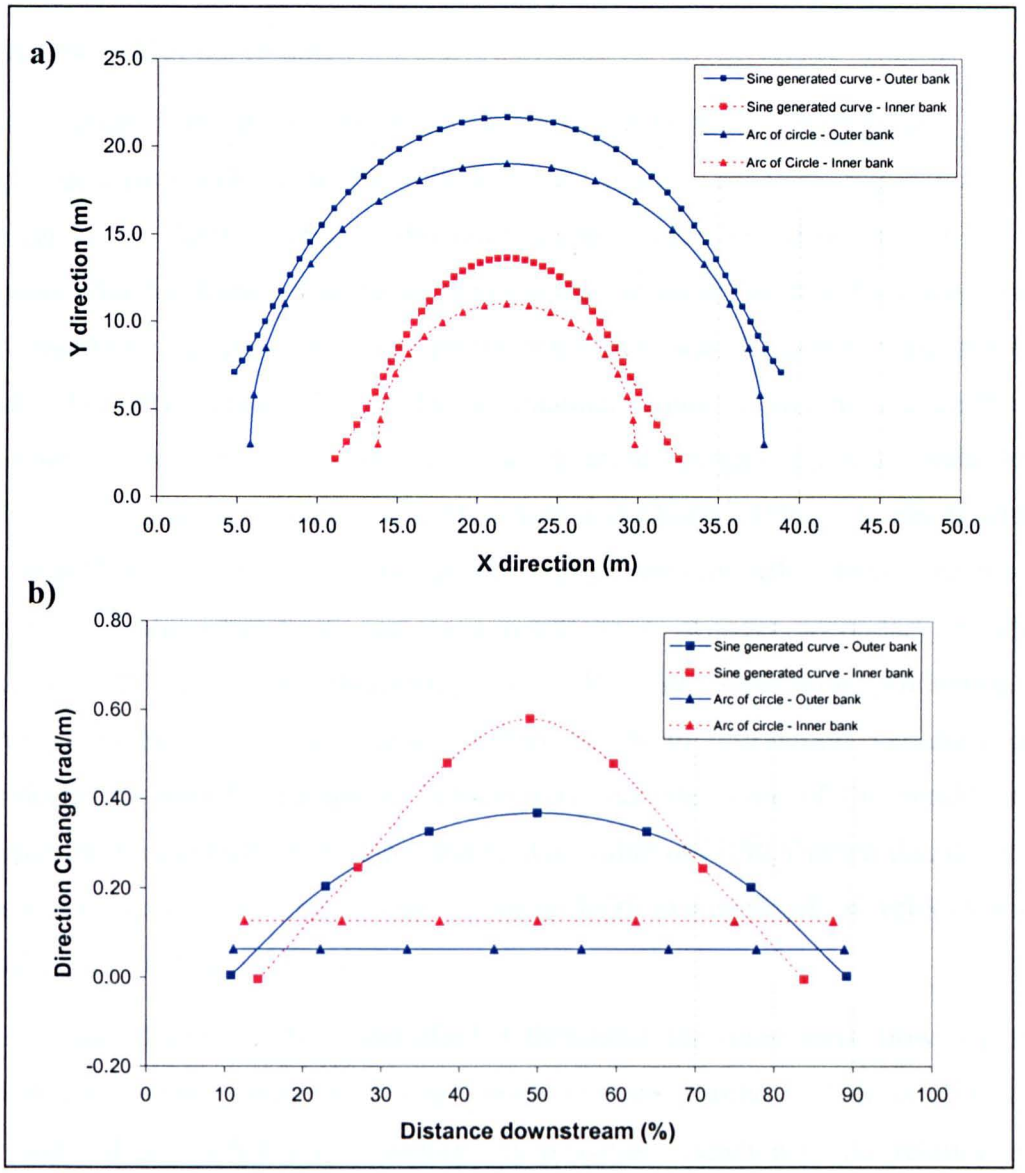

Figure 3.3: Idealised meander bends: planform traces (a) and curvature direction change series (b) to show streamwise variation of curvature in bends that are not arcs

Hodskinson and Ferguson (1998) showed that the inflow velocity distribution as controlled by upstream planform could have a significant effect on the flow structure within bends. The degree of flow asymmetry (ζ_{as}) at the bend inflow cross section was determined using a simple velocity index. The average velocity through each

half of the channel width was calculated and a percentage deviation between the two half's of the cross section was calculated. Thus, an index value of zero would imply that the flow is symmetrical and evenly distributed across the inflow reach. A negative value would mean that more flow is through the inner-bank section while a positive value would indicate that more flow is distributed towards the outer-bank section. An absolute index value of 100 would imply that velocity was twice as high in the one half of the channel.

The direction of the main core of inflow velocity was also determined as a deviation angle (φ_{in}) from normal to the inflow cross-section. As this section was placed normal to the channel banks, a deviation angle of zero would imply that flow was parallel with the banks; a negative deviation angle indicated that flow was towards the inner-bank and positive values implied that flow was directed towards the outer-bank. Velocity squared divided by the channel radius (U^2/R_c) is a hydrodynamic variable is a measure of the centrifugal acceleration strength and is the main driving force in secondary circulation (*e.g.* Markham and Thorne, 1992). In bends with the classical flow structure, tighter bends with higher velocity inflow have greater super-elevation at the outer-bank and as a result have stronger secondary circulation (Dietrich, 1987). The relationship of U^2/R_c with separation production was investigated as it combined flow (inertia) and form (curvature) variables into a physically meaningful parameter, which may indicate some of the conditions for separation, particularly at the inner bank. The value of U^2/R_c (herein denoted as ψ_{ur}) was calculated for each bend using the mean depth averaged inflow velocity and the bend average radius of curvature.

Leeder and Bridges (1975) identified a threshold for inner-bank flow separation based upon bend curvature (B_c) and local Froude number. This relationship is investigated for each bend, including any possible extension of the relationship to include bends exhibiting regions of outerbank flow separation.

3.3 RESULTS

3.3.1 Separation zone distribution

The distributions and sizes of separation zones at the inner and outer banks of the mid-level study bends are presented in Figure 3.4. As mentioned above a sample of

bends from the reconnaissance survey were chosen on an individual basis to provide a range of bend features including bends with no separation, separation at the inner-bank only, outer-bank only and separation at both banks. As the sampling procedure was in no way random or systematic, actual percentages of bends with given features are meaningless and the results discussed below focus on differences between bends to elucidate some of the processes controlling the production of separation.

As indicated by the reconnaissance survey (2.4), outer-bank separation zones are generally much larger than inner-bank separations. When outer-bank separation is present, a smaller inner-bank separation zone is generally present and the total area of flow separation within the bend is typically above 25% of the bend area (Figure 3.4). In some bends, the percentage area of total separation can be as high as 50%, with over 40% of the bend area occupied by an outer-bank separation cell. Inner-bank separations are generally smaller in terms of bend area, generally below 20% of the bend area and occur frequently without the presence of outer-bank separation.

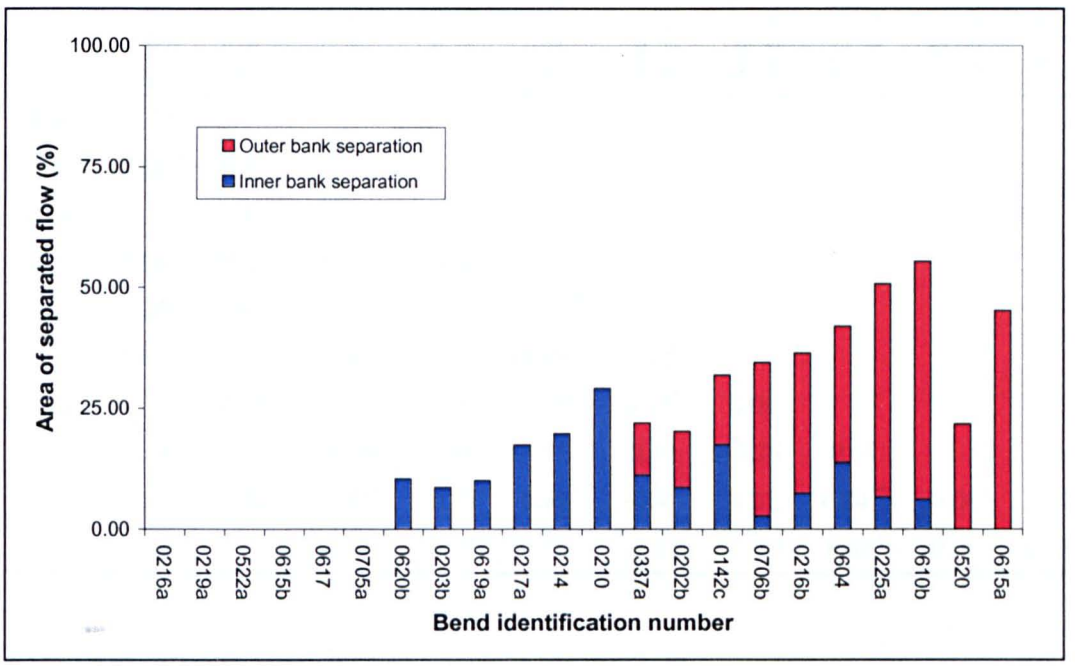

Figure 3.4: Distribution of separation zone size in the mid level study bends. Bend identification number refers to the reconnaissance survey cataloguing.

3.3.2 Parameter covariance

Many of the factors controlling the presence of flow separation are likely to co-vary between individual bends and between bends with separation and those without.

Therefore, initial investigations concerned analysis of the correlations between each parameter obtained from the field measurements (Table 3.2).

Significant negative correlations exist between the bend curvature (B_c) and depth ratio (R_d) (Figure 3.5), bed gradient (B_g), U^2/R_c (ψ_{ur}), and maximum direction changes at the inner (β_i) and outer (β_o) banks. Therefore, bends with high curvatures tend to be deeper, have higher riffle pool gradients, and have larger maximum direction changes per unit length at both banks.

Table 3.2: Correlation matrix for parameters investigated. Significant correlations are highlighted in bold and significance levels are indicated by *($p<0.05$) and **($p<0.01$).

	Bend Rc/w (B_c)	Width ratio (Rw)	Depth ratio (Rd)	Average width/depth ratio (Rwd)	Bed gradient (B_g)	Max outer bank direction change (β_o)	Max inner bank direction change (β_i)	Max depth averaged velocity (U_{in})	Inflow velocity direction (φ_{in})	Depth averaged U^2/R_c (ψ_{ur})
Rw	-0.39									
Rd	**-0.64****	**0.47***								
Rwd	-0.03	0.09	0.15							
B_g	**-0.56****	**0.56****	**0.61****	-0.06						
β_o	**-0.45***	**0.67****	0.39	0.09	**0.63****					
β_i	**-0.62****	0.24	**0.76****	-0.09	**0.58****	0.25				
U_{in}	-0.21	**0.47***	0.27	-0.01	0.30	**0.45***	0.08			
φ_{in}	0.14	-0.25	-0.08	0.04	-0.02	0.10	-0.28	0.07		
ψ_{ur}	**-0.52***	**0.42***	**0.43***	-0.21	**0.43***	**0.44***	0.27	**0.84****	0.04	
ζ_{as}	-0.04	0.18	-0.10	-0.02	0.01	-0.01	-0.20	**0.48***	0.07	**0.55****

The width ratio (R_w) is positively correlated with the depth ratio (R_d), the bed gradient (B_g), the ψ_{ur}, the maximum outer-bank direction change (β_o), and the maximum depth averaged inflow velocity (U_{in}). As R_w increases, the expansion of the channel at the apex becomes greater with respect to the inflow cross section. Thus, as bends become relatively wider at the apex, the gradient between the riffle and the pool generally increases, the pool shows a tendency to deepen, and the rate of change in direction of the outer bank increases.

As well as B_c and R_w, the depth ratio (R_d) is significantly correlated with increases in both B_g, and β_i. Interestingly, B_g is also significantly correlated with both β_i and β_o. Thus, bends with deeper pools tend to have larger bed gradients and generally have more rapid changes of bankline direction along both banks.

Maximum depth averaged inflow velocity (U_{in}) is significantly correlated with β_o, R_w, inflow asymmetry (ζ_{as}), and with the ψ_{ur} parameter. Indeed, ψ_{ur} is significantly correlated with the majority of other variables, reflecting the fact that it incorporates both flow and form variables. However, the relationships do contain significant amounts of variance (R^2 ~0.2). The average bend width-depth ratio (R_{wd}) and the deviation angle of inflow velocity (ϕ_{in}) are not significantly correlated with any other variables examined.

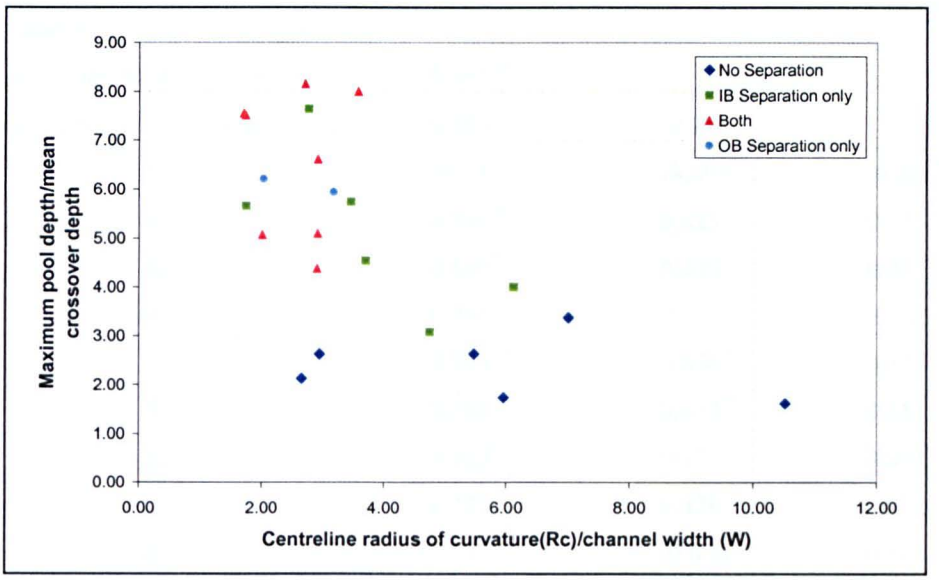

Figure 3.5: Relationship between bend curvature B_c and depth ratio Rd

The analysis presented above indicates that many of the factors investigated are related, at least weakly, to each other. However, the directions of cause-effect are difficult to discern. Moreover, as combined variations in each occur between bends and the variation of single parameters between bends is most unlikely, isolating the effect of one variable on the occurrence of flow separation is difficult. Thus, any interpretations drawn on the effect of individual variables on the occurrence of flow separation should consider the influence of other variables that are covariant with the specific variable under investigation.

3.3.3 Factors influencing separation: geometrical

The relationship of each variable obtained from the field measurements to the presence, position, and size of separation zones was examined. Initially, this involved examining the correlations of each variable with the percentage areas of separation in each bend (Table 3.3). Analysis then progresses to examine variables with significant relationships in more detail.

Table 3.3: Correlation coefficients for each variable against area of separated flow in the study bends. Significant correlations are highlighted in bold and significance levels are indicated by *($p<0.05$) and **($p<0.01$).

	Total area of separated flow	Area of outer bank separated flow	Area of inner bank separated flow
Total area of separated flow			
Area of outer bank separated flow	**0.897****		
Area of inner bank separated flow	**0.454***	-0.151	
B_c	**-0.533***	**-0.492***	**-0.446***
R_w	**0.805****	**0.829****	0.013
R_d	**0.607****	**0.488***	**0.457***
R_{wd}	0.204	0.263	-0.112
B_g	**0.793****	**0.656****	0.358
β_o	**0.880****	**0.675****	**0.511***
β_i	**0.423***	0.191	**0.491***
U_{in}	**0.427***	**0.428***	0.031
φ_{in}	0.018	-0.056	0.162
ζ_{as}	-0.046	0.226	**-0.484***
ψ_{ur}	**0.456***	0.345	0.164

The areas of separation considered in the analysis include the total area of separated flow and the areas of outer- and inner-bank separation individually. Analysis of the correlations between the calculated areas of separation reveals that the total area of separated flow in bends is strongly correlated with the area of outer-bank separation, and more weakly associated with the areal extent of inner-bank separation. This relationship reflects the relative contribution of the larger outer-bank separation to the total area of separated flow in the study bends. Areas of inner and outer-bank separation are not significantly correlated, indicating that relative sizes of separation

zones between bends do not systematically vary and that inner-bank separation does occur without outer-bank separation (Figure 3.4).

Bend average curvature (B_c) is significantly correlated with each of the areas of separated flow (Table 3.3). Figure 3.6a indicates that as B_c (R_c/w) decreases, the presence of flow separation within the bend becomes more likely. This relationship is stronger for the percentage area of outer-bank separation (Figure 3.6b), which does not occur for values of B_c above 4. Although the size of inner-bank separation also shows a similar trend, the relationship is not as strong and inner-bank separation occurs in one bend with a relatively high value of B_c (Figure 3.6c). Once a separation zone is present, there does not seem to be any dependency of percentage area of separation upon B_c.

The maximum direction change at the outer bank (β_o) also correlates significantly with both inner- and outer-bank separation size and with total separation area. β_i correlates with percentage area of inner-bank separation and the total areas of separation (Table 3.3). In bends of equal length, a decrease in bend radius would produce increases in the average direction changes per unit length along both banks, although the effect of sudden and irregular changes in bankline direction on the production of separation zones seems to be more significant (Figure 3.7a,b). Sharp peaks in the direction change series are followed by lengths of separated flow along both the outer- (Figure 3.7a) and inner- (Figure 3.7a,b) banks. However, where a peak in the series does not exist, even in a relatively tight bend, separation is not present (Figure 3.7c).

The relationship of the maximum changes in bankline direction for both the inner and outer banks are shown in Figure 3.8. The figures demonstrate that the formation of separation zones at both the inner and outer bank is accompanied by rapid changes in both β_i and β_o (Figure 3.8a,b). Indeed, non-parametric mean difference tests indicate that the difference between the presence and absence of inner-bank, outer-bank or any separation with the changes in β_i and β_o, is significant (Mann-Whitney, p=0.05). Moreover, a scaling of separation size with the maximum changes in bankline directions is also apparent, especially for total percentage area of separation and β_o (Figure 3.8c).

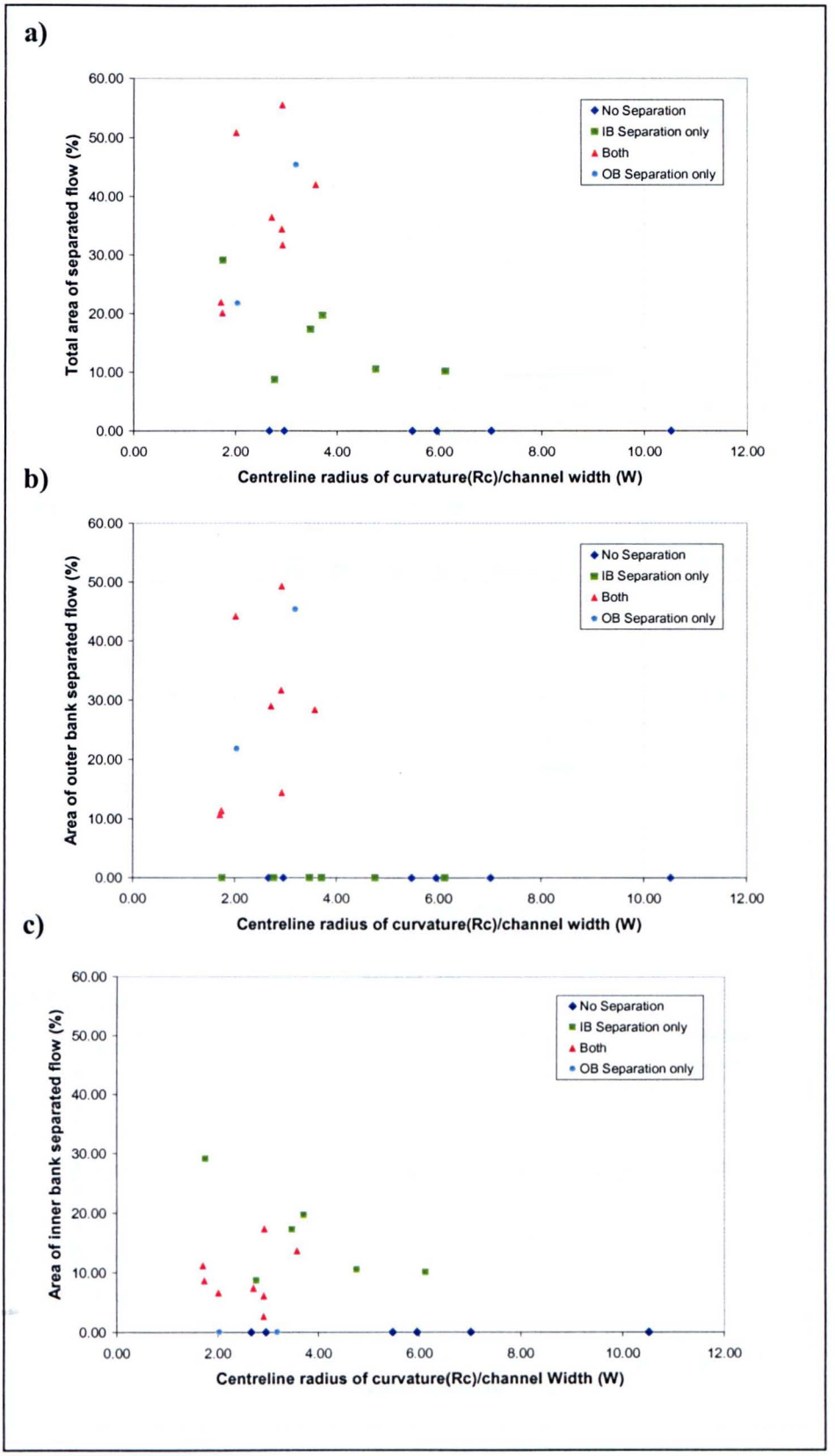

Figure 3.6: Relationship of centreline bend curvature (radius of curvature/channel width, R_c/w) with (a) total percentage area of separated flow (b) percentage area of outer-bank separated flow and (c) percentage area of inner-bank separated flow.

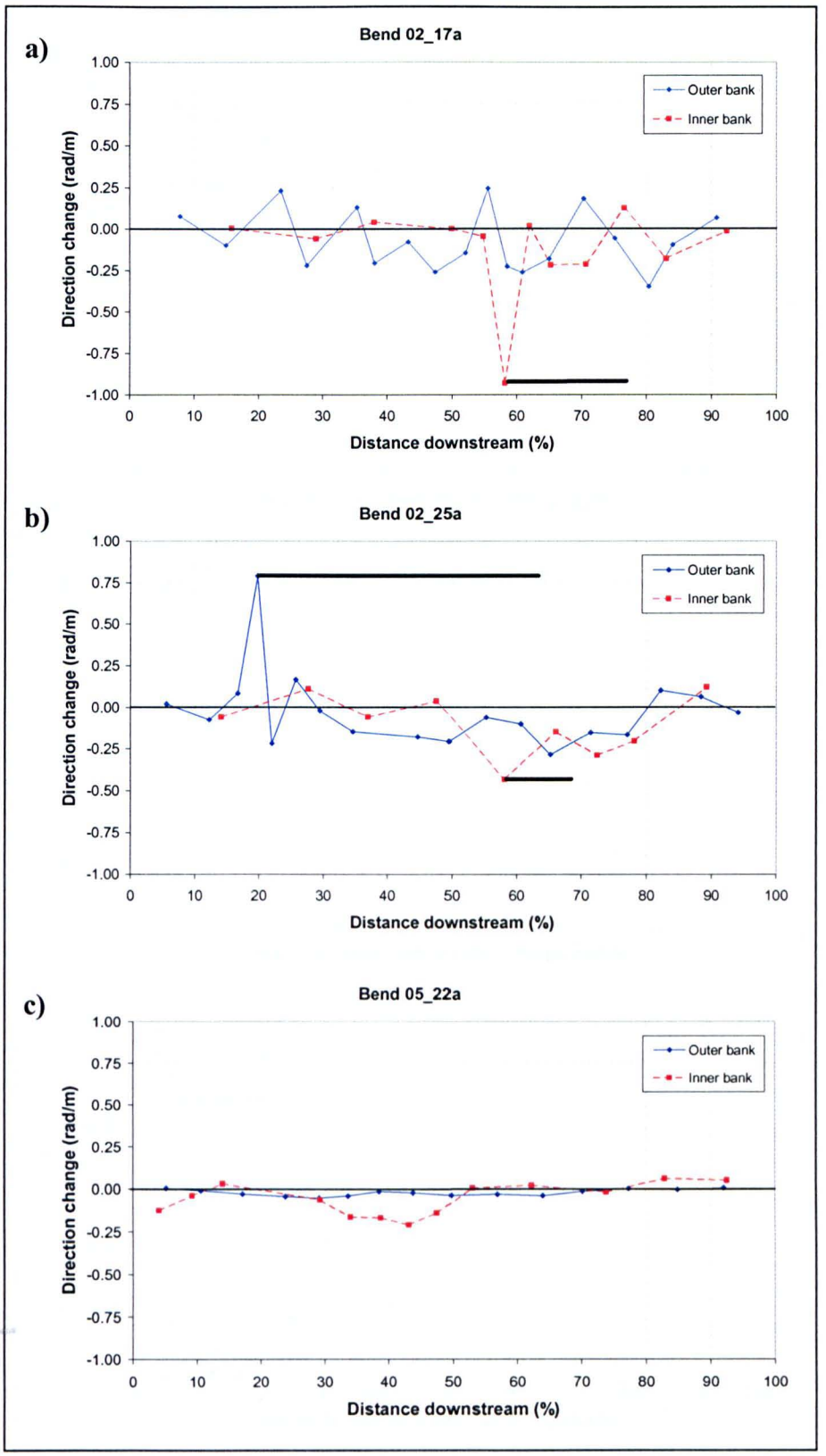

Figure 3.7: Direction change series along each bank for three representative bends of the twenty-two studied with (a) an inner-bank separation (b) a large outer-bank separation and smaller inner-bank separation and (c) no separation. Thick black lines indicate length of separation zone along the bank.

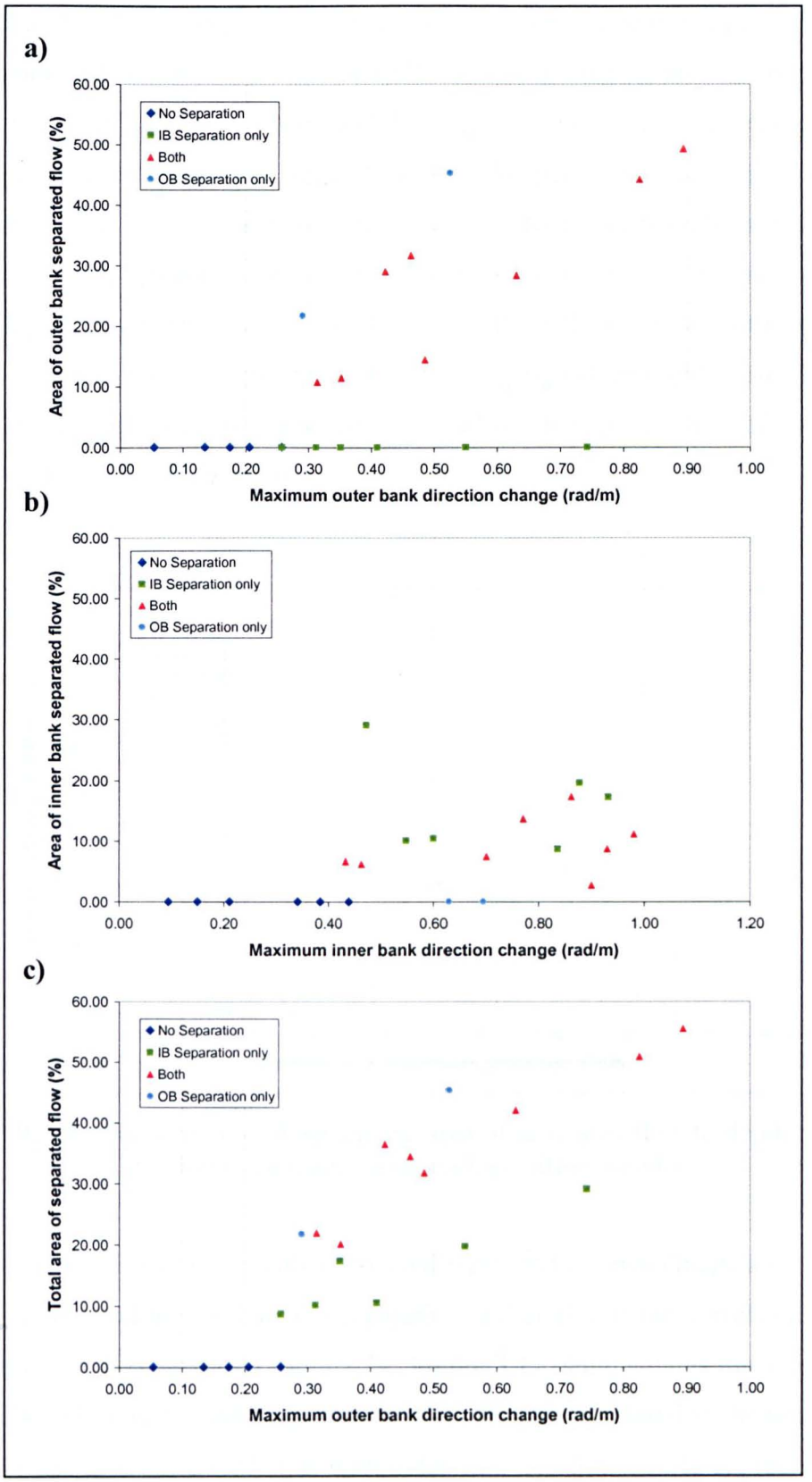

Figure 3.8: Relationships of maximum direction change in the bankline series to percentage areas of separated flow (a) β_o to area of outer-bank separation (b) β_i to area of inner-bank separation and (c) β_o to total percentage area of separated flow.

The bend average width/depth ratio (R_{wd}) does not correlate with the percentage area of separation. However, this is probably due to the averaging process as the depth ratio (R_d) is significantly correlated with the total percentage area of separated flow, percentage area of outer-bank separation and the percentage area of inner-bank separation (Table 3.3). Values of R_d are much greater in bends with separated flow, with values of R_d generally above 4 when separation is present (Figure 3.9). The relationship of separated flow area to the bed gradient (B_g) from the inflow riffle to the pool confirms this relationship, with increasing B_g values highly correlated with the total percentage area of separated flow and the percentage area of outer-bank separation (Table 3.3, Figure 3.10).

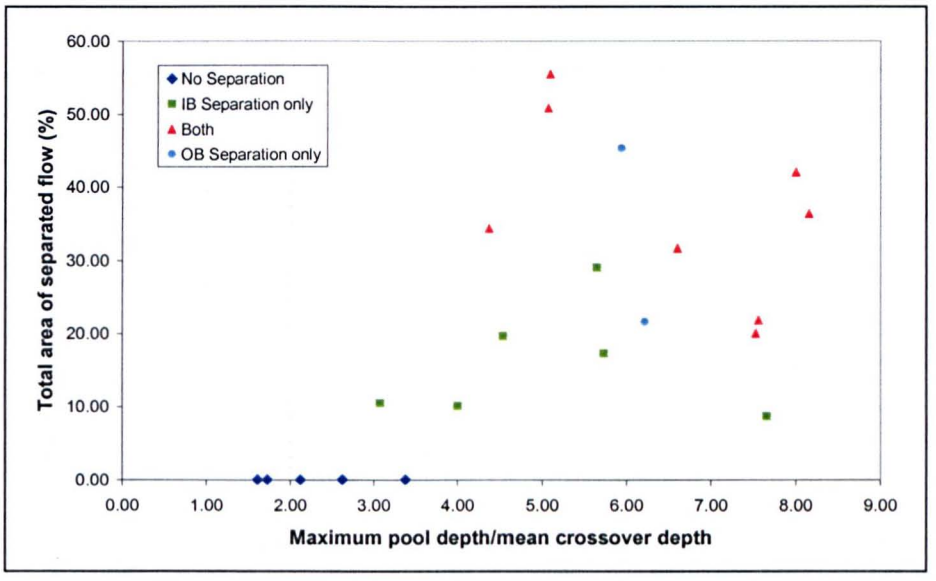

Figure 3.9: Relationship of total percentage area of separated flow to depth ratio (R_d; maximum channel depth/average inflow depth)

The width ratio (R_w) is also highly correlated with both the percentage area of outer-bank separation and the total area of separation, although it is not correlated with the area of inner-bank separation (Table 3.3). Figure 3.11 demonstrates this relationship graphically and indicates that large values of R_w are indeed related to the total area of separation and especially for bends with outer-bank separation. As R_w increases the presence of an outer-bank separation zone becomes more likely and the size of this zone increases with increasing values of R_w. Thus, outer-bank separation size is clearly related to bend apex width expansion, and does not generally occur where R_w is below 1.4.

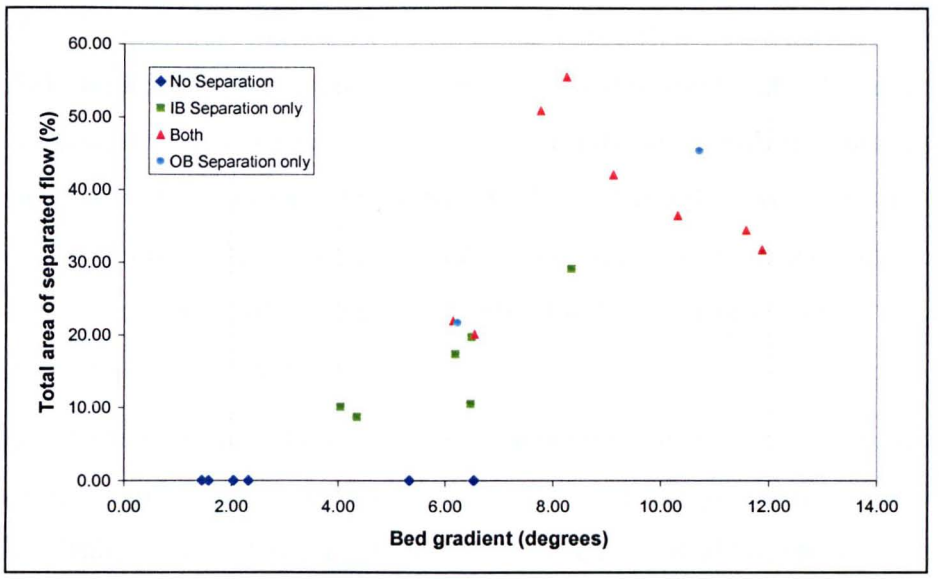

Figure 3.10: Relationship of separated flow area to bed gradient (B_g riffle/pool).

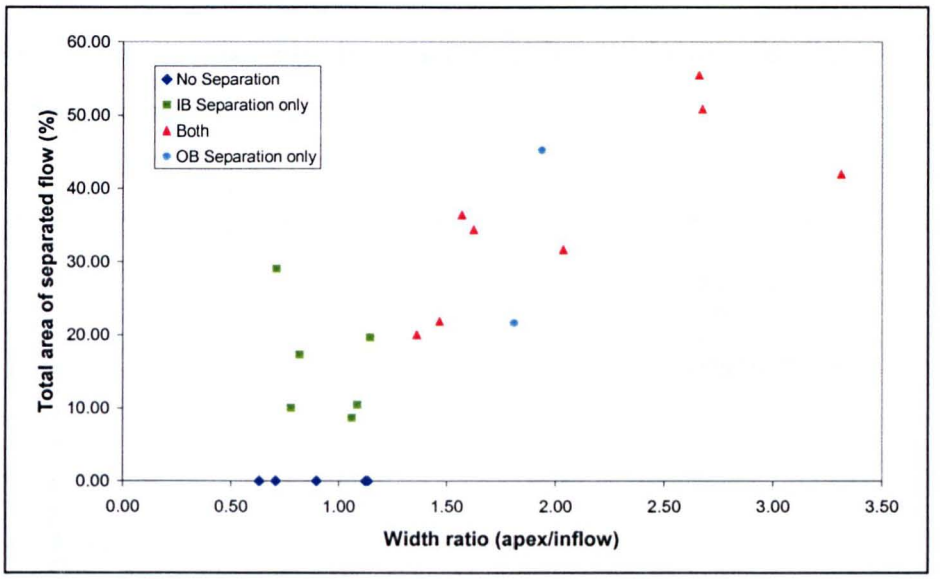

Figure 3.11: Relationship of total percentage area of separated flow to width ratio (R_w; apex width/inflow width)

3.3.4 Factors influencing separation: flow

The effect of inflow velocity distribution on the presence of separation was investigated with respect to three main variables: the maximum value of depth-averaged velocity at the inflow section (U_{in}); the flow deviation angle of the maximum depth-averaged velocity at the inflow section (ϕ_{in}); and the degree of inflow asymmetry (ζ_{as}).

Table 3.3 indicates that the flow deviation angle at the inflow cross section is not significantly related to the presence of separation within the bend. However, higher values of depth-averaged velocity do correlate significantly with the total and outer percentage areas of separation. Interestingly, the ζ_{as} variable correlates significantly with the U_{in} (Table 3.2), suggesting that as the flow is more asymmetrical, the confinement to one side of the channel leads to a higher inflow velocity and more chance of separation development.

The degree to which the inflow velocity is asymmetrical (ζ_{as}) at the inflow cross-section only significantly correlates with the percentage area of inner-bank separation (Table 3.3). However, Figure 3.12 reveals that although absolute values of ζ_{as} do not necessarily relate to the presence of separation, an interesting pattern exists whereby, with one exception, bends with only inner bank separation have inflow velocity skewed towards the outer bank (+ve ζ_{as}) and bends with outer bank separation zones consistently have main inflow velocity distributions skewed towards the inner bank (-ve ζ_{as}).

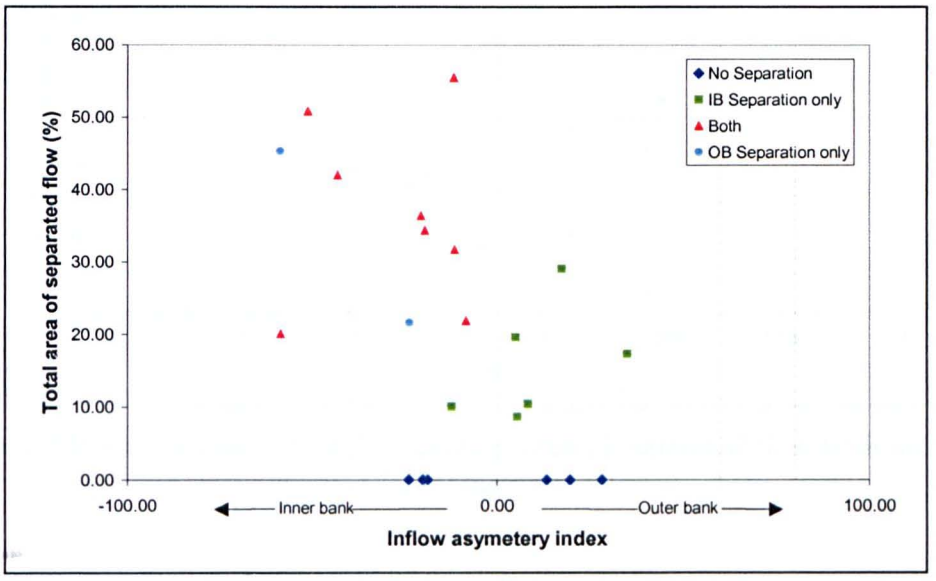

Figure 3.12: Relationship of separated flow area with the inflow velocity asymmetry.

Two calculated variables attempted to incorporate aspects of both flow and form in analysing the production of separated flow. Values of ψ_{ur} are positively correlated with the total percentage area of separated flow (Table 3.3) and statistical tests indicate that the medians are significantly different (Mann-Whitney p=0.01). Bends

with separated flow are generally sharper and/or have higher inflow velocities, although the spread in values is high (Figure 3.13).

The relationship between bend curvature and Froude number suggested by Leeder and Bridges (1975) for inner-bank separation occurrence in inter-tidal creeks is presented in Figure 3.14. The general trend in Figure 3.14 is similar to that found by Leeder and Bridges, with separation occurring in sharper bends and at higher Froude numbers. However, a cluster of points are close to their discriminatory curve and significantly one bend with a low B_c value and high Froude number does not have separation. Nevertheless, Figure 3.14 does indicate some discriminatory power if the curve was adjusted. Indeed, Leeder and Bridges (1975) do alter the position of the curve for experimental channels with different depths, suggesting that cross-sectional form has a greater control on separation occurrence.

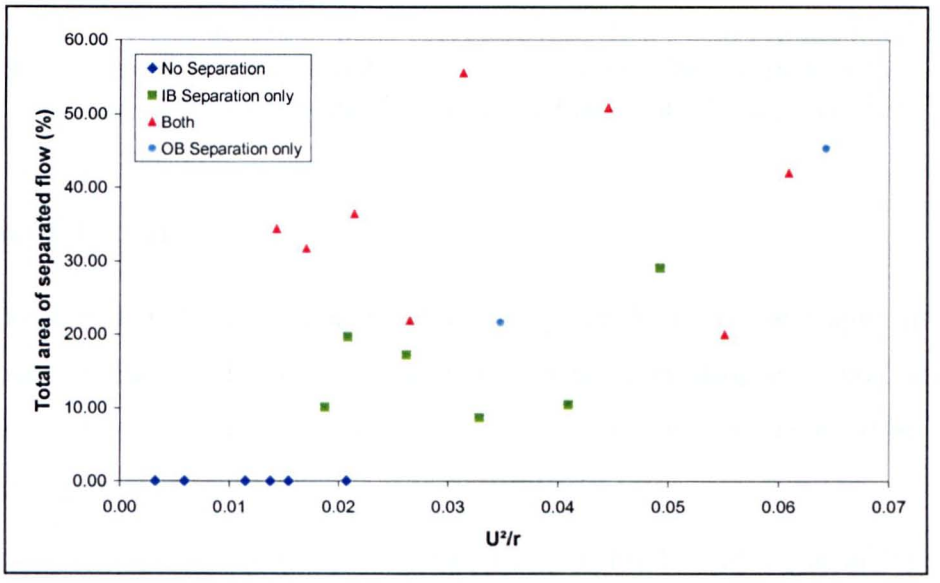

Figure 3.13: Relationship of total percentage area of separated flow with the U^2/R_c (ψ_{ur}) parameter.

In summary, the analysis presented above indicates that separation is associated with high average bend curvatures (B_c; R_c/w), deeper pools with high bed gradients from riffle to pool, and in bends where there are rapid changes in bankline direction. Outer bank separation is particularly associated with bends in which there are expansions in the channel width at the bend apex and where values of inflow asymmetry (ζ_{as}) are negative so that bend inflow is close to the inner bank. There is clearly some relationship between the inflow distribution to the bend and bend

geometry. However, both U^2/R_c (ψ_{ur}) and the bend curvature-Froude number relationships indicate that this relationship is a complex one.

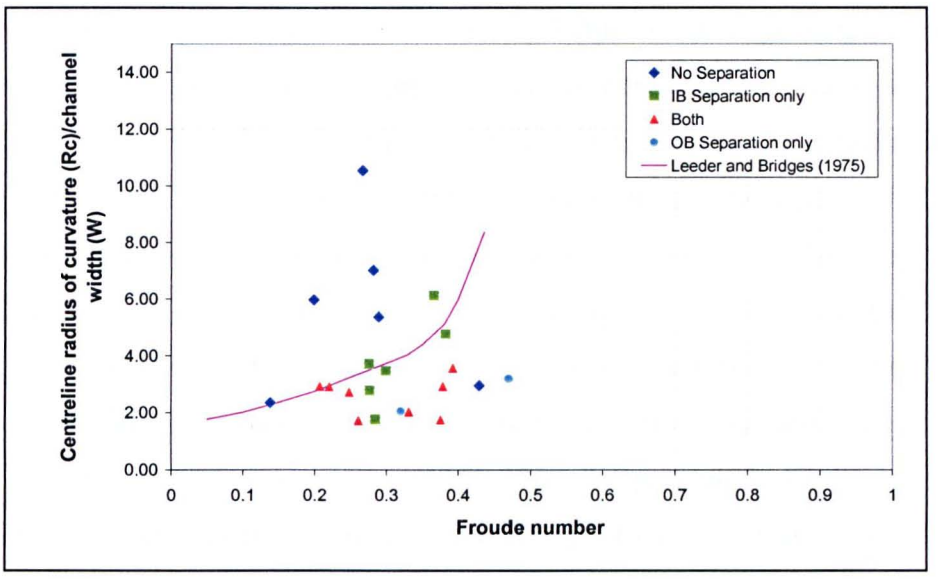

Figure 3.14: Relationship of bend curvature (B_c, R_c/w) with Froude number to predict occurrence of flow separation of various types. Discriminatory line is that determined for inner-bank separation by Leeder and Bridges (1975).

3.4 DISCUSSION

When combined with the reconnaissance survey results (2.4) the results presented above suggest that the processes responsible for the formation of bends with only inner-bank separation and those with outer-bank separation accompanied by smaller inner-bank separation zones may be significantly different.

The reconnaissance survey (2.2) identified that the total bend angle of turn (ω) is important in the production of both inner and outer bank separation in bends. The above results indicate that as bend curvature B_c (R_c/w) reduces, the occurrence of separation becomes more likely (Figure 3.6). Previous work has also found that bend tightness has a significant effect on the presence of inner-bank separation zones (Rozovskii, 1957; Leeder and Bridges, 1975) and other studies have postulated that the reduction in outer-bank bend migration rates in sharper bends is due to the onset of outer-bank separation (Hickin and Nanson, 1975; Hickin, 1986). Although Hodskinson and Ferguson (1998) did not investigate changes in total B_c, they found that the radius of the outer bank had a significant effect on the size of the outer-bank separation zone, which increased significantly with decreasing outer-bank radius.

The physical explanation for the increased occurrence of separation in sharper bends relates to the bend inflow being less able to adjust its momentum to the imposed curvature of the channel in tighter bends.

While the results indicated that gross bend curvature is an important factor in the presence of separation zones, sharp breaks in bankline curvature are a very significant factor (Figure 3.8), especially in the positioning of the detachment point (Figure 3.7). If sharp breaks in bankline curvature occur, the inertial effect of the flow discussed above is pronounced and these sharp breaks act as a location point for separation. Figure 3.7 demonstrates that sharp changes in bankline direction result in downstream flow separation adjacent to the bank downstream of the direction change. The flow is forced around the break in curvature and cannot adjust to this sudden change. This creates a zone of lower dynamic pressure in the lee of the break in curvature, where reverse pressure gradients act to create a zone of slowly re-circulating flow. Once flow separation has developed, the re-circulation will enhance the size of the separation zone by creating an adverse upstream pressure gradient, which will act to stall the downstream flow close to the point of detachment.

Separation therefore appears to occur in sharper bends and is enhanced by the presence of sharp breaks in channel curvature. However, from the data presented above it is difficult to establish whether low values of B_c or the breaks in bank curvature (high values of β_i and β_o) that are more important in the production of separation in bends. This is primarily due to the significant positive correlations between B_c and both β_i and β_o (Table 3.2). Thus, as B_c decreases, the probability of a sudden change in bankline direction increases. This covariation of β_i and β_o with B_c may be produced by the actual presence of separation within bends, which would affect the flow distribution through the whole bend. For example, the presence of flow separation within a bend could act to produce a sharp change in bankline direction within a bend by concentrating flow and erosive forces away from the point of separation. Moreover, a sharp bend may develop due to the presence in a sharp break in channel direction, produced by obstructions (*e.g.* Reid, 1984). This type of feedback may be strengthened by the fact that separation zone size seems to scale with values of maximum direction change (Figure 3.8).

Although the planform seems to exert a strong influence on the occurrence of separation, changes in the cross sectional form of the channel through the bend also seem to influence separation presence. Flow separation at both the inner and outer banks is more likely in bends with high depth ratios (R_d) and high riffle pool gradients (B_g) (Figure 3.9; 3.10). Equilibrium bend theory (*e.g.* Engelund, 1974) and empirical studies (Thorne, 1989; Markham and Thorne, 1992) have found that bend planform and pool depth are intricately linked. As bend curvature decreases the depth of the bend pools increase and the strength of secondary circulation increases. A possible explanation of this relationship is that large scour depths in bends promote high secondary circulation that may result in a positive feedback loop between migration rates, bend curvature and pool depth. Thorne (1989) found that on the Red River the relationship between curvature and pool depth is non-linear: bend scour depths increased rapidly as B_c fell below 5. However, the nature of this relationship in bends with separation is unclear, Thorne (1989) did suggest that there was some evidence that as B_c reduced below 2, where the formation of separation is likely, this trend levelled off and began to reverse. The results presented above confirm the general trend of increasing scour depth with reductions in B_c and that the possible reduction in scour depth in bends with separation does not occur (Figure 3.5; Table 3.2). Indeed, the trend continues with the highest R_d values, at pool depths up to eight times the mean inflow depth, occurring for bends with the largest separation zones. The positions of scour in bends with separation can be very different from classical type bends. For example, Andrle (1994) found that positions of maximum scour are near the inner bank in bends with outer bank separation. The bend with inner bank separation studied by Hodskinson and Ferguson (1998) had a zone of maximum scour very close to the outer bank at the bend apex. Thus, the processes responsible for the scour in classical bends may not be the same in bends with separation zones, especially in bends with outer bank separation, where pools are often found near the inner bank.

The presence of separation is also strongly correlated with the expansion of channel width at the bend apex and Figure 3.11 confirms that the size of outer bank separation is extremely sensitive to the width ratio (R_w). Hickin (1977) and Page and Nanson (1982) suggested that channel widening at the apex of sharp bends facilitates the flow expansion necessary for the presence of a large dead zone at the concave

bank. Lewin (1978), Reid (1984), and Andrle (1994) suggested that it is migration of the inner bank away from the outer bank that permits this width expansion. Hodskinson and Ferguson (1998), applying CFD to a hypothetical meander bend, found that widening the channel at the apex through decreasing the outerbank radius resulted in a larger separation zone at the concave bank. They also found that increasing the cross sectional area of the apex cross section through removal of the point bar resulted in the outer-bank separation zone increasing in size. However, expansion of channel width does not seem necessary for the formation of separation at the inner bank. For example, Rozovskii (1957) and Bagnold (1960) both noted the presence of separation at the inner bank of a uniform width channel. Indeed, Leeder and Bridges (1975) discuss the reduction in effective channel width produced by inner bank separation. This may also apply to outer bank separation, as an increase in total channel width is not necessarily incompatible with a reduction in the effective channel width. Thus, it may be that the increase in channel width required for the formation of a separation zone actually results in a reduction in the effective flow width. However, this proposition is difficult to assess without data on the flow structure through the bends.

The discussion above highlights the covariant nature of the channel form parameters investigated. In the cases of outer-bank separation, the width increases required at the bend apex have to be accommodated by a reduction in the outer-bank radius and an increase in the rate of change of outer bank curvature, which explains their significant correlation (Table 3.2), and an increase in cross sectional area. The values of R_d and R_w are also significantly correlated (Table 3.2), which is generally not the case of classical meander bend morphology. Bends with outer-bank separation zones develop areas of deep scour close to the inner bank and are often wide at the channel apex (Page and Nanson, 1982; Andrle, 1994), explaining the correlation. However, the processes responsible for the development of such features are poorly understood and require detailed investigations of the flow structure in such bends.

The inflow distribution inherited from upstream can have a significant effect on the flow structure present in the bend. The reconnaissance survey (2.5) identified that the angle of flow impingement (ϕ), as modified from upstream planform, at the outer bank can have a significant effect on the presence and size of separation within a

bend. However, the deviation angle of main inflow direction φ_{in} from normal to the channel banks had low correlation with the presence and size of separation within the bend. This suggests that it is the distribution of velocity, rather than the flow direction, at the inflow cross section that is important in producing separation within bends: the distribution of this velocity and its relationship with channel curvature then defines the impingement angle of the main flow at the outer bank. Indeed, the maximum depth-averaged velocity at the inflow section was found to be significant in the production of outer bank separation. The dominance of the flow velocity maximum and asymmetry over the flow direction in the production of separation reflects that separation is driven by flow inertia: that the flow cannot adjust its momentum to the imposed channel geometry. At higher velocities, flow inertia would prevent adjustment of the flow to the imposed curvature of the channel, resulting in the flow impinging on the outer bank at a higher angle. This would result in a breakdown in flow structure and the formation of a separation zone. Thus, as this parameter increases one would expect the formation of a separation zone to be more likely. Furthermore, the position of this main core of inflow velocity also seems to be important. Figure 3.12 demonstrates that in bends with outer bank separation the main core of inflow velocity is consistently near the inner bank with negative inflow asymmetry indices (ζ_{as}). The reverse seems to be true for the majority of bends with inner bank separation, with positive inflow asymmetry indices (ζ_{as}). Highly asymmetrical flows across the inlet cross section and the concentration of flow into one side of the channel are more likely to produce higher velocity inflow, which explains the significant correlation between ζ_{as} and U_{in} (Table 3.2). The asymmetry and high momentum of the inflow are more likely to produce a high angled collision with the outer-bank and lead to the creation of low-pressure regions and flow separation within the bend. Thus, the nature of the inflow to the bends has an important effect on the flow structure produced within the bend. Indeed, Hodskinson and Ferguson (1998) illustrate the significance of the velocity distribution, as modified by upstream planform, at the bend inflow. They demonstrated that as the inflow distribution was moved towards the inner bank the size of outer bank separation increased, although as the flow distribution was moved from the inner to the outer bank, the size of the outer bank separation zone decreased before being washed out entirely. Nevertheless, there are a number of bends that do not have large values of ζ_{as}, but still have large zones of separation. When individual

cases with low absolute values of ζ_{as} are considered, the deviation angle φ_{in} of inflow is generally higher. This suggests that it is a combination of the maximum inflow velocity, the degree of ζ_{as} and φ_{in} and their combined relationship with outer bank curvature which produces separation within bends.

The results discussed above highlight important parameters from both flow and form variables and how the inflow distribution interacts with channel form. Indeed, Table 3.2 indicates that there are significant correlations between some flow and form variables. The ψ_{ur} parameter was a first attempt at combining both flow and form variables into one value and as it includes both flow and form it is correlated to many of the other variables (Table 3.2). Values of ψ_{ur} are positively correlated with the total percentage area of separated flow (Table 3.3) and although the spread in values is high, Figure 3.13 indicates that bends with higher ψ_{ur} values are more likely to have separation. As discussed above, higher velocity inflow and a decrease in bend radius both have the effect of increasing the momentum of the flow towards the outer bank and increasing the angle at which the main current impinges onto the bank and the angle at which the flow departs from the inner bank. As both these effects combine, an upstream pressure gradient will develop at the outer bank and a region of low pressure will develop at the inner bank both of which create zones of separated flow. Figure 3.14 presents a similar attempt at combining variables to discriminate between bends with and without separation. The general trend is similar with separation occurring in sharper bends and at higher Froude numbers. Although both relationships demonstrate that they both have some discriminatory power, they also both have a significant amount of scatter that indicates incomplete capture of the significant factors in the production of separation.

The nature of the covariance between many of the variables discussed above results in distinguishing between cause-effect becoming extremely difficult, both between the variables and between factors producing flow separation. Thus, the analysis of how these interactions between variables alter once separation is present is problematic as once separation is present, it acts to modify the relationships between the parameters.

The study outlined above was only performed at intermediate to low flow stages, where flow is generally adjusting to an imposed topography. As changes in flow stage are likely to alter many of the variables outlined above, at different rates, the

effect of flow stage on the discussion above is difficult to comprehend. For example, changes in B_c will occur as width and channel radius alter, and with increasing flow, the asymmetry of the inflow may decline as topographic forcing by the riffle is reduced.

Thus, the presence of separation zones within bends is clearly complex and requires a more detailed understanding of both the immanent processes occurring within the bends at different flow stages and in different situations. There is also a need for studies of the long-term development of bends with separation zones.

3.5 CHAPTER CONCLUSION

This detailed field study of twenty-two bends presented in this chapter has shown that there are significant relationships between aspects of meander form, bend inflow distribution and the presence and size of separation zones. Building on the results of the reconnaissance survey, this chapter has identified that the bend curvature is significant factor in the development of separation in bends. However, it has also identified that breaks in bankline curvature in tight bends are perhaps more crucial to separation development, especially in terms of position within the bend. This relationship is complicated due to the covariant nature of variables considered: the occurrence of sharp breaks in bankline curvature is more likely in sharper bends. Width and depth ratios are also found to be significant factors: in both, the degree of expansion towards the apex was positively correlated with separation size. Depth ratio is correlated with bend tightness and continues to increase in sharp bends with separation zones: extending the previous results of Thorne (1989) into tighter bends with separation zones.

Although the reconnaissance survey found that the impingement angle of the main flow at the outer bank is important in generating both outer and inner bank separation, this chapter identified that it is the distribution of velocity and notably asymmetry at the bend entrance rather than the flow direction that is important in producing separation in bends. The nature of impingement at the outer bank is therefore governed more by the bend curvature and the inflow momentum rather than actual inflow deviation across the riffle. It is clearly a relationship between the bend inflow and channel form that produces flow separation, although simple parameters

such as ψ_{ur} and the B_c-Froude number relationships, which attempt to combine flow and form variables, do not provide much explanatory or discriminatory power.

Thus, although the variables measured and analysed have shown some interesting and significant relationships, the nature of the causal relationships is still speculative and unclear. This is primarily due to an incomplete understanding of the processes occurring within bends with separation zones and how these processes are modified by different conditions. The remaining chapters of this thesis address these issues though the application of numerical flow modelling (CFD), which is a powerful tool for understanding flow processes within different geometries. The next chapter introduces the background to the CFD model applied, with the following chapters detailing the use of this model to ascertain the process-form relationships initially in bends with inner bank separation before examining bends with outer bank separation.

Chapter 4
Numerical Modelling of Flow

4.1 INTRODUCTION

Recently, there has been a substantial increase in the use of numerical modelling applied in geomorphological study. The complexity of numerical models varies considerably: from simple one- (*e.g.* Hoey and Ferguson, 1994) and two-dimensional (*e.g.* Murray and Paola, 1994) sediment routing models to three-dimensional unsteady flow modelling (*e.g.* Bradbrook *et al.*, 2000b). In general, this movement towards more complex models has seen the incorporation of more physically based processes in the formulations. Although the *need* for the incorporation of more physically based approaches is hotly debated, especially when more uncertainty is introduced (*e.g.* Beven, 1992), the increase in model dimensionality often reduces the sensitivity of the model predictions to the parameters applied. The last few years has seen major progress in the application of high-resolution numerical flow models in geomorphology and hydrology in particular (*see* Bates and Lane, 1998). Recent enhancements of 3D Computational Fluid Dynamic (CFD) codes have seen their utilization in the fields of river mechanics, fluvial geomorphology, and engineering hydraulics to study flow structures in open channels. This has enabled an improved simulation of important flow processes, providing much richer prediction fields that enhance insight and understanding, where field and laboratory measurements can rarely provide a sufficient process representation. Their application has been especially valuable in areas of complex flow such as in confluences (Bradbrook *et al.*, 1998; 2000a) and where there is flow separation (*e.g.* Hodskinson, 1996; Hodskinson and Ferguson, 1998).

This type of modelling can be used for two main purposes: it can be used to improve the understanding and provide explanation of the linkages and relationships within a system (*see* Figure 1.2) or it can be used to provide predictions of system behaviour in given circumstances. The approach applied in this thesis is mainly within the first of these: initially flow modelling of specific bends is performed and then different

combinations of boundary conditions are used to examine the nature of causal linkages within the system (1.2).

This chapter aims to explain the basics of flow modelling in general and to outline the CFD model used in forthcoming chapters. The chapter begins by reviewing modelling approaches for understanding river channel flow processes (4.2), including the movement from one- to two- (4.2.1) and three-dimensional (4.2.2) modelling techniques, and the recent application of large eddy simulation in modelling transient flow processes (4.2.3). The following section (4.3) introduces the CFD model applied in this thesis, including an introduction to the conservation laws (4.3.1) upon which CFD is based, how these equations are solved numerically (4.3.2), and how this solution is controlled (4.3.3). Section 4.4 provides a brief introduction to turbulence in open channel flows (4.4.1) and deals with the different methods by which turbulence is incorporated in the solution of the equations. This includes time-averaged methods (4.4.2) and transient flow modelling techniques (4.4.3). The specific application of CFD to open channel flow is described in section 4.5, including grid construction (4.5.1), and boundary condition specification (4.5.2). Section 4.6 explains how the numerical flow models are verified (4.6.1) and validated (4.6.2) when applied to open channel flow.

4.2 MODELLING OPEN CHANNEL FLOW

There is a long history of modelling in the study of open channel flow and flow in meander bends in particular. Modelling has contributed significantly to the state of knowledge (1.3) of flow structure in bends. This section outlines this research, highlighting the developments in modelling approaches, including the recent application of CFD methods in open channel flow problems.

4.2.1 Two-dimensional approaches

Although one-dimensional models have a long history of application in modelling river flows for geomorphological study (*e.g.* Richards, 1978; Correia *et al.*, 1992; Niekerk *et al.*, 1992; Carling and Wood, 1994), their use in analysing flow distribution is now diminishing with their primary use being in sediment routing (*e.g.*

Hoey and Ferguson, 1994). Depth-averaged two-dimensional approaches have become a more common approach for analysing flow distributions in river channels (Lane, 1998a). This movement towards, and development of, two-dimensional approaches was primarily driven by modelling flow in bends (*e.g.* Dietrich and Smith, 1983; Odgaard and Bergs, 1998; Johansson and Parker, 1989a,b; Nelson and Smith, 1989a,b). The two-dimensional flow equations are produced through two main methods: (1) the integration of the fully 3D equations over depth or (2) assuming a hydrostatic pressure distribution in the vertical (see 4.3 for mathematical background). Flow dispersion terms are created to for this simplification. These terms, which arise in the equations, are used to effectively account for the effects of secondary circulations on the downstream flow. In meander bends, the convergence and divergence of flow caused by curvature and bed topography can produce significant variations in the cross-stream water surface and very strong secondary circulation and spatial variations of turbulent transport of momentum, the effects of which have to be included in flow models of bends.

Two-dimensional approaches to modelling bend flow began with the theoretical treatments of Boussinesq (1877) and Thompson (1876), who proposed explanations based on inviscid flow theories. Einstein and Harder (1954) introduced viscous effects via bed friction calculations. Seminal work by Rozovskii (1957) introduced perturbation techniques in analysing flow in bends and this method was developed, notably by Engelund (1974), who produced a theoretical model of meander flow based upon consideration of the forces acting as the flow moves through a curved path round a channel bend. Several authors have built on this work including Geldof and de Vriend (1983), de Vriend and Geldof (1983), and Odgaard (1986a,b). Although these models produced some acceptable results, the underling assumption of these perturbation approaches is that secondary circulation acts only to disturb a fully developed channel flow and its effects are often not incorporated adequately (Bridge, 1992). Thus, these models are only strictly applicable in conditions of uniform, fully developed bend flow, in mildly curved rectangular channels, after long exposure to the curvature, where the width is large in relation to the depth, flow is controlled mainly by friction, and has a low Froude number (<0.2).

In order to overcome some of these problems, Nelson and Smith (1989a), extending the pioneering work of Smith and McLean (1984), developed a flow model based on

the two-dimensional momentum equations, with a regular perturbation expansion that included zero order, vertically integrated, convective acceleration terms. Thus, the model had the ability to include cases where both depth and channel width could vary throughout the bends. The empirical field measurements of Dietrich and Smith (1983) were used to investigate the model's performance in the field. The model was found to reproduce realistic velocities, surface elevations, and boundary shear stresses. Johansson and Parker (1989a,b) developed a similar model to investigate flow redistribution in bends with encouraging results. These analytical methods to modelling secondary circulation effects have been described as taking the moment of momentum.

The main differences between the separate models of bend flow that are based on this moment of momentum technique (Odgaard and Bergs, 1998; Nelson and Smith, 1989a; Johansson and Parker, 1989a,b), concerns the representation of the effects of convective accelerations associated with secondary circulation on the primary flow field. There has been some debate over whether the convective terms should be included as downstream, cross-stream, or both. Researchers who have found the cross-stream term small have tended to be studying regular channels, whilst those studying irregular channels have found the cross-stream term becoming increasingly important (Lane, 1998a). Whiting (1997) recently commented that the importance of the convective acceleration terms diminishes with flow stage and that the divergent conclusions reached by different workers could be related to relative depth.

As the definition of streamwise and transverse directions becomes increasingly difficult in channels with non-regular boundaries or curvature (Bridge and Gable, 1992), the suitability of moment of momentum approaches in such situations has been questioned. Thus, Bernard and Schneider (1992) recommend a different approach based on qualitative arguments concerning the interaction of lateral curvature, bottom friction, and vertical non-uniformity (Lane *et al.*, 1995; Lane, 1998a). This reproduces the depth-averaged influence of the secondary flow by modelling the vertical dependence of the streamwise out of plane velocities, and the effects of centrifugal and friction forces on a vertical column of water. Shear stresses associated with secondary flow are calculated through the effects of streamwise vorticity, which includes empirically derived terms for production, dissipation, diffusion, and advection of vorticity. Vorticity production and dissipation are

proportional to both bottom friction and depth averaged velocity, and inversely proportional to the depth (Lane, 1998a). An additional term related to vorticity production caused by channel curvature is added to the vorticity production term. This type of secondary circulation correction has been found to work well both in open channel bends and at a diffluence-confluence unit in a braided river (Lane *et al.*, 1995; Lane and Richards, 1998). Although Lane and Richards (1998) noted that problems were still apparent where the flow is strongly three-dimensional.

One of the main advantages of two-dimensional approaches is the saving of computer processing time and the ability to incorporate sediment transport routines more easily. Indeed, recent developments of two-dimensional approaches have witnessed a movement to studies of morphological change through time with promising results. For example, Jia *et al.* (1999) demonstrate the predictions of channel change in a hypothetical meandering reach.

Although the two-dimensional depth-averaged treatments of flow in open channels do provide some good results, their success has been mainly confined to simplified cases. Even with recent developments of secondary circulation corrections, predictions remain poor in sharply curving bends (*e.g.* Bernard and Schneider, 1992; Lien *et al.*, 1999) where secondary circulation is strong. Results are also frequently poor close to channel banks, where topographic forcing produces high vertical velocities and in situations where turbulence structure is highly anisotropic. Indeed, research has shown that effects other than those described in the formulations above can be responsible for generating secondary circulation effects (*e.g.* Nezu *et al.*, 1993; Ashworth *et al.*, 1996). Furthermore, two-dimensional models tend to be very sensitive to the roughness parameter (Lane *et al.*, 1999a). Lane (1998a) suggests that three-dimensional approaches should be used to investigate ways of approximating secondary circulation effects more effectively. However, there are limits to the application of two-dimensional models, specifically in situations with large vertical velocities. For example, two-dimensional treatments are unsuitable for modelling high curvature bends with flow separation, as the separation is unlikely to extend throughout the depth creating large vertical velocities. Thus, to obtain adequate process representation three-dimensional approaches are required.

4.2.2 Three-dimensional approaches

Major progress in the application of three-dimensional computational fluid dynamics (CFD) codes in the study of complex flow structures in natural river channels have been made over recent years (*e.g.* Hodskinson, 1996; Lane, 1998a; Bradbrook *et al.*, 1998; Hodskinson and Ferguson, 1998; Lane *et al.*, 1999a; Nicholas and Sambrook Smith, 1999; Bradbrook *et al.*, 2000a,b). Indeed, such techniques have proved valuable in regions of complicated flow structure such as braid units, confluence zones and areas of flow separation.

Attempts at three-dimensional numerical flow modelling in open channel flow in river bends are well established. Leschziner and Rodi (1979) developed a three-dimensional finite difference method for calculating the turbulent flow in curved channels. The model calculated all the 3D velocity components using a k-ε turbulence model, but was restricted to rectangular cross sections. Demuren (1993) developed a curvilinear finite volume numerical model which has the ability to calculate the three dimensional turbulent flow in a meandering channel with natural bed topography. The model solves the Reynolds-averaged three-dimensional Navier-Stokes equations expressed in a general curvilinear coordinate system, with the Cartesian velocity components retained as dependent variables. A computational grid is constructed and the equations are solved iteratively in their full elliptic form. Thus, Demuren's model allowed for the possibility of flow separation and re-circulation, although no separation zones were present in the validation case used. The standard k-ε turbulence model was implemented to achieve closure of the averaged Navier-Stokes equations and the boundary conditions expressed for the inlet and outlet plane, the free surface and boundary wall. The experimental boundary conditions of Almquist and Holley's (1985) laboratory experiment were used to set the conditions for, and to evaluate, the computational simulation. Good agreement was apparent and the technique was found to give accurate three-dimensional flow estimates. Thus, Demuren (1993) stated that the model might provide a good hydrodynamic basis for the examination and prediction of meander evolution when combined with sediment transport algorithms. Ye and MaCourquodale (1998) applied a similar model to investigate flow in two different curved flume channels. They found generally good agreements between the predicted and observed in both cases. Hodskinson (1996) and Hodskinson and

Ferguson (1998) applied CFD to a natural bend with flow separation at the inner bank. The model successfully simulated the qualitative features of the flow (Figure 4.1), but the quantitative comparisons were not as impressive (Table 4.1). The model's robustness was tested for grid resolution, water surface specification, and choice of turbulence model closure: insensitivity to each was found. Hodskinson and Ferguson (1998) were also, by systematically altering aspects of the geometry of an idealised bend, able to examine the geometric controls on the occurrence of flow separation. The results were then analysed with reference to previous work in the area of meander bend flow separation (*e.g.* Hickin, 1977; Page and Nanson, 1982; Andrle, 1994). Thus, Hodskinson and Ferguson (1998) were able to consolidate earlier research, showing that the extent of flow separation at the concave bank seems to be strongly related to changes in upstream planform, bend planform and point bar topography.

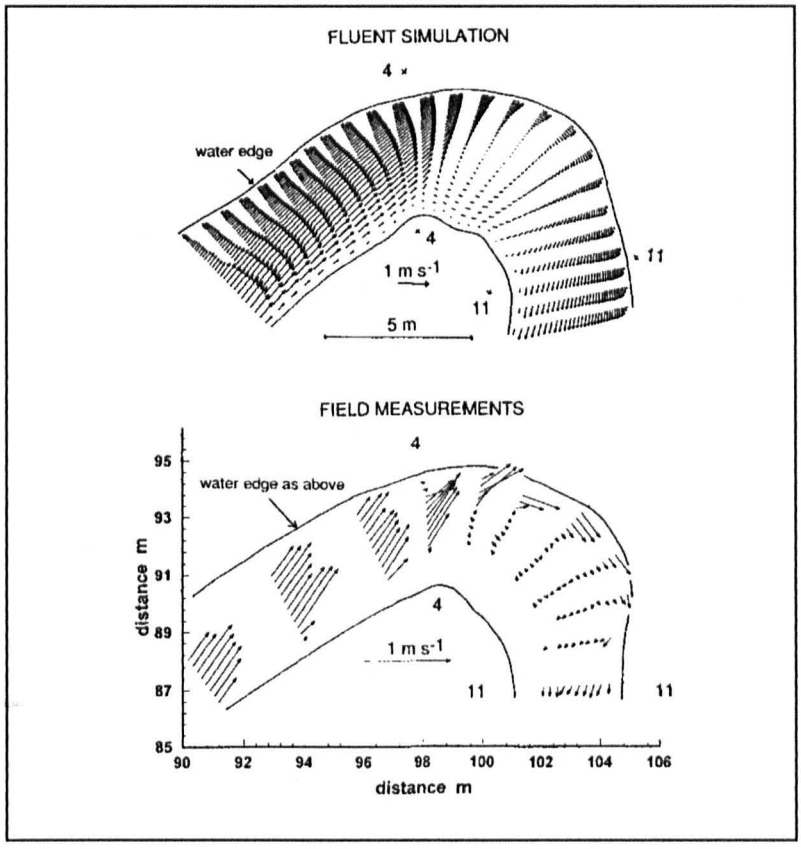

Figure 4.1: Simulated and observed near surface velocity patterns in a bend with inner bank flow separation (Hodskinson and Ferguson, 1998)

Three dimensional numerical flow models have also been successfully applied to confluence flow. Well validated simulations (Table 4.1) of different confluence

geometries, both laboratory (Bradbrook *et al.*, 1998; 2000a; Huang *et al.*, 2002) and field (Bradbrook *et al.*, 1999; 2000a), have permitted detailed investigations of flow structures. Experimentation of different combinations of boundary conditions has helped to solve the debates as to the relative controls on flow structure generation at confluences.

Table 4.1: Previous applications of 3D CFD to natural river channels in which a quantitative assessment of model predictions has been undertaken. Values given are for R-squared (the coefficient of variation obtained using ordinary least squares regression between model predictions and field or laboratory observations).

Authors	Description of study	Flow speed	Downstream velocity	Vertical Velocity
Bradbrook *et al.*, 1998	Laboratory study with smooth bed of a junction of parallel tributaries with a step.	Not reported	0.95	0.75
Hodskinson and Ferguson, 1998	Field study of a sharp meander bend with flow separation. Rough bed (D_{50} = 0.054 m).	0.89	Not reported	Not reported
Lane *et al.*, 1999a	Field study of a tributary junction in a gravel-bed river. Rough bed (D_{65} = 0.050 m).	Not reported	0.50	0.25
Nicholas and Sambrook-Smith, 1999	Field study of flow around a gravel bar in a braided river. Rough bed (D_{50} = 0.064 m).	0.78	Not reported	Not reported
Booker *et al.*, 2001	Field study of a riffle-pool sequence in a woodland stream. Rough bed (D_{50} = 0.019 m).	0.77	Not reported	Not reported
Bradbrook, 2000b	Field study of a tributary junction in a sand-bed river. Rough bed (D_{65} = 0.050 m).	Not reported	0.50	0.01
Bradbrook *et al.*, 2001	Laboratory study of a tributary junction angled at 30° degree to the post-tributary channel.	Not reported	0.53	0.59

Very recent developments in three-dimensional modelling have extended consideration to sediment transport. Gessler *et al.*, (1999) used a three dimensional hydrodynamic model to solve the depth-averaged velocity correctly which is used to drive sediment transport. Although, the model only included sand fractions, it performed well for several reaches of the Mississippi, with error estimates close to

13% volume in certain cross sections. Wu *et al.* (2000) have developed a three-dimensional model that calculates both suspended and bed load movements along with the resultant bed deformation. Bed load transport is calculated using a non-equilibrium method and the bed deformation is obtained from mass balance equations with the position of the grid re-calculated at the end of each time step. It was tested for the 180° bend of Odgaard and Bergs (1988), starting from an initially flat bed. Calculations continued until an asymptotic state was reached. Results were compared to measurements: the main features were reproduced, including scour at outer bank and point bar development at the inner bank.

Although the recent development of three-dimensional hydrodynamic models with simple morphological change incorporated is an important development, the application of three-dimensional models to open channel flow is still in its infancy and the flow structures themselves are not always adequately reproduced. Moreover, the sensitivity of these models to certain conditions, such as topographic representation, is still undetermined. Furthermore, the predictions of current three-dimensional models are steady state and the effects of turbulent flow structures, particularly upon shear stress at the bed, are not presently incorporated in the solution.

4.2.3 Three dimensional transient flow modelling

Although the three-dimensional models described above have provided significant spatial information, they have only simulated the time-average flow field, accounting for the effect of turbulent structures on the mean flow using techniques based on Reynolds averaging (RANS) (see 4.3 for mathematical background). This averaging is necessary as direct numerical simulation (DNS) of the time varying flow at the high Reynolds numbers encountered in river channels is computationally infeasible with current hardware capabilities (Friedrich *et al.*, 1991; Lesieur *et al.*, 1997 Speziale, 1998). Thus, Reynolds averaging of the Navier-Stokes equations is adopted, with a turbulence closure model simulating the effects of fluctuating components of the flow on the main flow. For open channel flow problems, this turbulence model is often based on a modified two equation k-ε model, which

models the effects of transport of turbulence on the main time-averaged flow field (*e.g.* Bradbrook *et al.*, 1998).

However, there is mounting evidence that coherence and structure exists in the turbulent boundary layer of river channel flows (*e.g.* Ferguson *et al.*, 1996; McLelland *et al.*, 1996; Rhoads, 1996). Hence, some flow structures may themselves fluctuate in a coherent manner over time. Such flow structures include the formation of Kelvin-Helmholtz instabilities in shear layers (*e.g.* Leeder and Bridges, 1975; Kimura and Hosoda, 1997; Best and Roy, 1991; Sukhodolov and Rhoads, 2001), longer-term shear layer migration (*e.g.* Biron *et al.*, 1993b), and periodic upwelling and downwelling at certain positions in the channel (*e.g.* Bradbrook *et al.*, 1998). Thus, flow structures such as secondary circulation cells, inferred from time-averaged measurements or modelling, may not be steady features but derived from the averaging of an intermittent or periodic process (*e.g.* Shi *et al.*, 1999; Lane *et al.*, 1999b; 2000). Moreover, the presence of these coherent flow structures could have a significant control on river flow processes which could each be several orders of magnitude greater than the time-average mean (Lane *et al.*, 1999c; 2000). This has significant implications for flow mixing, solute mobility, and pollution dispersion (Lane *et al.*, 1999c), notably in relation to periodic sweeps and ejections of fluid with different concentrations. Periodic structures will also lead to fluctuations in boundary shear stress, sediment entrainment and transport, and thus changes in overall channel geomorphology. Therefore, there is a need for measurement and modelling techniques that can identify three-dimensional flow fields instantaneously and simultaneously from a large number of measurement locations throughout the flow.

The periodic fluctuations that are known to exist, for example in shear zones, cannot be modelled by time-average CFD techniques. Indeed, many time-average techniques, especially those involving the k-ε turbulence model, have problems resolving accurate and stable, time-averaged, open channel flow fields. However, recent research (*e.g.* Thomas and Williams, 1995a,b; Bradbrook *et al.*, 2000b) has made progress in applying a technique that has the potential of addressing this difficulty. Large Eddy Simulation (LES) is a compromise between DNS and Reynolds averaging. It computes directly the scales of flow that contain the most mass and momentum transfer using the full Navier-Stokes equations, but

parameterises the smaller features of the flow through a sub-grid scale turbulence closure model (Deardorff, 1970; Rogallo and Moin, 1984; Meneveau and Katz, 2000). In the spectrum of turbulent motions within fully developed open channel flow, a scale must be defined where sub-grid scale parameterisation is superseded by DNS of the flow. This cut-off scale is often based upon the average local grid spacing, such that eddies larger than the grid scale are subject to DNS and a turbulence model is applied to the smaller sub-grid scale eddies (Meneveau and Katz, 2000). The larger scales of flow are likely to be directly affected by site-specific boundary conditions. The effect of the smaller scale motions on larger ones can be specified by certain parameters. LES is now a well-established technique and it has been applied in complex engineering and geophysical flows for many years (*e.g.* Friedrich *et al.*, 1991). For example, Sagaut (1996) used LES successfully to simulate time-averaged separation length and the dominant frequency in the time series of streamwise velocity for flow over a backward facing step. Lu *et al.* (1997) and Manhart (1998) applied LES in modelling the flow around a circular cylinder and a hemisphere respectively, finding vortex shedding rates in the wake comparable to experimental values. Nevertheless, application of LES to open channel flow problems has been limited. Exceptions to this include Thomas and Williams (1995a,b), who have used LES to improve flow modelling of asymmetric and symmetric compound channels, and Shi *et al.* (1999) and Li and Wang (2000) who applied LES to model flow in straight, rectangular, open channels. These studies found that LES was able to produce predictions of mean velocities, velocity profiles, turbulent intensities and distributions of boundary shear stress that compared well with experimental data.

Application of LES to model and to investigate the turbulent unsteady components in open channel flows is a recent development. Bradbrook *et al.* (2000b) used LES to model the production and evolution of individual large-scale eddy structures in two open channel confluences. This approach has the ability to provide insights into both the spatial and temporal properties of flows in open channels. Indeed, Bradbrook *et al.* (2000b) found that, for a simple parallel confluence (similar to the Best and Roy (1991) set-up) LES was able to predict some of the observed periodic flow structures, such as eddy shearing and shear layer fluctuations. Comparison of spectral analysis power spectra from 30 ADV time-series in the flow field indicated

matches in the dominant frequency for eighteen. However, a further eight points only yielded matches for a dominant frequency in the first harmonic and in the other four, no frequency match was determined. Moreover, only the three largest peaks were identified in each time series and only a few of these matched up for each point. Indeed, the smaller scale, higher frequency, flow structures such as Kelvin-Helmholtz instabilities are not reproduced whatsoever by their LES model. Bradbrook *et al.* (2000b) suggest that this is due to the lack of incoming flow instabilities and/or grid size dependency on the scale of eddy reproduced. Indeed, Manhart (1998) and Hardy *et al.* (in press) highlight the importance of grid resolution for the reproduction of temporal aspects of the flow field.

In an exciting development, Zedler and Street (2001) report the successful modelling of the coherent flow structures and shear stress distribution over a sub-aqueous dune. By applying an advection-dispersion model for sediment transport, they were also able to reproduce some of the sediment dynamics over the dune.

Its potential recognised, further work is required to develop and improve the applicability of LES modelling techniques in natural river channels. Once established, LES could provide very detailed predictions of flow fields with potentially critical periodic fluctuations. For example, LES may have the ability to identify the factors controlling the generation and modification of specific channel scale flow structures and indicate the effects they may have upon sediment transport and mixing processes. These processes are of particular importance where flow separation and re-circulation zones are present and suggest that LES will be required to fully investigate and understand flow processes in meander bends with separation zones.

4.2.4 Summary

A range of modelling approaches have been applied in the studying flow processes in river bends. There has been a recent trend towards three-dimensional CFD modelling in fluvial geomorphology in order to investigate the flow structures present in complex areas of flow deflection, combination, and shear. The potential of LES has also been recently highlighted, and substantial work is required to ascertain its ability to simulate periodic aspect of the flow field. However, the

application of CFD to natural channel involves a number of assumptions and simplifications, which raise specific issues in each application. The following sections consider the background mathematics to modelling turbulent river flows and the assumptions and simplifications that are required.

4.3 CONSERVATION LAWS OF FLUID MOTION

This thesis applies a commercial software package called Parabolic, Hyperbolic Or Elliptic Numerical Integration Code Series (PHOENICS) produced by Concentrated Heat And Momentum (CHAM) Ltd. PHOENICS is an excellent code with add-on utilities for user developed code and has successfully been applied to fluvial problems in the past. This section outlines the numerical methods used by this software to discretize the equations and to couple the pressure and velocity equations, as well as the way in which the flow is treated at boundaries.

4.3.1 Background equations and derivation

Three-dimensional CFD flow simulation calculations are based upon the application of the fundamental conservation laws of physics, namely the conservation of mass, the conservation of momentum (Newton's 2^{nd} Law) and the conservation of energy (1^{st} Law of thermodynamics) to fluids. These laws were developed for application to rigid bodies or particles and thus they need modification for application to fluids. These commence with the assumption that the fluid can be regarded as a continuum. For the analysis of fluid flows at macroscopic length scales, the effects at the molecular scale are averaged over a suitably large number of molecules and are represented through their overall effect on the macroscopic flow properties. These macroscopic properties include the velocity, pressure, density, and temperature: each in their space/time derivatives (Tritton, 1988). The laws have to be further modified by the Eulerian transform in that the continuum that represents a fluid can be considered as an individual element of arbitrary volume (Figure 4.2) that moves through time and space (Versteeg & Malalasekera, 1995).

Consideration of a mass balance for the element, where the rate of increase of mass within the element is equated to the net flow rate of mass into the fluid element leads

to the derivation of the law for mass conservation. Mass flow rate across each face of the element can be calculated by the product of density, area, and perpendicular velocity component. The combination of these equates the rate of increase of mass within the element to the net rate of flow across all faces. For an incompressible fluid where density is constant, this simplifies to a simple law equating the mass inflow into the element to the mass outflow [4.1].

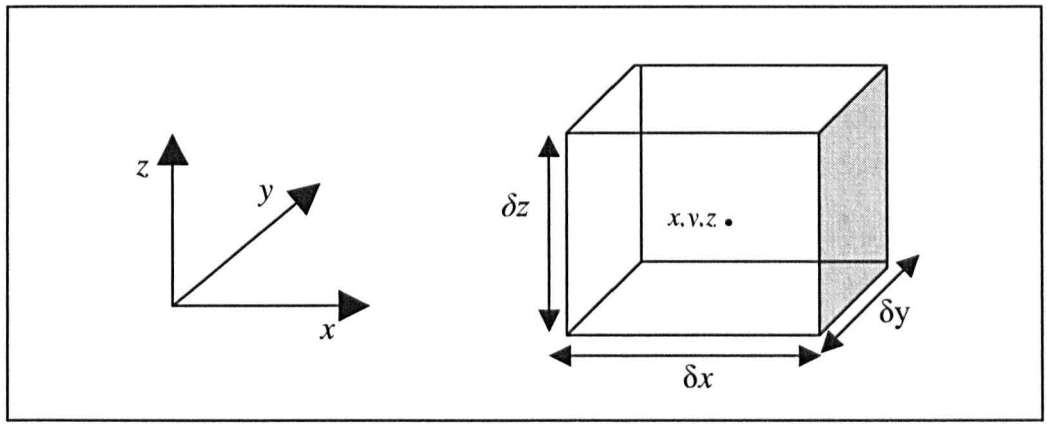

Figure 4.2: (a) Velocity vectors components (b) Fluid element considered for Eulerian transform.

The application of the Newtonian conservation of momentum law to fluid flow is achieved firstly by two assumptions. First, we observe that the rate of increase of the *x, y* and *z* momentum directions is equal to the sum of the vector forces acting in each. Second, we assume that the forces acting on fluid particles can be split into two distinguishable types: (i) body forces which are applied to the fluid mass; and (ii) surface forces which are applied by adjacent parts of the fluid (Versteeg and Malalasekera, 1995). The first type includes gravity, centripetal, Coriolis, and electromagnetic forces although only the former is significant in reach-scale open channel flow problems and the centripetal, Coriolis and electromagnetic forces can be ignored (Lane, 1998a). There are two types of surface forces: those due to pressure gradients within the fluid and those due to viscous action between the fluid particles. The viscous stresses exerted on each face were found to be twice the local rate of linear deformation times the dynamic viscosity, μ. Consideration of the pressure gradients and these viscous shear stresses on each of the six sides of the element, in the three Cartesian directions, yields the Navier-Stokes momentum equations with source terms accounting for the body forces [4.2] (Versteeg & Malalasekera, 1995).

Thus, a systematic account of the changes in mass and momentum of the fluid element due to fluid flow across its boundaries and action of sources within the element leads to the derivation of two key equations. These are the law of conservation of mass for an incompressible fluid in Eulerian form [4.1] and the Navier-Stokes momentum equations for an incompressible fluid [4.2a,b,c].

$$\frac{\partial u}{\partial x}+\frac{\partial v}{\partial y}+\frac{\partial w}{\partial z}=0 \qquad [4.1]$$

$$x\text{-}direction: \quad \rho\left(\frac{\partial u}{\partial t}+u\frac{\partial u}{\partial x}+v\frac{\partial u}{\partial y}+w\frac{\partial u}{\partial z}\right)=-\frac{\partial p}{\partial x}+\mu\left(\frac{\partial^2 u}{\partial x^2}+\frac{\partial^2 u}{\partial y^2}+\frac{\partial^2 u}{\partial z^2}\right)$$

$$y-direction: \quad \rho\left(\frac{\partial v}{\partial t}+u\frac{\partial v}{\partial x}+v\frac{\partial v}{\partial y}+w\frac{\partial v}{\partial z}\right)=-\frac{\partial p}{\partial y}+\mu\left(\frac{\partial^2 v}{\partial x^2}+\frac{\partial^2 v}{\partial y^2}+\frac{\partial^2 v}{\partial z^2}\right)$$

$$z-direction: \quad \rho\left(\frac{\partial w}{\partial t}+u\frac{\partial w}{\partial x}+v\frac{\partial w}{\partial y}+w\frac{\partial w}{\partial z}\right)=-\frac{\partial p}{\partial z}+\mu\left(\frac{\partial^2 w}{\partial x^2}+\frac{\partial^2 w}{\partial y^2}+\frac{\partial^2 w}{\partial z^2}\right)-\rho g$$

[4.2a,b,c]

where u, v and w are the Cartesian velocity (m s^{-1}) components in the x, y and z directions respectively, ρ is the density of the water (in kg m^{-3}), μ is the coefficient of laminar viscosity (in kg m^{-1} s^{-1}) and g is the acceleration due to gravity (in m s^{-2}) and p is the pressure (Tritton, 1988; Versteeg & Malalasekera, 1995).

The application of these equations to open channel flow problems may require some modifications and additions. First, the pressure is made up of two components; the dynamic pressure produced by the flow itself and the hydrostatic pressure produced by gravitational forces. If the water surface is horizontal, a simplification of the z-direction Navier-Stokes equation (4.2c) is possible as the hydrostatic pressure and gravitational body force will balance and can thus be neglected (Lane, 1998a). If the water surface is not horizontal then the full forms of the equations must be maintained. Second, at both the channel boundaries and the free surface, special treatments will be required, as particles cannot cross either margin. In both cases, the normal velocity must reduce to zero. At the channel boundary this will result in the

exertion of a shear stress, whilst at the water surface this can be achieved mainly through vertical movement (Lane, 1998a).

4.3.2 Generic conservation equations

An analytical solution to the equations presented above is still a distant prospect. Thus, numerical methods are used to solve the equations. The transformation of the Navier-Stokes [4.2] and mass continuity [4.1] equations into a numerical model algorithm involves expressing them in a generic conservation form [4.3], which permits the use of the same solution procedure to be applied to each (Versteeg & Malalasekera, 1995).

$$\underbrace{\frac{\partial}{\partial t}(\rho f)}_{\text{Transient term}} + \underbrace{\nabla.[\rho \boldsymbol{u}.f}_{\text{Convective term}} \underbrace{- G_f.\nabla f]}_{\text{Diffusive term}} \underbrace{- S_f}_{\text{Source term}} = 0 \qquad [4.3]$$

where t is time, ρ is the density, f is the variable in question, $\mathbf{u}$ is the vector velocity, G_f is the diffusive exchange coefficient for f, and S_f is the source term. With appropriate settings for f, G_f and S_f, this general equation can be used to solve for all variables including pressure, velocity, temperature, and turbulence parameters. Solution of the equations representing the continua requires discretisation in both space and time. In PHOENICS, this is achieved using a finite volume approach (Versteeg and Malalasekera, 1995), where the domain is split into three-dimensional grid of cells (units) that have six faces. In a Cartesian grid these cells are cuboidal, although in representing more complicated geometries, cells are distorted in real space but are treated as cuboidal in computational space and in the solution procedure. Once the discretisation has been preformed, the general conservation equation [4.3] can be integrated over the cell volume. This produces (Versteeg and Malalasekera, 1995):

$$\underbrace{a = Au\rho}_{\text{Convective term}} + \underbrace{\frac{AG_f}{\Delta x}}_{\text{Diffusive term}} + \underbrace{\frac{V\rho}{\Delta t}}_{\text{Transient term}} \qquad [4.4]$$

where a is the flow across a particular face, A is the face area, u is the velocity component perpendicular to the face of interest, V is the cell volume, Δx is the

distance between cell centres and Δt is the time interval. Convection, diffusion, and transience across the face of interest are represented respectively by the first, second and third terms on the right hand side of the equation [4.4]. In steady state flows, the transient term can be neglected.

4.3.3 Numerical solution

In PHOENICS, scalar values are stored at cell centres and vector values are stored at the centres of each cell face. Thus, interpolation is required in the solution procedure to obtain scalar values at faces and vector values at cell centres. In steady flows, the main problem concerns the calculation of the convection between cells. The convective and diffusive parts of the mass flux across a cell face can be separated [4.4], which permits separate calculation. If the convected variable is a scalar quantity, its value must be determined by interpolation methods and many schemes exist for doing this. The most obvious approach is central differencing where values are calculated at the cell face using the average of the values at the two cell centres. This scheme is 2^{nd} order accurate and it is excellent for calculation of diffusion problems where properties of the flow are influenced equally in all directions. However, in problems with convection, properties do not spread equally in all directions (Roache, 1976) and downstream effects on the upstream values become less important or irrelevant. Thus, where convection is high, the central differencing scheme can become unstable and false (numerical) diffusion becomes a significant problem. The upwind differencing scheme takes into account the direction of flow: the convected variable at the cell face is equal to the upwind cell centre. This scheme is very stable in flows with very high convection. However, it is only 1^{st} order accurate, and problems occur in regions of low convection and where flow is skewed to the grid lines. Thus, careful design of the grid is required. As the grid becomes finer, this becomes less of a problem, although it may become too computationally expensive.

In open channel flow problems, where geometries are complex, there will be regions of both high and low convection. The hybrid-differencing scheme (Spalding, 1972) is based on a combination of central differencing and upwind approaches. The filter for applying the two schemes is based on the on the local Peclet number (P_e), which

is the ratio of convective mass flux per unit area by diffusion conductance at each control volume face. Where diffusion dominates (P_e<2), central differencing is applied and where convection is high (P_e>2), the upwind scheme is applied. Thus, the hybrid scheme exploits the favourable properties of both central and upwind differencing. The scheme has been widely used in most branches of CFD work and has proven very useful for simulating practical flow problems. It is fully conservative and since the coefficients are always positive, it is unconditionally bounded. Moreover, transportivness is satisfied by the switching of schemes with P_e number. The scheme produces physically realistic solutions and is highly stable when compared to higher order schemes. The main disadvantage is that the hybrid scheme is only 1st order accurate, although Waterson (1994) has demonstrated that errors due to interpolation scheme are not likely to be significant, especially when compared to boundary condition specification. Moreover, it has been the choice of scheme in most applications to natural river flow problems (*e.g.* Hodskinson, 1996; Hodskinson and Ferguson, 1998, Lane *et al.*, 1999a; Nicolas and Sambrook Smith, 1999). Thus, the hybrid-differencing scheme was applied in all solutions presented in this thesis. However, further research is required into the effects that the choice of scheme has on solutions of river channel flow problems, especially given the recent developments and improvements in higher order schemes such as the Quadratic Upwind Interpolation for Convective Kinematics (QUICK) scheme (Leonard, 1979) and X-CELL (Spalding, 2001). QUICK uses second order interpolation and is third-order accurate for convective terms (volume integrals) and second-order accurate for surface integrals or diffusive terms. Ferziger and Peric (1997) note that although the QUICK scheme is more accurate than central differencing, the differences are rarely large.

Computation of the entire flow field requires coupling of the mass continuity equation with the Navier-Stokes equations and the pressure field that drives the flow. The three momentum equations are intricately linked as each velocity component appears in each momentum equation and in the mass continuity equation. The complex issue surrounds resolving the pressure field as it appears in the momentum equation but there is no other equation for pressure. Therefore, an iterative solution procedure must be applied to fully couple the equations. In PHOENICS, this is achieved with the SIMPLEST algorithm: a variation of the SIMPLE algorithm of

Pantaankar and Spalding (1972). Although it requires more equations to be solved, it ensures more rapid convergence (Anderson *et al.*, 1984).

SIMPLEST is one version of a whole series of numerical solution schemes (SIMPLER, Patankar, 1980; SIMPLEC, van Doormal and Raithby, 1984; PISO, Issa, 1986), all of which are variants of the SIMPLE algorithm (Versteeg & Malalasekera, 1995). It is essentially a guess-and-correct procedure for the calculation. A pressure field is guessed and the discretized momentum equations are solved using this guessed pressure field. Mass continuity errors are then calculated for each cell and the pressure field and velocity are corrected for mass continuity. The velocities will now satisfy continuity but not momentum. The momentum equations are then used to re-calculate the velocities with the new pressure field and this procedure continues until errors in continuity and momentum are acceptably small. There are no set rules for convergence *per se*. In this thesis, a solution was deemed converged when the mass and momentum flux residuals reduced to 0.1% of the inlet flux and individual values in a critical part of the flow (*e.g.* close to a shear layer) were changing by less than 0.1%.

The solution of the discretized equations for the full flow field involves the transmission of the boundary conditions through the flow field. This can be done by iteratively solving the equations in a whole-field manner, which solves and stores values for each cell at once. Although this is the most accurate method of solution, it requires large amounts of memory. Thus, it tends to be very slow for large problems. Other methods exist which iteratively solve for individual slabs of cells, with other areas of the domain temporally ignored. The fluxes from the slab of interest are transmitted to adjacent slabs with sweeps through the domain. The balance of iterations and sweeps is dependent on the flow field being solved. In this study, the whole field solver was used for the pressure calculations and slab-wise procedures used for all other variables. To obtain a converged solution between 5 and 10 iterations were used for several thousands sweeps in the streamwise direction.

4.3.4 Controls on numerical solution

Convergence on a solution through the iterations can be controlled using initial conditions, value controls, and relaxation methods that can both accelerate

convergence on a solution and in some cases promote convergence rather than divergence.

Initial values of variable fields can be specified throughout the domain and should not alter the final solution. The specification of realistic values can accelerate the convergence and can prevent divergence that could lead to the solution crashing. Value controls concern specifying realistic minimum and maximum values for a certain variable during simulation and so constraining the path taken to convergence.

Relaxation involves limiting the amount of change permitted in any variable at each iteration, which can damp out oscillatory behaviour in the solution. In PHOENICS, there are two ways of implementing relaxation: linear; and false time-step. With linear relaxation, which is used primarily for the pressure correction, only a proportion of the change calculated at each iteration is added to the value for the next iteration. Linear relaxation can also be used for other variables, but when a conservation equation is being solved, false-time step relaxation can also be used. This views the change between iterations as analogous to change over time. In that the change that would occur in the absence of any relaxation requires an infinite time-step, and if this time-step is reduced, so is the amount of change that can occur. Although often some form of relaxation is usually necessary to prevent oscillations, very small values of either relaxation method will prevent any change taking place, and hence delay convergence indefinitely. The choice of relaxation will not effect the fully converged solution obtained but only promotes or accelerates the process of attainment. Unfortunately, the optimum values of relaxation to obtain convergence most rapidly are flow dependent and must be identified on a case-by-case basis.

4.4 MODELLING TURBULENCE

4.4.1 Turbulence in open channels

In open channels, the flow is highly turbulent with individual fluid particles following irregular paths. Thus, their motion displays random behaviour although this may be organised within distinct transient flow structures (*e.g.* Nezu and Nakagawa, 1993). The motion is intrinsically unsteady even with constant boundary conditions. At-a-point measurements show fluctuations in three dimensions with frequencies exhibiting random noise superimposed upon fluctuations with a range of

identifiable frequencies (Nezu and Nakagawa, 1993). Visualization studies have shown that these transient structures have the form of a rotational vortex known as an eddy. Within a flowing fluid, individual eddies exhibit cycles of generation, development, interaction and decay. The turbulent eddies have a wide range of length scales with the largest eddies determined by the channel boundary conditions. These large eddies interact with and extract energy from the mean flow through a process called vortex stretching. The mean velocity gradients distort the rotational motion of the large eddies and they are stretched in the direction of the flow. Large eddies are of the same scale as the mean flow and are dominated by inertial effects and viscous effects are negligible. Smaller eddies are stretched by large eddies and the main flow. Thus, kinetic energy is handed down to the smaller eddies in what is termed an energy cascade. The smallest turbulent motion is determined by the viscosity of the fluid. Increased energy losses are associated with turbulent flows as energy is dissipated in overcoming the action of these viscous stresses at smaller scales.

The structure of the largest eddies is stretched in the direction of the mean flow to produce anisotropy. The diffusive action of viscosity and the reduced effect of inertia at the smaller scales tends to smear out directionality and at these scales the eddies become more isotropic. The larger scale eddy motions have been observed as coherent flow structures (Nezu and Nakagawa, 1993; Ashworth *et al.*, 1996), which have a quasi-periodic or quasi-organised structure. Both bursting phenomena and large-scale vortices (Nezu and Nakagawa, 1993) have been observed in open channel flows. For example, large-scale clasts such as pebble clusters (Lawless and Robert, 2001) on the riverbed have been observed to intermittently shed eddies. The passing of busts and sweeps of fluid from the bed to the surface has also been identified (Yalin, 1992; Ferguson *et al.*, 1996; Buffin-Belanger *et al.*, 2000a,b). Coherent structures are also known to exist in and close to the shear layers between combining flows or between areas of slow and faster flows (*e.g.* Biron *et al.*, 1993b; Biron *et al.*, 1996; Bradbrook *et al.*, 2000b; Sukhodolov and Rhoads, 2001). Turbulent flow is therefore a complex mix of developing, interacting, and decaying eddy motions of different sizes, frequencies, and orientations.

4.4.2 Time-averaged methods (RANS)

Being a set of closed equations, it is theoretically known that equations [4.1] and [4.2a,b,c] can accurately describe fully turbulent flows. However, it is, in practical terms, computationally difficult to obtain a direct numerical solution of all turbulent motions in a flow field of high Reynolds number (*Re*). The required grid spacing would have to be smaller than the smallest turbulent motion and the time steps would have to be smaller than the movement of the fastest eddies. Thus, the number of grid nodes required for solving the equations shows a *Re* dependence (Younis, 1992). In the early 90's, Speziale (1991) calculated that direct numerical simulation of turbulent pipe flow (*Re* = 500000) required a computer that was 10 million times faster than the fourth generation CRAY supercomputer. Thus, even with very recent developments, the computing levels required to simulate the time-dependent Navier-Stokes equations for high *Re* flow are truly phenomenal and must await major developments in computer hardware.

To resolve these limitations in practical applications, two main approaches have been applied: (1) a statistical theory of turbulence; and (2) semi-empirical modelling of the effects of turbulent motions on the mean flow field (Rodi, 1993).

This latter approach has been the most commonly used and is based upon Reynolds (1885) averaging (RANS) (Rodi, 1993). Reynolds (1885) showed that a continuously varying signal could be split into a slowly varying mean value and a rapidly varying (random) component [4.5].

$$u_i = \overline{u}_i + u_i' \qquad [4.5]$$

where u_i is the instantaneous velocity in any given direction, $\overline{u}_i$ is the mean flow value and u_i' is the time-variant component.

Time-averaging of the mass continuity [4.1] and Navier-Stokes equations [4.2a,b,c] is carried out for a period that is long in relation to the frequency of the largest turbulent fluctuations. Although the time-averaging process [4.5] does not alter the form of the mass continuity equation [4.1], it introduces six new terms into the Navier-Stokes equations [4.2a,b,c]: the Reynolds stresses. They represent the convective momentum transfers that are produced by the instantaneous velocity fluctuations (Rodi, 1993). The Reynolds stresses are composed of three normal

stresses and three shear stresses: one of each for the three Cartesian directions. The normal stresses $-\overline{u_i'^2}$ contain squared velocity fluctuations and the shear stresses $-\overline{u_i'u_j'}$ are associated with correlations between velocity components. They are non-zero in turbulent flows and are usually very large compared to the viscous stresses (Rodi, 1993). The incorporation of the Reynolds stress terms into the Navier-Stokes equations results in the Navier-Stokes equations no longer closing. There is no direct way of obtaining the Reynolds shear stresses and they have to be modelled to allow the Reynolds averaged Navier-Stokes equations to become closed (Rodi, 1993).

Thus, the time-averaged flow field is analysed and an empirically derived turbulence model is used to account for the influence of turbulent momentum transfer on mean flow properties. Thus, the main task of a turbulence model prediction of the Reynolds stresses sufficiently accurately for this purpose. Over the years this has been a very active area for research and very many models have been developed, with increasing complexity and physical realism been incorporated as development has progressed (Rodi, 1993).

Most turbulence models apply the Boussinesq (1877) assumption that Reynolds stresses can be modelled as being proportional to the mean rates of strain with the eddy viscosity as the coefficient, ν_t (Versteeg and Malalasekera, 1995).

$$-\overline{u_i u_j} = \nu_t \left(\frac{\partial \overline{u}_i}{\partial x_j} + \frac{\partial \overline{u}_j}{\partial x_i} \right) \qquad [4.6]$$

The logic behind this equation is that turbulence production will be greatest where the flow strain rates are greatest. However, the model requires the determination of eddy viscosity ν_t. This can be done with a number of turbulence models, the pertinent ones to open channel flows will be discussed below.

4.4.2.1 Zero-equation models

In its simplest form, the Boussinesq approximation is a zero-equation model, which specifies a constant eddy viscosity throughout the flow. This closure has been applied to open channel flow problems with some success (*e.g.* Nelson and Smith, 1989a,b; Bridge, 1992), however, eddy viscosity, is difficult to measure and unlike molecular viscosity is not a constant throughout the flow field (Versteeg and

Malalasekera, 1995). As a result, formulations have been developed to relate ν_t to the flow so that its value can be calculated from the mean properties of the flow and thus account for the spatial variation of ν_t. In order to achieve this, an analogy is drawn with molecular viscosity that is known to be proportional to average velocity and the mean free path of molecules. Thus, it is assumed that turbulent eddies can be treated as parcels of fluid and ν_t can be considered as proportional to velocity and a length scale that characterizes the fluctuating motion (Prandtl, 1925):

$$\nu_t = l^2 \left(\frac{\partial \overline{u}_i}{\partial x_i} \right) \qquad [4.7]$$

It is then possible to specify simple empirical formula for the mixing length l, such as $l=kz$, where z is the distance from the nearest wall and k is the von Karman constant (Schlichting, 1955). Thus, eddies are compressed as a wall is approached. This has seen widespread application in geomorphology, as it is the basis for law-of-the-wall (Lane, 1998a). However, zero-equations implicitly assume that turbulence is dissipated where it is generated. Thus, no transport of turbulence is included in the formulation. Furthermore, they are incapable of describing flows with separation and re-circulation (Versteeg and Malalasekera, 1995).

4.4.2.2 One equation models

More complex one-equation models have been developed that attempt to model the transport of turbulence. This is based on Rodi (1980) who argues that ν_t should be characterized by the square root of the kinetic energy of turbulence per unit mass (k) as this is the most physically meaningful variable (Rodi, 1993). The kinetic energy is mainly contained in the large scale eddies and the square root of k is thus a velocity scale for the larger scales of turbulent motion. The eddy viscosity can be determined from:

$$\nu_t = c'_\mu \sqrt{k} l \qquad [4.8]$$

where C'_μ is an empirically derived constant and l is the length scale. The distribution of k can be calculated by a transport equation (Kolmogorov, 1942; Prandtl, 1945).

$$\frac{\partial k}{\partial t}+v_i\frac{\partial k}{\partial x_i}=\frac{\partial}{\partial x_i}\left(\frac{v_t}{\sigma_k}\frac{\partial k}{\partial x_i}\right)+v_t\left(\frac{\partial u_i}{\partial x_j}\frac{\partial u_j}{\partial x_i}\right)\frac{\partial u_i}{\partial x_j}-C_d\frac{k^{3/2}}{l} \qquad [4.9]$$

The equation is from left to right composed of the following terms: the rate of change of k, convective transport owing to the mean flow, diffusive transport owing to velocity fluctuations, transfer and production of k from the mean flow to turbulent motion, and transfer and dissipation of k through viscous processes (Rodi, 1993; Versteeg and Malalasekera, 1995). The equation has three empirically derived constants C'_μ, C_d, and σ_k, which have been determined experimentally (Launder and Spalding, 1972).

4.4.2.3 Two equation models

Although one-equation models represent the effect of the transport of turbulence, they fail to specify correctly the transport of the length scale. Two-equation models build on this and, in a similar way to the k, derive a transportable mixing length scale (Versteeg and Malalasekera, 1995). The length scale would be expected to show some spatial variation as eddies are transported downstream. For example, vortex shedding would reduce the size of eddies and dissipation would destroy small eddies. The most commonly used two-equation model is the κ-ε model (Launder and Spalding, 1974) where:

$$\varepsilon=\frac{k^{3/2}}{l} \qquad [4.10]$$

where ε is the dissipation rate that can be substituted into [4.9] and a transport equation can be written for ε:

$$\frac{\partial \varepsilon}{\partial t}+\bar{u}_i\frac{\partial \varepsilon}{\partial x_i}=\frac{\partial}{\partial x_i}\left(\frac{v_t}{\sigma_e}\frac{\partial \varepsilon}{\partial x_i}\right)+C_{1\varepsilon}\frac{\varepsilon}{k}\left(v_t\left(\frac{\partial u_i}{\partial x_j}\frac{\partial u_j}{\partial x_i}\right)\frac{\partial u_i}{\partial x_j}\right)-C_{2\varepsilon}\frac{\varepsilon^2}{k} \qquad [4.11]$$

The equation is, from left to right, composed of the following terms: the rate of change of ε, convective transport owing to the mean flow, diffusive transport owing to velocity fluctuations, transfer and production of ε from the from the mean flow to turbulent motion, and transfer and destruction of ε. The two equations combined have five adjustable constants C'_μ, σ_k, σ_ε, $C_{1\varepsilon}$, $C_{2\varepsilon}$. The standard κ-ε model employs

values for the constants that are arrived at by comprehensive data fitting for a very wide range of turbulent flows (Versteeg and Malalasekera, 1995). However, these values may not be constants and Rodi (1993) gives functions for the values in specific circumstances. Nevertheless, the two-equation model is the most widely applied turbulence model in CFD calculations and has been shown to give accurate results in a wide range of practical flows (Versteeg and Malalasekera, 1995), including open channel flow in a braided river (Lane *et al.*, 1995).

4.4.2.4 RNG modification

The standard κ-ε model performs poorly in flows where strain rates are high as found in swirling, rotating, curved boundary layers, or re-circulation zones. For example, Lien and Leschziner (1994) and Bradbrook *et al.*, (1998) have shown an under prediction of separation zone length with the standard κ-ε model. Thus recent applications of CFD to open channel flow problems have applied a modified form of the κ-ε model based on re-normalization group theory (RNG) (Yakhot and Orszag, 1986; Yakhot *et al.*, 1992). This has different values for the constants and an extra production term for ε. These modifications result in greater dissipation of turbulence in areas of strong strain, which reduces eddy viscosity and thus increases the length of separation zones (*see* Bradbrook *et al.*, 1998). The RNG closure is theoretically and empirically superior to the standard κ-ε model in flows with regions of significant mean strain, as found in shear layers and separation zones, and it has been the standard choice in recent open-channel CFD applications (*e.g.* Hodskinson and Ferguson, 1998; Bradbrook *et al.*, 1998; Lane *et al.*, 1999a; Nicholas and Sambrook Smith, 1999; Bradbrook *et al.*, 2000a; Ma *et al.*, 2002). It is the model of choice in all time-averaged simulations applied in this thesis.

4.4.2.5 Other time-averaged models

All the turbulence models outlined above rely upon the Boussinesq approximation and have limitations in computing turbulence-driven secondary circulation. Alternative approaches are now being developed that avoid the use of the Boussinesq approximation by determining, directly or indirectly, the Reynolds stresses through consideration of their own differential transport equations (Younis, 1992; Versteeg

and Malalasekera, 1995). However, these models are more computationally demanding, only provide a slightly better time-averaged solution and have only been applied to simple geometries (Lane, 1998a). Moreover, the American Society of Civil Engineers task committee on turbulence models in computational hydraulics (ASCE, 1988) noted that the application of sophisticated turbulence closures to open channel flow problems was proceeding without due consideration to whether this amount of sophistication was required, especially given the problems in boundary conditions specification in open channel flow applications (Lane, 1998a). However, with a suitable increase in computing power over the next decade, the use of Reynolds stress models will become more widespread in future applications to open channel flows and will provide an approach at obtaining a more accurate time-averaged solution which would incorporate the effect of turbulence driven secondary circulation that is produced by shear layer flows.

4.4.3 Transient flow modelling

The use of Reynolds averaging (RANS) and the Boussinesq approximation for the Reynolds stresses makes the Navier-Stokes equations tractable by 'averaging' temporal aspects of the flow field. RANS can thus yield important information regarding the temporally averaged flow field, but does not provide details of the structure of individual turbulent eddies or coherent flow structures, which are often present. Hence, time-averaged approaches may not adequately describe the turbulent structures that are important in system formation and alteration and the most important processes can be missed or misinterpreted (Lane *et al.*, 2000). To investigate the instantaneous flow fields and unsteady coherent flow structures numerically, a transient modelling approach is required. This can be done in one of two ways: Direct Numerical Simulation (DNS), or Large-Eddy Simulation (LES).

As mentioned above, DNS is a computationally demanding method of generating flow information as it solves the Navier-Stokes equations directly. It has recently been performed for simple situations with excellent agreement between predictions and observations (*e.g.* Le *et al.*, 1997). However, application is still restricted to low *Re* numbers because, as *Re* increases, the range of eddy sizes with significant energy dissipation also increases (Moin and Mahesh, 1998). Consequently, alternative

methods are needed for modelling flows where there is a wide range of dissipative turbulence scales, which is typically the case for open channel flow.

4.4.3.1 Large eddy simulation

LES attempts to model the larger scales of the flow directly, but approximates the smaller scales with a sub-grid scale model. RANS approaches manipulate the Navier-Stokes equations through a decomposition of instantaneous values into mean and fluctuating quantities. With LES, the re-organisation is based upon a characteristic length scale (Δ) (Ferziger and Peric, 1997; Lesieur *et al.*, 1997), which is usually the grid-size employed in the finite-volume solution of the equations (Silviera Neto *et al.*, 1993). LES is thus a compromise between RANS, where the time-averaged flow field is computed and the effect of the fluctuating components on the mean flow is modelled, and DNS, in which all turbulent fluctuations are resolved and no turbulence model is required. In LES, only the larger, slower, turbulent motions are computed directly, with a sub-grid scale model (SGS) accounting for the effect of the smaller, faster, motions on the larger ones. The main advantage of LES is that it can be applied to more complex flows at higher Reynolds numbers than currently possible with DNS. Moreover, the larger scales of flow are likely to be directly affected by site-specific boundary conditions and are thus characteristic of the system. The effect of the smaller scale motions on larger ones can be specified by certain 'universal' turbulence parameters obtained from the SGS model (Rogallo and Moin, 1984).

Within the spectrum of turbulent scales, a level has to be defined which separates those scales of motion that are solved directly, and those that are modelled by the SGS model. As mentioned above, in the model applied in this study, the separation of these scales is based upon the average grid spacing. The large, directly resolvable scale of a quantity f, is given by (Leonard, 1974):

$$\bar{f}(x) = \int_D G_\Delta (x - \tilde{x}) f(\tilde{x}) d\tilde{x} \qquad [4.12]$$

where D is the integration control domain and G_Δ is a filter function of length Δ that is obtained from the grid cell size Δx_i (Lesieur *et al.*, 1997):

$$\Delta = \left[\prod_{i=1}^{3} \Delta x_i \right]^{\frac{1}{3}} \qquad [4.13]$$

Application of a filter function through the equations enables quantity f to be decomposed into grid-scale ($\bar{f}$) and subgrid-scale ($\breve{f}$) components. Thus ($\breve{f}$) represents the effects of fluctuations in the subgrid scale flow upon the grid-scale flow obtained from the filtering process. Many different types of filters can be applied to perform this separation of scales, and Pope (2000) provides a discussion on the various type and their relative properties. The most commonly used filters are the box or top-hat filter (Lilly, 1967; Deardorff, 1970; Silveira Neto *et al.*, 1993), the Gaussian filter (Lesieur *et al.*, 1997) and the spectral filter (Härtel and Kleiser, 1997). The box filter has good spatial localization but does not allow unambiguous separation between scales because of spectral overlap. The spectral filter cleanly separates between the scales but when filtering spatially localized phenomena it can cause non-local oscillatory behaviour (Meneveau and Katz, 2000). However, according to Härtel and Kleiser (1997) and reflecting the philosophy of LES, the choice of filter should make little difference to the solution, particularly as cell size reduces.

Averaging [4.11] over the cell volume for both the mass conservation [4.1] and Navier-Stokes equations [4.2] results in the filtered terms ($\bar{f}$) replacing the full terms (f). It also results in an additional stress tensor term T_{ij} appearing in the Navier-Stokes equations. The stress tensor T_{ij} is produced by the subgrid-scale (SGS) fluctuations acting on the grid scale in the flow field:

$$T_{ij} = \bar{u}_i \bar{u}_j - \overline{u_i u_j} \qquad [4.14]$$

The important difference between RANS and the averaging of [4.11] in the Navier-Stokes equations [4.2] is that the latter retains a time derivative, permitting the solution of problems involving unsteady flows. However, T_{ij} remains unknown and must therefore be modelled using a subgrid scale model (Rogallo and Moin, 1984; Lesieur *et al.*, 1997).

4.4.3.2 *Subgrid scale models*

Subgrid models (SGS) act to approximate energy exchange between the grid and subgrid scales (Rogallo and Moin, 1984). The direction of this energy transfer is mainly from the larger to the smaller eddies ('the energy cascade'). However, an inverse transfer of energy ('backscatter') from small to larger spatial eddy scales can occur and is particularly important in the wall region and in shear layers (Leith, 1990; Kosovic, 1997). An ideal SGS model should be able to capture both the forward and backscatter energy transfers as both wall regions and shear layers are of importance when modelling open channel flow. The importance of SGS model accuracy to the solution of a given flow is highly dependent upon the relationship between the scales of turbulent flow present and the grid size employed in the solution of the flow. Open channel flows have complex boundary conditions and high *Re* numbers which result in a large range of eddy size and a greater proportion of flow energy contained in the smaller scales of motion. Under these circumstances, computational limits mean that coarser grids are often required and the importance of the SGS model performance increases significantly (Rodi *et al.*, 1997). Indeed, Hardy *et al.* (in press) highlight the importance of grid resolution for the reproduction of temporal aspects of the flow field. They found that the use of coarse grids in the LES model could result in no flow periodicities being reproduced, although as grid resolution was increased, some periodicities are reproduced. Further refinement in the grid resulted in higher frequency flow structures being reproduced. Hardy *et al.* (in press) noted that the definition of a grid independent solution in LES was thus problematical.

4.4.3.3 *The Smagorinsky SGS model*

The aim of a SGS model is to estimate T_{ij} accurately. The simplest and most widely applied SGS model follows Smagorinsky (1963) and this SGS model is applied in this thesis. It has been used in modelling many types of flow (*see* Ferziger and Peric, 1997) including recent applications to open channel flow problems (Thomas and Williams, 1995; Shi *et al.*, 1999; Bradbrook *et al.*, 2000b; Li and Wang, 2000). Applying an eddy-viscosity (Boussinesq, 1877) and a mixing-length (Prandtl, 1925) assumption Smagorinsky (1963) calculated the SGS stresses as:

$$\tau_{ij} = -2\rho\nu_t \vec{S}_{ij} \qquad [4.15]$$

where ρ is fluid density, ν_t is eddy viscosity and S_{ij} is the local mean strain rate, given by:

$$\vec{S}_{ij} = \frac{1}{2}\left(\frac{\partial \vec{u}_i}{\partial x_j} + \frac{\partial \vec{u}_j}{\partial x_i}\right) \qquad [4.16]$$

where $\vec{u}_i$ is the component of velocity in the direction x_i, and the eddy viscosity is calculated using a mixing length hypothesis similar to that of Prandtl (1925):

$$\nu_t = l^2\left(2\vec{S}_{ij}\frac{\partial \vec{u}_i}{\partial x_i}\right)^{\frac{1}{2}} \qquad [4.17]$$

where l is the mixing length of the unresolved eddies defined by:

$$l = \min(C_s h_s, \kappa . d_w) \qquad [4.18]$$

where C_s is the Smagorinsky constant, h_s is the average mesh interval spacing, d_w is the normal distance to the closest wall and κ is the von Karman constant (0.4). Thus, the two adjustable parameters within the Smagorinsky SGS model are the Smagorinsky constant C_s and the local grid spacing.

Grid resolution should be sufficient that the scales of interest are adequately resolved. As the grid is refined, the accuracy of the SGS model matters less (Rogallo and Moin, 1984). Indeed, Fureby *et al.* (1997) confirmed that if grid resolution is adequate, the SGS model is not critical for correctly reproducing the macroscopic flow properties. Thus, the philosophical basis for LES is that a mesh resolution is chosen such that the sub-grid scales can be assumed to isotropic and homogeneous. If this is the case, the majority of the flow energy will be contained in directly resolved grid scales. Equation [4.18] demonstrates that the application of LES to anisotropic grids will become a problem because the definition of the length scale filter [4.18] will vary over the domain. Thus, as anisotropy increases the rate of strain of the flow becomes ambiguous and is more a function of grid anisotropy rather than flow property (Scotti *et al.*, 1993). As one of the objectives of this thesis is to ascertain the applicability of LES to open channel flow, this effect will be examined.

The value of the Smagorinsky constant has been determined both experimentally and using DNS and it is thought to range between 0.07 and 0.24 (Rogallo and Moin, 1984). Lilly (1966) through theoretical calculation based on the Kolmogorov spectrum obtained a value of 0.17. However, Deardorff (1970) found that a value for C_s of 0.1 gave improved results, although he also found that values of C_s reduced with increasing rates of strain in homogenous turbulence damping out some large-scale motions. Piomelli *et al.* (1988) proposed a value of 0.10 and Lesieur *et al.* (1997) suggested a value of 0.18 for shear layer flows. Although it could be important in damping out fluctuations, as the grid spacing reduces, the less the stresses computed by the Smagorinsky model will affect the solution, and the less the value of the constant will matter (*c.f.* Rogallo and Moin, 1984).

4.4.3.4 Limitations of Smagorinsky SGS model and alternatives

Although the Smagorinsky SGS approach is a popular method, it suffers from being only dissipative. Thus, it does not account for backscatter effects (Lesieur, 1997; Kosovic, 1997). Furthermore, although C_s is known to vary, the Smagorinsky SGS model applies a uniform C_s value throughout the solution that inevitability introduces errors into the simulation. This has led to a number of alternative approaches that can improve the formulation. These include: SGS models that relate eddy viscosity to the kinetic energy of the SGS eddies (Schumann, 1975); SGS models that use transport equations for individual SGS stresses (Deardorff, 1973); SGS models that have the ability to incorporate some backscatter effects, including a scale-similarity model (*e.g.* Kosovic, 1997) and a spectral eddy-viscosity model (Chollet and Lesieur, 1981); and other models that incorporate dynamic functions which adjust C_s values (*e.g.* Germano, 1992). Meneveau and Katz (2000), Vreman *et al.* (1997), and Silveira Neto *et al.* (1993) provide comparisons between several SGS models for 3D flow in several situations that include a temporal mixing layer and flow over a backward-facing step. They all found that the recent dynamic SGS models offer a number of advantages over simpler approaches and that the Smagorinsky model was consistently the weakest of the SGS models examined. However, these newer models tend not to have been tested as rigorously as the simpler and earlier methods, especially at higher *Re* numbers. Moreover, Rodi *et al.*, (1997) note that as the grid resolution is improved and the energy of subgrid-scale motions becomes smaller with

respect to the grid scale flow, the type of SGS model used is not of great importance because its primary function increasingly becomes that of dissipation.

4.4.3.5 Time solution

In LES, time remains in the Navier Stokes for grid scale fluctuations, and the formulation therefore requires a time-dependent solution. There are two main approaches to the incorporation of time into unsteady solutions: explicit, where values at a given time step are calculated directly from values at the previous time step; and implicit, where time dependence enters as a boundary condition to the solution.

Shorter time steps in the solution will mean that fewer iterations are required at each time step and the solution will be temporally more accurate, but there is a trade off with computation time. The time step applied in the solution must be faster than the smallest grid scale large eddy. Moreover, the time step must also be small to ensure convective stability of the solution. In applications where time is incorporated explicitly, the Courant number (Cr) is a key parameter and can be used to characterise the stability of the solution (Ferziger and Peric, 1997). The Courant number represents the ratio of the time step of the solution to the typical convection time and is defined by:

$$Cr = u\frac{\Delta t}{\Delta x} \qquad [4.19]$$

When diffusion is negligible, an explicit time dependent solution will be stable if the value of Cr is < 1. PHOENICS employs an implicit solution scheme and Cr is not strictly applicable. Nevertheless, Bates *et al.* (1997) argue that the Courant number has a physical basis, and so even in implicit schemes, it can be a good measure of solution stability. They recommend that a Cr value below 50 demonstrates sufficient stability of implicit schemes. The Cr value is therefore computed for each LES application in this thesis.

4.4.3.6 *Additional considerations in LES applications*

There is some evidence to suggest that the choice of numerical scheme applied in solving LES may be more critical than for the solution of RANS. This is especially true for schemes such as upwind difference, where artificial viscosity can become high. High levels of artificial viscosity and false diffusion are dissipative mechanisms that can damp and distort the physical representation of both the large and small eddies (Rogallo and Moin, 1984). However, the nature of this effect is difficult to quantify and requires further research. This is beyond the scope of this thesis.

The relaxation applied in the solution of the equations also becomes an issue in LES. If the relaxation applied to the equations is very high, fluctuations in the flow field may be damped out. Thus, the false time step applied in the relaxation must be below or equal to the time step applied in the LES.

The upstream boundary conditions applied in LES could have a significant effect on the variability of the flow field within the computed domain. In simple applications where the planes of the upstream and downstream sections are the same size, a periodic boundary condition can be applied, where the flow at the downstream outlet becomes the upstream inlet (*e.g.* Deardorff, 1970; Thomas and Williams, 1995a,b). Other methods include superimposing a random perturbation on the mean inflow velocity, such as the use of spectral line processors (Li and Wang, 2000), or using another LES model to generate unsteady inflow conditions to a second model. However, the sensitivity of LES to different inflow conditions remains difficult to determine. As the aim was to model inherent instability in the flow produced by the shear effects no fluctuations were superimposed on the main incoming flow. Nevertheless, it is an area future research on LES application to open channel flow should consider especially in light of possible short-term flow pulses (Grass, 1971; Buffin-Belanger *et al.*, 2000a,b).

4.4.3.7 *LES summary*

At present, for high *Re* flows over complex geometries, LES is the only method that can provide a transient flow solution. LES solves directly for the large eddies using a SGS model to simulate the effects of the SGS stresses on the large eddies.

Although the Smagorinsky model would appear to be the least effective of a range of SGS models, it is the most popular model and has been the choice of recent applications of LES to open channel flow. The Smagorinsky model is applied in all LES model runs in this study, although to counter some of its limitations a very fine grid resolution is used. Sensitivity checks for grid resolution are performed, analysed and detailed.

4.5 APPLICATION OF CFD TO OPEN CHANNEL FLOW

Sections 4.1 to 4.4 outlined the basic equations, solution methods, and turbulence closure schemes. This section addresses the specific application of CFD to modelling open channel flow problems.

4.5.1 Numerical grid

4.5.1.1 Grid construction

The geometry of the domain over which fluid flow is calculated must be defined. The finite volume approach to solving the Navier-Stokes equations requires the discretisation of this solution domain into a number of six-sided cells. In a CFD model, a distinction is made between Cartesian space (x,y,z) and computational space (i,j,k). The latter is regular, while the Cartesian space may or may not be regular. However, for complex geometries such as natural river channels, the grid cells in Cartesian space must be distorted to fit the domain using boundary fitted co-ordinates (BFC). Thus, the spatial domain is divided into cells that are regular in the computational domain, but irregular in the Cartesian domain. The discretisation process can have a large effect on the model's performance and careful consideration has to be given to the way in which the grid is constructed (Lane *et al.*, 1999a). This is because grid distortion can control the numerical stability of the solution and may result in numerical diffusion. Numerical instability was therefore minimised by keeping changes in grid line direction between cells to <30° and avoiding rapid changes in cell aspect ratio.

In PHOENICS, grid generation begins by defining the points along the boundary of two or more cross-sectional frames. Points along the boundaries are then connected

using linear interpolation or curve fitting techniques. The corner points on each frame are defined, creating a four-sided plane onto which a 2D grid of specified dimensions is mapped. A specified number of additional frames with constant grid dimensions are then linearly interpolated between those defined, creating a 3D grid. Thus, a curvilinear computational grid with fixed user-specified numbers of cells in the streamwise, transverse, and vertical directions is created.

4.5.1.2 Grid resolution

The number of cells determines the resolution of the flow details calculated and the amount of error in the discretisation process, but the finer the grid the greater the computational time. Moreover, the grid spacing must be small enough to obtain a solution that is independent of the grid being used. In order to demonstrate grid-independent or grid-convergent results and to systematically evaluate truncation error and accuracy, solutions over a range of significantly different grid resolutions should be performed.

The approach applied in this thesis was to perform an initial solution with a grid spacing identified from experience as that required for the flow domain under consideration and then coarsening (x 0.5) and fining (x 2) the grid spacing. Error estimates based on Richardson extrapolation were then performed to demonstrate solution accuracy (4.6.2) as part of model verification.

4.5.1.3 Topographic representation

In Cartesian grids, the number of planes, either defined or interpolated, merely affects the grid resolution of the solution. In a BFC grid, the number of planes also affects the resolution. However, the ratio of defined planes to interpolated planes has a significant effect on the representation of the 'real' geometry. The quality of the representation of the 'real' topography also depends upon the number of points used in definition of a frame and any adjustments that are required to improve the numerical stability of the grid.

Thus, one of the main issues in the application CFD models to natural open channel flow problems is the representation of the channel morphology through construction

of a BFC grid. In open channel flow problems, the defined frames in the BFC grid are cross sections that are either directly surveyed (*e.g.* Hodskinson and Ferguson, 1998) or extracted from a digital elevation model (DEM) of the channel geometry (*e.g.* Lane, 1998b). This poses a problem, as discrete point sampling is required to represent the continuous surface of a natural channel.

This process of obtaining field topographic data and incorporating it within a model involves filtering the topographic detail present within reality. In reach scale flow modelling, co-incidence of the grid nodes and sampled points is unlikely. For reasons of grid independence, the grid size within the model is much smaller than the sampling interval in the field. Thus, interpolation techniques are required that replace the information that is 'lost' in this field sampling process. This interpolation effectively creates an artificial surface (Lane, 1998b), where the interpolated surface is unlikely to represent the exact surface between the surveyed points. The surface created by interpolation is then sampled to create the geometry for the construction of the computational grid, which is another layer of spatial filtering. Therefore, as the grid size reduces below the resolution of the field data, the model increasingly becomes dependent upon field sampling, point interpolation, and grid interpolation. This has significant implications for grid independence: how does one obtain a grid independent solution over a continuously varying topography?

The topographic detail not represented at sub-grid scales is often incorporated in the model through an increase in the bed and bank roughness parameter, although variation at scales above the sub-grid scale but smaller than that represented by the survey is lost. The topography represented in the model and the specified boundary roughness are thus intrinsically linked. The importance of topographic representation in open channel flow modelling and how the spatial filtering that occurs in the construction of the grid affects the predicted flow field has not been addressed and is a consideration of this thesis.

Adjustments to the grid are sometimes required to improve numerical stability. For example, the inclusion of small sections of vertical lines is often required at the top of the banks, especially where shoaling occurs at a bankline with a point bar. Furthermore, sudden changes in direction produced by large boulders on the bed or small bank collapses have to be removed from the computational grids (*e.g.* Bradbrook, 1998).

4.5.1.4 Turbulence model implementation

All time-averaged solutions obtained in this thesis used the RNG modified form of two-equation κ-ε model. As mentioned above, this model performs better in areas where flow separation is present and has become the standard choice in recent applications of 3D CFD to open channel flow.

Large eddy simulation was applied with the initial conditions of the flow field specified as the RANS solution. These initial conditions will affect the progression of the LES solution. However, after a sufficient number of time steps most flows will develop a statistically stable state. Checks were performed to certify that a statistically stable state had developed; this often required that at least the first 1000 solution time steps of each LES solution was disregarded. In the LES model solutions, sensitivity to grid resolution is likely to be significant and is assessed. However, the PHOENICS default value for the Smagorinsky constant of 0.17 was used and the sensitivity of the solution to this value was not assessed. This assessment is left as an avenue for further research.

4.5.2 Boundary conditions

4.5.2.1 Wall treatments

It is necessary and extremely important to specify the conditions at the solid boundary interface. At the solid boundary, the normal velocity components will reduce to zero. If a no-slip condition is assumed at the bed, then u and v must also be zero and a bottom stress must be derived from the surrounding flow properties.

Classic boundary-layer flow close to a wall consists of a viscous sub-layer adjacent to a turbulent region (Schlicting, 1979). There are very strong velocity gradients away from the wall in this region that generate the large amount of turbulence (Grass, 1971; Grass and Mansour-Tehrani, 1996), which are responsible for energy dissipation due to friction at the wall. Satisfactory solution of the flow close to the wall requires a very fine grid to resolve the viscous effects within the sub-layer. However, in practice, the large-scale flow dynamics are of interest and the resolution of these strong gradients is not practical. Thus, a suitable empirical approximation is introduced which models the effect of the near-wall flow on the outer flow. This is achieved by ensuring that the centre of the first cell lies outside the laminar sub-layer

and a wall function is used to estimate the velocity and turbulence parameters at the centre of this cell. Shear further from the boundary is modelled explicitly.

The size of the laminar sub-layer is important in modelling the effects of the wall. Thus, in the treatment of the wall region, distance from the wall, y, is often normalised with respect to laminar viscosity (υ), bed shear stress (τ_b), and the density of water (ρ) to give a non-dimensional wall unit measurement (y^+):

$$y^+ = \frac{\sqrt{\tau_b / \rho}}{\upsilon} y \qquad [4.20]$$

The depth of the laminar sub-layer immediately next to the wall (δ) is then given as $11.6y^+$ (Keulegan, 1938). Above this laminar layer, a defect region develops that is affected by the wall and where velocities are reduced and eddies are damped. Prandtl, (1925; 1952) derived a logarithmic relationship which describes the effects of the wall in this region:

$$\frac{u}{u_*} = \frac{1}{\kappa} ln\left(\frac{y}{y_o}\right) \qquad [4.21]$$

where u is the velocity, u_* is the shear velocity $= \sqrt{\tau_b / \rho}$, κ is the Von Karman constant (=0.4), y is the distance from the bed and y_o is the height of zero velocity which depends on the bed roughness. This is the standard law-of-the-wall, which has been extensively applied in open channel flow problems. The relationship between y_o and the bed roughness has been found to vary depending on the relationship between the depth of the sub layer and the size of roughness elements on the bed (Nikuradse, 1952).

$$\begin{aligned} y_o &= \frac{\upsilon}{9u_*}, \quad \text{for smooth beds } (D_{65} < \delta) \text{and} \\ y_o &= \frac{1}{30} D_{65}, \quad \text{for rough beds } (D_{65} > 5\delta) \end{aligned} \qquad [4.22]$$

where D_{65} is defined by the size of the sixty-fifth percentile of the grain size distribution of the surface (Nikuradse, 1952).

The distinction between rough and smooth beds depends whether viscous effects or roughness elements dominate the energy dissipation, and there is a zone of transition

($\delta < D_{65} < 5\delta$). The law-of-the-wall only applies in the region of the flow affected by the wall above the laminar sub layer, standards are applied such that suggests that y^+ values should be between the values of 30 and 300. However, in boundary fitted co-ordinate grids constructed for natural channels it is often difficult to achieve this over the whole bed region since cell heights can differ greatly across the channel.

As mentioned above, the standard law-of-the-wall function is simply based upon the standard near-wall logarithmic velocity profile and it assumes that turbulence production and dissipation are equal. However, this is not the case in many situations and the use of the standard law in areas of high roughness and where flow separation is present, has been questioned (*e.g.* Ferro and Baiamonte, 1994). The non-equilibrium wall treatment (Launder and Spalding, 1974) relaxes this assumption. It applies $\sqrt{K}$ (the square root of turbulence energy) rather than u^* (the shear velocity) as the characteristic velocity scale, consequently providing a more realistic approximation of the wall conditions in separated flows. This is because separated flows diffuse a significant quantity of turbulence towards the wall, breaking the conditions of local equilibrium upon which the u^* formulation is based (Launder and Spalding, 1974). Thus, for the flows considered in this thesis, the non-equilibrium wall functions are employed. However, as LES does not solve for turbulent kinetic energy the standard law is applied in LES model runs.

The roughness parameter (D_{65}) applied in both formulations is defined by the size of the sixty-fifth percentile of the grain size distribution (Nikuradse, 1952). However, this formulation is based upon sand distributions. The use of the grain size in estimating y_o is not appropriate with wide ranges of grain size or where bedforms are present. In such situations, the value of D_{65} requires adjustment. For example, in gravel bed rivers, the Nikuradse roughness height, k_s, has been found to be dominated by the larger clasts and bedforms and, k_s has been put at 3.0 to 3.5 times the D_{84} or D_{90} or 5.2 times the D_{65} (Bray, 1980; Ferguson, 1986; Clifford *et al.*, 1992a,b and many others). The amount of adjustment required in the roughness parameter is dependent on the amount and size of bedforms and the scales of topographic variation that is represented within the grid (4.5.1.2) and the two are linked. In this thesis, application to natural channels used a roughness bed formulation with k_s based on 3.5 times the D_{65} of the sediment distribution on the inflow riffle to each bend.

Most applications of three-dimensional numerical flow models have applied a constant bed roughness height throughout the domain. However, in many situations in open channel flow, such as meander bends, reach scale sorting can be significant. This may causes large variations in k_s over the bed and banks. Although studies have shown that three-dimensional models are less sensitive than two-dimensional models to roughness specification (Lane *et al.*, 1999a), Booker *et al.* (2001) have suggested that velocities close to the bed and banks are very sensitive to roughness. The effect of a spatially variable roughness is unknown and could have a significant effect in near-bed velocity and shear stress predictions. The investigation of model sensitivity to spatially variable roughness is not explicitly assessed in this thesis and is left as an area that requires more research.

4.5.2.2 Inflow distribution

To provide an inflow velocity distribution for the model, the inflow characteristics in the furthest upstream reach are required. The inflow data must comprise velocity vectors in all three dimensions and turbulence parameters κ and ε for each grid cell. Two main approaches can be applied: specifying constant values for all cells in the inflow section and allowing the flow to develop; or specifying individual values for each cell based on theoretical considerations or empirical measurements.

To avoid the extra computation of including upstream flow development, in the case of a rectangular cross section inflow, such as in a flume, a fully developed inflow can be prescribed by a separate model that calculates a fully developed flow profile. The model requires the dimensions of the channel and the mass-flow rate to be defined and the fully developed flow profile is derived for an infinitely long channel. The mean axial pressure gradient required to generate the desired mass flow rate is calculated from overall continuity considerations (Pantaankar and Spalding, 1972) using:

$$\frac{dp}{dx} = 0.5\frac{f\rho(u_{in})^2}{D} \qquad [4.23]$$

$$f = 1/(1.82\log_{10}(Re) + 1.64)^2 \qquad [4.24]$$

where u_{in} is the cross-sectional average velocity, f is a friction factor and D is the hydraulic radius. The calculated velocity profile provided the inflow conditions for all model runs of the laboratory flume.

This fully developed flow profile model is only applicable to regular channels and could not be applied for irregular inflow cross sections. The inlet flow distributions for the field case bends were therefore prescribed by different methods. Where field measurements had been made, law of the wall was fitted to each vertical profile. The values for each grid node were then calculated for the correct height in the profile. Estimations for each vertical profile of grid cells between those measured were performed using linear interpolation. This was performed for velocities in each direction, which provided the inflow velocity distribution for the bend. Values of kinetic energy of turbulence were also calculated from the measurements and were interpolated across the section in a similar manner.

In modelling some hypothetical cases and field bends with only a specified discharge for the inflow, a different method of inflow distribution was required. This was achieved using the total discharge and calculating the velocity in each cell based upon the cell distance from any boundary using law of the wall. Uniform values of turbulent kinetic energy, κ, and dissipation, ε, were calculated by:

$$\kappa = (T_i u_{in})^2 \qquad [4.25]$$

$$\varepsilon = 0.1643 \frac{\kappa^{\frac{3}{2}}}{l} \qquad [4.26]$$

where T_i is turbulent intensity, which was set at a nominal value of 10%, where u_{in} is the cross-sectional average velocity, and l is a mixing length taken as $0.1d$ where d is the average depth of the channel across the section.

4.5.2.3 Outflow conditions

At the outlet profile, a hydrostatic pressure distribution was applied across the cells and calculated pressure values in the domain were defined relative to this. Consequently, the outlet had to be far enough away from the effects of any negative

dynamic pressure zone within the domain and where the flow was approximately hydrostatic.

4.5.2.4 Free surface

The spatial variation in the position of the free surface, through superelevation or depression, is a significant degree of freedom in open channel flow (*e.g.* Dietrich, 1987; Bridge, 1993; Rhoads, 1996). Temporal variation in free surface elevation could also be related to the flow structures (*e.g.* Kimura and Hosoda, 1997). However, many applications of numerical models to open channel flow have applied a 'rigid lid' assumption (*e.g.* Demuren, 1993; Noat *et al.*, 1993; Meselhe and Odgaard, 1998). This involves setting a symmetry plane at the water surface, across which all the normal derivatives and velocities are set to zero (Bradbrook *et al.*, 2000a). The pressure at the surface is not set to zero and varies to reflect the effective free surface if the lid were not fixed (*e.g.* Meselhe and Odgaard, 1998). As a result, the free surface is accounted for in the pressure gradient term in the momentum equations and will accurately represent the effects of surface deviation upon the momentum equations (Leschziner and Rodi, 1979). However, the pressure terms do not enter the mass continuity equation. This may result in overestimation of velocity in zones of superelevation and underestimation in zones of depression (Bradbrook *et al.*, 1998; 2000a). This effect has also been shown to alter predictions of re-circulation zone length downstream of obstacles (Ouillon and Dartus, 1997).

These free surface effects can be included in the solution through a number of different treatments. Direct treatments of the free surface effects such as the marker and cell method (MCM) and the volume of fluid technique (VOF) (Hirt and Nichols, 1981) involve re-calculating the vertical extent of the grid or considering the fractions of gas and liquid in interface cells as the solution proceeds. Indeed, Ma *et al.* (2002) recently applied the VOF method in simulating open channel flow in a straight reach. However, these direct treatments have been shown to have severe stability restrictions, especially where dynamic pressure fluctuations are high (Casulli and Stelling, 1998) and where the grid is irregular.

Alternatively, a free surface can be defined by implementation of a porosity correction. This applies a symmetry plane across the free surface and accounts for

the effects of the free surface by specifying a variable porosity in the surface layer of cells (Spalding, 1985). In this formulation, the porosity for each surface cell is calculated, with the flux across any cell face equal to the porosity multiplied by the area of the face and the perpendicular velocity component. A perturbation of porosity from 1.0 represents an effective change in height of the cell. The porosity is calculated so that the pressure deviation on the rigid lid is satisfied by this effective change in height:

$$P_f = 1 + \frac{S_p}{\rho g h_c} \qquad [4.27]$$

where P_f is the cell porosity, S_p is pressure on the surface, ρ is the density, g is the acceleration due to gravity and h_c is the surface cell thickness. Therefore, porosity is greater than 1.0 where surface pressure is greater than zero and below 1.0 where pressure is below zero. This correction represents the free surface in the mass continuity equation by altering the effective discharge through the surface cells. Thus, the effective discharge is increased in cells where the surface is superelevated, resulting in a reduction of predicted velocity, and reduced where the surface is depressed, resulting in an increase in predicted velocity. This correction is introduced once a solution has been obtained with a normal rigid-lid treatment.

This free surface approximation has been successfully applied to many three-dimensional open channel flow problems including flow around groynes (Ouillon and Dartus, 1997) and flows in open channel confluences (Bradbrook *et al.*, 1998; 2000a). Recently, Biron *et al.* (in press) found that measured spatial patterns of free surface elevation in a natural confluence broadly correspond to those simulated using this free surface approximation.

4.6 VALIDATION AND VERIFICATION

These CFD models have been developed by applied mathematicians and civil, mechanical and chemical engineers. They are therefore designed for general application to many types of flow process. Hence, application to open channel flow processes raises a number of methodological and philosophical issues (Lane and Richards, 2001), which have to be addressed.

The terminology applied in this process is that validation refers to the correct determination of variables predicted by the model and verification is associated with the correct solution of the model to produce these predictions. Thus, verification involves checking for coding errors as well as errors associated with both spatial and temporal discretisation and numerical solution. If these errors have been minimised then validation will yield the error due to the specification of system geometry, initial conditions, boundary conditions and parameters, as well as to process representation decisions, such as law of the wall or turbulence closure applied. Thus, validation is a fuller model assessment process with significant linkages with verification, which can be seen as the first step towards model assessment.

4.6.1 Model development

The development of a numerical model involves many stages, the first of which is the construction of a conceptual model (Howes and Anderson, 1988). It involves the translation of conceptual linkages to mathematical formulations, and transference of these formulations into numerical algorithms that requires discreteisation of the continuous variables through time and space. The use of a computer in the numerical calculations requires programming of the numerical algorithms into computer code. This is a cyclical process through model development and then refinements. Certain assumptions have to be made at each of the stages of model development and their effects must be analysed, both in general and for each application of the model to specific problems (Lane and Richards, 2001).

4.6.2 Verification

As mentioned above, verification is concerned with obtaining the correct solution to the equations applied. Coding of numerical algorithms should be assumption and error free, and it has to be assumed that PHOENICS had been verified by the developers at CHAM for internal consistencies within the code. Thus, verification focused upon errors associated with spatial and temporal discretisation specific to this study. Many editorial statements for engineering journals (*e.g.* AIAA; ASME) state that the most important activity in verification testing is systematically refining the grid size and time step to estimate the discretisation error in the numerical

solution. Indeed, most state that validation by comparison with check data is not necessary and is no substitution for verification.

As the discretisation interval (Δ) tends to zero the code should converge mathematically upon the correct solution of the continuum equations. The solution is verified at a given discretisation interval if model predictions are within some acceptable range of the correct solution. However, as discretisation interval (Δ) reduces, computational costs increase. There is therefore a need to specify a grid resolution that produces a sufficiently grid independent solution.

Although CFD models have been applied in fluvial geomorphology for a few years, there are still few formal frameworks for the systematic verification of numerical models. For example, many studies state that mesh independence was determined, although few provide the details. Those that do (*e.g.* Bradbrook *et al.*, 1998) based grid independence on the variations in predictions of key parameters, and used a mesh resolution in which variation was slight from the finest used. The choice of variation is commonly arbitrary and difficult to conceptualise in terms of significance. Furthermore, except for the Courant number indicating solution stability, no methods whatsoever have been introduced to check for the effect of the time step on LES calculations in open channel flow modelling (*e.g.* Bradbrook *et al.*, 2000b).

In order to address the issue of verifying grid discretisation in simulations of open channel flow, Hardy *et al.* (in press) have recently applied an approach, applied in engineering for many years, which provides a systematic method to report the credibility of simulations: this method is based upon a Grid Convergence Index. The section below is based on the derivation in Hardy *et al.* (in press).

4.6.2.1 Grid convergence index (GCI)

The grid convergence index (GCI) is a general method for reporting the sensitivity of model solutions to numerical discretisation. It was originally proposed by Roache (1994, 1997, 1998). Using the theory of generalised Richardson extrapolation, it is an index of the uncertainty associated with a solution at a particular grid resolution, based on comparison with the solution at other resolutions. This theory assumes that, within a certain radius of convergence, the discrete solution for some flow variable f

converges monotonically at all points in the continuum as the grid spacing h tends to zero (Roache, 1997). The error is given by a power series in h:

$$f = f_x + g_1 h + g_2 h^2 + g_3 h^3 + \ldots \quad [4.28]$$

where f_x denotes the exact solution and g is defined in the continuum which is not dependent on the discretisation. For a solution method accurate to order p,

$$f = f_x + g_p h^p + \text{higher-order terms} \quad [4.29]$$

If two such solutions exist, f_1 on a fine grid of resolution h_1 and f_2 on a coarser grid of resolution $h_2 = r\,h_1$, then elimination of g_p yields

$$f_x = f_1 + (f_1 - f_2)/(r^p - 1) \quad [4.30]$$

If the higher-order terms can be neglected, error estimates for the two solutions can be obtained:

$$E_1 = f_x - f_1 = \varepsilon/(r^p - 1) \quad [4.31]$$

where $\varepsilon = f_1 - f_2$ for the fine mesh, and

$$E_2 = f_x - f_2 = \varepsilon\, r^p/(r^p - 1) \quad [4.32]$$

for the coarse mesh.

In the particular case of grid doubling with a second-order solver, these reduce to $E_1 = \varepsilon/3$ and $E_2 = 4\varepsilon/3$. These are absolute errors, which can be expressed as absolute percentages. Roache (1997) defined the GCI for a particular grid as the error estimate multiplied by a factor of safety F_s:

$$GCI^{fine} = F_s\,|E_1| \quad [4.33]$$

$$GCI^{coarse} = F_s\,|E_2| \quad [4.34]$$

$F_s = 1$ makes the GCI a median error, whereas $F_s = 3$ gives a conservative upper limit akin to a 99.9% statistical confidence interval. For the latter, it reduces simply to ε for $r = p = 2$, but has the advantages of allowing for the formal order of accuracy of the solution method and application to any degree of grid refinement, not just doubling. This is important as where computational limits prevent a mesh doubling, it will still be possible to get an estimate of the GCI provided the refinement is sufficient. Roache (1994) recommended a minimum 10% change in r since as r tends to zero, f1-f2 may become swamped by noise due to other influences. It is also

recommended that where mixed grid resolution changes are made (i.e. one orthogonal axis is changed by a different r than another) the highest value of r is taken.

The assumption of asymptotic convergence is especially important and applies to any sort of grid convergence study. Although the leading order term in a Taylor series analysis of a spatial discretisation scheme provides a meaningful estimate of convergence rate, this only holds as the grid spacing approaches zero (Haworth *et al.*, 1993). Extrapolation to zero mesh spacing of results computed on two or more finite resolution grids will be misleading if the solutions are outside the convergence radius, and it is not possible to know *a priori* if a given mesh and numerical scheme lie within this limit. Moreover, the effective order of accuracy may be unclear in hybrid numerical schemes where the cell Peclet number controls whether or not upwind or central differencing is used. When the true solution is unknown the only way to establish that a given solution is within a radius of convergence, and to estimate the effective order of solution accuracy, is to compare it with solutions on two or more other grids and check that E (or the GCI) scales as a power function of r. With three grids, labelled from 1 = finest to 3 = coarsest, repeated use of (4.30) gives:

$$\varepsilon_{23}/\varepsilon_{12} = r_{12}^{p}(r_{23}^{p} - 1)/(r_{12}^{p} - 1) \qquad [4.35]$$

where in an extension of the previous notation $\varepsilon_{23} = f_2 - f_3$, $\varepsilon_{12} = f_1 - f_2$, $r_{23} = h_3/h_2$, and $r_{12} = h_2/h_1$. This can be solved for p, either iteratively or directly as $p = \ln(\varepsilon_{23}/\varepsilon_{12})/\ln r$ if $r_{12} = r_{23} = r$.

In summary, [4.32] and [4.33] provide an objective and reliable method for the determination of truncation error in CFD applications. Thus, in each set of model applications, the effect of grid resolution on numerical error is established using the GCI index to indicate definitively whether a specific grid resolution is acceptable for the results to be analysed.

4.6.3 Validation

4.6.3.1 Conventional approaches

The conventional approach to model validation relies upon comparison of prediction with empirical measurements, with tests for goodness of fit, precision and accuracy (Lane and Richards, 2001). However, this cannot resolve the source of any error between predicted and observed, as much as it cannot categorically resolve whether agreement is achieved for the right reasons (Beven, 1989). Indeed, Oreskes *et al.* (1994) suggest that it is only possible to falsify a model of an open system. However, all models representing open systems can be falsified (Lane and Richards, 2001). This is because the model will require some form of closure and the full open-ness will therefore not be represented within the model. There is also appreciable uncertainty in both field data as well as the model predictions. Lane and Richards (2001) suggest that this places fundamental limits on the ability of empirical data to provide adequate basis for model validation. Thus, the process of validation must contain more than checking against empirical data.

4.6.3.2 Model assessment

Howes and Anderson (1988) emphasise that model assessment is thus more than testing against empirical data but a continuous set of procedures, which attempt to understand model behaviour and the system it represents. Validation as an exercise should be performed in terms of both the assumptions at each stage of model development and model refinement and the error that process creates.

As it is impossible to identify all variables and relationships in an open system, a conceptual model must capture what is thought to be the processes that matter in the system under consideration (Usunoff *et al.*, 1992). Model assessment has already begun in the selection of the complexity required, and the considerations of the implications these choices have on model predictability. The translation of conceptual linkages to mathematical formulations requires further assumptions to be made, such as reliance on mathematical theoretical reasoning and more importantly on empirically derived constants used in the formulation. It is also common to introduce further simplifications at this stage, which can introduce parameters that have less physical meaning (Lane and Richards, 2001). For example, a number of

different mathematical models are available to describe turbulence, bed roughness and water surface effects. Each of these incorporate simplifications that not be appropriate for natural flows. However, it can be difficult to separate out conceptual and mathematical model development. This type of internal *validation* of the representation of physical processes at each stage of model devolvement can provide an understanding of model performance in relation to each application.

4.6.3.3 Sensitivity analysis

The boundary conditions and parameters used in a model are defined by theoretical reasoning, empirical measurement or informed knowledge. Each of these is likely to have errors of uncertainty attached. Thus, sensitivity analysis has become an essential part of modelling process permitting an understanding of the consequences of this uncertainty. Sensitivity analysis can be used: (1) to determine if model behaviour is realistic; (2) identify sensitive boundary conditions and input parameters; (3) to improve model representation through limiting sensitivity of one component; (4) to assess the uncertainty in model predictions (Lane *et al.*, 1994b). All of these inform and improve the understanding of the internal structure and the applicability of the model to given situations. Recent approaches have applied sensitivity analysis thoroughly using Monte Carlo or generalized likelihood uncertainty estimation approaches (Beven and Binley, 1992), where combinations of input data are varied and sensitivity of output examined.

4.6.3.4 Validation summary

In conventional approaches to model validation, a fundamental assumption has been made that the validation data are better than the model predictions (Lane and Richards, 2001). However, error exists in both and significant errors can exist in both the empirical data used in model boundary conditions and in the validation data itself. Indeed, empirical data tend to be very poor at representing the spatio-temporal dynamics of the system and model predictions of systems can be richer in space and sometimes time.

Lane and Richards (2001) question this focus on model validation to empirical data and argue that progress can be better made using wide ranging, complementary,

holistic treatments, of model assessment that recognise contributions from model assumptions and specific model application. Indeed, Oreskes *et al.* (1994) suggests that models can be most useful in advancing understanding when it makes us think differently, ask new questions and challenge formulations, rather than validating them. However, a dichotomy arises with this approach because without good model validation, it is difficult to identify which new questions need asking and answering. When the model is used to predict spatial variations in processes that empirical measurements cannot produce, the sampled empirical data within that space become a control rather than a validation exercise. The coincidence of the two at sampled locations provides an indication of the predictive performance of the model in rest of the space, which is a powerful combination.

The assessment and validation of model performance in this thesis initially considers the development and assumptions applied in each application and uses spatially distributed empirical data to validate model performance. As error and uncertainty exists in both data sets, linear regression is performed in both directions or the reduced major axis regression is applied.

4.7 CHAPTER SUMMARY

This chapter reviewed application of flow modelling to open channels, highlighting the progression from two to three-dimensional flow models, and the recent application of transient flow modelling techniques based on large eddy simulation (LES). The chapter also introduced the background to the three-dimensional numerical flow model PHOENICS which is applied in the following chapters. This introduction included derivation of the conservation laws and details of the finite volume method used to solve the equations. The fundamentals of turbulence modelling were introduced, including a range of time-averaged models as well as LES treatments that permit investigation of the unsteady components of the flow field.

Application of this model to open channel flow requires a number of modifications. For application to natural channels, boundary fitted co-ordinates may be required in grid construction. Wall treatments based upon law of the wall are applied to represent the effects of bed and bank roughness, and methods by with inflow profiles

could be distributed across the model inlet have been identified. A porosity based free surface approximation can account for the free surface effects in the momentum equations.

The application of numerical models to different situations require consideration of the assumptions and simplifications applied. The methods applied for both validation and verification of model application have been identified.

The following chapter details the use of this numerical model in simulating and investigating the time-averaged flow structure in meander bends with flow separation zones.

Chapter 5

Time-averaged Flow Structures in Bends with Separation

5.1 INTRODUCTION

Chapters 2 and 3 detailed the use of a reconnaissance survey and a detailed field study comprising 635 and 22 bends respectively. Both levels of investigation identified variables that were significantly correlated with the occurrence of separation. However, there were large amounts of scatter and the direction of cause-effect within many of the relationships remains unclear.

This chapter aims to examine the 3-D time-average flow structure in meander bends with separation zones using a combination of computational fluid dynamics (CFD) simulations that are validated against detailed field observations, including 3-D velocity measurements. The next section (5.2) provides a brief background to intensive case study research of reach-scale river channel flow structures. The flow structures in two natural meander bends with separation zones at the inner bank are examined (5.3), before the flow structure in a natural bend with outer bank separation is investigated (5.4). Stage dependence of the flow structures are explored, permitting a discussion of the geomorphological implications of the findings (5.5). The chapter ends with a brief summary of the findings presented (5.6).

5.2 BACKGROUND

Many intensive field studies have examined the flow structure in small reaches of open channels in an attempt to elucidate the nature and direction of relationships between variables at the reach scale (Figure 1.1). This type of investigation has been important in ascertaining information on the flow dynamics in a number of open channel situations including classical type meander bends (*e.g.* Hey and Thorne, 1975; Bathurst *et al.*, 1977; Dietrich and Smith, 1983; and Markham and Thorne, 1992) and in braided reaches and confluences (*e.g.* Ashmore *et al.*, 1992; Rhoads and

Kenworthy, 1995, McLelland *et al.*, 1996; De Serres *et al.*, 1998 and Rhoads and Sukhodolov, 2001).

However, some of these studies have found differences in the flow structure and reached different conclusions on the factors responsible for those structures. For example, in meander bends, Bathurst *et al.* (1977) identified helical motion that extended throughout the channel width whilst Dietrich and Smith (1983) found that flow across the point bar could be outwardly directed throughout the vertical. Other differences between separate studies have included the effect flow asymmetry on delayed inflection through bends and the presence of the small outer bank cell with a reverse vorticity to the main skew induced cell. Similar differences have been found in studies of field confluences. For example, Ashmore *et al.*, (1992) and Rhoads (1996) identified counter-rotating helical cells driven by planform curvature whereas De Serres *et al.* (1998) identified a different flow structure driven by turbulent shear. Many of the differences found between field sites can be related to the different morphological conditions of each particular field site. However, the different methodologies under which measurements were taken and analysed (*see* 1.4.2) may also affect the results obtained (Dietrich and Smith, 1983; Lane *et al.*, 2000). This makes ascertaining which factors drive the flow field in generic terms extremely difficult.

As discussed in the previous chapter, use of computational fluid dynamics (CFD) is a relatively novel approach to addressing some of these difficulties. CFD has been applied to meander bend flow with some success (*e.g.* Demuren, 1993). Moreover, Hodskinson (1996) and Hodskinson and Ferguson (1998) used it to simulate the flow in a bend with inner-bank separation and found fairly good agreement with field measurements (velocity magnitude $R^2 = 0.89$; Table 4.1). They were able to use CFD to explore the dependence of outer-bank separation in hypothetical bends on radius of curvature, upstream planform, and other geometric factors. Bradbrook *et al.* (1998; 2000a; 2001) used CFD to disentangle the different theories of flow structure generation in river channel confluences. As mentioned in 4.2.2, CFD provides three-dimensional flow data at a high resolution, providing spatially rich three-dimensional prediction fields that can enhance insight and understanding of flow processes. Moreover, models can also be used to provide additional

information on pressure gradients, near bed velocity and bed shear stress predictions and estimates of water surface elevation.

Although, bends with separation and a shear layer between the main flow and re-circulation zone are known to have quasi-periodic flow structures (*e.g.* Hickin, 1978; Rhoads and Sukhodolov, 2001), this chapter concentrates exclusively on the time average flow structure. The following chapter (6.1) examines the unsteady nature of the flow processes in such situations.

5.3 INNER BANK SEPARATION

5.3.1 Introduction

This section investigates the flow structure in two bends with inner-bank separation zones. Initially, the two study bends are introduced (5.3.2) and the field methods applied in gathering necessary data are outlined (5.3.3). Application of the numerical model to both bends, with respect to the methodological issues discussed in section 4.6, are detailed (5.3.4) and the assessment of model performance in terms of verification and validation is presented (5.3.5). The details of the flow structures in both bends are presented and explained (5.3.6), before the differences and similarities between the two bends are highlighted (5.3.7). Section 5.3.7 explores the differences between the flow structures in classical meander bends (*e.g.* Dietrich, 1987) and in bends with inner bank separation, before the possible controls on the flow structure are discussed. The section concludes with a brief consideration of the implications of the flow structure in bends with inner bank separation for sediment transport and bend morphology (5.3.8) and a summary of both research findings and unresolved issues (5.2.9).

5.3.2 Study bends

The two bends studied in detail in this section are close together on the River Dean (Figure 3.1; 5.1). The first bend ('bend 17') has an inner-bank re-circulation zone extending almost halfway across the channel; the second ('bend 37') has an inner-bank separation extending over three-quarters of the channel width. Both bends were included in the reconnaissance survey (2.3) and the mid-level study (coded 02_17a

and 02_37) (3.1). These particular bends were selected as well-developed and representative examples of large inner-bank flow separation, not significantly confined by valley terraces or trees or obstructed by large woody debris. These particular bends were also chosen as access was relatively easy and both bends had unobstructed sightlines for surveying.

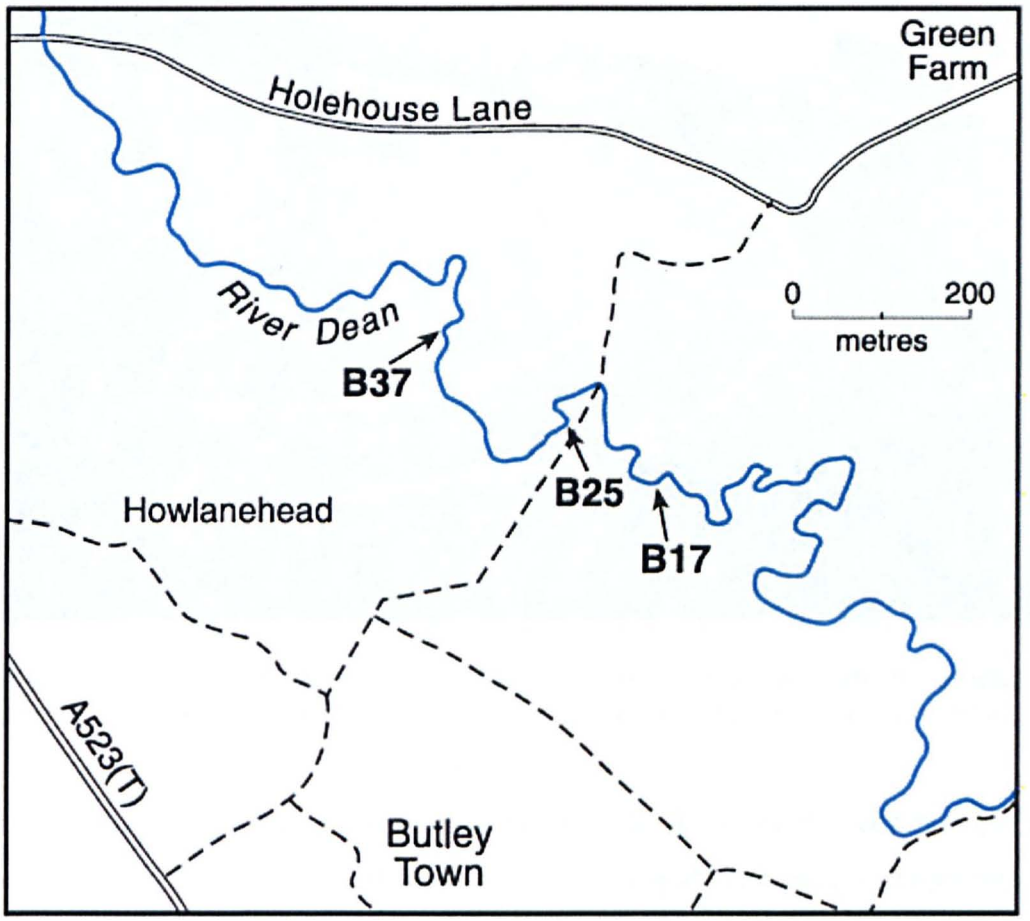

Figure 5.1: Location of the study bends

5.3.2.1 Bend 17

Bend 17 (on the 4th of July 2000) is a sharp bend which turns ~80° to the right over a centreline distance of approximately 10 m (Figure 5.2; 5.3). The stage was fairly low at the time the flow measurements were made (~0.4 m^3/s). At this flow discharge, the bend had a large inner bank separation, although the bend was observed to maintain a large inner-bank re-circulation zone in near-bankfull conditions. The channel has a bankfull width of 5-6 m and mean R_c/W is therefore <2. Total relief from the grassy left-bank floodplain to the deepest part of the pool is ~1.4 m. The

left, outer bank is ~0.9 m high and eroding over its full length. The right, inner bank is less steep and is vegetated down to the low-flow waterline.

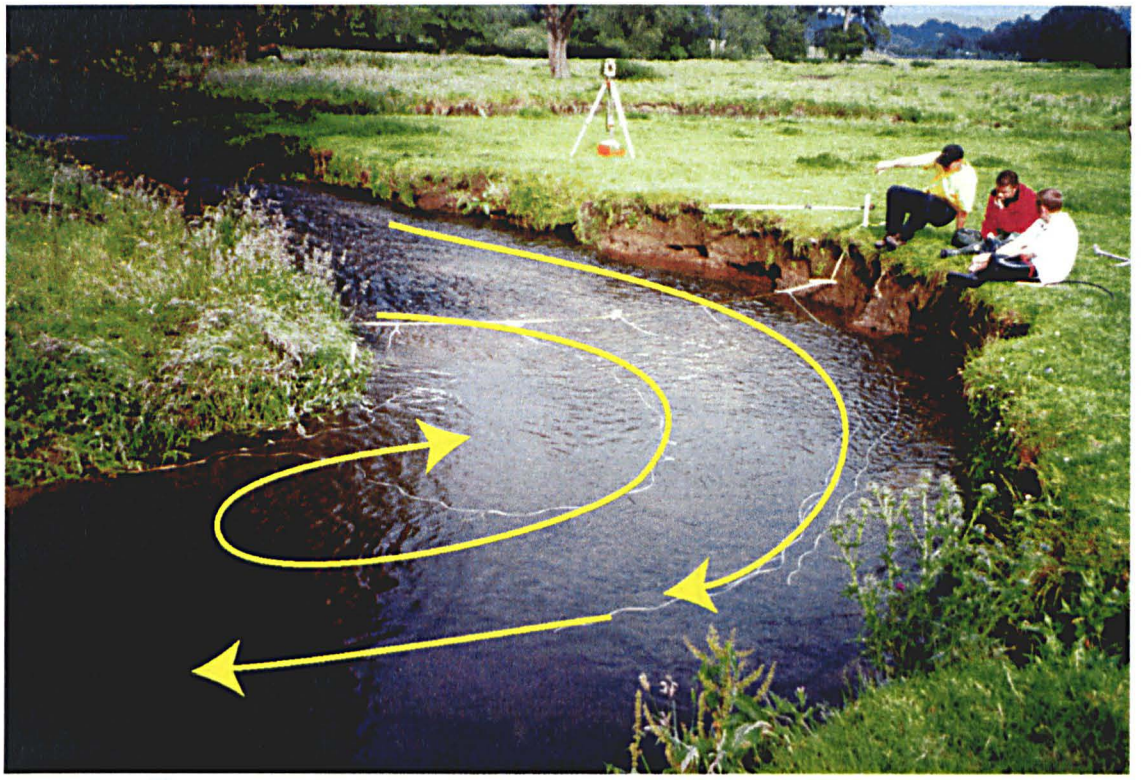

Figure 5.2: Bend 17 during normal flow. The inserted arrows indicate general direction of surface flow, as do the floating streamers (Taken on 4th July 2000).

Neither bank is uniformly curved in plan: the inner bank follows the common pattern of turning sharply at the apex. The outer bank has a slight reverse curve opposite the apex separating two zones of fairly high curvature (Figure 5.3). This irregularity in outer-bank curvature does not appear to be due to any variation in bank materials and probably reflects the location and size of cantilever failures of the more cohesive upper bank as the basal gravel is eroded during floods. Remains of collapsed blocks are responsible for local irregularities in the bed topography near the left bank downstream from the pool and the banks may be the source of the large gravel elements found in the pool. Flow enters over a gravelly riffle, highest in midstream and with the left talweg deeper and faster than the one on the right. The deepest part of the pool is past the apex, as normal in meander bends, but is unusually close to the centreline rather than the outer bank. The mean flow depth at the stage studied varied considerably around the bend, from a maximum of 0.34 m at the inflow to

0.76 m in the pool and 0.51 m at the outflow from the bend (Figure 5.3). The central and outer parts of the bed are gravel throughout, with D_{84} ranging from 69 to 54 mm, but most of the small point bar in the region reverse flow at and beyond the apex of the inner bank is sand.

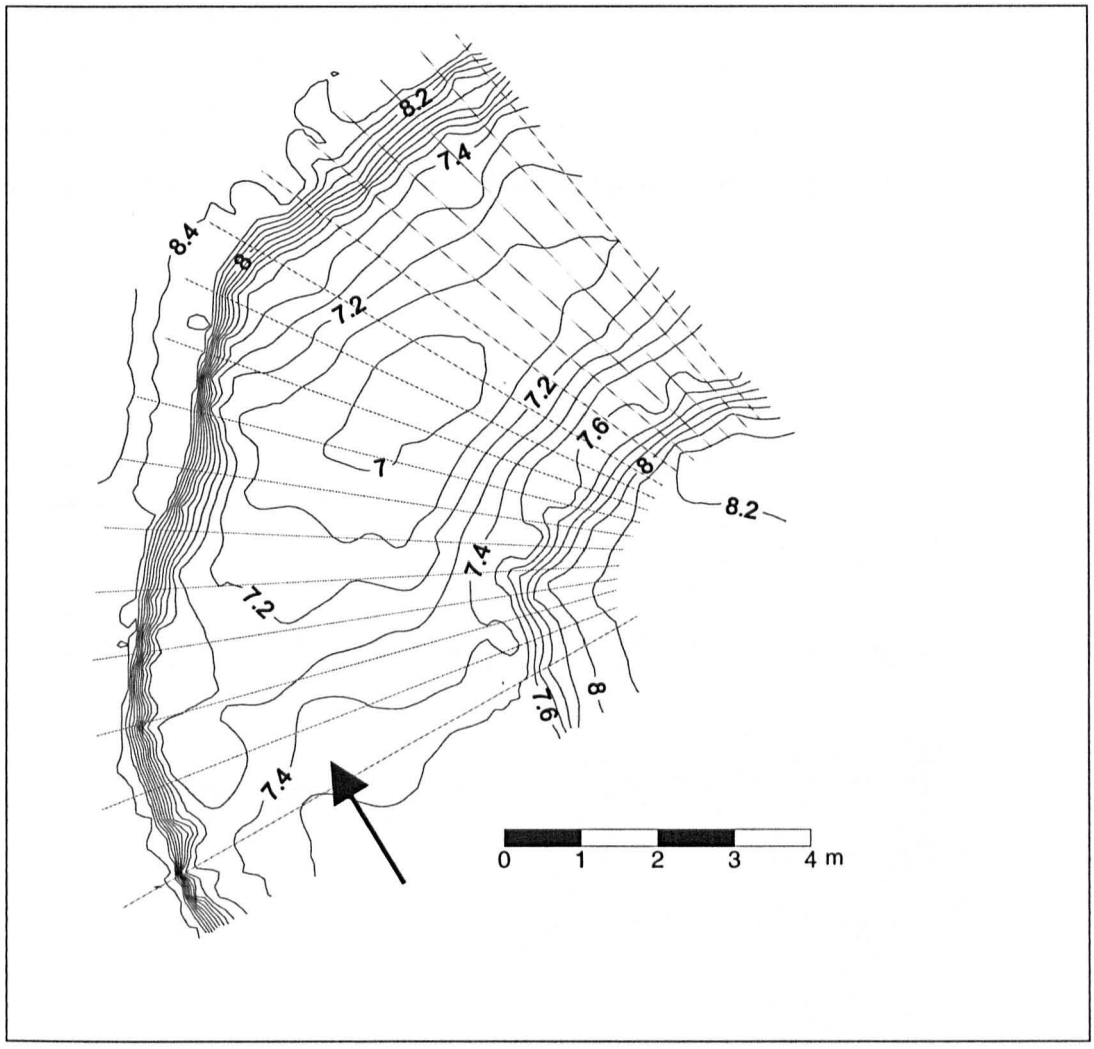

Figure 5.3: Bed morphology of bend 17 (4th July 2000). Elevation contours are in meters relative to an arbitrary datum. The arrow indicates flow direction and the cross section lines indicate cross section used to construct the numerical mesh.

5.3.2.2 Bend 37

The morphology of bend 37 was measured on the 8th August 1995 and it is described and modelled in Hodskinson (1996) and Hodskinson and Ferguson (1998). It is a sharp right-hand bend with a deep pool towards the outer bank and a small partially submerged point bar (Figure 5.4). It follows a long, almost straight, riffle and leads immediately into a sharp left-hand bend. The pool and its eroding outer bank consist

of gravel but the point bar is sand-covered. The inner bank is grassed down to the waterline. The outer bank is capped by overbank fines with a grass root layer. When surveyed in 1995 by Hodskinson (1997) bend 37 turned ~130° to the right over a distance of ~15 m along the outer bank and only ~7 m along the inner bank. These figures together with the mean channel width of 5.5 m give mean R_c/W ratios of 1.2 and 0.6 at the outer and inner banks. In 1995, the upstream riffle and outer parts of the bed are gravel throughout, with D_{84} of 66 mm, but most of the bed within the separation zone is sand. This morphology produced an inner-bank separation, which extended most of the way to the outer bank at the time of data collection.

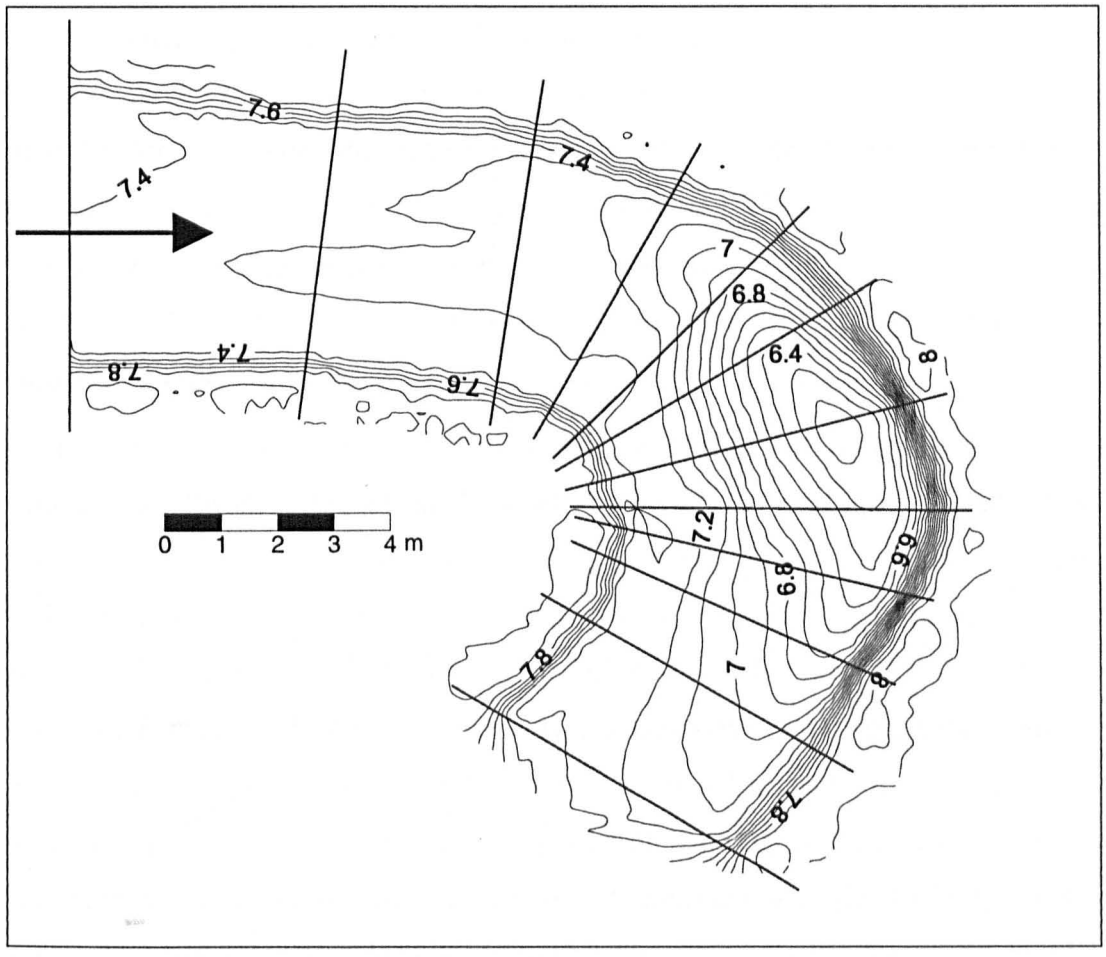

Figure 5.4: Bed morphology of bend 37 (8th August 1995). Elevation contours are in meters relative to an arbitrary datum. The arrow indicates flow direction and the cross section lines indicate cross section used to construct the numerical mesh.

By 2001, the outer bank had retreated substantially, especially upstream of the apex, which increased the radius of curvature. The separation zone was still present but less extensive.

5.3.3 Field monitoring methods

Bend 17 was investigated in July 2000 during a period of fairly low and slowly-falling discharge (~0.5 m^3/s). Stage did not change by more than 4 mm during the flow velocity measurement period. The methods used to obtain the field measurements were based upon techniques outlined in Lane *et al.* (1998). The banks and bed of the bend were mapped using a total station and a digital elevation model (DEM) was created from the survey data, using 404 data points. A kriging algorithm was applied to interpolate the surveyed points onto a regular DEM grid (*e.g.* Figure 5.3). The points surveyed along bank tops and bottoms were used to construct breaklines, which indicate the position of breaks of slope and act as information barriers to the kriging algorithm. The water surface elevation at 104 points within the submerged area was obtained by recording the vertical angle to the intersection of the reflector rod with the water surface. The estimated precision of these measurements of water surface elevation is ±0.02m. The approximate margin of surface flow separation was also mapped. Size counts of 100 surface pebbles were made in 1 m^2 quadrats at 7 locations in the bend for use in deriving values of bed roughness for the CFD models.

Velocity measurements were made across the inflow, to initialise the inflow boundary conditions, and within the bend, to assess the numerical model. These measurements were made using a Sontek™ acoustic Doppler velocimeter (ADV), which measures three orthogonal components of velocity at 25 Hz in a sensing volume of less than ~1 cm^3 which is ~5 cm below the probe. The ADV was mounted on a custom-made wading rod (Figure 5.5) that had a pair of reflectors on a crossbar. These were surveyed from the total station to allow subsequent calculation of ADV location and its orientation into the same coordinate system used in the DEM and CFD model. The rod also had a spirit bubble to help maintain the ADV in a vertical plane. Full details and estimates of the error in positioning and rotation involved using this field methodology at a similar scale of application are provided by Lane *et al.* (1998).

The bend inflow discharge and velocity distribution were quantified by sampling the velocity for 2 minutes at 0.25 m intervals across the first upstream cross section at 0.05 m intervals in each vertical. These data were used to calculate stream discharge

and interpolate the inflow velocity distribution as a boundary condition for the CFD model.

Figure 5.5: Positioning and Field methods. Total station (background) is used survey the bend morphology and position the ADV wading rod (foreground) into the same co-ordinate system. ADV data is downloaded onto a laptop.

Velocity measurements were also made at spatially distributed locations throughout the bend to obtain data with which to validate the CFD model. This data was collected by fixing the ADV at two separate heights and recording for at least 1 minute at a number of locations that were approximately 1-2 m apart throughout the

bend. The two heights selected were 0.435 m, which approximated the mean bend flow depth and a lower height of 0.225 m, which approximated 0.5 the mean bend flow depth. The position of the rod was surveyed using the total station during the measurement period. This procedure was then repeated at a lower height of 0.225 m, which was close to the mean depth, providing a well-distributed sample of points within the bend (Figure 5.6).

Longer time series were obtained at selected points across the shear layer and into the re-circulation zone for purposes of turbulence analysis (7.1). For all velocity measurements, the signal-to-noise ratio (SNR) and correlation coefficient were used to check the quality of the velocity measurements. Measurements when the signal correlation was less than 0.7 or when the SNR values exceeded 30% were removed from the signal series. The mean velocities were then computed and the series were subject to a low-pass Gaussian filter (see Lane *et al.*, 1998) before turbulent kinetic energy (*tke*) was calculated.

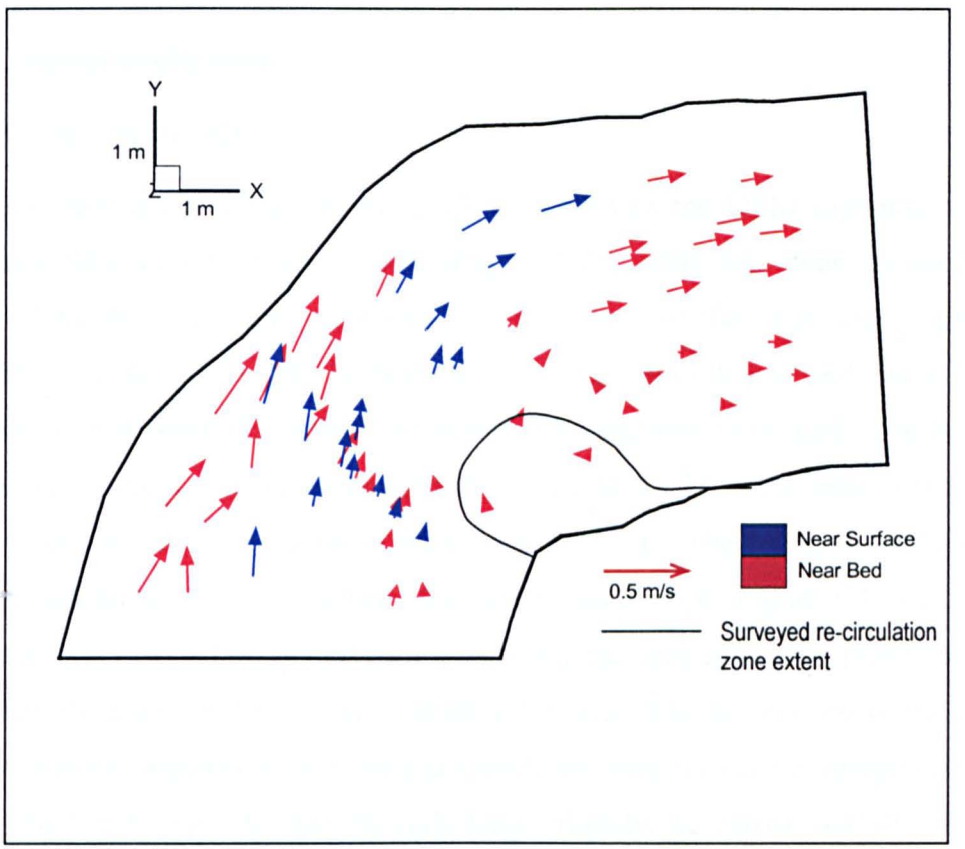

Figure 5.6: Velocity vectors obtained using the ADV, with the surveyed re-circulation zone delineated.

Field measurements in bend 37 were made in August 1995 by Hodskinson (1997) and used the more traditional approach in which measurements are made only at selected cross sections (Figure 5.3). Flow stage was again low (approximately 0.5 m^3/s) and falling very slowly (Hodskinson and Ferguson, 1998). Twelve sections, approximately perpendicular to the local channel direction, were surveyed using a total station. The sections were more closely spaced in the sharpest part of the bend. Water surface elevation was obtained at the left and right water edges along each section. Velocity measurements were made using a Marsh-McBirney™ two-component electromagnetic current meter (ECM). Streamwise and lateral components were measured to define the inflow and at two heights in eight verticals across sections 4 and 11. Additional measurements were obtained along the outer bank between sections 5 and 10 and within the separation zone at section 8. The estimation of boundary roughness was based upon a sample of 500 pebbles from the upstream riffle taken at the time of the measurements (full details are available in Hodskinson, 1997 and Hodskinson and Ferguson, 1998).

5.3.4 Model application

5.3.4.1 Numerical grid

For each bend a 3D computational grid was fitted to the DEM topography using boundary-fitted coordinates (*see* 4.5) (Figure 5.7). This was done by specifying points along the boundaries of a series of 2D planes of the 'real' topography and connecting these points into a four sided plane using linear and curve fitting techniques. For bend 37, the field-surveyed cross-sections were used. For bend 17, a series of 17 cross-sections were extracted from the DEM of the bend, which gave greater freedom in the position of each cross section. The sections used for grid construction are marked on the bed elevation contour maps (Figure 5.3; 5.4). A 2D grid was then mapped on to each cross-section plane and additional planes between those specified were interpolated creating a 3D grid. The dimensions of the grid in the streamwise, transverse, and vertical directions were set before interpolation (see 4.4). The bend 17 model had 96 cells longitudinally, 42 across, and 10 vertically (Figure 5.7). This means that cells along the outer bank have average dimensions of

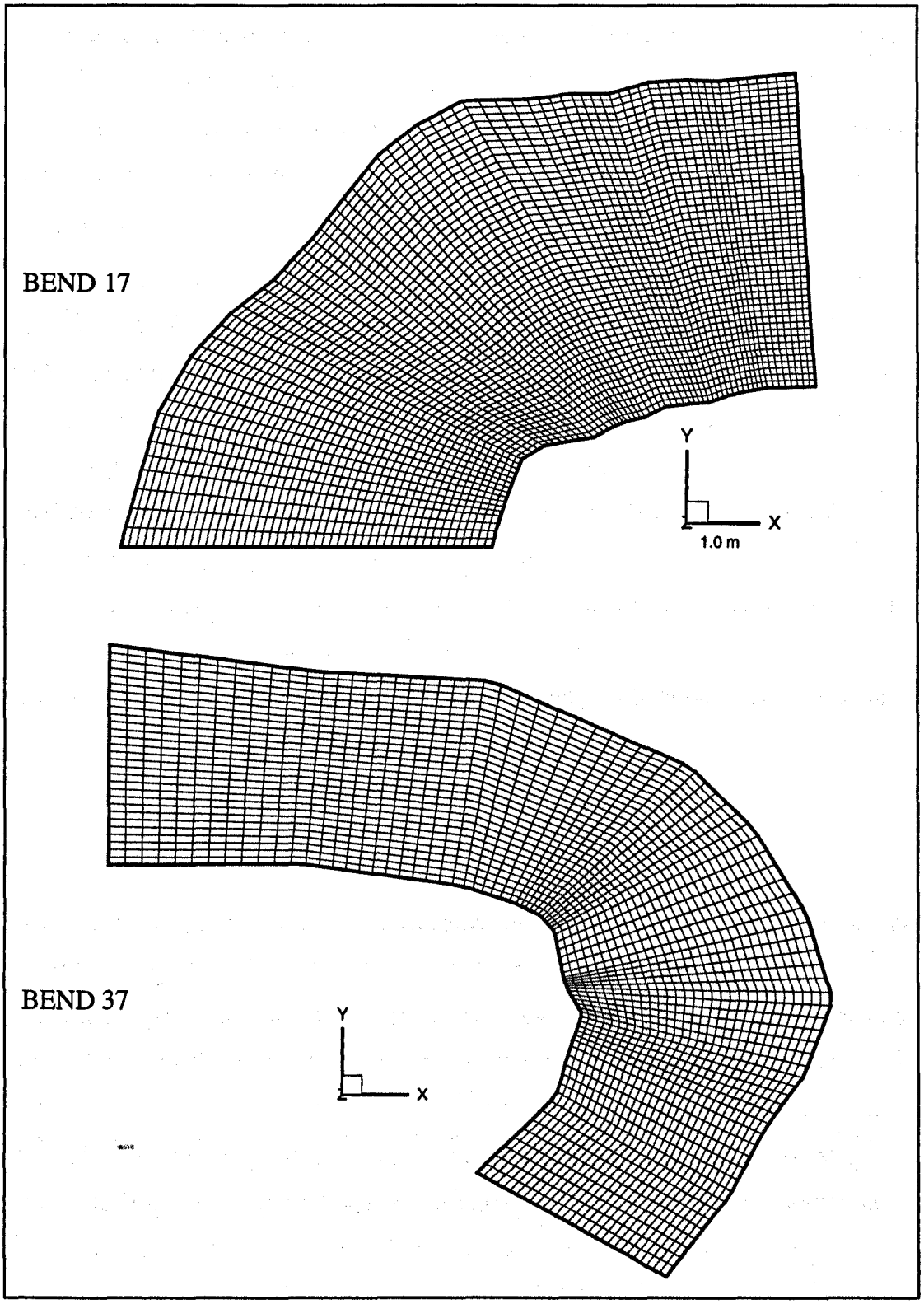

Figure 5.7: Planform view of the computational grids constructed to obtain solutions for bend 17 and 37.

~0.12 x 0.12 x 0.06 m, in the x, y, and z directions respectively. Mean cell length decreases across the channel to ~6 cm at the inner bank. Cell height varies between ~1 cm and ~9 cm according to local flow depth. The bend 37 model comprised a grid of 80 cells longitudinally, 30 across, and 10 vertically (Figure 5.7). Cells along the outer bank therefore have average dimensions of ~0.28 x 0.18 x 0.05 m, in the x, y, and z directions respectively. These cell dimensions were adopted after grid independence checks, the results of which are detailed below (5.3.5.1).

Grid construction of complex forms such as these two bends is a difficult and trying task (see 4.5), involving a significant amount of trail and error. Both bend 17 and 37 took approximately a week each. In the first instance only simple planform topography was modelled, followed by incorporation of simple representations of bed topography and then an increasing amount of topographic information, until a final converged solution of the bend was obtained. To obtain a converged solution, slight changes to the geometry of the inner banks had to be made: rounding off the inner bank apexes by 0.1 m to avoid excessive change in direction at the apex section, and making the sloping banks of the point-bars beyond the apex vertical for at least 0.05 m at the waterline to avoid vanishing cell heights (see Lane *et al.*, 1999a).

5.3.4.2 Boundary conditions

Inflow conditions are defined by specifying the velocity distribution at the upstream section. In bend 17, the 3D velocity measurements and turbulence parameters were interpolated linearly across the section. The law of the wall was used for quadratic interpolation in the vertical. For bend 37 the discharge measured by Hodskinson (1997) was used to distribute the velocity of the flow across the section using law of the wall. *tke* was given uniform values of 10% of the average inflow velocity (Lane *et al.*, 1998). A constant boundary roughness height, estimated from grain size surface counts on the upstream riffles, was used for both the bed and banks. Using $k_s=3.5D_{84}$ this gave roughness height values of 0.242 m in bend 17 and 0.231 m in bend 37. This exaggerates the skin roughness of the sandy parts of the bed, but the sand was rippled which adds some form resistance that is not represented in the model grid geometry. Use of a gravel roughness is also deemed appropriate for the

cut banks that are gravelly throughout, and is probably reasonable for those banks that were not eroding since they were all heavily grassed. A hydrostatic pressure distribution was specified at the outflow cross section and both models were run using the free surface approximation (4.5).

5.3.5 Model assessment

5.3.5.1 Verification

Verification of the solutions in terms of grid resolution for both bend 17 and 37 is demonstrated by the global convergence index (GCI)(4.6.2.1) results presented in Table 5.1. To obtain the results, both models were run with the number of cells in each direction doubled (*High*) and then halved (*Low*) from the baseline run (*Mid*) and the nodes common to all simulations were subject to GCI error analysis. Thus, the GCI analysis was based on 4,320 and 3,000 points for bend 17 and 37 respectively. The GCI analysis was performed between the low and mid resolution grids and the mid and high resolution grids. The GCI values quoted were obtained using a factor of safety of 3, such that the quoted GCI percentages are similar to a 99.9% statistical confidence interval (see 4.6.2.1).

The low GCI values obtained between the high and mid resolution meshes indicate that the mid resolution grid for both bend 17 and 37 is suitably verified for the three components of velocity (Table 5.1). However, the convergence for the turbulence parameters, except for turbulent kinetic energy in bend 37, is generally poor with relatively high GCI values. Hardy *et al.* (in press) found a similar pattern of poor grid convergence of turbulence parameters where a shear layer is present.

Table 5.1: GCI results for bend 17 and 37 in percentage terms. Velocity components in *x*, *y*, and *z* directions, the turbulent kinetic energy (*tke*) and turbulent dissipation rate (*ep*)

Variable	B17		B37	
	High/Mid	*Mid/Low*	*High/Mid*	*Mid/Low*
x-component	4.45	15.01	3.44	5.88
y-component	3.03	6.17	7.28	12.05
z-component	6.60	4.15	4.80	19.02
tke	21.44	37.08	1.39	7.81
ep	15.12	22.70	69.20	80.28

The velocity components are suitably verified using the GCI results therefore indicating that the mid resolution grid for both bend 17 and 37 is verified for analysis of the simulation results.

5.3.5.2 Validation

Before flow structures are analysed using CFD models it is essential to validate the solution against measured flow properties. For bend 17 this is achieved mainly by comparing measured and predicted values of velocity components in the x, y, and z directions, the velocity magnitude calculated from all three components, and the turbulence parameters. The comparisons are made at 62 field measurement points, using the simulated values for the nearest cell face in the CFD results.

The scatter plots are in Figure 5.8 and the associated correlation and regression statistics in Table 5.2. All the correlations are statistically significant at p=0.05, but a high correlation indicates small scatter rather than lack of bias so it is also necessary to check that the regression slopes and intercepts are not significantly different from 1 and 0 respectively. Error is possible in field measurements as well as CFD predictions so both forward and backward least-squares regressions are reported. Fitting methods that assume error in both measurements and predictions, for example reduced major axis (RMA) regression, gave lines between the backwards and forwards least-squares regression lines. The forward regressions, labelled 'CFD on ADV' in Table 5.2 and represented by the flatter of the two trend lines in each scatter plot, are appropriate if error is assumed to exist only in the CFD predictions. The steeper ADV-on-CFD fits are more appropriate if error is only in the measurements.

The results can be summarised as showing good agreement in velocity magnitude and its horizontal components, but less good for the vertical component and for *tke* as is commonly the case (*e.g.* Bradbrook *et al.*, 1998; Lane *et al.*, 1999a). The general tendency is for the model to predict rather less spatial variability in flow properties than is shown by the measurements. None of the backward regressions shows any significant difference from the 1:1 line of perfect agreement, and none of the intercepts of the forward regressions is appreciably different from 0, but the slopes are all significantly lower than 1: only just so for u, v and magnitude, but drastically

for *w* and *tke*. The RMA fits (not shown in Figure 5.8 for clarity) again all have slopes <1, though not significantly so for *u*, *v* or magnitude.

Table 5.2: Validation results for bend 17: comparison of ADV measurements at 62 field points with CFD model predictions. Forwards and backwards regression intercepts (*a*) and slopes (*b*) are shown, each with 95% confidence intervals, together with the correlation coefficient (r). Velocity variables are components in Cartesian *x*, *y*, *z* directions (as shown in Figure 5.2), *Magnitude* is the resultant of the *x* and *y* components, and *tke* is turbulent kinetic energy.

Variable	CFD on ADV			ADV on CFD	
	a	b	r	a	b
x-component ($m\ s^{-1}$)	0.01±0.01	0.83±0.08	0.94	0.00±0.01	1.08±0.10
magnitude ($m\ s^{-1}$)	0.02±0.02	0.82±0.10	0.91	0.01±0.02	1.01±0.12
y-component ($m\ s^{-1}$)	0.01±0.01	0.91±0.08	0.95	0.01±0.01	0.99±0.08
z-component ($m\ s^{-1}$)	0.00±0.02	0.37±0.10	0.66	0.00±0.00	1.19±0.35
tke (m^2s^2)	0.00±0.00	0.40±0.12	0.66	0.00±0.00	1.06±0.32

The scatter plots for *x* and *y* velocity components and velocity magnitude (Figure 5.8a-c) show close linear correlations (r >0.9) between measurements and predictions, but with a slight tendency for high measured *x* and *y* velocity to be underpredicted. Some negative *x* values are predicted as small positive values, and one positive value is greatly overpredicted. These discrepancies are near the margins of the recirculation zone, which is slightly bigger in reality than in the model (see the difference between Figures 5.6 and 5.9). This is probably due to the need to round off the abruptness of the inner-bank apex, though it may also be that the time-averaged turbulence model does not capture the full effects of the strong shear between main and separated flow. Underestimation of the width of the re-circulation zone implies overestimation of the width over which flow is downstream; this could explain the slight underestimation of the higher velocities. Note also that no optimisation of roughness height or topographic representation has been attempted. The higher velocities are mostly fairly near the surface, and could be underestimated if the effective roughness of the bed is greater than assumed in the simulation.

The correlation for *w* velocity is substantially lower (r <0.7) than those for *u* and *v*, and the tendency to predict less spatial variation than is measured is much clearer

(Figure 5.8d). Small measurement errors in w are possible because of the difficulty of holding the ADV wading rod exactly vertical and the contamination of the vertical velocity with horizontal velocity components, but the measured values greater than $\pm$0.02 m/s seem too big to be explained in this way. The biggest discrepancies are at locations near the edge of the re-circulation zone or near the outer bank. The differences close to the shear zone and within the separation zone could be related to macroturbulent structures generated by the shear, especially in view of the short duration of most measurements. However, stationarity analysis of longer-duration measurement records revealed that this effect is minor. Differences close to the outer bank seem to be related to bed and bank irregularities not included in the model geometry. For example, the bed of the outer side of the pool had some large protruding clasts, which had presumably fallen in from the eroding bank, which must deflect the flow to some extent. Lane *et al.* (in press) discuss the significant improvements that full topographic representation of the bed can have on the predicted vertical velocity. The correlation of *tke* is also much lower (r <0.7), although the general range is good (Figure 5.8e). The main discrepancies in the *tke* results relate to drastic under-prediction at a handful of points. ADV measurements of turbulence are not totally unproblematic (Lane *et al.*, 1998; McLelland and Nicholas, 2000), so despite efforts at quality control and post-processing there is likely to be some data error. Moreover, the time-average κ-ε turbulence model, even with the RNG modification, is unlikely to predict turbulence intensities correctly near shear layers and within separation zones. This is a cell size issue in terms of how fine the grid is relative to the local shear process. The relatively fine grid employed in this study explains the higher correlations obtained in compassions with previous applications of CFD to open channel flow (Table 4.1).

Although the CFD predictions do not always match perfectly with measured velocity and turbulence values, the agreement is generally good. Moreover, most of the discrepancies can be explained. The validation results obtained are better than previous applications of CFD to natural channels (Table 4.1) and are comparable to what has been regarded as acceptable by researchers modelling flume data (Bradbrook *et al.*, 1998; Huang *et al.*, 2002). In view of the additional uncertainties of field data collection the model is considered adequately validated for use in discussing the flow structures present in bend 17.

a)

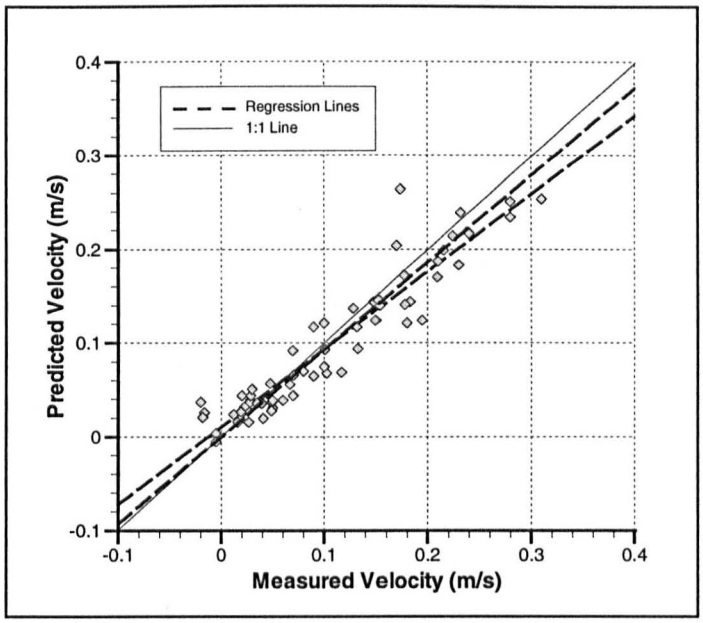
Regression Lines
1:1 Line
Predicted Velocity (m/s)
Measured Velocity (m/s)
0.4
0.3
0.2
0.1
0
-0.1
-0.1
0
0.1
0.2
0.3
0.4

b)

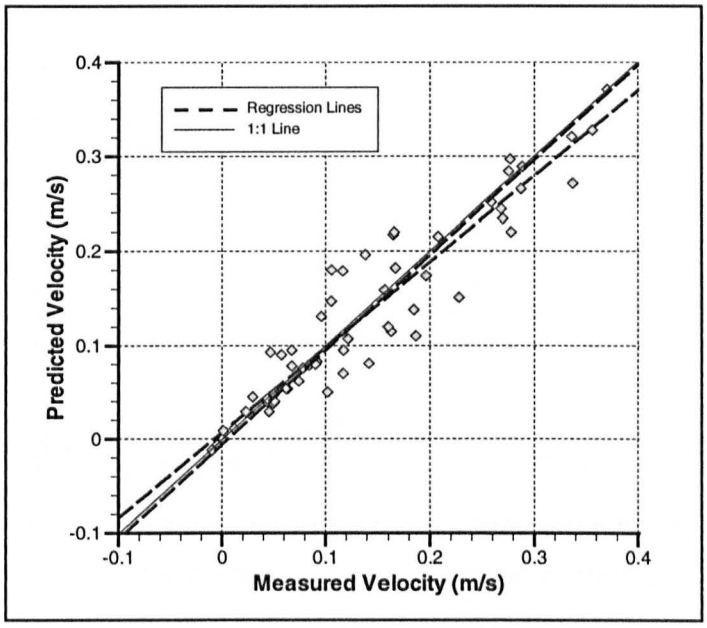
Regression Lines
1:1 Line
Predicted Velocity (m/s)
Measured Velocity (m/s)
0.4
0.3
0.2
0.1
0
-0.1
-0.1
0
0.1
0.2
0.3
0.4

c)

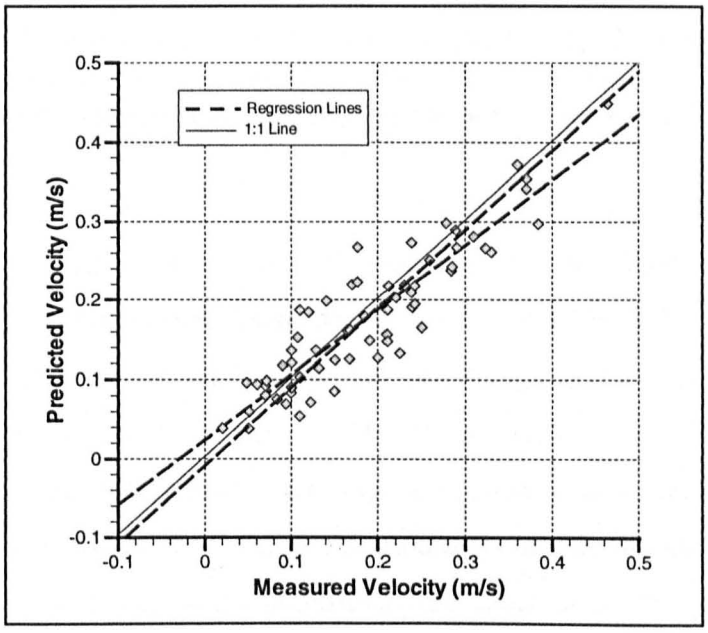
Regression Lines
1:1 Line
Predicted Velocity (m/s)
Measured Velocity (m/s)
0.5
0.4
0.3
0.2
0.1
0
-0.1
-0.1
0
0.1
0.2
0.3
0.4
0.5

d)

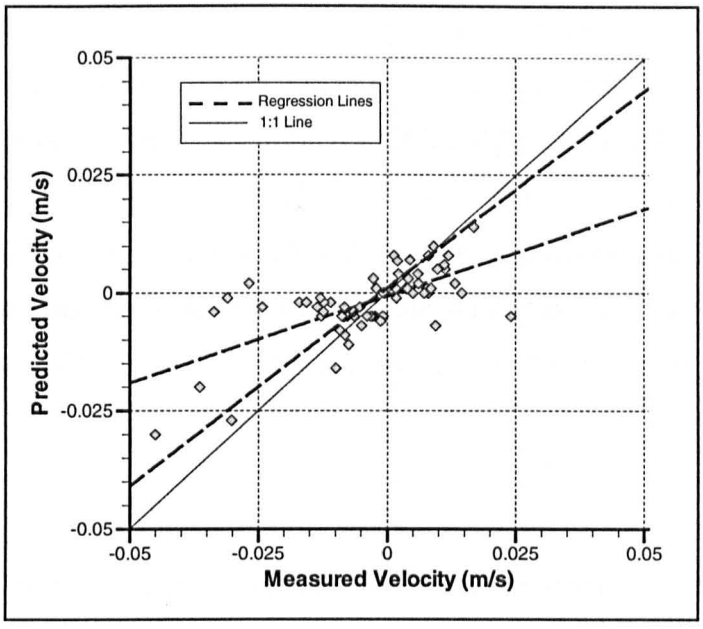

e)

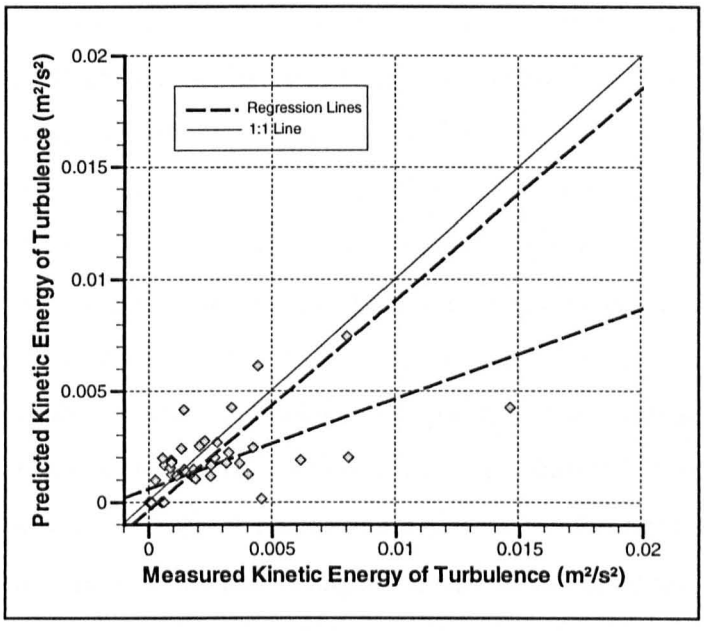

Figure 5.8: Comparison of predicted and observed values for bend 17: (a) *x*-component velocity; (b) magnitude velocity; (c) *y*-component velocity; (d) *z*-component velocity; and (e) turbulent kinetic energy per unit mass.

Full quantitative validation of the bend 37 model is not performed as the data is no longer available. As mentioned above, bend 37 is the one modelled by Hodskinson and Ferguson (1998). Although they did not examine the 3D flow structure produced by the model, they used the validation to justify idealized experiments of outer bank separation. Hodskinson and Ferguson (1998) found good qualitative and adequate qualitative validation of the two components of velocity that they measured in the field (R^2 =0.88), but noted significant problems in correctly specifying the

correct roughness over the shallow riffle inflow that resulted in over prediction of velocity in the riffle and under prediction in the pool. The new simulation performed here does not experience the same problems with roughness specification as the non-equilibrium version of law of the wall is applied. Comparison of planform maps from Hodskinson and Ferguson (1998) with the new simulation also indicate that the flow structures produced by the new model are qualitatively similar, although bed velocities in the riffle are slightly lower, indicating that they are closer to those measured.

5.3.6 Results: flow structure in bends with inner bank separation

Discussions of flow structures in meander bends, and in other channel features such as confluences and braids, have nearly always been based on detailed field measurements at a number of cross sections (*e.g.* Dietrich and Smith, 1984; Ashmore *et al.*, 1992; Rhoads and Sukhodolov, 2001). Results have typically been visualised using cross-section plots with isovels of the streamwise velocity component (denoted hereafter by u) and vectors calculated from the v (transverse) and w (vertical) components. These plots have been used to infer patterns of secondary circulation, although not without controversy since such patterns may appear very different according to the orientation chosen to define the u component (Lane *et al.*, 1999b; Rhoads and Kenworthy, 1999). A downstream sequence of such plots is often used to infer the nature of streamwise changes in the flow structure. This can be somewhat speculative in the absence of data between cross-sections. Moreover, the densities of measurements in the cross-stream and vertical dimensions at each cross section are much higher than the density of measurements in the streamwise direction. Some authors have also presented maps with u, v vectors, typically just for near-surface and near-bed measurements (*e.g.* Ashmore *et al.*, 1992; Andrle, 1994).

As the CFD results are spatially much richer, with velocities known at upwards of 10^4 points in each bend, compared with ~10^2 in studies based entirely on field or laboratory measurements, there is a wider choice of ways to identify, to describe, and to illustrate the flow structures present. This study uses a combination of near-surface and near-bed vector and streamline plots; cross-section vector plots; and isopleth maps of individual velocity components, *tke*, dynamic pressure, and shear

stress. Planform maps show the spatial patterns of velocity magnitude and orientation, and the extent to which magnitude and orientation alter in the vertical. Selected cross-section plots show patterns in the vertical component of velocity more effectively.

5.3.6.1 Bend 17: Horizontal components of velocity

Simulated near-surface and near-bed flow patterns are shown in Figure 5.9. The unit vectors show the resultant direction of the u (streamwise) and v (rightwards) components of velocity at alternate cells in each direction, with the velocity magnitude shown by the background contours. The magnitude is calculated from all three velocity components but is dominated by the horizontal components. The use of unit vectors and magnitude contours, rather than the more conventional scaled-vector map, makes it easier to see flow directions in the extensive areas of very low velocity. To help locate particular flow features within the bend, seven equally spaced section lines are marked on the maps and labelled A-G in downstream order. Section A runs across the riffle face not far from the inflow, C close to the inner-bank apex at the upstream edge of flow separation, D through the re-circulation zone and the deepest part of the pool, and E just downstream of the flow reattachment point.

As noted above, the inflow to the bend is over a riffle, with shallow flow midstream and talwegs on either side. The left talweg was much deeper and contains the majority of the flow. The riffle is much shallower than the rest of the bend, with flow depth <0.25 m over most of its width compared to >0.5 m across most of the pool, so the inflow velocities are relatively high. Their lateral pattern reflects the morphology of the riffle.

There is a general rightwards decrease in surface velocity, from ~0.7 m s^{-1} near the left bank to <0.1 m s^{-1} three-quarters of the way across, but with an increase to nearly 0.3 m s^{-1} close to the right bank. The vector directions indicate a general divergence of the slow central part of the inflow towards the deeper and faster areas towards the banks, though there is also local convergence in the lee of one part of the riffle about 80% of the way towards the right bank. The existence of two filaments of high velocity is a site-specific feature, which can be expected to complicate the flow

structure in the rest of the bend. At high discharge, with a much higher mean depth over the riffle, the relative variation in depth would be less, the associated topographic forcing reduced and the lateral distribution of velocity should be simpler.

The patterns of near-surface and near-bed velocity magnitude in Figure 5.9 are much more complicated than flow structures found in laboratory experiments or in idealised CFD simulations. Nevertheless, a number of key flow features can be identified. There is a general deceleration of the flow from the shallow riffle to the deep pool and some subsequent acceleration to the outflow section as the pool shallows towards the bend exit. The deceleration is most prominent in the near surface flow at the outer bank where the maximum velocity declines from >0.6 m s^{-1} at the inflow to a minimum of ~0.3 m s^{-1} and is still <0.4 m s^{-1} at the outflow. Moreover, the lateral distribution of flow through the whole bend is strongly asymmetric. A narrow zone of fast flow is concentred into an outer bank 'streamtube' (mostly over 0.35 m s^{-1} at the surface, 0.3 m s^{-1} at the bed), which is in stark contrast to the extensive area of slow flow extending across the channel from the inner-bank 'dead zone' of stagnant flow (<0.1 m s^{-1} at both surface and bed). The periphery of the re-circulation zone, as indicated by the 0.2 m s^{-1} surface isovel, comes close to the outer bank at sections C and D near the bend apex, although the near surface and near bed isovels have different patterns. This is apparent if the 0.1 and 0.2 m s^{-1} isovels are traced in Figure 5.9. Low near-bed velocities extend closest to the outer bank at the start of the bend (near section A), in the lee of the riffle face. Further round they are restricted to the right-hand half of the channel, before the velocity near the inner bank begins to increase towards the bend exit (sections F and G). Low surface velocities extend closest to the outer bank on the left side of the deepest part of the pool, rather more than half way round the bend. Interestingly, the surface velocity through sections C, D and E is actually lower than the near-bed velocity.

The region of stagnant flow is extensive within which a zone flow separation occurs. There is also an area of reverse flow immediately after the inner-bank apex, between sections B and C. Flow reattachment is located between sections D and E, midway from the apex to the end of the model domain. The separated zone has a clockwise circulation in plan view, with full-depth reverse flow in the dead zone downstream of

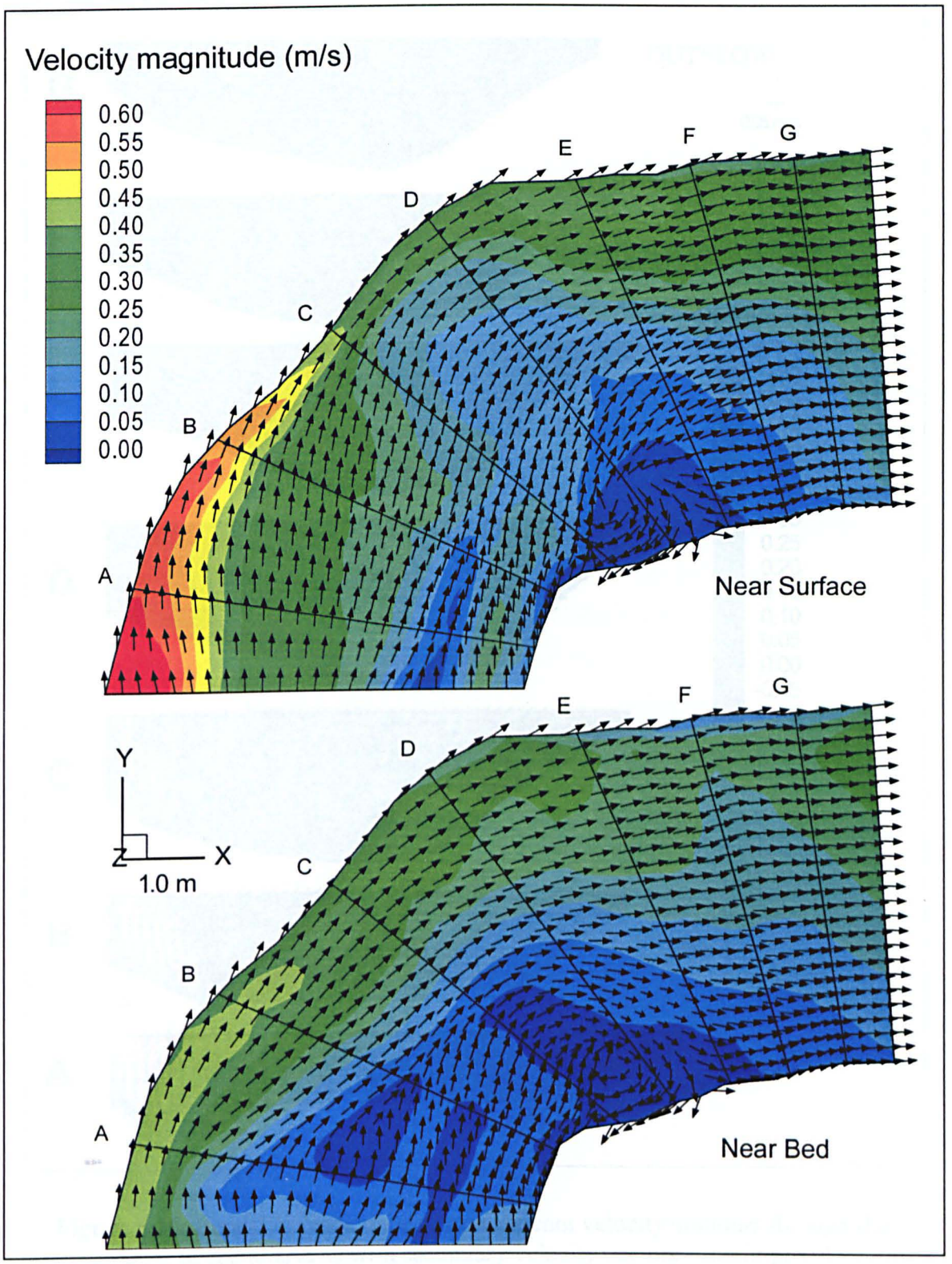

Figure 5.9: Bend 17: predicted planform maps of velocity magnitude with superimposed unit vectors showing flow direction near the surface and near the bed.

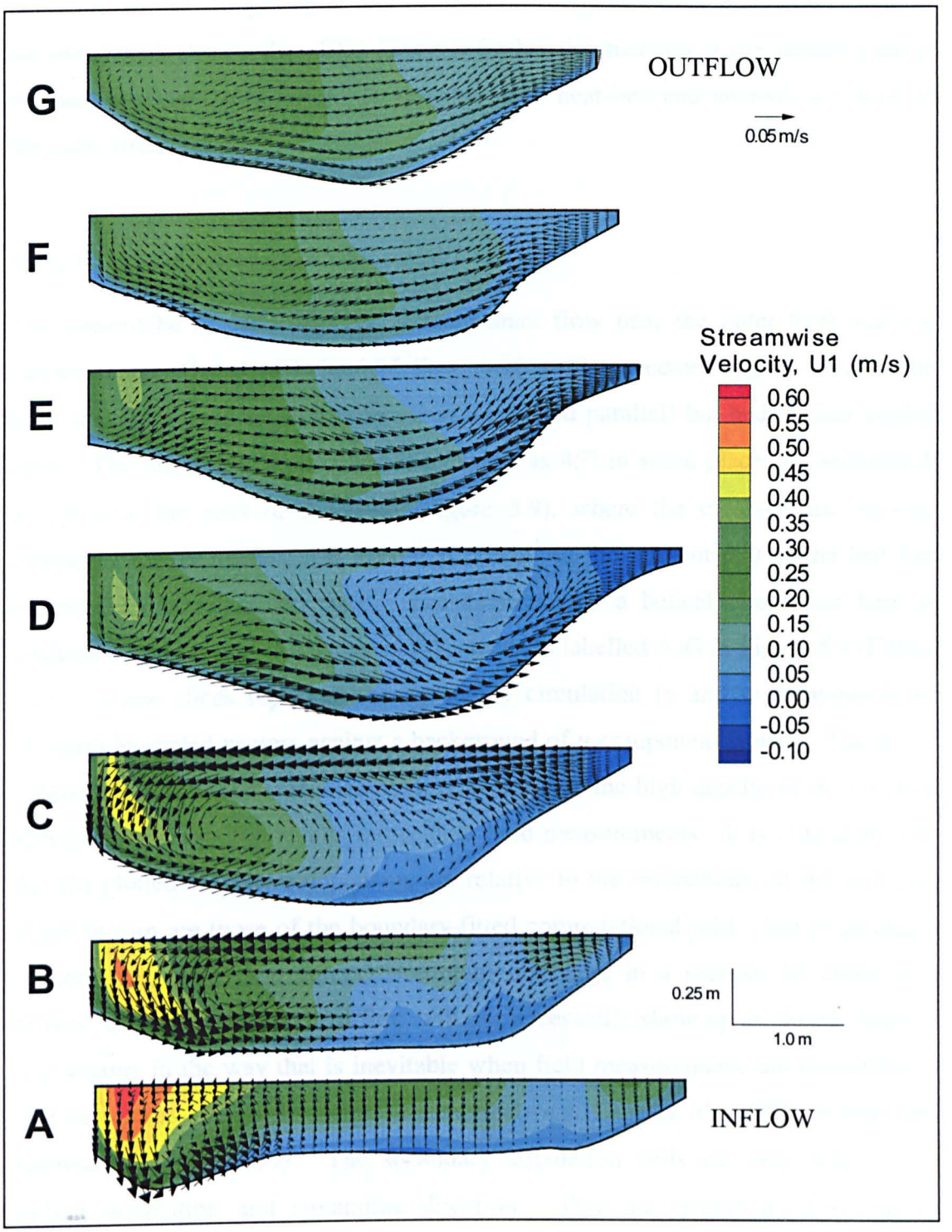

Figure 5.10: Bend 17: Predictions of downstream velocity contours through the planes of sections A-G with secondary velocity vectors superimposed.

the apex. Separation appears to be due to the sharp change of direction along the inner bank past section B. The moderately fast current entering this side of the bend continues straight on and a separation eddy develops in the expansion zone between it and the bank line. The main downstream flow to the left of the separation

continues almost straight on at first. It then turns rightwards as it converges against the outer-bank streamtube. This happens further downstream at the surface than at the bed, because the difference in orientation of near-bed and near-surface flow in the outer streamtube.

5.3.6.2 Bend 17: Secondary circulation

The streamtube of relatively fast downchannel flow near the outer bank has the classic characteristics of helicoidal flow, with surface vectors angled towards the bank (except very close to it where they are forced parallel) but bed vectors angled away. The difference in direction is as much as 45° in some places on sections A and B near the start of the bend (Figure 5.9), where the cross-stream velocity component at the surface can exceed 0.1 m s^{-1} to the left but that at the bed can exceed 0.15 m s^{-1} to the right. The existence of a helical circulation here is confirmed by cross-sectional slices of the sections labelled A-G in Figure 5.9 (Figure 5.10). These slices represent the secondary circulation (v and w components of velocity) by scaled vectors against a background of u-component isovels. The major difference from previous studies of flow in bends is the high density of information afforded by using CFD results rather than field measurements. It is critical to note that the plotted velocity components are relative to the orientations of the sections, which in turn are those of the boundary-fitted computational grid. The orientations do not necessarily yield zero cross-stream discharge in a section, let alone at a vertical, so the classical helical flow will not necessarily show up as closed loops of v, w vectors in the way that is inevitable when field measurements are reoriented to give zero cross-stream discharge at a vertical (*e.g.* Lane *et al.*, 2000; Rhoads and Kenworthy, 1998; 1999). The secondary circulation cells are very sensitive to section orientation and streamline direction. Thus interpretation of secondary circulation is therefore based upon differences between the near bed and the near surface velocity magnitude and direction, combined with the cross section plots and the vertical velocity predictions within them.

Figure 5.9 combined with the pattern of vertical velocities revealed by Figure 5.10 indicates that two areas of significant secondary flow exist. The first is close to the outer bank in the upper portion of the bend, where the strength of helical motion is at

a maximum. This cell is produced by the upstream riffle driving flow into the outer bank (Figure 5.9; 5.10). This strong helical circulation, anticlockwise looking downstream, can be seen in the left-hand half of the channel at sections A-C. This feature is produced by the contrast between outwards flow at the surface and inwards flow at the bed, and is essentially the same as in the classical model of curvature-induced flow structure in bends. The circulation is clearly demonstrated by plunging at the bank and upwelling in midstream. The strength of the circulation is enhanced by the asymmetric inflow impinging at the outer bank and the reduction in effective width past the dead zone. The axis of the vortex is well left of centre at each cross-section plane so the plunging near the outer bank is stronger than the upwelling on the midstream side of the vortex where streamwise velocities are low. Beyond section C the downwelling appears to weaken considerably, in contrast to the conventional assumption that the outer bank downwelling associated with one meander bend persists part way into the next before being replaced by one of opposite sense (*e.g.* Wilson, 1973). The difference is partly due to varying obliqueness of the sections relative to the irregular planform of the outer bank, but it also reflects the acceleration of near-bed flow around the outer edge of the bend followed by deceleration where the downstream flow expands rightwards past the end of the re-circulation zone in sections F and G.

The second area of significant secondary flow is also of anticlockwise vorticity in the downstream direction. It is found in the right-hand half of the channel at sections D and E, with upwelling next to the inner-bank separation cell and downwelling in the centre of the channel above the lowest part of the bed (Figure 5.10). This vortex approximates the part of the dead zone that has low, but downstream, velocity, where the flow decelerates considerably into the pool. It moves leftward and upward through section E before dissipation at the downstream limit of the dead zone at section F. This v, w vorticity seems to be generated by near-bed and near-surface flow convergence around the outer margin of the dead zone.

The two areas of secondary flow create a shear interface between upwelling flow on the midstream side of the outer helix and downwelling flow on the adjacent side of the inner helix. As the strength of the outer bank helical cell declines through sections A to C, the midstream upwelling at section C is replaced by upwelling by section D as the inner bank cell begins to dominate this interface. The structure here

is further complicated by the lateral gradient of streamwise velocity and a slight convergence of flow in the centre of the bend. Upwelling flow from the outer helix at section D and E appears to escape rightwards and join the downwelling side of the inner helix.

Flow is entrained into the separation cell at the downstream limit of the inner vortex in section E, where the inner portion of the flow field is entirely directed towards the inner bank. This reverse flow moves along the inner bank through section D until, at section C, it flows upwards and outwards to join the main cross-stream flow at the surface, completing the twin hairpins of the reverse flow circuit. The reverse flow thorough section D illustrates that the shear layer between the upstream flow and dead zone is not vertical, with a larger area of reverse flow near the surface.

5.3.6.3 Bend 37: Horizontal components of velocity

The simulated near-surface and near-bed flow patterns in bend 37 are mapped in Figure 5.11. Many of the flow features identified in the bend 17 analyses are also found in bend 37. There is a deceleration from riffle to pool then slight acceleration towards the bend exit. Strong flow asymmetry exists past the apex with fast flow in a narrow outer-bank streamtube that has a strong helical motion in the upper portions of the bend. There is an extensive inner-bank re-circulation zone within which flow separates, re-circulates, and re-attaches towards the bend exit. However, there are two major differences: the re-circulation zone in bend 37 is far bigger, and the flow structure is substantially simpler. These differences perhaps reflect the even sharper curvature of bend 37 and the simpler, more symmetric velocity distribution across its inflow. The discussion locates features with reference to six sections labelled A-F from bend entrance to exit.

Two dominant flow structures are apparent: a large zone of recirculating flow in an area which extends outwards from the inner bank to beyond the centreline of the channel; and, wrapped around it along the outer bank, a streamtube of relatively fast downchannel flow containing the classical curvature-induced helical circulation. Vorticity in the re-circulation zone is clockwise around a near-vertical axis. Vorticity in the outer-bank streamtube is anticlockwise around a streamwise axis. The maximum shear is at the interface of the two structures.

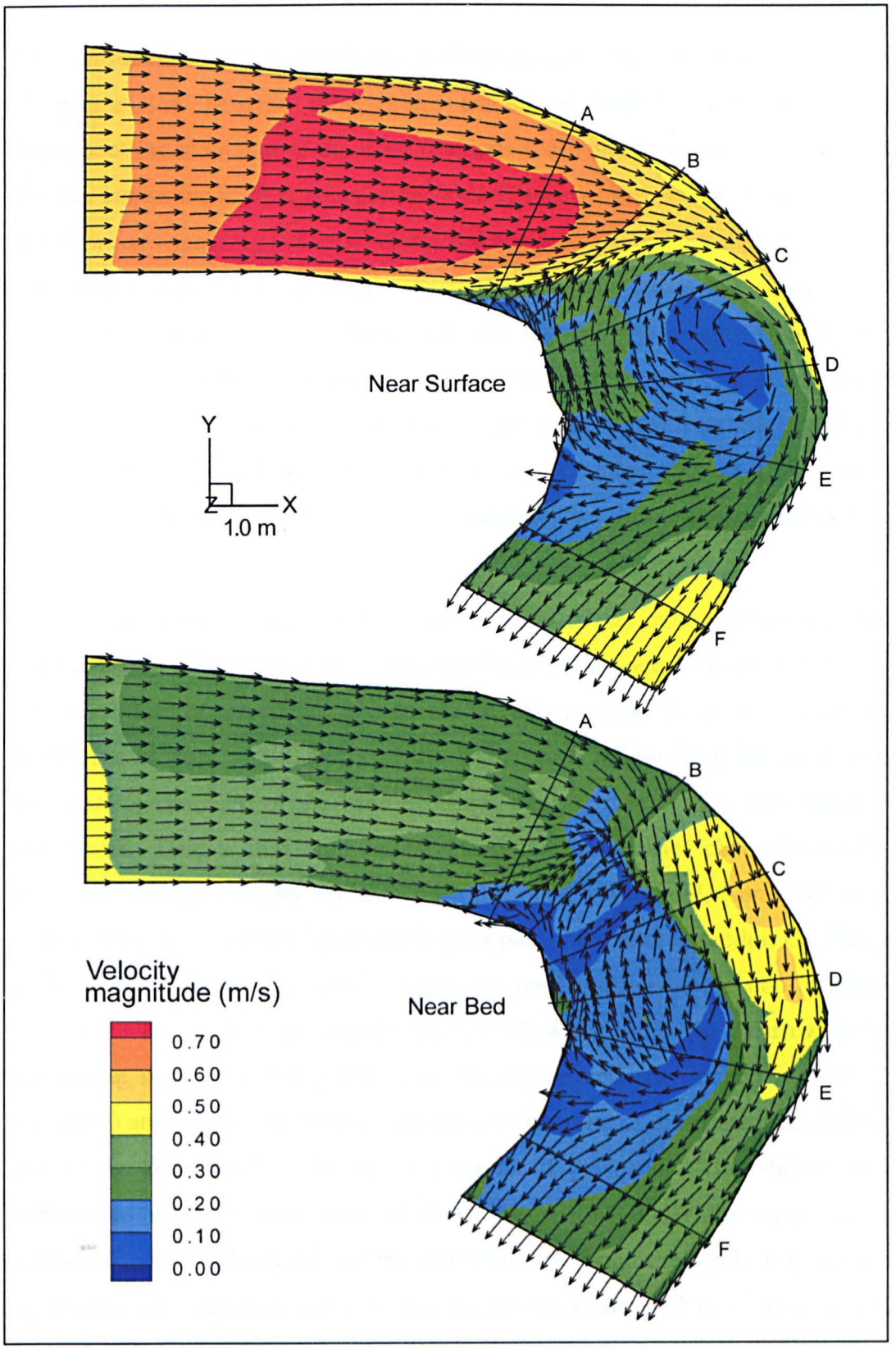

Figure 5.11: Bend 37: predicted planform maps of velocity magnitude with superimposed unit vectors showing flow direction near the surface and near the bed.

The extensive zone of reverse flow occurs at both the surface and the bed, just before the right, inner bank starts to turn sharply at section A. Reattachment occurs

between sections E and F, not far short of the crossover into the next bend. The zone of reverse flow between these points extends at least halfway across the bed throughout the main part of the bend (sections C-E), and to a maximum of ~75% of the way across the surface between sections C and D. The reverse flow is relatively fast flowing, exceeding 0.2 m s^{-1} close to the inner bank at both the surface and the bed. The lowest velocities within the separation zone are at the surface near the points of separation and reattachment, and towards the outer boundary of the separation zone between sections C and D. The lowest velocities at the bed are less localised, and are found in zones extending across the stream from the separation and reattachment points. Indeed the extent of the separation zone at the bed in mid-stream is greater than at the surface, extending further upstream between sections A and B.

Downstream flow through the bend is restricted to the outer part of the channel beyond the re-circulation zone. This would imply an acceleration of flow as the effective width of the stream is reduced, but this is offset by the increase in depth from riffle to pool. The inertia of the fast surface inflow from the shallow riffle immediately upstream of the bend produces convergence of flow into the curving outer bank. Despite this rapid convergence, due to increased channel capacity the maximum surface velocity declines from the riffle to the pool, from >0.7 m s^{-1} at section A to only ~0.4 m s^{-1} past the deepest part of the pool at section D. There is a slight acceleration to ~0.5 m s^{-1} towards the bend outflow as the pool shallows at section F. The asymmetric convergence of full-width inflow to a narrow left-bank streamtube implies a strong leftwards velocity component (locally >0.4 m s^{-1} at section B) and has the effect of increasing the curvature of the streamlines relative to that of the outer bank in the upper portions of the bend. This surface flow is constrained into a narrow zone of downstream flow under the outer bank and continues to have a leftwards component until well round the bend. It then expands rightwards, with cross-stream velocities locally exceeding 0.2 m s^{-1} at section E, as the re-circulation zone narrows and disappears.

The detailed pattern of flow at the bed in the outer part of the channel is not the same as that at the surface. Leftwards convergence at the start of the bend is restricted to the right-hand half of the bed, in contrast to the surface flow, where the leftward component extends the full width of the channel from the separation point (section

A). In the streamtube under the outer bank, the flow at the bed has a substantial rightwards component, locally exceeding 0.2 m s^{-1} between sections B and C, while the surface flow continue to have a significant rightwards component. Thus, the surface and bed flow directions differ considerably in the streamtube, implying a three-dimensional helical circulation (anticlockwise looking downstream) that is completed by plunging at the bank and upwelling at the edge of the re-circulation zone (Figure 5.12). The velocity of the near bed flow in the streamtube accelerates from sections A and B where velocity is <0.3 m s^{-1}, through to sections C, D and E where near bed velocity locally exceeds >0.4 m s^{-1}. This is in direct contrast to the near surface flow which experiences significant deceleration into the bend apex. At sections C, D and E this results in a reversal of the velocity gradient, with near bed flow velocity exceeding the near surface.

5.3.6.4 Bend 37: Secondary circulation

The progressive movement of the locus of maximum *u* down the outer bank from the surface at B, to part way down the bank at C, the base of the bank at D, and finally the talweg at E is clearly shown by the cross section plots Figure 5.12. This downward plunging of fast surface water is accompanied by a large deviation in near bed and near surface flow direction close to the outer bank in the upper part of the bend (Figure 5.11). The fast inflow to the bend at section A crosses leftwards at all depths and begins to plunge downwards near the outer bank. At B and C, the classical helical circulation is fully developed, but is restricted to the outer part of the channel: only half the width at B, and less at C. The compression in vortex width accentuates the helical circulation, with v >0.4 m s^{-1} at B and w < -0.1 m s^{-1} close to the outer bank at C. This is the classical pattern of curvature-induced circulation, although it is rapidly dissipated downstream. Thus, at D the remains of the helix can still be seen between the talweg and the base of the bank, but there is no longer a leftwards flow at the surface. At section E, the outer bank helix is completely dissipated and is replaced by an upwelling and inwards movement of flow (Figure 5.11; 5.12). Finally, at section F which is beyond the reattachment point and is much shallower as the channel approaches the crossover to the next bend, the secondary flow becomes wholly rightwards and the fastest flow is once again at the surface and towards the left bank.

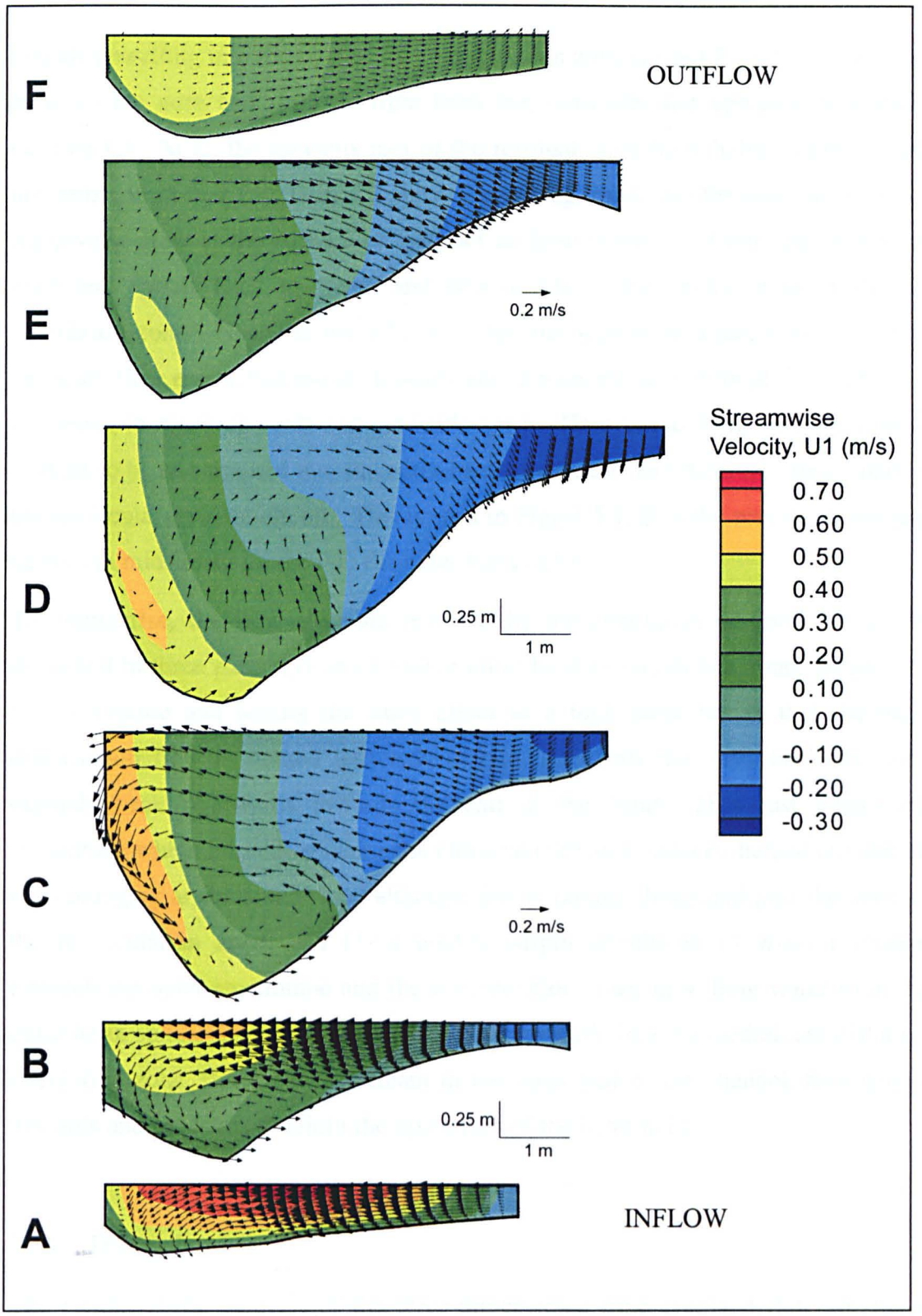

Figure 5.12: Bend 37: predictions of downstream velocity contours through the planes of sections A-F with secondary velocity vectors superimposed.

In plan (Figure 5.11) the re-circulation zone has the appearance of a simple separation vortex, with clockwise circulation about a vertical axis, but Figure 5.12

reveals upwelling into the core of the re-circulation zone (D and E) and downwelling between the core and the true right bank but outwards and upwards proximally (section C). At D, the upwards part of the residual outer-bank helix and the strong upwards component (>0.03 m s^{-1}) above the talweg, links into the outermost part of the reverse flow at the surface of the pool as flow is entrained into the separation zone and spirals back upstream and downwards in the central core of the re-circulation zone. Near the inner bank within the separation zone, a main core of upstream flow exists, that moves inwards and downwards at E through D, but by C it is starting to move upwards and outwards again. Here and at B, the reverse flow is starting to be re-entrained into the outer-bank streamtube and the downstream part of the re-circulation zone circuit. This is seen in Figure 5.12B in the way the secondary vectors in midstream merge into the outer-bank helix.

To summarise, the flow structure revealed by the simulation of bend 37 can be described in three parts: (1) an extensive inner-bank re-circulation zone, induced by high curvature and having the same effect as a high point bar in that the main downstream flow is steered leftwards around it towards the outer bank and then expands back rightwards towards the end of the bend; (2) a fast outer-bank streamtube which initially contains the classical curvature-induced helical circulation with plunging at the outer bank, although this is rapidly dissipated past the apex of the re-circulation zone; and (3) a double-hairpin circulation of water exchange between the outer streamtube and the re-circulation zone: upwelling water from the outer helix spirals inwards, backwards and downwards into the medial and distal re-circulation zone, flows back upstream in the inner half of the channel, then spirals upwards and outwards to rejoin the upper part of the outer helix.

5.3.7 Discussion

The results of the analysis of the three-dimensional time-averaged flow structures presented in this study reveal significant differences, but some similarities between the classical models of flow structure in meander bends (*e.g.* Dietrich, 1987) and bends where significant zones of inner-bank separation are present. The results also demonstrate notable similarities but important differences between the two bends with inner-bank separation. This permits tentative suggestions about generic features

and contingent differences in the flow structures in the two bends. Thus, the rest of this discussion focuses on these similarities and differences, and also on how flow structures in bends with inner-bank separation compares with that in 'classical' bends without separation.

There are several important similarities in the results for the two study bends. Both have 'dead zones' of slow and/or recirculating flow close to the inner bank just past its apex, extending nearly halfway across bend 17 and considerably further in bend 37. The presence of a re-circulation zone acts to confine the main downstream flow into a streamtube of relatively high velocity close to the outer bank. The streamtube in both bends has increased velocity near the bed and at the toe of the outer bank (Figures 5.10 and 5.12). In both cases, flow in the streamtube initially has the classical helical motion with flow directed outwards at the surface but inwards at the bed, with plunging flow at the outer bank. This flow pattern is extremely strong in the first half of the bend, but past the apex it is rapidly dissipated in both bends as the near surface and near bed velocities are in a similar direction (Figures 5.9 and 5.11). This dissipation of helical motion can be attributed to a number of factors: (1) acceleration of near bed flow results in less deviation of near bed flow towards the inner bank, whereas the simultaneous deceleration of near surface flow reduces the outwards component; (2) the deceleration and asymmetric expansion where the streamtube spreads back rightwards past the end of the re-circulation zone; (3) turbulent diffusion in the shear layer between the streamtube and the adjacent re-circulation zone.

Despite differences in dead-zone extent in the two bends, the flow structure in and around the re-circulation zone is similar. In both bends, the strongest upstream current is near the bed, close to the inner bank, with a zone of near surface stagnant flow in the centre of the channel. The movement of flow into and out of the reverse flow zone in both bends is also very similar. In both bends, a double hairpin motion of fluid exchange exists. Flow seems to enter the reverse flow circuit via inward and downwards movement at the downstream limit of the upwelling edge of the streamtube helical vortex (close to section D in Figures 5.9 and 5.10 and close to section E in Figures 5.11 and 5.12). At the upstream limit of the reverse flow, an upwards and outwards movement of fluid interacts with the strong streamtube vortex as fluid is entrained back into the main downstream flow (close to section C in

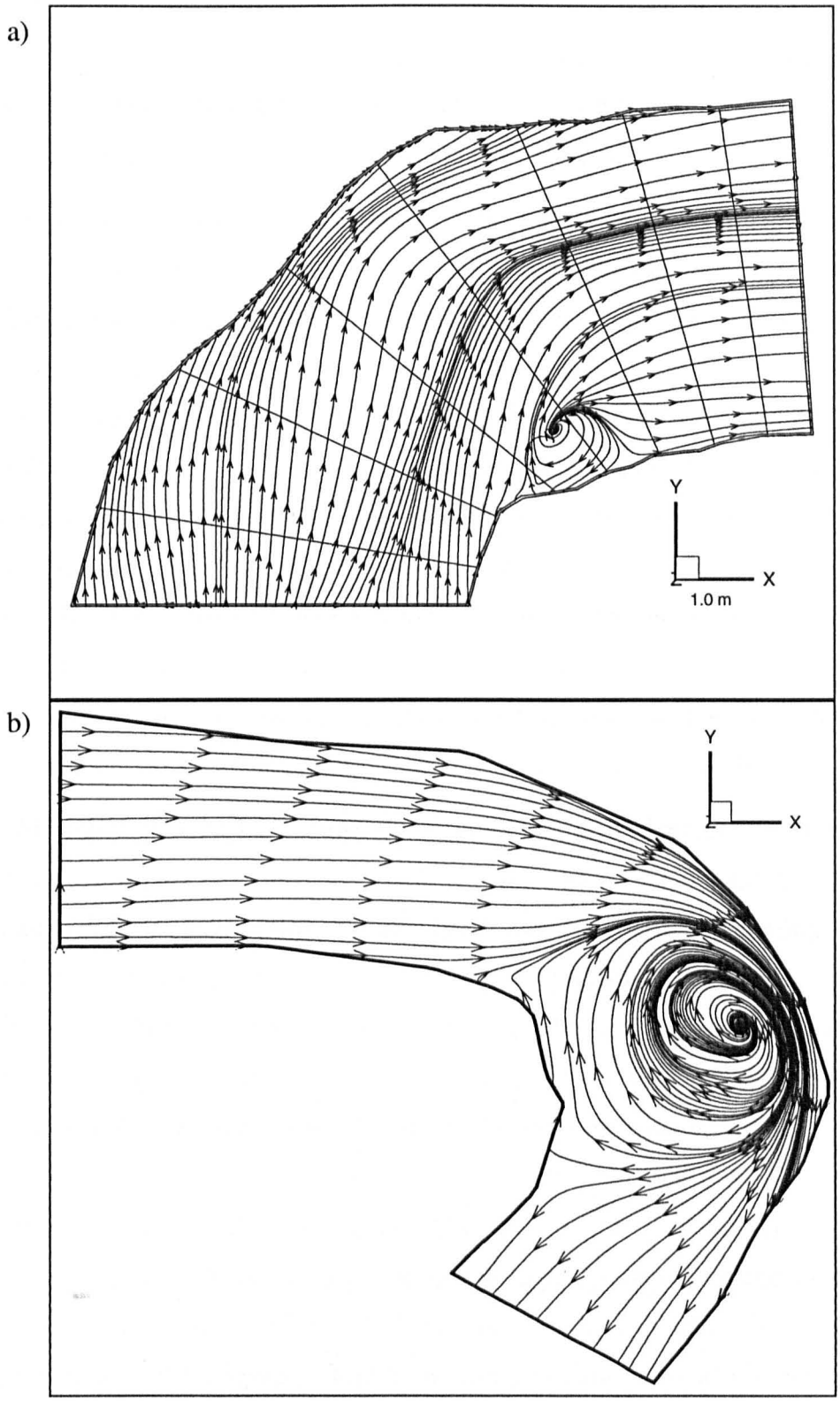

Figure 5.13: Surface streamline plots in (a) bend 17 and (b) bend 37.

Figures 5.9 and 5.10 and close to section B in Figures 5.11 and 5.12). However, Figure 5.13 seems to demonstrate that the fluid within the separation zone is poorly

mixed with the main downstream flow, and continually re-circulates around an axis close to the centre of the channel. The transfer and entrainment of fluid into and out of the separation zone and turbulent diffusion across the shear layer interface both providing energy to a central vortex system of re-circulation.

There are however notable differences between the two bends. The flow structure in bend 37 is simpler than in bend 17. Bend 37 is dominated by two large vortices: the classical helical cell in the streamtube, and a zone of recirculating flow at the inner bank, with intense shear between these features. Bend 17 has the same features but they are separated by a large area of slow downstream flow, so that there are effectively two zones of high shear: a main one at the mid-channel side of the streamtube of fast downstream flow close to the outer bank, and a weaker one between the slow flow in the centre of the channel and the reverse flow close to the inner bank. Thus, bend 37 does not have the interacting effect of these two shear layers and resulting combination of two helical cells rotating in the same direction (Figure 5.10 sections C and D). These differences seem primarily to do with the simpler inflow and higher curvature of bend 37 in comparison with bend 17.

It is difficult to isolate the factors that control the flow structures in these bends. However, it seems possible to identify three inter-related factors: streamline curvature; inflow distribution to the bend; and topographic forcing. Strong streamline curvature produced by the local bankline direction acts to produce a region of high dynamic pressure against the outer bank as the inertia of the flow is too great to adjust to the imposed curvature of the bend. This impingement creates a region of high dynamic pressure (Figure 5.14) some distance before the outer-bank apex of both bends, and results in a region of relatively low or negative dynamic pressure opposite the outer bank apex. The general flow structure and free surface elevation (Figure 5.15) are a response to the high dynamic pressure on the outer bank. The inflow distribution, which is governed by a combination of upstream planform and local topographic forcing on the upstream riffle, also seems to have a pronounced effect on the flow structure observed. The inflow distribution can act to enhance or diminish the potential pressure gradients produced by streamline curvature by acting to drive flow into the outerbank at a higher or lower angle than the local bankline direction. The bed topography also acts to promote flow separation through the effect of deceleration from shallow riffle to deep pool; the

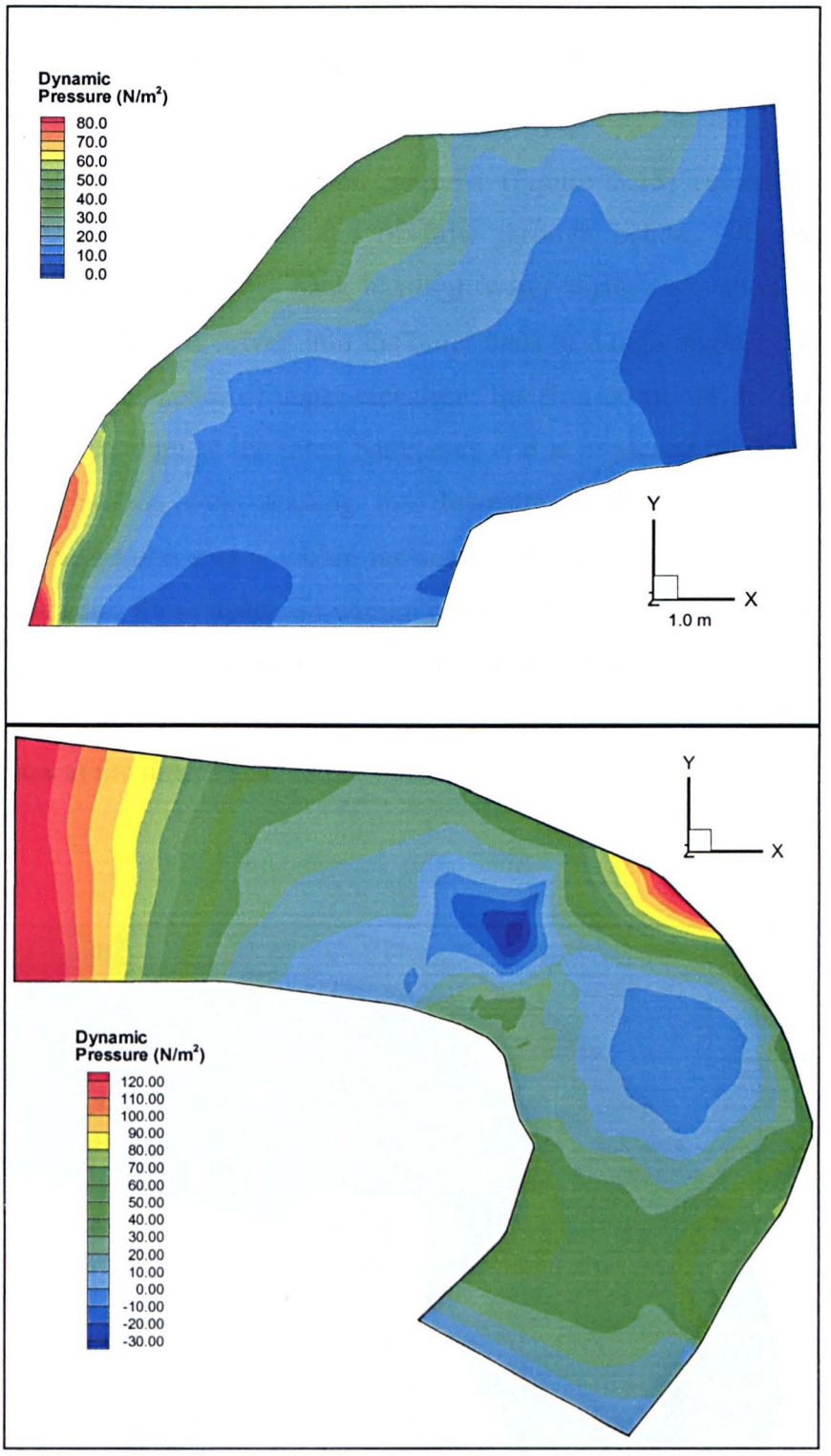

Figure 5.14: Dynamic pressure distributions at the bed in bends 17 and 37.

transverse location of the deepest part of the pool also matters. Once produced, the re-circulation zone acts as a fourth factor modifying the flow structure through the bend by steering the main downstream flow into a narrow core around outer bank.

The interaction between the streamtube of downstream velocity and the regions of slow or reverse flow within the separation zone produces intense shear along the boundary.

The predicted free surface elevation patterns (Figure 5.15) reveal a significant difference from the classical model of flow through bends. As expected the impingement point at the outer bank has high water surface elevation produced by super-elevation as flow is driven into the outer bank at a high angle. There are also two other significant zones of super-elevation; the first occurs at the point of flow separation just upstream of the inner bank apex and is produced by the reverse flow within the separation zone stalling the downstream flow in an area of flow stagnation. The second area is within the separation zone close to the inner bank as flow reattaches and flows upstream within the reverse flow cell. Areas of significant surface depression occur upstream of the point of separation opposite the super-elevation at the outer bank and in the centre of the channel as the bed deepens and flow separates at the inner bank.

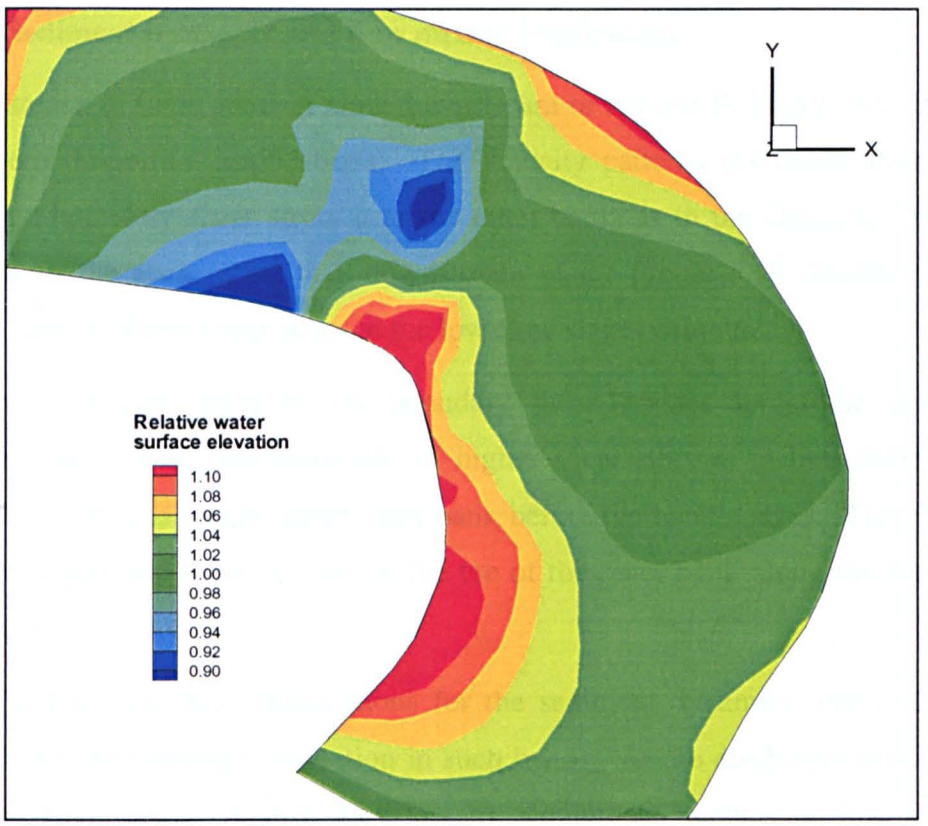

Figure 5.15: Relative water surface elevation patterns in the main part of bend 37

Flow in both bends is driven into the outer bank some distance before the bend apex, which produces the pressure gradients discussed above (Figure 5.14). This is different from the classical model in which the main impingement of flow into the outer bank occurs after the bend apex, maintaining the helical structure to or beyond the bend exit. However, the relative contribution of each factor to the production of separation seems to differ between bend 17 and bend 37. In bend 17, the cause of flow separation seems to be the upstream riffle, where the majority of inflow is very and driven into the outer bank. In bend 37, separation seems to be caused by the high curvature of the inner bank rather than the specific details of the inflow. The main topographic control in the bends is the relative position of the deepest part of the pool. In bend 37 this is close to the outer bank just upstream of the apex, whilst in bend 17 the pool is more centrally placed and closer to the bend apex. Thus, although the main flow processes occurring within these bends are very similar, site-specific details complicate the picture. These site-specific details become less important in bends where separation is more dominant and the flow structure becomes more coherent.

5.3.8 Sediment transport and flow mixing implications

The existence of large areas of slow downstream or reverse flow in bends like these has several important implications. The velocity patterns discussed above imply maximum boundary shear stress near the outer bank, as in the classical model, but upstream of the apex rather than downstream of it. Figure 5.16 demonstrates this general pattern of bed shear stress at the low flow stages examined.

There are extensive areas of low boundary shear stresses across the inner bank separation areas with concentrations of higher shear stresses in both bends in the upstream riffles and on the upper outer bank before the bend apexes. There are also zones of higher bed shear stresses at the toe of the outer bank along the path of the streamtube.

These patterns will have implications for the sediment dynamics within the bend, bank erosion and meander migration in such bends. At the discharges studied here, the inner-bank zones of slow flow act to accumulate patches of fine sediment. Indeed, at the flow stages examined above the Shields criterion suggests that the

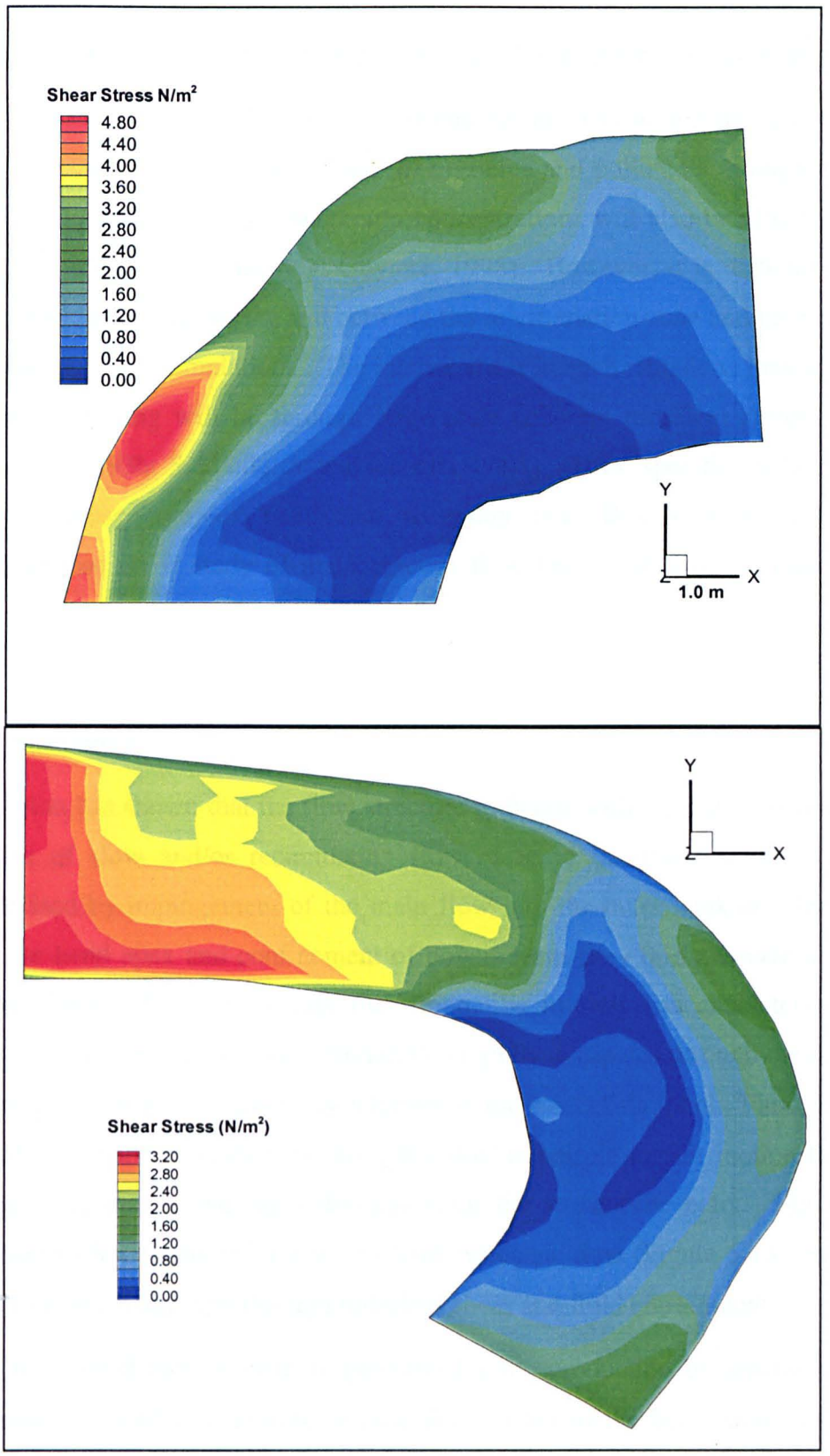

Figure 5.16: Predicted bed shear stress patterns in bends 17 and 37.

maximum size of entrained material through the upstream riffle in bend 17 is approximately 7 mm. Thus, little morphological change should occur at these flow

stages and the mobile sediments are likely to be deposited in the separation zones where flows are only capable of transporting particles an order of magnitude smaller.

The nature and timing of the mixing between the main flow and the re-circulation zones will clearly affect the movement of nutrients and pollutants through the river system. Residence times and maximum concentrations will also be affected by the presence of separation zones (*e.g.* Guymer, 1998). However, it is difficult to draw any conclusions on the mixing and between the re-circulation zone and the main flow from time-averaged simulations. The intense shear in such situations may mean that most of the mixing will be through large-scale coherent turbulent structures (*e.g.* Biron *et al.*, 1993b; Sukhodolov and Rhoads, 2001). Thus, specific studies of flow mixing in these complex bends are necessary (*e.g.* Boxall *et al.*, 2002) and techniques that allow study of instantaneous flow fields will also be required (*see* 6.1).

5.3.9 Summary

This section has shown that the flow structure in bends with separation is dominated by zones of slow and/or recirculating flow close to the inner bank. They are characterised by impingement of the main flow into the outer bank at a high angle before the bend apex and confinement of downstream flow into a streamtube along the outer bank. The flow within the streamtube initially has characteristics that suggest a strong helical motion, although this rapidly dissipates through the bend past the apex as the near bed velocity accelerates in the base of the pool. Fluid exchange into and out of the separation is through a double hairpin circuit motion that links into the accentuation and rapid dissipation of the streamtube helix. Fluid in the separation vortex seems to have a very high residence time (Figure 5.13), extracting energy from the main flow through turbulent shear and fluid entrainment.

Three interrelated factors seem responsible for the production of separation at the inner bank: streamline curvature; inflow distribution to the bend; and topographic forcing through the bend. However, the relative importance of these factors varied between the two bends investigated. Moreover, how these factors vary through time and at different flow stages is uncertain. Indeed, the presence and nature of separation zones are likely to alter with flow stage as the relative influence of the

controlling factors outlined above varies. For example, the influence of the upstream riffle bed topography is likely to reduce as discharge increases. Thus understanding of how these bends change requires investigations of the flow structures at higher channel formative flow stages. Therefore, section 5.5 examines the flow structure in bend 37 at a near bankfull flow.

5.4 OUTER BANK SEPARATION

5.4.1 Introduction

This section investigates the flow structure in a bend with a large outer bank separation zone. Initially, the study bend is introduced (5.4.2) and the field methods particular to data gathering in the bend are outlined (5.4.3). The specific application of the numerical model in the bend is detailed (5.4.4) and the assessment of model performance in terms of verification and validation is presented (5.4.5). The flow structures in the bend are presented and explained (5.4.6). A discussion of the similarities and differences between bends with outer bank separation, inner bank separation and bends with a classical flow pattern then follows (5.4.7). The implications these similarities and differences have are then explored and discussed (5.4.8). The section closes with a brief summary (5.4.9).

5.4.2 Study bend

Bend 25 (Figures 5.17; 5.18) is a sharp right-hand bend along the same reach of river as bend 17 and 37. It turns ~100° in 10 m and has a large outer-bank re-circulation zone which has been observed to be present at a range of flow stages.

There is a large concave-bank bench within the re-circulation zone and large amounts of floating debris including small woody debris are trapped in it after floods. The left-hand bend immediately upstream is fairly sharp so the talweg at the entrance to bend 25 is under the right-hand bank. The latter is undercut right to the apex of the bend but then lies back and becomes a point bar towards the exit of the bend. To the left of the talweg in the entrance to the bend is a high gravel bar with sand drapes and grass, separated from the grassy left-bank floodplain by a shallow chute channel that only carries water during very high flows. Bankfull width here is

~9 m but flow is normally restricted to a width of only 2-3 m in the true right-bank talweg.

Downstream from the entrance the left-side of the channel opens into a fairly elevated backwater area with a muddy bed. The right hand side of the channel then deepens into a deep pool (~ 0.95 m) which extends past the apex, after which the channel becomes shallower again and also narrower with an exit width ~4 m normally, but upwards of 6 m at bankfull flow when the point bar is submerged.

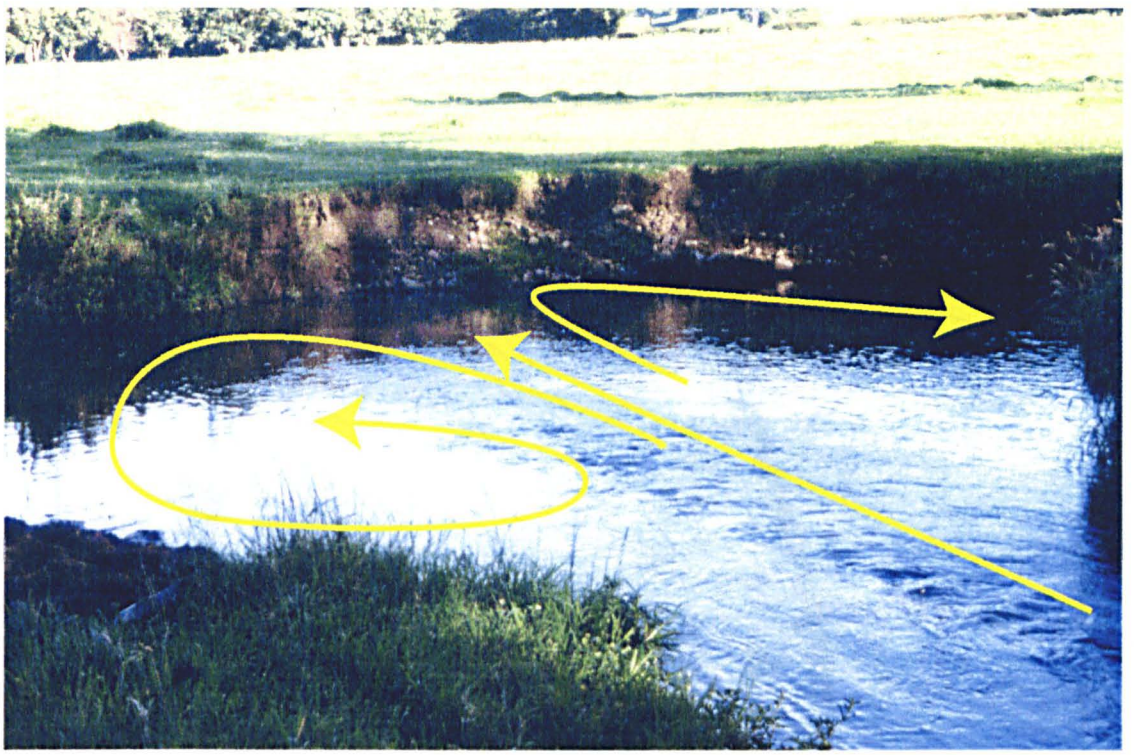

Figure 5.17: Bend 25 (looking downstream) during normal flow. The inserted arrows indicate general direction of surface flow (Taken on the 4th August 2000).

The outer bank of the pool is high (~1.1 m), quite uniformly-curved, and is composed of gravel with a thin capping of fine floodplain sediments. From the apex onwards it is actively eroding with undercutting of the grassy floodplain. The fastest flow in the bend hugs the inner bank and the entire central and outer part of the pool is a dead zone. To the left of the pool beyond the elevated backwater and towards outer bank opposite the apex the channel expands to upwards of ~12 m and a concave bank bench of fine material is present, around which a deeper trench has been cut around the outer bank. The highest point of this bench was ~0.9 m above

the two deepest parts of the pool, ~0.6 m below the floodplain, and just submerged. Since the survey, the bench has continued to grow and has become vegetated.

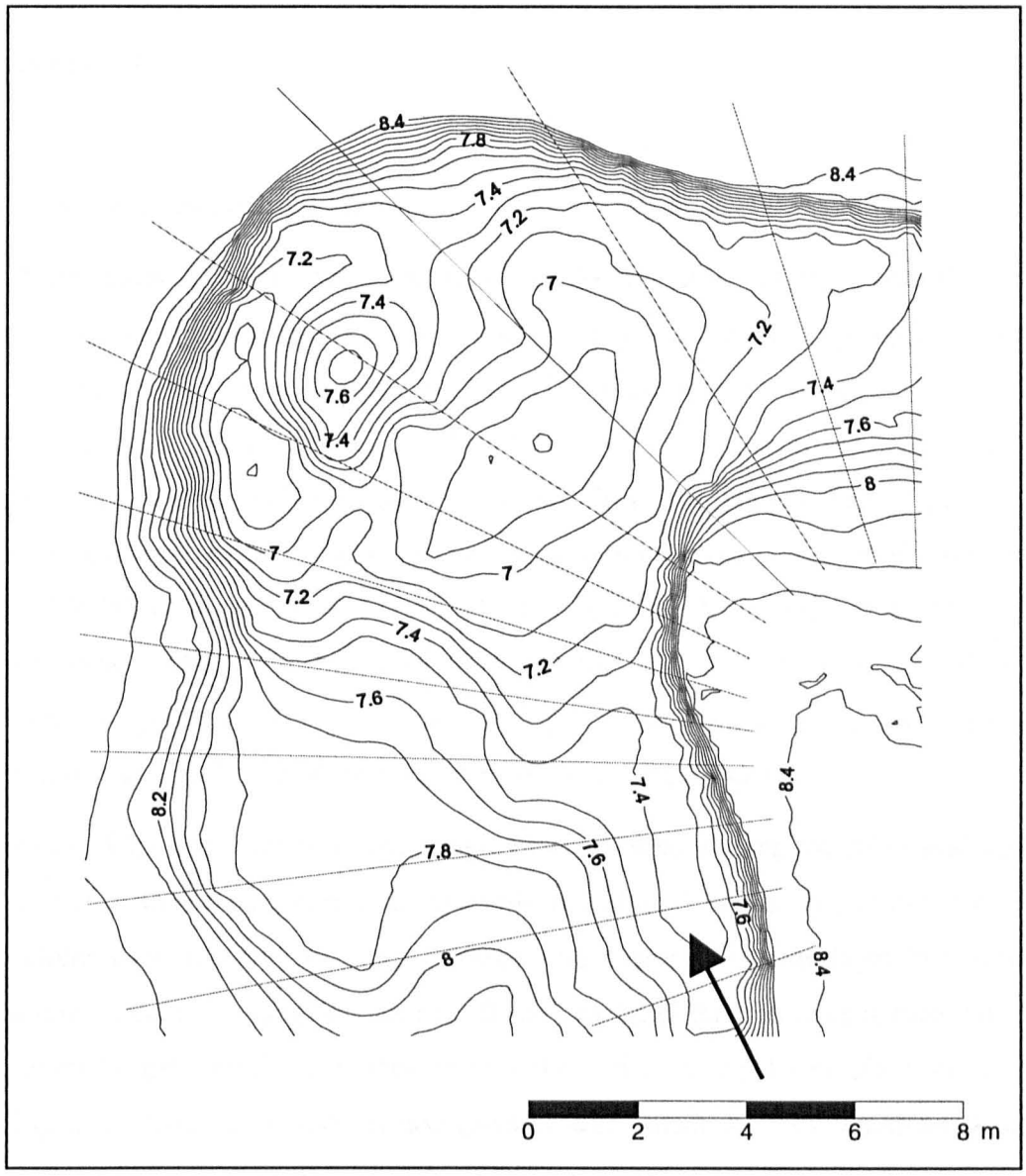

Figure 5.18: Bed morphology of bend 25 (4th August 2000). The arrow indicates inflow direction and the cross-section lines indicate slices taken through the DEM to produce the numerical mesh.

Bend average D_{84} is 34 mm, although this varies considerably through the bend, from 55 mm on the upstream riffle and 78 mm in the pool to 0.44 mm on the concave bank bench and 0.31 mm in the elevated backwater area. The grab sediment samples taken from the concave bank bench area had an average organic content of 3.2%.

The variation in both width and bank curvature around the bend makes it difficult to define an overall R_c/W ratio. However, the radius of curvature of the inner bank near the apex is <4 m and that of the outer bank right round the pool is no more than 6 m; since the channel is ~10 m wide here the R_c/W value is of order 1, which is extremely low.

5.4.3 Field monitoring methods

Field measurements were made on the 4th of August 2000 during a period of fairly low and slowly-falling discharge (~0.35 m^3/s). Stage did not change by more than 6 mm during the flow measurement period. The methodology applied is identical to that described for bend 17 (5.3.2). The banks and bed of each bend were mapped using a total station and a DEM was created from the survey data (Figure 5.18), using 566 survey points. Water surface elevations were also taken at 102 points. A general kriging algorithm was applied to interpolate the surveyed points onto a regular grid. The points surveyed along bank tops were used as breaklines to represent the position of major breaks of slope. Breaklines were also used along the edge of the pool and around the base of the concave bank bench.

As for bend 17, the velocity measurements were obtained using the ADV and wading rod at the inflow cross section, at spatially distributed points throughout the bend, and along two transects that cut through and along the shear layer between the separation zone and main downstream flow. As bend 25 was deeper than bend 17, the spatially distributed test data were collected at three fixed positions on the wading rod. Counts of 100 surface pebbles were made in 1 m^2 quadrats at seven locations and grab samples of fine sediment were taken from within five 1 m^2 quadrats in the dead zone. These samples were taken back to the laboratory where they were sieved for the size distributions quoted above.

5.4.4 Model application

5.4.4.1 Numerical grid

A grid was fitted to the irregular topography using boundary fitted co-ordinates (Figure 5.19). For this purpose, 23 cross sections from the DEM (Figure 5.18) were

used. The model had 110 cells longitudinally, 56 across, and 10 vertically. This means that cells along the outer bank close to the apex have average dimensions of ~0.28 x 0.22 x 0.06 m, in the x, y, and z directions respectively. Mean cell length decreases across the channel to ~0.11 m at the inner bank, and cell height varies between ~0.10 m and ~0.006 m according to local flow depth. These cell dimensions were used for validation and flow structure analysis after verification checks had been performed, the results of which are detailed below (5.2.5.1).

Construction of the grid was key to obtaining numerical convergence, slight modifications to the grid had to be made. This included placing vertical banks of 0.05 m near the point bar on the upstream riffle and around the elevated bed region in the upper portion of the bend before the pool. The abruptness of the angle at which the outer bank turned away from the inner bank just downstream of the inlet also had to be rounded. The construction of this grid was extremely difficult and took over a month to complete.

5.4.4.2 Boundary conditions

Inflow conditions were defined by fitting log laws vertically to the ADV profiles and linearly interpolating the velocity measurements to each grid node across the upstream section. *tke* at each node was given uniform values of 10% of the average inflow velocity. A constant boundary roughness height, which was estimated from the grain size surface counts on the upstream riffles, was used for both the bed and banks throughout the bend. Using $k_s=3.5D_{84}$ this gave a roughness height value of 0.193 m. As for bend 17 and 37, this significantly exaggerates the skin roughness of the sandy parts of the bed across the re-circulation zone, but the sand was rippled which adds some form resistance that is not represented in the model grid geometry. A hydrostatic pressure distribution was specified at the outflow cross section downstream of any negative dynamic pressure effects. The free surface approximation could not be used in the bend 25 simulations due to the vanishing cell heights over the concave bank bench. Thus, all model runs were performed using a planar fixed lid. Assessment of the sensitivity of the inclusion of the free surface approximation suggested it had a negligible effect in idealized bends with outer bank separation zones.

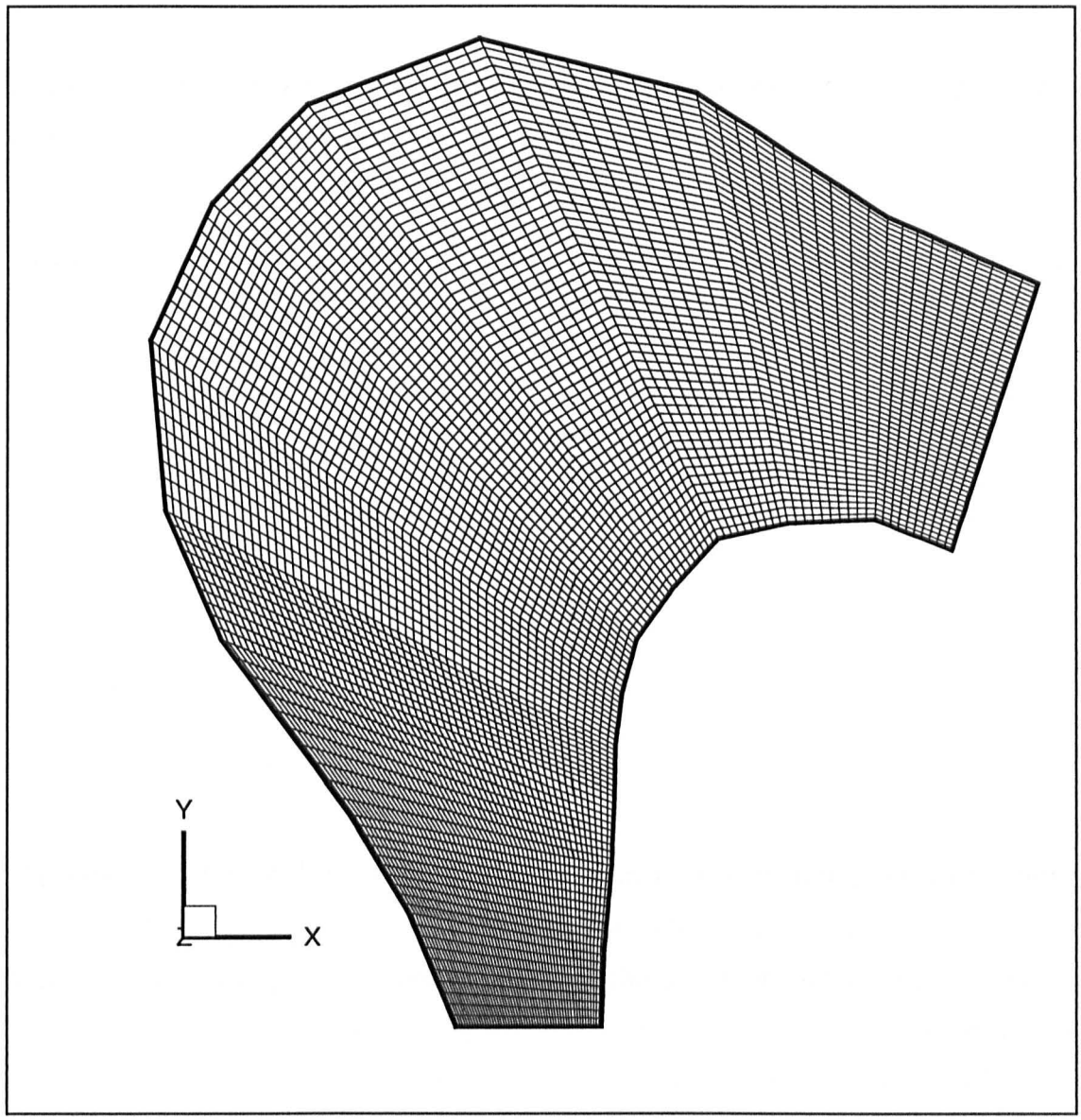

Figure 5.19: Numerical grid constructed

5.4.5 Model assessment

5.4.5.1 Verification

The GCI analysis was performed to ascertain that the solution from the grid resolution quoted above was independent of the grid spacing. Three simulations were performed with a doubling and halving of the mesh resolution. The GCI values obtained are presented in Table 5.3 and indicate that the mid-resolution grid is suitably verified for the three components of velocity. However, as for the results in

both bend 37 and 17 the convergence for the turbulence parameters is poor, reflecting the large amount of shear present within the bend and the fact that at the grid resolutions examined the RNG turbulence model is unable to fully capture this intense shear process.

Table 5.3: GCI results for bend 25 in percentage terms. Velocity components in *x*, *y*, and *z* directions, the turbulent kinetic energy (*tke*) and turbulent dissipation rate (*ep*)

Variable	B25	
	High-Mid	*Mid-Low*
x	5.23	15.01
y	4.58	22.17
z	5.11	14.15
tke	40.44	77.08
ep	35.12	42.70

5.4.5.2 Validation

Validation of the model solution was performed by comparing the mean flow velocities in the co-ordinate system Cartesian directions (*x*, *y*, and *z*), the resultant velocity magnitude, and turbulent intensities with those obtained using the ADV. Field sampling was performed using two main methods, resulting in 40 distributed sampling points and 35 points located along two transects that were positioned along the length of the shear layer. Comparisons between simulated and observed measurements are made for all 75 field-sampled points, although the two data sets are kept distinct for assessment purposes. The simulated values were taken from the nearest cell face in the CFD results, reflecting the fact that the grid cell size is much larger than the ADV sampling volume.

Scatter plots of predicted and observed values are presented in Figure 5.20 and the associated correlation and regression statistics in Table 5.4. As mentioned above error is possible in field measurements as well as model predictions, so both forward and backward least-squares regressions are reported. Analysis was performed for the full field sampling dataset and with the shear layer transect points removed.

a)

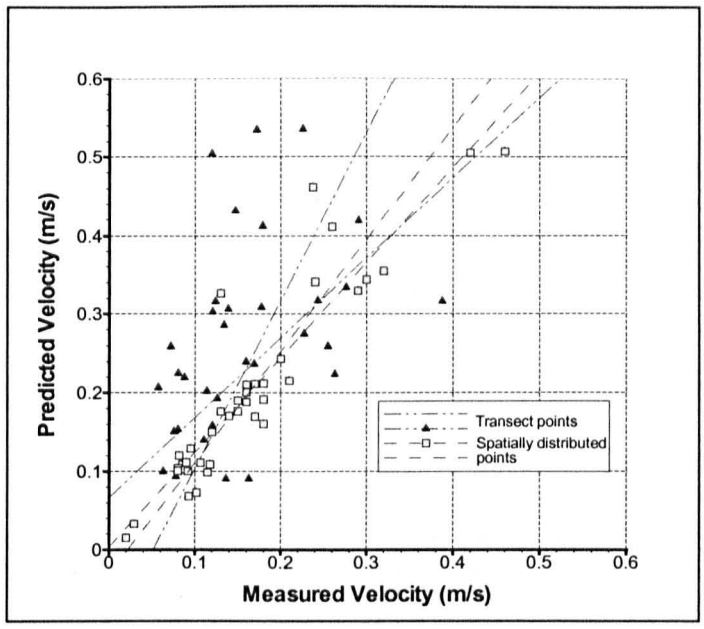
Predicted Velocity (m/s)
Measured Velocity (m/s)
Transect points
Spatially distributed points

b)

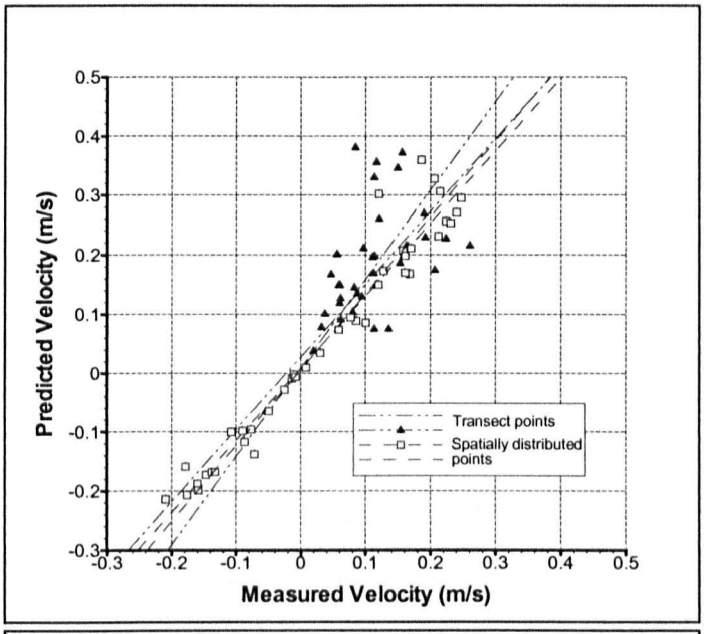
Predicted Velocity (m/s)
Measured Velocity (m/s)
Transect points
Spatially distributed points

c)

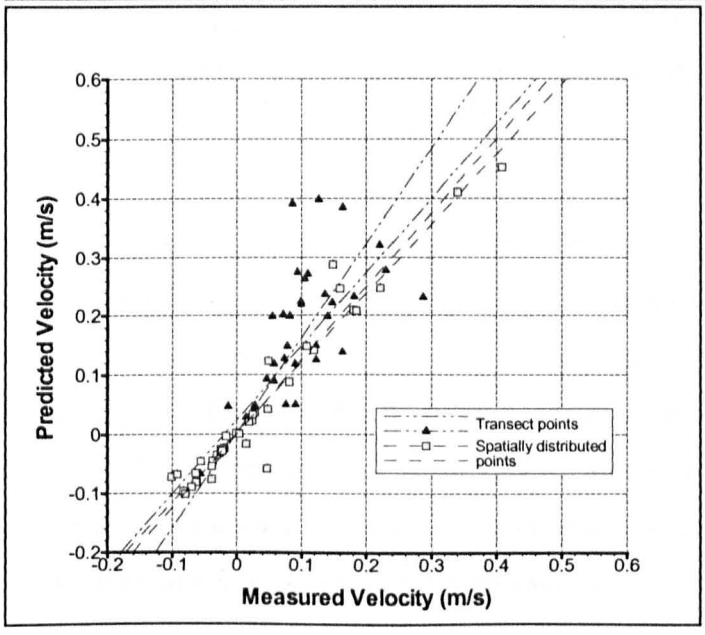
Predicted Velocity (m/s)
Measured Velocity (m/s)
Transect points
Spatially distributed points

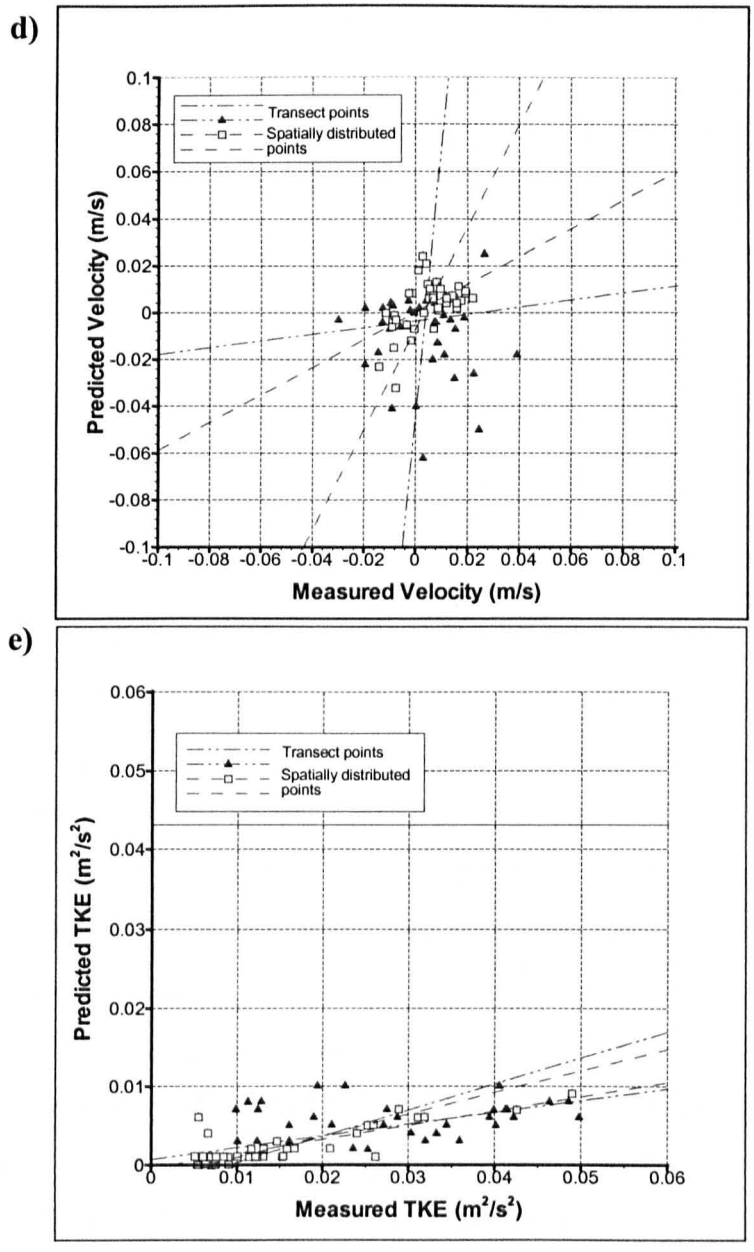

Figure 5.20: Comparison of predicted and observed values for bend 25: (a) velocity magnitude; (b) *x*-component velocity; (c) *y*-component velocity; (d) *w*-component velocity; (e) turbulent kinetic energy per unit mass.

When the full data sets are considered the agreement for the horizontal velocity components (*u, v*) is generally good (r ~0.9) (Figures 5.20a,b; Table 5.4), although both the forward and backward regression slopes deviate notably from the line of equality and the signs of *y* velocity component are incorrectly predicted for three points (Figure 5.20c). This is perhaps not surprising as the velocity is likely to fluctuate around zero at some points and the time-averaged values will not reflect this process. The agreement for velocity magnitude (*magnitude*), which combines

the errors in the horizontal components, is significantly inferior (r ~0.7), with deviations from the line of equality and in the intercept from zero (Figure 5.20a; Table 5.4a). There is a general trend of over prediction of velocities, although this error is mainly associated with the transect points (Figure 5.20a,b,c). Both the vertical velocity (z) and the *tke* also have poor agreement between predicted and observed values. The poor relationship for z reflects the low magnitudes and range of the values. However, the direction of flow at a number of points is incorrectly predicted with the model predicting negative values at points where positive values were observed. The ability of CFD to predicting vertical velocity can be poor when applied to natural river channels (Table 4.1) and is thought to be mainly associated with inadequate topographic representation in the grid (Lane *et al.*, 1999a). The points where the w direction is incorrectly predicted again relate to the transect points from within the shear layer. Predicted values of *tke* are considerably lower than observed, although the general trends are correctly predicted by the model. As discussed in the validation of bend 17, this probably relates to the time-average turbulence model, even with RNG modification, not providing adequate process representation of the fluctuating components of velocity.

All the regressions equations improve significantly when the shear layer transect points are removed from the analysis (Table 5.20b) with both the forward and backward regression lines falling closer to the lines of equality in all five scatter plots (Figure 5.20). The transect points represent a stringent and rigorous test of the numerical model as the points are concentrated through and adjacent to the shear layer where the time-averaged CFD model is known to perform imperfectly. Moreover, due to the presence of strong shear, this area is extremely sensitive to small errors in both model predictions and in the field positioning and sampling. For example, in areas across the shear layer, a 0.3 m movement can result in a five-fold increase in predicted velocity. Many of the transect points are significantly over predicted by the model and when the transect sample points were transversed 0.25 m towards the shear layer the regression equations all significantly improved. This suggests that the position of the shear layer is incorrectly predicted. A number of factors could explain this including: (1) that the shear generated momentum extraction from the mean flow may not be adequately represented by time-averaged modelling methods; (2) the use of a constant roughness height on the bed of the

channel may reduce velocities within the separation zone, reducing its return into the shear layer; and (3) the need to round-off the outer bank close to the point of detachment may result in more upstream flow into this region and a resulting migration of the incoming jet or streamtube to the left of its true position.

Table 5.4: Validation results for bend 17: comparison of ADV measurements at 62 field points with CFD model predictions. Forwards and backwards regression intercepts (*a*) and slopes (*b*) are shown, each with 95% confidence intervals, together with the correlation coefficient (*r*). Variables *x*, *y*, *z* are velocity components in Cartesian directions (as shown in Figure 5.21), *magnitude* is the resultant of the *x* and *y* components, and *tke* is turbulent kinetic energy.

Variable	CFD on ADV			ADV on CFD	
	a	b	r	a	b
a) For all data points					
magnitude ($m\ s^{-1}$)	0.05±0.03	0.47±0.12	0.69	0.07±0.04	1.02±0.25
x ($m\ s^{-1}$)	0.00±0.01	0.67±0.10	0.90	0.03±0.02	1.23±0.14
y ($m\ s^{-1}$)	0.00±0.01	0.62±0.08	0.88	0.02±0.02	1.25±0.16
z ($m\ s^{-1}$)	0.00±0.00	0.09±0.35	0.11	0.00±0.00	0.15±0.30
tke (m^2s^2)	0.01±0.00	1.56±0.32	0.61	0.00±0.00	0.24±0.07
b) Excluding transect points					
magnitude ($m\ s^{-1}$)	0.02±0.02	0.70±0.10	0.92	0.00±0.29	1.05±0.33
x ($m\ s^{-1}$)	0.00±0.01	0.78±0.06	0.97	0.01±0.00	1.22±0.09
y ($m\ s^{-1}$)	0.00±0.00	0.80±0.06	0.96	0.00±0.01	1.18±0.10
z ($m\ s^{-1}$)	0.00±0.00	0.46±0.25	0.52	0.00±0.00	0.59±0.32
tke (m^2s^2)	0.01±0.11	1.88±0.53	0.76	0.00±0.00	0.31±0.09

Although the exclusion of the transect points from the analysis results in an improvement in the model validation, a very slight tendency for *u* and *v* velocity over-prediction remains. The *w* correlation and regression equations are significantly improved (Table 5.4b) and although some scatter does remain, the regression lines are much closer to the 1:1 line. *tke* also improves with the removal of the transect points, with loss of many points where there was an order of magnitude difference between predicted and observed. Nevertheless, many of the predictions are still significantly under-predicted.

The assessment results presented above show a generally good and encouraging agreement between predicted and observed velocity, especially given the extreme test of a CFD model that this bend represents. The validation of the simulation is therefore considered adequate for the full results to be used in examining the general flow structure present within the bend, albeit with some caution with interpretation of the shear layer position.

5.4.6 Results: flow structure in a bend with outer bank separation

The simulated near-surface and near-bed velocity magnitude patterns with unit vectors are shown in Figure 5.21. Figure 5.22 shows 6 evenly spaced cross sections, labelled A-F, through the bend. Section A runs across the riffle face not far from the inflow, D from close to the inner-bank apex through the deepest part of the pool and across the top of the concave bank bench, E from the inner bank after the apex to the impingement point of the flow on the outer bank, and F close to the bend exit as the pool shallows.

The inflow into the bend is over a shallow riffle (<0.25 m), which has relatively fast flow. The riffle is strongly asymmetric, being deepest on the true right where the majority of the flow is concentrated. It follows on from a sharp upstream bend, which results in a strong cross-stream component to the flow.

The fast inflow filament from the riffle face jets straight into the pool and is confined into a streamtube close to the inner bank. There is a considerable reduction in surface velocity magnitude within the streamtube from ~0.7 m s^{-1} at section A to ~0.3 m s^{-1} through cross sections C to D. The rapid expansion in the cross sectional area produces this rapid decline in velocity, as jet (or streamtube) flow expands and diffuses in both cross-stream and vertical directions (Figures 5.21; 5.22; 5.24). As flow decelerates in the central part of the pool area, the flow slowly begins to turn right towards the bend exit (Figure 5.21). However, this deviation of flow does not occur very rapidly resulting in a high angle impingement of flow into the outer bank close to section E. The impingement of flow into the outer bank is characterised by a region of very low velocity magnitude as flow stalls in the region of high dynamic pressure (Figure 5.23). Separation of flow occurs around the area of stalled flow with some flow forced upstream along the outer bank by the region of relatively high

dynamic pressure. Flow within the re-circulation zone is similar at the bed and the surface with the main vertical axis of flow rotation around a distinct region of stagnant flow in the centre of the bend. Interestingly, this axis is not centred on the concave bank bench, although an additional, smaller, axis exists around a low velocity zone in the lee of the bench. The region of highest velocity within the re-circulation zone (~0.2 m s^{-1}) occurs close to the outer bank around the back of the concave bank bench through section D. This higher velocity zone splits either side of the concave bank bench, producing the two axes of rotation. The main re-attachment and re-entrainment of flow out of the re-circulation zone occurs in the centre of the channel between section C and D, although low velocity reverse flow continues along the outer bank almost to the inflow cross section. There is a significant difference in the re-attachment at the bed and the surface. Reattachment of reverse flow at the surface is to the mid-channel side of the inflow jet, but recirculating water near the bed is directed to the true right bank and crosses beneath the jet and is reattached to the upwelling side of the streamtube at the inner-bank (Figure 5.21; 5.25). Intense shear at the boundary between the main downstream flow and the adjacent water in the re-circulation zone exists between sections B to C, and is strongest at the surface. This shear layer is characterised by intense turbulent activity (Chapter 6), although the time-averaged position of the shear layer is approximately vertical through sections B to D.

At section E, the shear layer is significantly slanted away from the bed as the area of reverse flow at the bed is larger than at the surface presumably due to the greater stalling of the flow at the bed. To the right of the stagnation zone flow is forced out towards the bend exit by the zone of high dynamic pressure at the outer bank. This zone of high pressure at flow impingement would be associated with super-elevation at the outer bank. Interestingly, there is little downwelling at this point with most of the flow at impingement being translated into lateral flows. Between sections E and F, flow continues to cross rapidly from near the inner bank towards the outer bank, as the inner bank continues to turns rapidly away from the flow. This rapid crossover produces a small separation zone in the lee of the inner bank apex, with the time-averaged shear layer again slanted towards the bed.

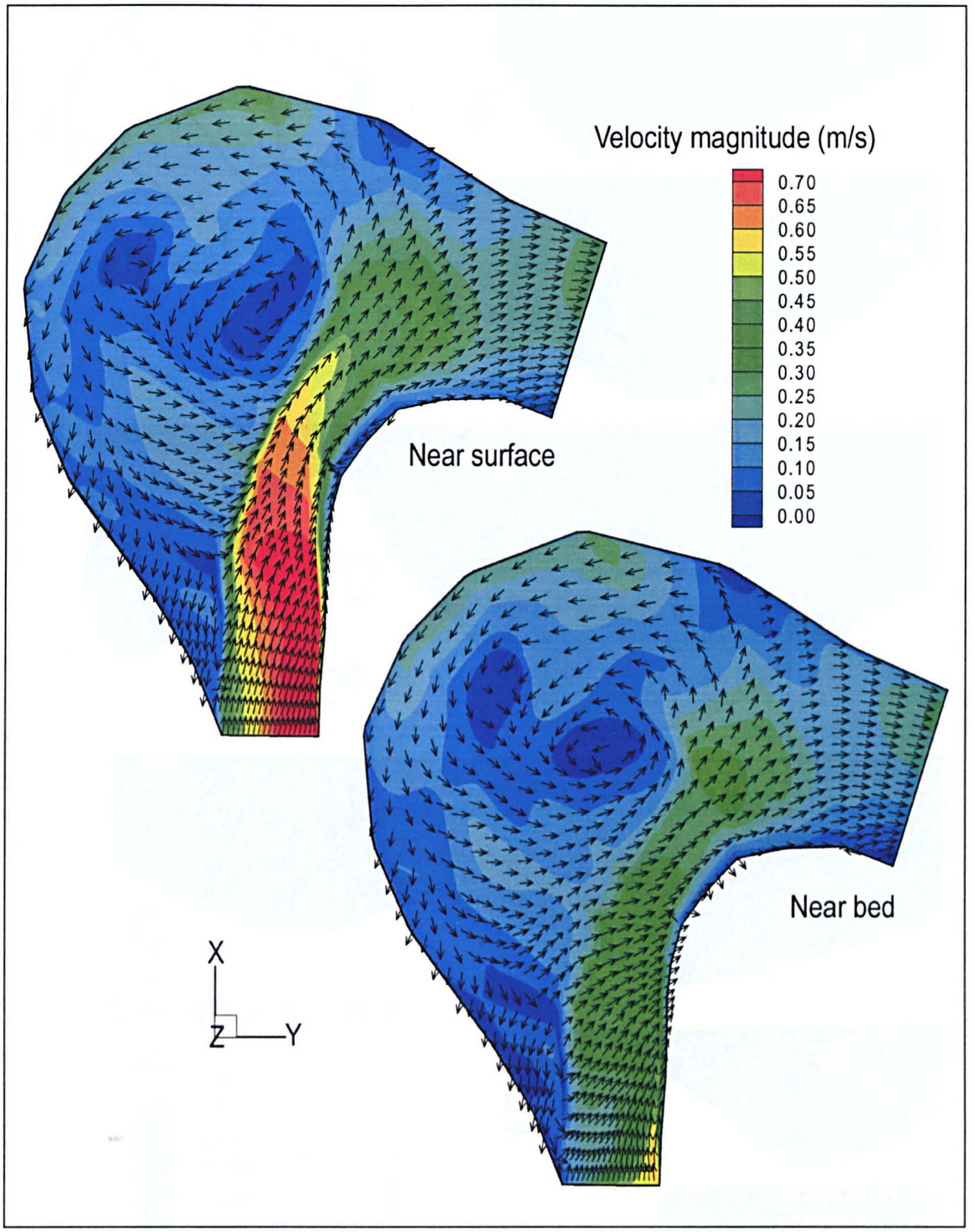

Figure 5.21: Bend 25: predicted planform maps of velocity magnitude with superimposed unit vectors showing flow direction near the surface and near the bed.

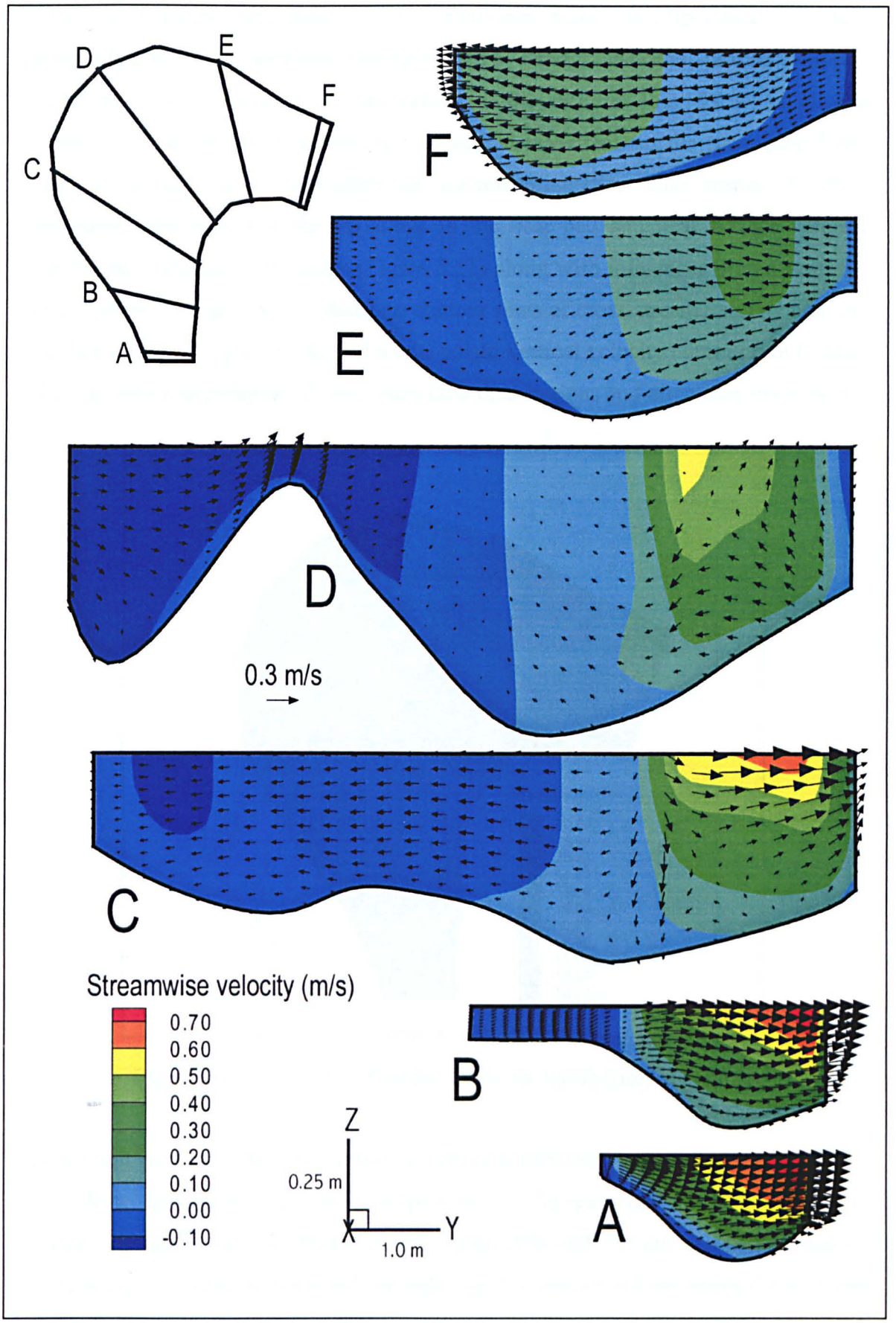

Figure 5.22: Bend 25: predictions of downstream velocity contours through the planes of cross-sections A-F with secondary velocity vectors superimposed (x4 vertical amplification).

The highly asymmetric nature of the banklines makes it impossible to obtain perpendicular cross sections throughout the bend. As the plotted velocity components are relative to the orientations of the sections, they do not yield zero cross-stream discharge in a section, let alone at a vertical, so the secondary flows represented are highly dependent on section orientation with respect to flow direction. Nevertheless, the variations in the near bed and near surface velocity directions in the planform maps (Figure 5.21) along with inferences drawn from the cross-sections (Figure 5.22), planform contour plots of cross-stream velocity near the surface and bed (Figure 5.24), and a mid-height vertical velocity contour plot (Figure 5.25) permit interpretation of secondary flow distributions and directions in the bend.

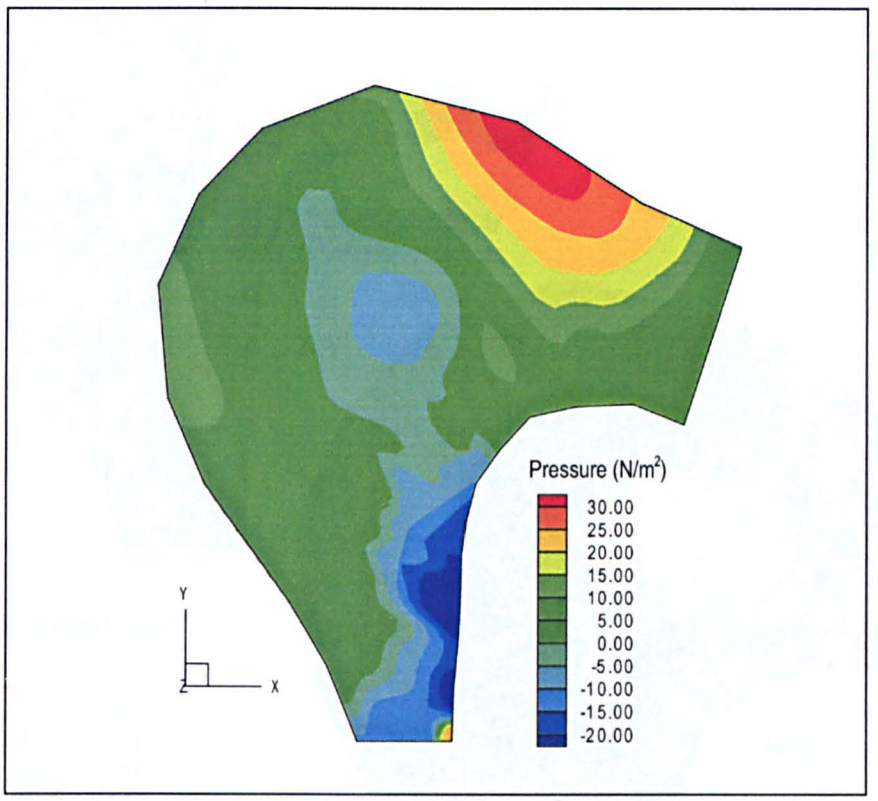

Figure 5.23: Predicted dynamic pressure distribution in bend 25.

At section A, flow is highly asymmetric, concentrated adjacent to the true right bank with flow through the section directed towards the true right bank (Figure 5.21; 5.24). Through section B, flow remains asymmetric with the left half of the channel containing slow reverse flow and the right half the main jet of incoming flow. Flow through the section retains a strong cross-stream component with upwelling at the inner bank. Figures 5.21 and 5.24 indicate that secondary flows close to section C

have a classical like helical flow structure within the streamtube, with near surface flow orientated towards the centre of the channel and near bed flow oriented towards the inner bank. There is also upwelling at the inner bank and downwelling adjacent to the shear layer (Figure 5.22; 5.25), highlighting the helical structure.

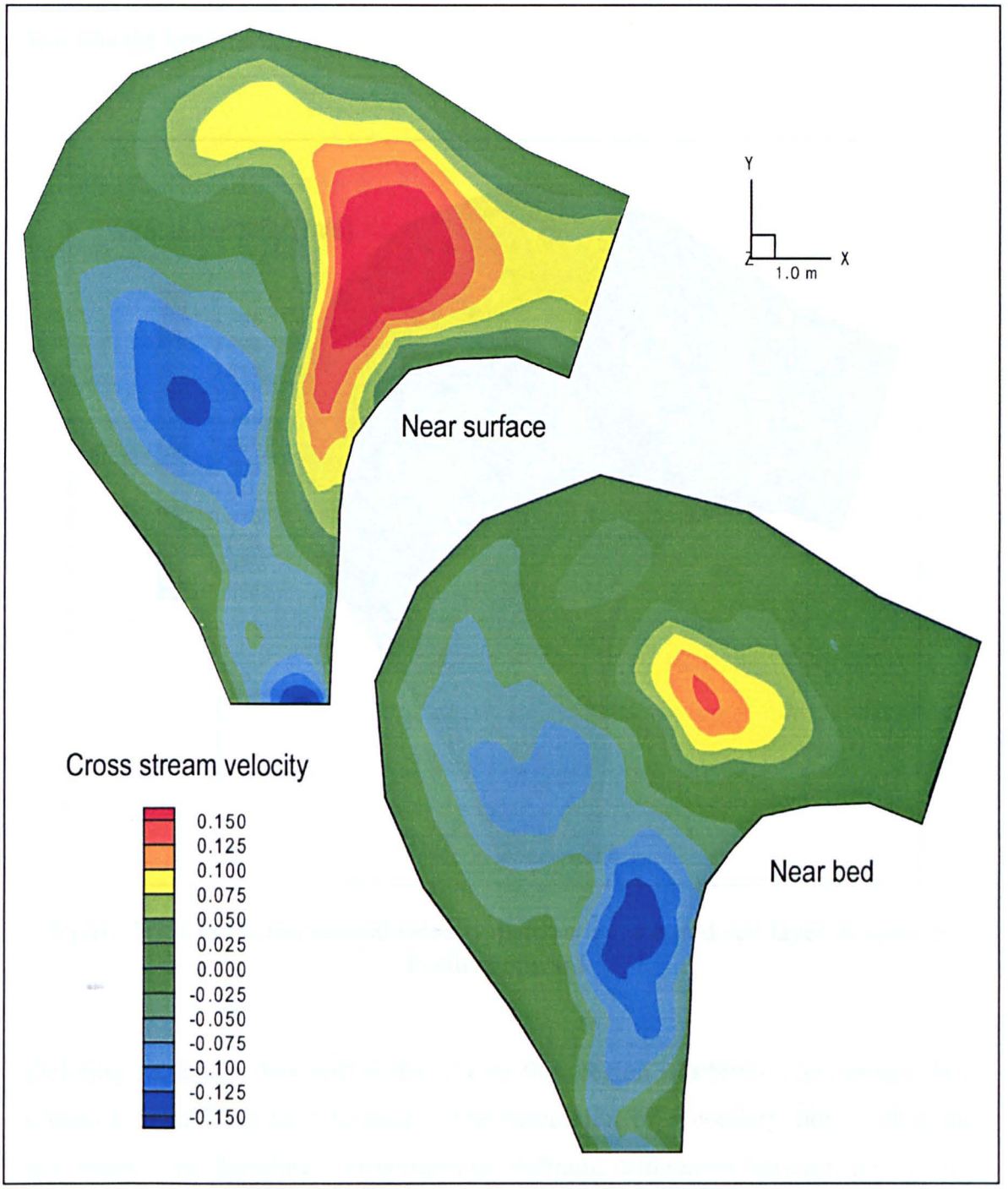

Figure 5.24: Predicted cross-stream velocity distribution in bend 25. Positive is towards the true left channel.

This flow structure in the streamtube continues into section D at the inner bank apex, with relatively strong downwelling over the pool (Figure 5.25). However, after the apex the intensity of helical motion declines significantly (Figure 5.21; 5.24; 5.25) as the flow expands past the bend apex and the near bed and near surface flow vectors are closely realigned once more. Towards section E, the more rapid crossover of flow towards the outer bank results in a weak leftwards component to the flow towards the bend exit.

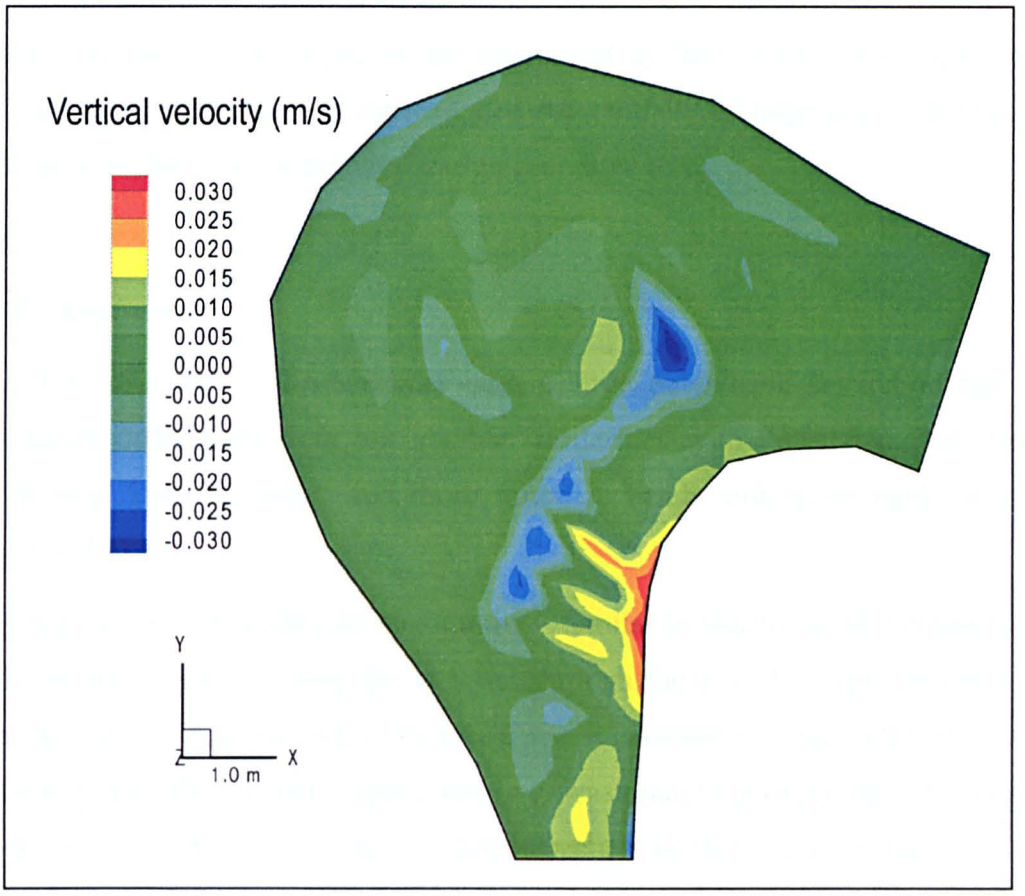

Figure 5.25: Predicted vertical velocity distribution at a mid cell layer in bend 25. Positive upward.

Defining secondary flow within the reverse flow region is arbitrary, as primary flow direction is difficult to determine. The discussion of secondary flow within the separation zone therefore concentrates on defining differences between the surface and the bed in certain areas. In absolute terms the secondary flows within the separation zone are weak, as all flow within the zone are relatively weak. Close to section E, to the left of the main impingement on the outer bank, a leftwards

component of surface velocity (Figure 5.21; 5.24) highlights the entrainment of flow into the separation zone. At the bed the flow is entrained into the re-circulation zone slightly more inwardly directed (Figure 5.21; 5.24), primarily a result of the slanted shear layer at the outer bank (Figure 5.22E). The main point of re-attachment at the proximal end of the dead zone is dominated by a zone of high rightward cross-stream velocities between sections B and C (Figure 5.21; 5.22; 5.24). At the bed, flow is turned into the streamtube slowly and re-attaches to the upwelling side of the helix at the inner bank. Return flow from the dead zone at the surface tends to impinge into the streamtube at a relatively high angle, which contributes to the intense shear across this zone. The nature of the movement of fluid across this shear zone is difficult to ascertain and will be mediated substantially by large-scale coherent flow structures produced by turbulent shearing processes (6.1).

5.4.7 Discussion

The flow structure in this meander with a large outer bank separation has some significant differences from but notable similarities with those found in classical bends (*e.g.* Dietrich, 1987) and those found in bends with inner bank separation (Section 5.3).

The velocity pattern within the streamtube is similar to that found in a classical bend with the main flow crossing the channel through the pool towards the outer bank after the apex. However, the collision of the streamtube into the outer bank occurs some distance after the bend apex, further downstream than expected in the classical model and a movement in the opposite direction to that found in the inner bank separation cases, where impingement occurs upstream of the apex. The helical flow pattern within the streamtube is also similar to that in a classical bend with downwelling along the shear layer and upwelling near the inner bank: the shear layer effectively replacing the outer bank as a barrier to the flow. The separation zone acts as the outer boundary to this helical flow structure and is somewhat isolated from the general helical pattern within the streamtube. However, as found for the inner bank separation cases, the intense helical motion found in the inflow streamtube is rapidly dissipated downstream past the bend apex. In classical bends, this helical structure can exist into the entrance of the next bend (*e.g.* Thompson, 1986). A dynamic shear

layer between the re-circulation zone and main downstream streamtube flow is present in bends with inner and outer bank separation. However, in the outer bank case, the shear layer is present on the downwelling side of the streamtube helix whereas in the inner bank case it is on the upwelling side. This has the effect of enhancing the time-averaged vertical distortion of the shear layer in the inner bank case as the near bed velocity within the streamtube is lower at the bed and as free surface variation can mediate the downwelling within the helix in the outerbank case. These differences are also likely to affect the shear-generated turbulence production across these regions within the bends.

The mechanism through which separation occurs is dissimilar in outer and inner bank separation cases. In outer bank separation, flow separates distally against the outer bank at the point of highest dynamic pressure and re-attaches proximally, along the upstream edge of the shear layer. In the inner bank cases, separation occurs proximally at the inner bank apex and re-attachment occurs distally, some distance downstream along the inner bank. Thus, inner bank separation is produced by a region of low relative dynamic pressure in the lee of the inner bank apex, whereas outer bank separation is produced by a region of high pressure at the impingement point after the bend apex. This is likely to affect the turbulent flow structures produced along the shear layer and their advection into the separation zone. This is examined in the following chapter (6.1).

The separation zone in the outer bank case is much larger than in either of the inner bank cases examined above. Indeed, the reconnaissance survey identified that although they are slightly less frequent, outer bank separation zones tend to be much larger than inner bank separation zones. As they are larger features within the fluvial system, and occupy greater areas of the bed and larger volumes of recirculating flow, outer bank re-circulation zones are likely to be more significant in controlling fine sediment dynamics and flow residence times through the reach.

It is difficult to isolate the factors that control the nature of the flow structure present within bend 25. However, some of the controls on the presence of outer bank separation in idealized sharp meander bends were elucidated by the numerical experiments of Hodskinson and Ferguson (1998) and similar features are also present in this bend. These include: (1) sharp curvature in both banks and a large and rapid expansion in channel width; (2) no point-bar present at the inner bank; and (3) a main

core of inflow velocity that is close to the inner bank at the inflow section. The high curvature of the bend, and the inertia of the high velocity inflow act to drive the flow into the outer bank at a high angle. As no point bar is present, the inflow streamtube enters the bend and follows the line of the inner bank until its apex where a delayed but rapid crossover produces a region of high dynamic pressure at the outer bank downstream from the outer bank apex. Flow stalls and separates within this region with a portion of the stalled flow being forced upstream into the re-circulation zone. Flow forced to separate into the dead zone slowly recirculates, producing intense shear between the streamtube and the dead zone. The shear layer and the pressure gradients produced by reattachment act to confine the inflow in the streamtube region close to the inner bank. However, unlike in the inner bank separation case the presence of the re-circulation zone does not reduce the effective width of the downstream flow past the apex. The reduction in vorticity of the streamtube helix seems to be produced by the general deceleration of flow as it enters the deep pool, where the cross sectional area increases significantly.

Hodskinson and Ferguson (1998) demonstrated that the character of the bend inflow was a critical factor in the size and extent of separation zone. Thus, it is likely that the character of the inflow streamtube in this bend, which is governed by a combination of upstream planform and local topographic forcing on the upstream riffle, will be a sensitive and a significant control on the flow structure within the bend. For example, if the inflow were directed towards the centre of the bend, the production of a larger inner bank separation and smaller outer bank separation would perhaps be more likely. Moreover, an increase in velocity, produced by an increase in discharge or reduction in pool depth would reduce the effect of deceleration through the bend and collision of the streamtube into the outer bank would perhaps move upstream, increasing the velocity in the dead zone. This mechanism is likely to be self-regulatory. If the impingement point moves upstream, a greater proportion of flow will be forced into the separation zone. This will cause the streamtube to be forced toward the inner bank at reattachment, which will result in the impingement point moving back downstream. However, time did not permit the sensitivity of the flow structure within the bend to such factors to be examined, although this avenue of research could be followed using numerical experiments where the geometry or inflow distribution of the 'real' rather than an idealized channel could be altered.

5.4.8 Implications

The result and implications of this complex flow structure in bend 25 are illustrated in the bed shear stress distribution (Figure 5.26), which is very different from that found in classical bends. The bed shear stress pattern through the bend indicates that the highest shear stresses occur over the shallow inflow riffle, where the bed material is relatively coarse. The majority of the bend has very low shear stresses indicating its depositional nature at this flow stage. The rapid reduction in velocity from the riffle into the pool of the bend and entrainment of fluid into the separation zone will act to trap fine sediments moving through the system as they are dropped out of suspension within the region of re-circulating flow. Given the size and volume of the separated flow region, this bend is therefore a significant sink for the fine sediments within the reach and is thus extremely important in regulating the dynamics of fine sediment through the system.

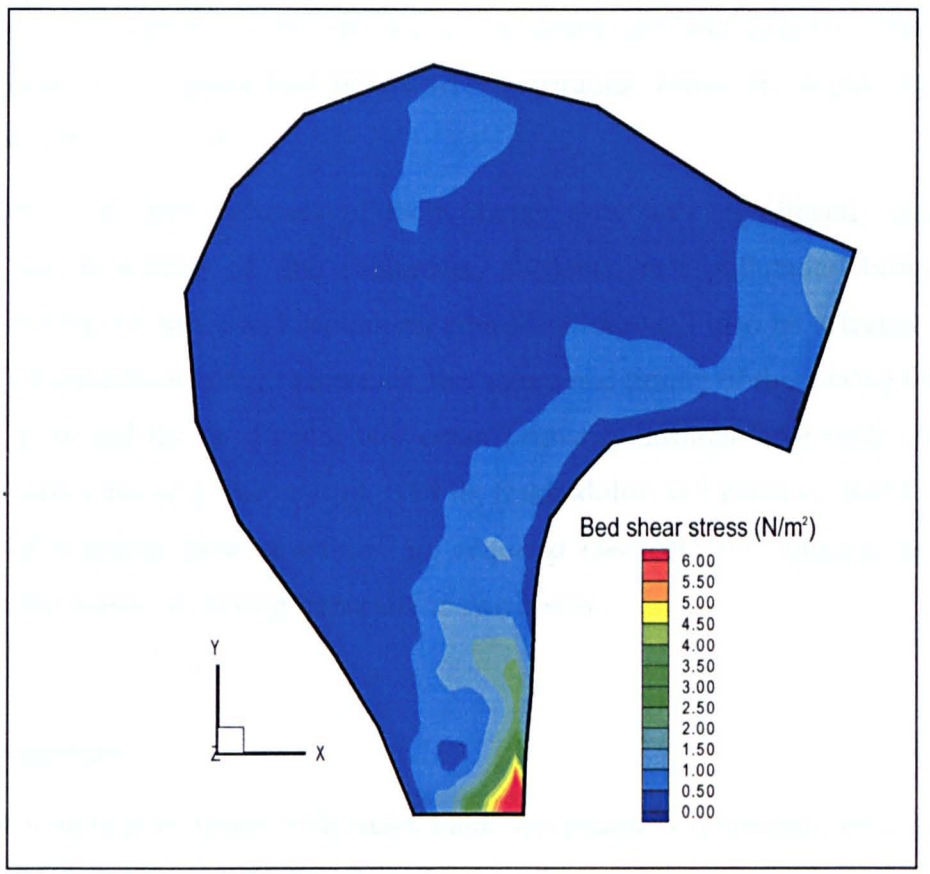

Figure 5.26: Predicted bed shear stress patterns in bend 25 at normal flow.

The pattern of flow through the bend also indicates that the migration patterns of bends with outer bank separation are likely to be very different from both more classical bends and bends in which inner bank separation occurs. The presence of the streamtube close to the inner bank at a higher flow and the collision of flow into the outer bank is likely to result in erosion of the convex bank and erosion of the outer bank around the point of impingement. This is confirmed by Figure 5.27, which indicates that bend 25 has indeed migrated downstream through erosion of the inner bank up to the point of the apex where the main streamtube departs and collides into the outer bank where another zone of significant erosion also exists. The bed elevation within the separation zone also increased during this period with the backwater area in the proximal part of the re-circulation zone being a concentrated area of deposition. The concave bank bench expanded into the pool and increased in height by approximately 0.25 m at its highest point. Whether the separation zone remains a sink for fine sediment during bankfull stage is difficult to determine, although the large amount of deposition within the zone indicates that it may. Figure 5.27 illustrates a significant amount of erosion, deposition, and migration during the study period and suggests that bends with separation zones are highly dynamic features within the system.

The presence of large volumes of recirculating flow will significantly alter and mediate the movement of fine sediments, nutrients, and pollutants through the system. Residence times and maximum concentrations will also be affected by the presence of separation zones. However, the nature and timing of the mixing between the main flow and the dead zones will occur primarily through large-scale coherent turbulent structures (*e.g.* Biron *et al.*, 1993b; Sukhodolov and Rhoads, 2001). Thus, analysis of transient flow structures are required (*see* 6.1) for conclusions to be drawn on the nature of mixing between the two zones.

5.4.9 Summary

The flow structure in bends with outer bank separation is dominated by a zone of slow recirculating flow at the outer bank. These bends are characterised by impingement of a streamtube into the outer bank at a high angle after the bend apex and a stalling of the flow in a region of high dynamic pressure produced. As found

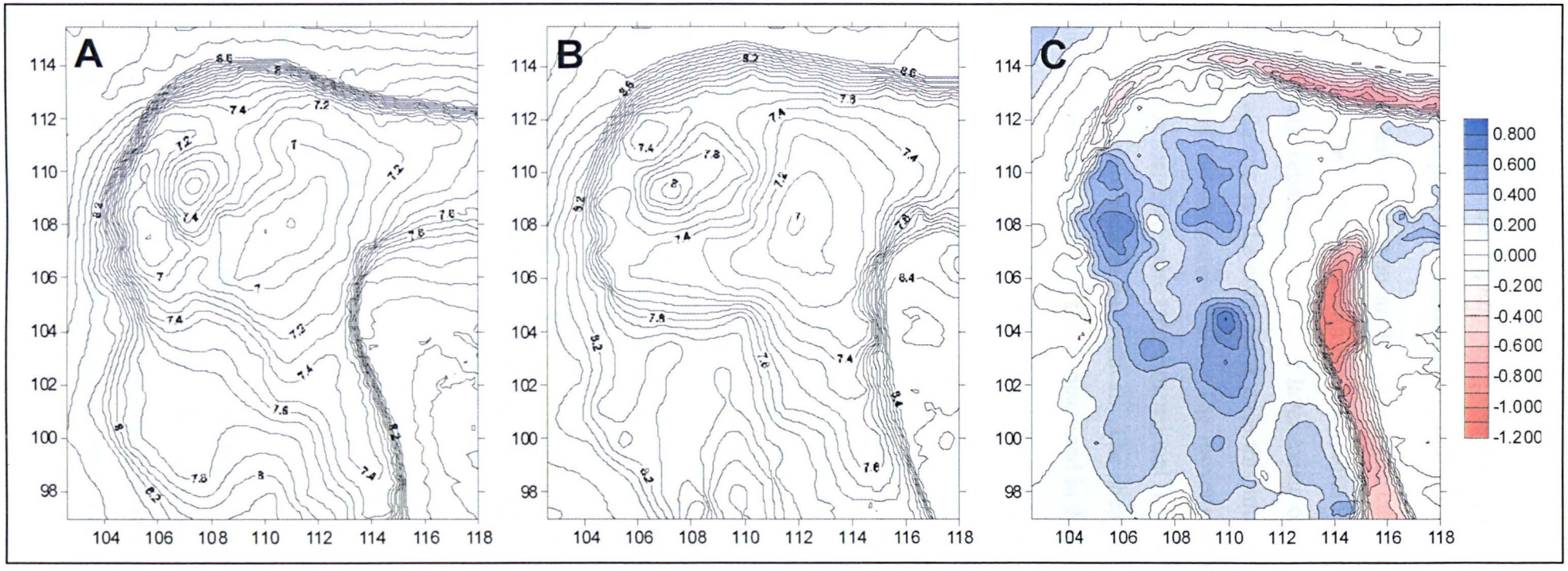

Figure 5.27: Digital elevation models of bend 25 (A) 4th August 2000; (B) 28th February 2002; (C) identified difference. Units in meters.

in the bends with inner bank separation, flow within the streamtube initially has a strong helical motion, although this rapidly dissipates through the bend past the apex as flow decelerates into the pool and turns after the impingement at the outer bank.

The shear layer is less deformed than in the inner bank case and results from the different interactions of the streamtube with the re-circulation zone in the two cases. In bends with inner bank separation, the shear layer exists on the upwelling side of the streamtube helix whereas in the outer bank case this interaction is produced on the downwelling edge of the streamtube helix. The movement of flow into and out of the separation zone is therefore more two-dimensional than in the inner bank case as the shear layer is less deformed in the vertical. The shear along the boundary is dominated by large-scale turbulence and this is discussed in detail in chapter 6.

The significant factors responsible for the production of separation at the outer bank identified by Hodskinson and Ferguson (1998) exist in bend 25: the bends are tightly curved with a rapid expansion in the apex channel width; no point-bar is present within the bend; and the inflow is asymmetrically skewed towards the inner bank.

The presence of separation at the outer bank radically alters the shear stress distribution through the bend and the low stress across the re-circulation zone indicates the depositional nature of the bend. Migration patterns are significantly different than more classical bends, with erosion occurring along the convex bank and at the outer bank well past the bend apex. This results in deposition within the separation zone as the bend slowly abandons the region. To completely understand the complex morphological change in bends with separation there is a need to investigate the flow structures present at channel forming discharges. The next section details an initial attempt at this.

5.5 STAGE DEPENDENCE

5.5.1 Introduction

Understanding how flow structure changes with discharge is one of the fundamental limitations of most studies of reach scale channel flow structures. This is because the vast majority of investigations have only analysed the flow structure at one discharge (*e.g.* Bathurst *et al.*, 1977; Carson and Lapionte, 1983; Van Alphen *et al.*, 1984;

Ashmore *et al.*, 1992; Lane *et al.*, 1995; Hodskinson and Ferguson, 1998), which is often at low to intermediate discharges. This is primarily due to the low frequency and short duration of higher flows in many of the rivers investigated. However, it can also be due to logistical and safety reasons. Thus, little may be known about how flow structure changes with stage and the nature of flow structures present at higher flow discharges, which are primarily responsible for determining channel form. Moreover, the contrasting conclusions drawn by different studies of the importance of different convective acceleration terms in the production of secondary flows has been attributed relative flow stage differences between studies (Whiting, 1997). Hence, studies are often analysing and interpreting the effect of channel form on flow processes rather than truly exploring the feedback linkages highlighted in Figure 1.1.

Current understanding of three dimensional flow structures at high flow stage is based upon a few field studies that have examined the influence of flow stage, including Jackson (1975) who presented the flow field at different stages at a single cross section in a bend. Dietrich and Smith (1984) investigated the topographic and shear stress adjustments at two flow stages in a classical mender bend, one of which was 70% of the bankfull discharge. Through detailed velocity measurements in three cross sections, Markham and Thorne (1992) examined the effect of flow stage on the flow structure through a meander. Bridge and Gabel (1992) and Whiting (1997) both examined how patterns of flow alter as flow increases around and over a mid-channel bar, and Rhoads and Kenworthy (1995) did likewise in a river channel confluence. However, many of these studies have experienced significant problems in gathering the required data. For example, Markham and Thorne (1992) were only able to obtain measurements at three widely spaced cross sections through a bend and encountered difficulties in obtaining cross-section velocity measurements at comparable flow discharges for both high and low flow stage situations.

Nevertheless, these findings and theoretical based studies suggest that strength of the helical circulation in bends generally increases with streamline curvature, velocity, degree of super-elevation, and depth of the pool (Dietrich, 1987). This is because each of these factors will increase the magnitude of the centrifugal acceleration and thus the pressure gradient force. Therefore, there is a positive feedback relationship between channel form and flow processes, whereby deeper sharper bends have

higher secondary circulation velocities. This produces a co-variation of channel morphology in both the cross-section and the planform directions of the channel. The relationship between discharge and strength of secondary circulation therefore depends on the relative variation in the above factors, especially velocity and curvature, in individual bends (Hooke, 1975; Bathurst *et al.*, 1979; Markham and Thorne, 1992). As a result, the strength of secondary circulation has been found to increase to a maximum at intermediate discharges. As stage increases, primary currents dominate and secondary circulation strength declines due to the main flow following a straighter path and shoaling over the point bar (Dietrich and Smith, 1983).

An extension of this analogy to flow separation may suggest that at higher flow stages than those measured and modelled in sections 5.3 and 5.4, separation at the inner bank could be 'washed' out while at the outer bank the separation zone may grow. Indeed, the occurrence and size of flow separation will depend on how the hydraulic geometry of the channel alters as stage varies and several authors have noted some changes in the occurrence and extent of flow separation zones according to flow stage. For example, Bridge and Jarvis (1982) found that inner-bank separation in steep-sided intertidal creeks was transient and only occurred at a range of intermediate flows. Its disappearance at high tide is consistent with a reduction in topographic steering as just discussed. The likelihood of separation at lower tides is diminished as the main flow velocity is lower and the curvature of the bend is reduced due to a greater decrease in width than in bend radius with stage. However, the conclusions of this study are difficult to interpret due to its tidal setting: high tides result in deeper slower flows rather than deeper faster flows.

Despite the problems with fieldwork outlined above, Markham and Thorne (1992) were able to report that outer-bank separation occurred at bankfull stage in a bend on the River Roding, but not at lower discharges. They identified alteration in the impingement angle of the main flow current on the outer bank as the likely explanation. As stage and velocity increase, the main flow encounters the bank at a higher angle, resulting in a greater portion of the incoming flow being forced to flow upstream. However, Andrle (1994) found that this was not the case with outer-bank reverse flow in Mansfield Creek, which was found to be persistent at all flow levels.

Although the three bends investigated above (Sections 5.2 and 5.3) have been observed to have separation zones at higher flow stages, the relationship between flow stage and the presence and extent of flow separation is poorly understood. Moreover, the flow structure at channel forming flow stages in bends with separation is also unknown. This section examines the flow structure in bend 37 at near bank-full flow. Bend 37 was the ideal choice for investigation at high flow as the inflow is relatively simple and is some distance upstream of the bend. The methods through which the higher discharge inflow was calculated and modelled are detailed (5.5.2). Specific attention is also paid to how the grid was re-constructed for the increase in the size of channel geometry, how the bank-full discharge was computed, and how this discharge was distributed through the inflow cross section. The modelling results obtained are presented and explained (5.5.3), before the flow structures through the bend at the high and low flow are compared and contrasted in a general discussion (5.5.4). The section ends with a brief exploration of the implications of the findings (5.5.5) and concludes with a brief summary (5.5.6).

5.5.2 Methods

No high flow measurements could be made in bend 37. Thus, to model the flow structures at a higher stage, the boundary fitted grid had to be re-generated for the increased volume of flow and the bankfull discharge had to be calculated and the velocity distributed across the upstream cross section.

The discharge was calculated by computing the water surface slope at the normal flow discharge at which measurements were made modelled in 5.3. The DEM (Figure 5.4) was then used to ascertain the approximate elevation of the water surface in the bend at a discharge close to bankfull and the average depth of flow across the inflow cross section was calculated. With an assumption that the water surface slope does not change appreciably as stage increases, the standard law-of-the-wall (4.5.2.1) was applied to calculate an average inflow velocity. This average velocity was then used to provide an estimate of bankfull discharge in the reach, which was almost six times the normal flow stage investigated above (Table 5.5). This agreed well with the Environment Agency gauging station stage curve, which is located 5.4 km downstream. The computed bankfull discharge was then used to

distribute the flow across the inflow cross section according to law-of the-wall. Thus, a fully developed inflow velocity for the bankfull stage was produced and was used as the boundary condition in the high flow model runs.

Table 5.5: Change in variables with discharge

Variable	Normal flow	High flow	Ratio
k_s (m)	0.231	0.231	1
Water surface slope	0.00266	0.00266	1
Inflow width (m)	4.80	5.70	1.2
Mean inflow depth (m)	0.18	0.45	2.5
Mean inflow velocity (m/s)	0.58	1.08	1.9
Discharge (m^3/s)	0.50	2.77	5.5

It should be noted that although the mean water surface slope is unlikely to alter greatly, differences over the pool-riffle topography are likely to change as stage increases. However, a sensitivity analysis revealed that even a 10% change of the water surface slope from the constant value used only resulted in only 3% change in the computed average inflow velocity.

The same 12 cross-sections used for the normal discharge simulation (5.3) were extracted from the DEM (Figure 5.4) to the elevation of the higher flow through the bend. These cross-sections were then used as planes through which a 3D grid is interpolated (4.6). The same grid resolution used for the normal flow stage was applied for the high flow case, despite the grid occupying a greater volume and greater lengths in both the vertical and cross-stream directions. Thus, the grid resolution applied had 80 cells longitudinally, 30 cells across, and 10 cells vertically. This means that the grid resolution is slightly lower than in the low discharge model (5.3) with cells along the outer bank having average dimensions of ~ 0.28 m x 0.22 m x 0.12 m, in the x, y, and z directions respectively.

5.5.3 Results: flow structure at high flow stage

5.5.3.1 Horizontal components

The simulated near-surface and near-bed flow patterns at both the lower flow discharge and high discharge are shown in Figures 5.28 and 5.29 respectively. The unit vectors show the resultant direction of the u (streamwise) and v (rightwards) components of velocity at alternate cells in each direction, with background contours of velocity magnitude. Figures 5.28 and 5.29 demonstrate that the main features of the flow are maintained at the higher flow discharge, although several significant alterations in flow detail are evident.

As flow stage increases, the sloping nature of both banks towards the bed, especially along the banks of the inflow riffle, results in a general widening of the channel. The mean inflow velocity into the bend is more than twice as high at bankfull flow stage (~1.5 m s^{-1}), with the main core of velocity occupying a greater width of the channel. Impingement of this main flow core on the outer bank occurs further downstream than at normal flow stage, but still upstream of the bend apex.

The strong flow asymmetry through the bend continues to exist past the apex at bankfull stage, with the inner bank separation remaining present and the downstream flow still confined into an outer-bank streamtube. Although the separation zone remains at bankfull stage, it is smaller and the flow structure within and around it is altered considerably. The upstream extent of the reverse flow is curtailed by the high velocity inflow and the point of detachment likewise is further downstream along the inner bank. The area of very slow velocity in midstream remains, although it is significantly smaller in the high flow case. Downstream of this slow velocity area, the return flow into the separation zone towards the inner bank is at a much higher angle with the point of reattachment slightly further upstream. The velocity within the separation zone is much higher at bankfull stage, with the flow towards the inner bank and the reverse flow at the surface both exceeding 0.75 m s^{-1}.

The near bed flow pattern also alters appreciably (Figure 5.29). The size of the separation zone generally reduces from about 2/3 of the channel width to approximately 1/3, primarily due to the corresponding expansion of the streamtube at the bed. The upstream extent of the separation zone is reduced, although the point of reattachment remains relatively similar at high and normal flow stages. The velocity

within the streamtube is much greater at high flow stage, with large regions of very high near bed velocities along the outer bank, especially downstream of the bend apex. The direction of the flow within this region is more inwardly directed than at lower flow discharges as the flow is less influenced by the presence of the smaller separation zone. Like the surface flow pattern, flow within the separation zone at the bed turns upstream rapidly, accelerating to ~0.9 m s^{-1} close to the inner bank. Thus, the vertical axis vorticity of the flow within the separation zone is much higher at bankfull discharge as the flow turns and recirculates more tightly and at a higher velocity.

5.5.3.2 Secondary circulation

The large difference in near-bed and near-surface velocity vector directions indicates intense secondary circulation at high flow stage. This difference in direction is as much as 80° in the streamtube of fast downchannel flow in the first part of the bend. The presence of more intense helical flow at high flow stage is confirmed by the cross-section plots (Figure 5.30). Moreover, the cross-section plots also demonstrate that the nature of the secondary flow structure and locus of maximum u also alter with flow stage.

Similar to the lower discharge, at bankfull stage there is a progressive movement of the locus of maximum u down the outer bank and into the base of the pool. This movement occurs as rapidly as at normal flow stage, although the areas of high downstream u are much larger and occupy greater portions of the bed through sections D, E, and F. These areas of high downstream u occupy the main areas of the scoured pool up to the crest of the submerged point-bar.

As in the lower flow stage case, the changing location of the high u component through the bend is strongly related to the patterns of upwelling and downwelling. At high flow stage, the increase in depth and width at section A, are associated with patterns of upwelling and downwelling that suggest a coherent secondary circulation cell close to the outer bank. Although the beginnings of such a flow pattern are present at the normal flow stage, it is not as clearly defined or developed. At section B in the high flow stage case, this streamtube secondary cell is more intense and much larger, occupying half the channel. Upwelling dominates the inner half of the

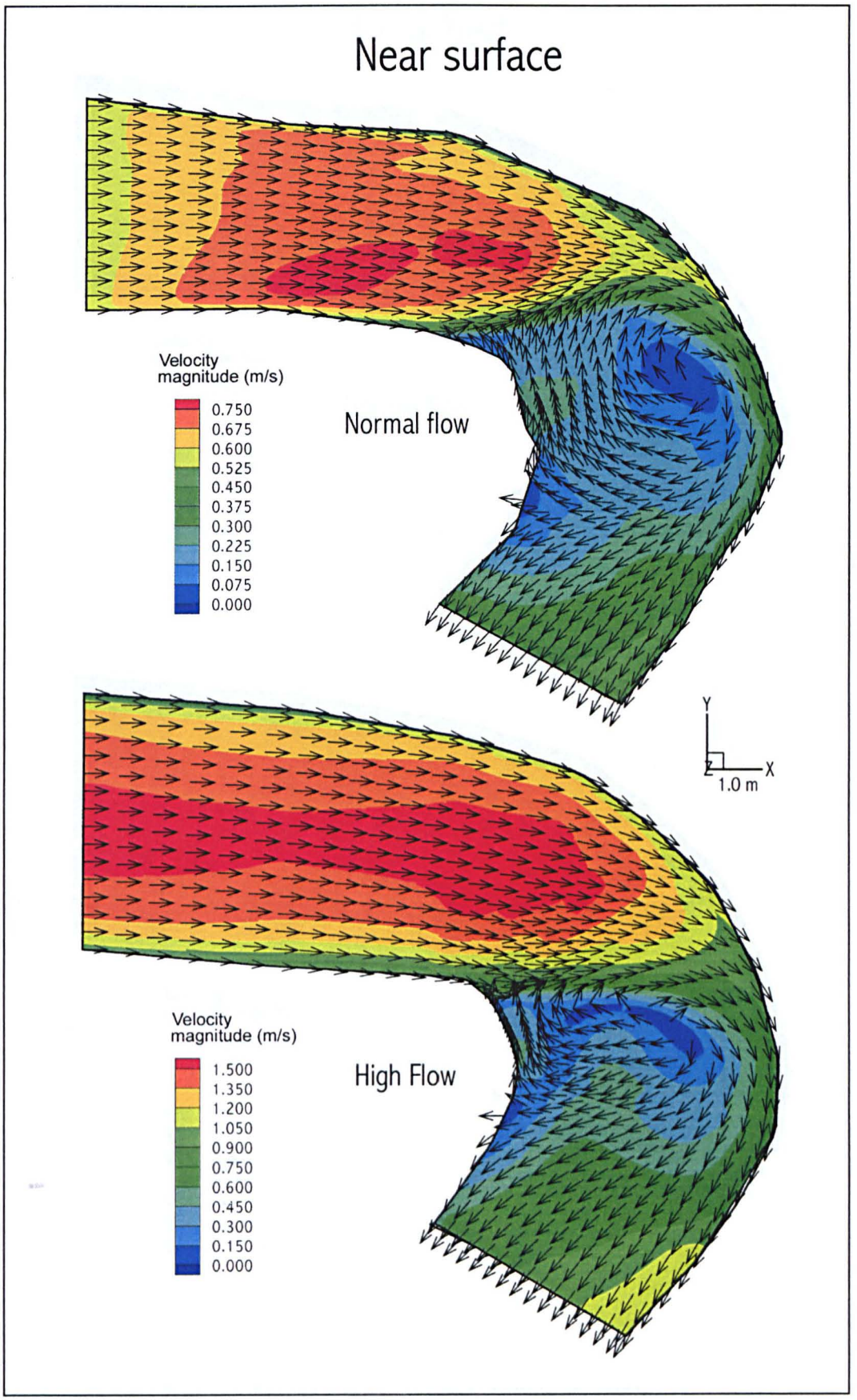

Figure 5.28: Bend 37: predicted near surface velocity magnitude with superimposed unit vectors of direction for a normal flow stage and a high flow stage. Note the change in scale between plots.

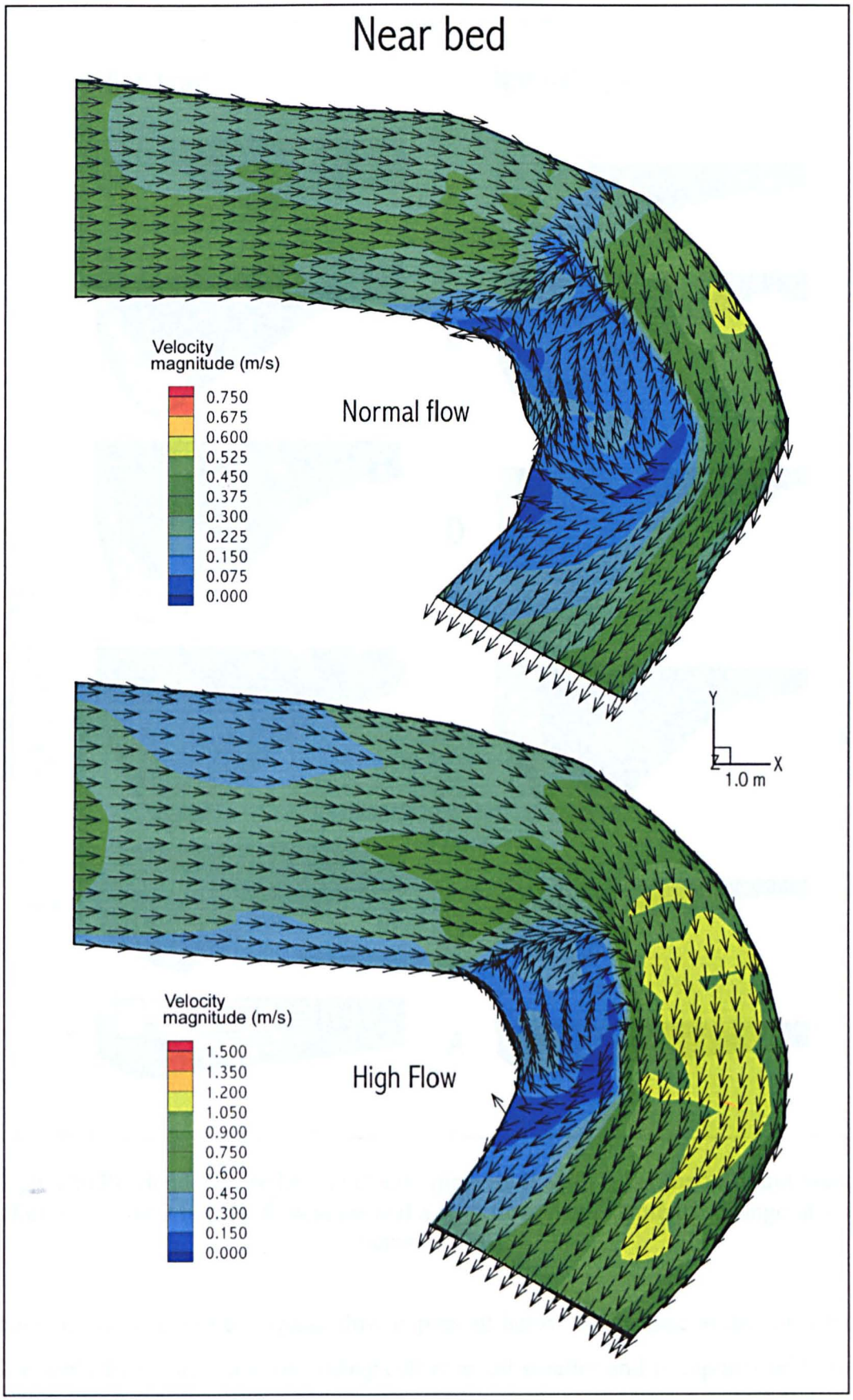

Figure 5.29: Bend 37: predicted near bed velocity magnitude with superimposed unit vectors of direction for a normal flow stage and a high flow stage. Note the change in scale between plots.

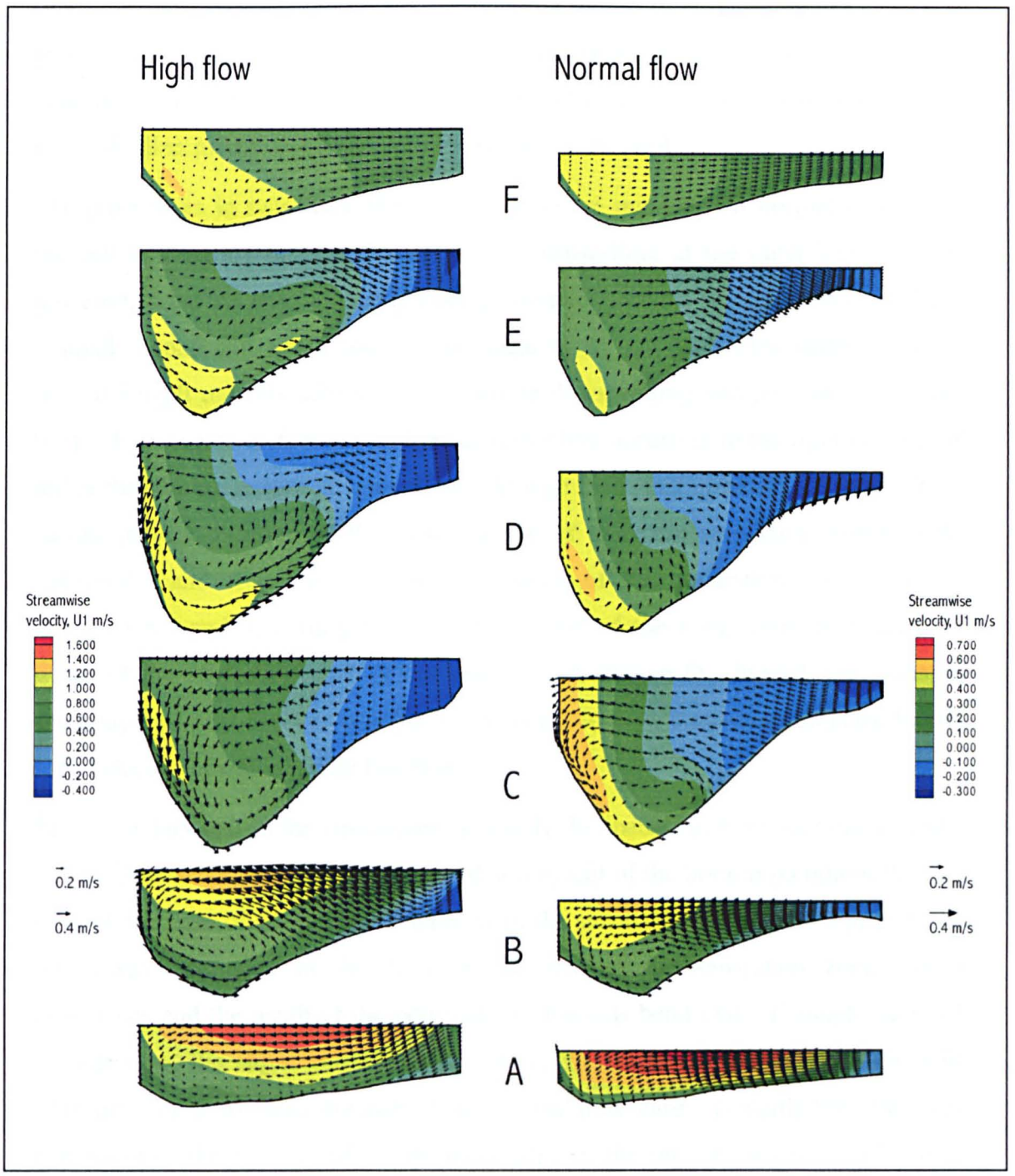

Figure 5.30: Bend 37: predicted velocity magnitude with superimposed unit vectors of direction for a normal flow stage and a high flow stage. Note the change in scale between plots.

channel, and a region of reverse flow is present below the surface at the inner bank. At normal flow stage, this secondary cell is much smaller and is suppressed towards the bed. The intensity of the helical circulation at section B is much higher in the bankfull case, with downwelling at the outer bank in excess of 0.2 m s^{-1}, while in the normal flow stage case this downwelling is less than 0.1 m s^{-1}. At section C, at high

flow, the secondary cell extends through more of the flow depth, with outer bank downwelling and upwelling midstream being particularly noticeable. The flow patterns at the normal flow stage are similar, although the cell is less coherent and much smaller, mainly occupying the lower part of the pool.

The differences in secondary flow at section D are notable. At normal flow stage, the cell has mainly dissipated with weak downwelling at the outer bank and the upwelling from the base of the pool being entrained into the separation zone and into a small second cell at the base of the shear layer. At high flow stage, the main secondary cell remains dominant, with strong downwelling still present at the outer bank. This results in stronger midstream upwelling occurring to the right of the pool rather than from the base at lower flow. At high flow, this upwelling diverges at the surface with a partition of flow into the top of the main secondary vortex in the streamtube and flow into the outer portions of the separation zone. Strong downchannel and upwelling flow along the base of the pool seems to restrict the width of the separation zone at the bed through section D. Indeed, the S-shaped shear layer present between sections C and D at low flow stage is accentuated by this high velocity, upwelling, near bed flow.

The secondary cell in the streamtube is mainly dissipated between sections D and E at high flow stage. Although there is still a remnant of the bottom section of this cell through the base of the pool, the majority of the secondary cell in E is replaced by a rightwards expansion of the flow as the size of the separation zone rapidly diminishes and the depth of the pool reduces towards bend exit. Through section F at high flow, the slight midstream upwelling, present in section E, is still evident. This flow structure does not persist in the low flow case. Nevertheless, the main expansion of the flow at the downstream edge of the separation zone is present at both flow stages.

The changes to the flow structure with stage are accompanied by significant alterations to the patterns of water surface elevation. At high flow (Figure 5.31), there is super-elevation along the length of the outer bank curve, whereas in the low flow case (Figure 5.15) this super-elevation is less extensive and concentrated close to the point main flow of impingement. At high flow these is also a region of super-elevation distally located close to the inner bank. This region is also super-elevated in the low flow case and is produced by the impingement of reattaching flow up the

point bar and onto the inner bank. Areas of water surface depression occur at the inner bank and extend towards the centre of the channel. This pattern is significantly different from that at low flow and more closely reflects that expected in a more classical bend. Nevertheless, within the zone of depression a region of super-elevation exists close to the point of detachment and separation at the inner bank.

Although the planform patterns of flow within the separation vortex change appreciably at bankfull stage as the size of the separation zone reduces, the cross section plots reveal that the flow patterns within the vortex are similar, and that movements into and out of the separation zone seem to occur in a similar double hairpin movement. However, the secondary flows are much intense in the high flow case, reflecting the increased volume of flow transported through the separation zone and bend as a whole.

5.5.4 Discussion and implications

Although both the width and depth, and the velocities throughout the bend all increase, the main qualitative features of the flow present at the lower discharge investigated in 5.3 are retained at bankfull flow stage. This illustrates that inner bank separation zones are not always 'washed out' at high flow as suggested by some workers.

There are notable differences as flow is increased, including the impingement of the main flow occurring slightly further downstream. Nevertheless, it still occurs upstream of the bend apex, which is in contrast to the classical model of flow through bends. The inner bank separation is still present at bankfull stage, although it is somewhat reduced in size and extent. This change in flow structure with discharge is similar at the surface and bed, with a curtailing of the upstream extent of reverse flow near the inner bank and a narrowing of the point of reattachment. The flow structure around the separation zone is also similar and the movement of flow into and out of the separation zone is through an analogous double hairpin motion identified at low flow. The patterns of near surface and near bed velocity vectors (Figure 5.29) indicate that secondary flows in the streamtube remain present at high flow stage. At high flow the magnitude of secondary flow is enhanced and it exists for longer through the bend to section D, although it is still dissipated before the

bend exit and does not exist into the next bend as would be expected in the more classical case (*e.g.* Wilson, 1973; Dietrich and Smith, 1983; Dietrich, 1987).

The progressive movement of the streamtube core towards the bed through the bend also occurs at high flow stage, with a large region of fast near bed flow present in the outer half of the channel downstream of the bend apex. The size and shape of the separation zone and the alterations at bankfull stage seems highly dependent on the position and size of the pool in the bend. The extent of the separation zone and its 3D shape are seemingly controlled by the progressive movement of the main centre of velocity down the outer bank and into the base of the pool and the upwelling from this area out of the base of the pool towards the shear layer. In bend 37, this produces the S-shaped nature of the shear layer at the bend apex, reducing the extent of the separation zone at the bed in relation to the surface. At higher flow these features are accentuated, as the velocity through the base of the pool and upwelling out of the pool both increase.

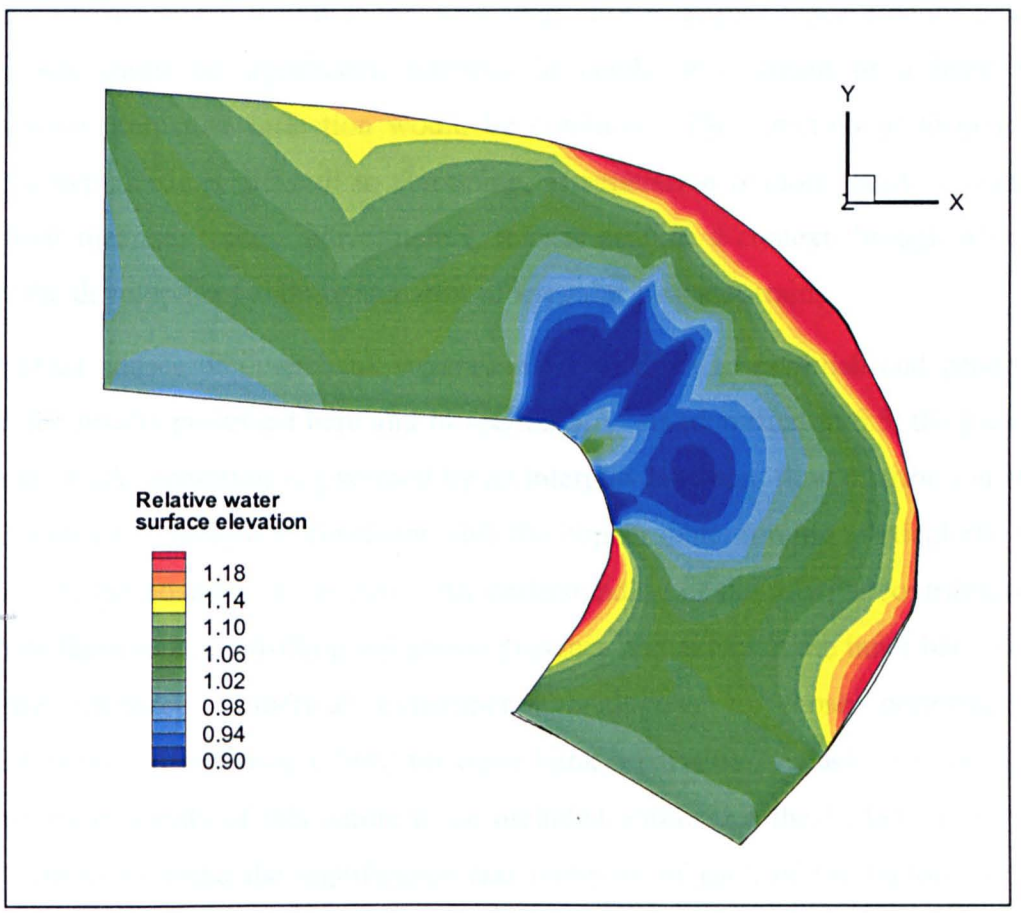

Figure 5.31: Predicted water surface elevation in bend 37 at high flow stage

Significant alterations occur to the patterns of water surface elevation in the bend as discharge increases. The areas of super-elevation at the outer bank increase and areas of depression occur around the inner bank and across the separation zone. However, significant areas of super-elevation remain at the inner bank at the points of detachment and separation where reverse flow stagnates as it collides with the main downstream flow and at the point of reattachment as flow impinges into the inner bank.

The rapid dissipation of the secondary flow vortex shown by the common alignment of the near surface and near bed vectors in the streamtube implies that the effect of a bend with separation would be unlikely to affect the flow distribution in downstream bends. Among others, Thompson (1986) and Furbish (1991) both suggested that the secondary cells advected from upstream bends could persist into downstream bends and so delay the development of secondary circulation in the downstream bend. In meander trains where separation zones are common, this could result in the development of an irregular meandering pattern through the effect of separation in a bend upstream on the inflow to the next bend. For example, in some bends delayed inflection could be significant, whereas in bends downstream of a bend with separation premature inflection would be common. The direction of feedback in such a hypothesis is difficult to determine, as separation is more likely to occur in irregular meander trains. Nevertheless, it does provide a context through which to view the development and maintenance of irregular meander trains.

The exact causes of inner bank separation are difficult to establish and generalize from the results presented here and in section 5.3. As identified in 5.3, the presence of inner bank separation is governed by an interplay between, flow distribution at the bend entrance, planform curvature and the topographic forcing particularly with respect to the position of the pool. An understanding of the relative contribution of each of these to in controlling separation presence and extent at the inner bank would require idealized numerical experiments analogous to those performed by Hodskinson and Ferguson (1998) for outer bank separation. A lack of time did not permit experiments of this nature to be included within this thesis, but future work will aim to examine the significance and interplay of each of the factors outlined above in the production of inner bank separation.

The patterns of the flow through the bend at bankfull stage and noteworthy differences in flow structure between high and low flow have several important implications. The progressive movement of the main core of downstream velocity down the outer bank into the base of the pool explains the deep scour through this region. Indeed, the high near bed velocities produce shear stress values that indicate particles up to 15 mm would be entrained out of the pool at bankfull stage. More generally, this process of the main velocity core approaching the base of the pool, combined with stronger secondary circulations, provides a physical explanation of the deep scour present in many tight mender bends.

As discussed above (5.3.7), at normal flow discharges, the separation zone acts to trap fine sediments, nutrients, plankton, and pollutants. However, at bankfull stage, the high magnitude of velocity through the regions of separation will result in removal of accumulated sediments into the main downstream flow and the potential mobilization of both nutrients and pollutants. Predicted shear stress values within the separation zone indicate that particles up to 4 mm within the separation zone could be mobilised at bankfull stage. This evacuation of materials from within the separation zone will act to maintain the presence of the separation zone at low flow stage by effectively preventing significant point-bar development and permitting erosion of the inner bank. The implication is that bends with inner bank separation could be self-maintaining features in the meander train.

The nature and type of outer bank erosion acting in bends with separation are likely to be very different to classical models of bend migration patterns. The presence of a region of high velocity in a streamtube around the outer bank will create high shear stresses on the outerbank (Figure 5.32). As a result, the migration rates are likely to be relatively high in bends with inner bank separation zones. This is in contrast with the accepted theories that suggest the formation of a separation zone as a likely cause of a reduction in migration bend rates (*e.g.* Hickin and Nanson, 1975). Thus, the reduction in migration rate in low radius of curvature bends may only relate to bends with outer bank separation.

This supposition is confirmed by Figure 5.33, which demonstrates the morphological change in bend 17 over approximately two years. The first DEM (A) corresponds to the survey used for model grid construction and boundary condition specification (5.2.3) and the second (B) was produced from a separate survey taken approximately

two years later. The third DEM (C) was produced by differencing the second from the first such that negative values correspond to areas of erosion. The difference DEM (C) reveals that, during this period, the bend has migrated substantially, with almost 2 m of planform erosion along the length of the outer bank. The migration of the outer bank has occurred in conjunction with deposition at the inner bank. This deposition has been concentrated at, and downstream of, the inner bank apex reflecting the depositional environment indicated by the numerical modelling.

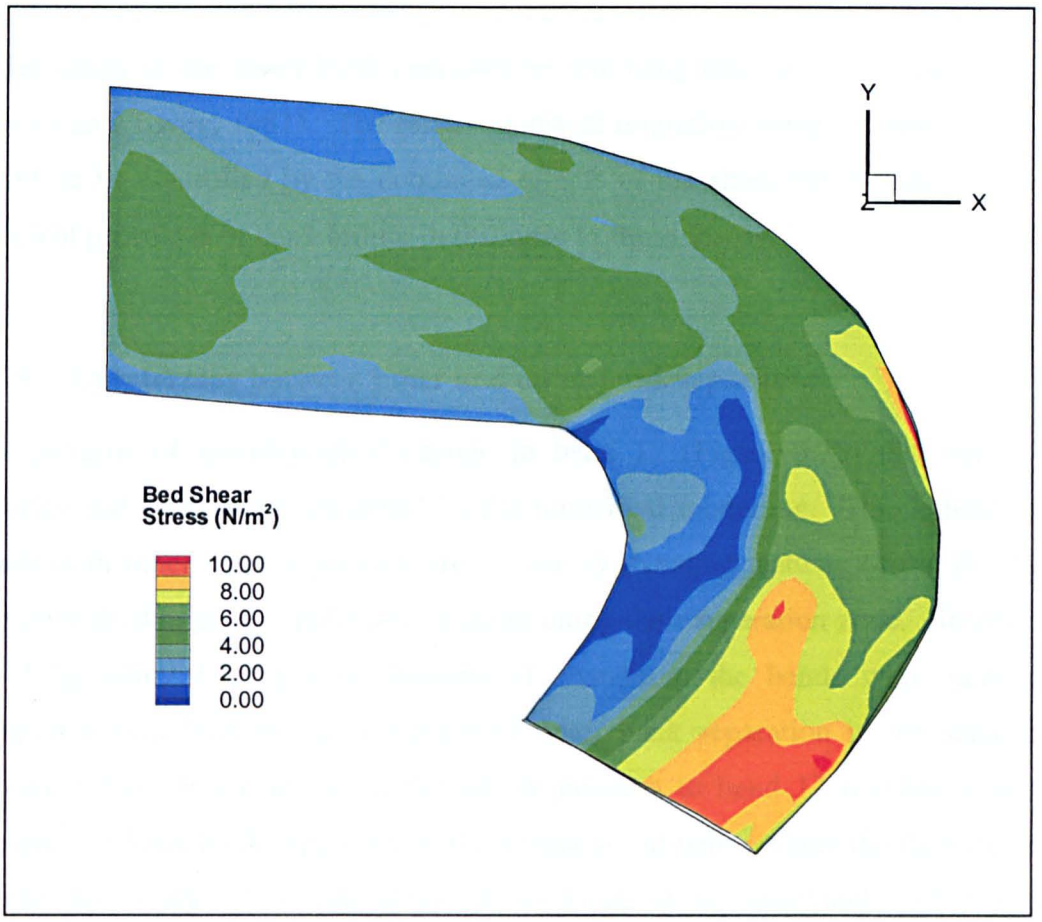

Figure 5.32: Predicted bed shear stress patterns in bend 37 at high flow stage

The pattern of outer bank erosion through the bend is slightly different, with the main concentration of bank erosion having occurred in the first two thirds of the bend. The small area of convexity in the bankline has remained in a similar position and downstream of this the bank erosion has been less extensive. This area of convexity does not seem to have been produced by heterogeneous bank material and seems to reflect the stress patterns produced by the flow. This alteration can perhaps be

explained by a variation in bank erosion process through the bend. The numerical modelling has revealed that in the upper portions of the bend before the apex, the main core of high velocity is near the surface and strikes the outerbank at a high angle producing highest shear stress values high on the outer bank. After the bend apex however, the main core of velocity moves towards the base of the pool, producing highest shear stress values through the outer sections of the bed and at the base of the outer bank. This pattern of shear stress through the bend is likely to alter the mechanism of bank erosion through the bend, from slab or mass failure in the upper part of the bend (*e.g.* Osman and Thorne, 1988) to cantilever failure, where undercutting of the lower bank generates an overhang that fails, after the apex (*e.g.* Thorne and Tovey, 1981). The relative rates of migration along the outer bank will therefore be controlled by the combined effects of the shear stress patterns and the different processes of bank failure in response to those forces.

5.5.5 An interplay between inner and outer bank separation?

The patterns of morphological change in bend 17 (Figure 5.33) thus reflect the velocity and shear stress predicted by the numerical modelling. This indicates that bends with inner bank separation are extremely dynamic features of the floodplain and do indeed migrate rapidly whilst maintaining their separation zone. However, in the long term, these general patterns of change in the bends with inner bank separation may lead to the formation of outer bank separation in the same bend (Figure 5.34). For example, if the inflow position to bend 17 remains fixed, the presence of inner bank separation will continue to influence where the flow impinges on the outer bank. A continued high erosion rate of the outer bank will eventually lead to the formation of an embayment, where a reverse flow could develop. The formation of a small outer bank separation would force the position of flow impingement further downstream and possibly reduce the size of the inner bank separation. Thus, there may be a self-regulating interplay between inner bank separation and outer bank separation in bends, which ultimately controls the position of outer bank impingement. The impingement on the outer bank influences the size of separation at both banks and controls where erosion and deposition occur within the bend. Changes in bend 25 (Figure 5.27) also support this hypothesis. The tightening of the bend through inner bank erosion before the apex has lead to a

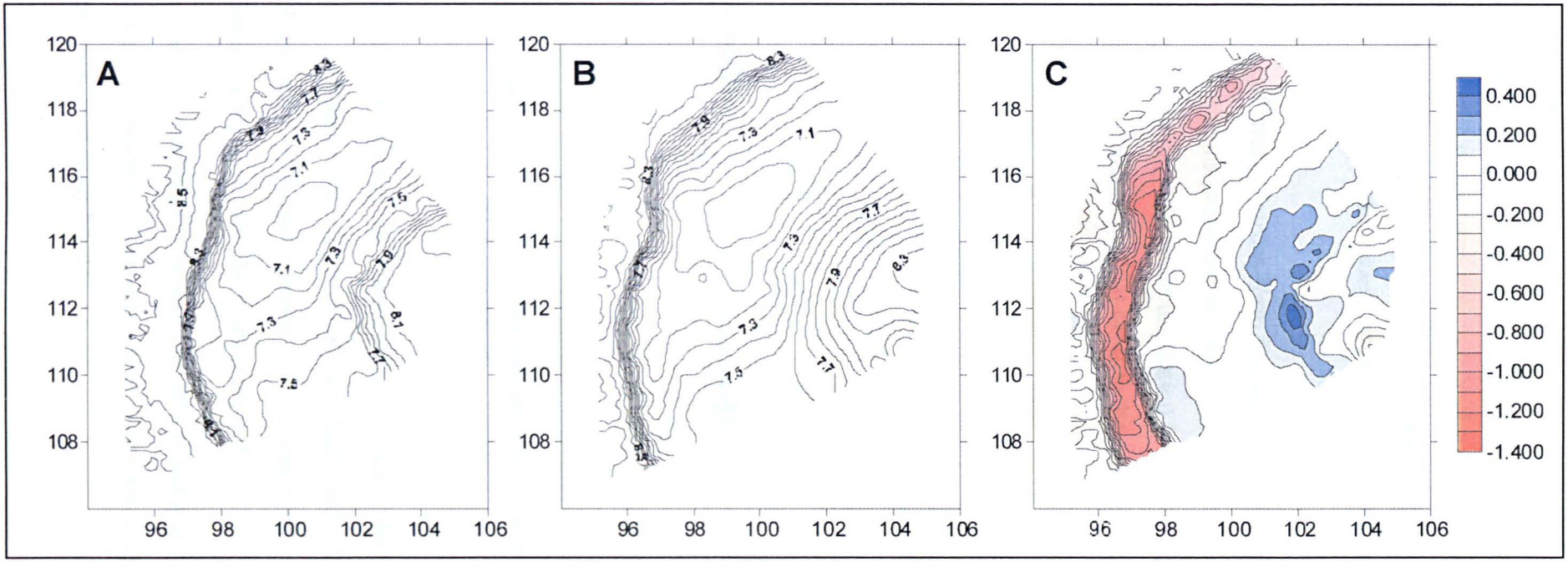

Figure 5.33: Digital elevation models of bend 17 (A) 4th July 2000; (B) 12th September 2002; (C) identified difference. Units in meters.

downvalley shift in the position of the channel and a tightening of the inner bank apex. If the outer bank erosion downstream of the apex continues the downstream section, of the channel will widen and this will lead to an increase in inner bank separation size. This increase will tend to push the impingement of flow on the outer bank back towards the outer bank apex, reducing the size of the outer bank separation zone.

This conceptual model of strong process-form linkages can partly explain the scatter in the lower level investigations presented in chapters 2 and 3. The data collected is heavily influenced by the timing of sample in relation to the interplay between inner and outer bank separation in each individual bend as the channel migrates.

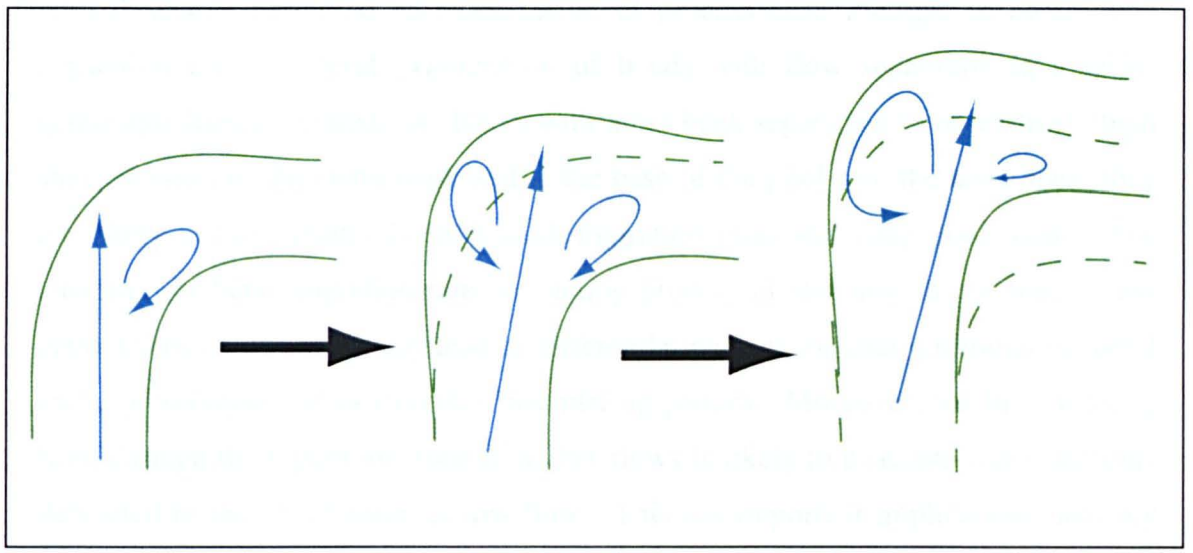

Figure 5.34: Conceptual model of outer bank separation development from inner bank separation.

However, this conceptual model is complicated by any changes in upstream planform that will influence the position of the bend inflow. For example, Hodskinson and Ferguson (1998) have shown that the inner/outer bank interplay is also heavily influenced if the upstream planform is altered.

The confirmation and/or formalization of this theoretical interplay require long-term monitoring of whole river reaches where separation zones are common and detailed monitoring of individual case study bends.

5.5.6 Summary

The simulation of bend 37 at high flow stage demonstrates the maintenance of inner bank separation at bankfull flow. There are some notable differences between the flow structure at bankfull stage and that at a normal flow discharge. These differences include a general doubling of velocity throughout the bend including within the separation zone itself, a slight reduction in the size and extent of the separation zone, a movement of impingement point closer to the bend apex, a widening of the streamtube and persistence of the streamtube secondary vortex further towards the bend exit. Nevertheless, the qualitative features of the flow field are similar at both flow stages investigated.

The flow structure at bankfull stage and the nature of alterations in flow structure with discharge permitted an examination of process-form linkages in bends with separation and a general examination of bends with flow separation in a wider geomorphological context. As bends with inner bank separation have relatively high shear stresses on the outer bank and at the base of the pool past the bend apex, they are likely to have relatively high bank migration rates and deep pool scour. The alteration of bank migration rate and acting process in response to the shear stress pattern through the bend may lead to differential rates of migration through the bend and a preservation of an irregular meandering pattern. Moreover, the high velocity flow through the separation zone at higher flows is likely to evacuate fine sediments deposited in the 'dead zone' at low flow. This has important implications not only for the self-maintenance of separation zones within the meander train but also for the sediment dynamics of the system and the potential reactivation of pollutants.

The inflow distribution, planform curvature of the bend and the nature of topographic forcing produced by the pool all interact in generating separation at the inner bank. However, it is difficult to generalise and to isolate the factors responsible for separation presence at the inner bank. Future work should apply numerical modelling in a structured set of idealised experiments to fully elucidate the controlling factors of separation at the inner bank.

5.6 SUMMARY AND CONCLUSIONS

This chapter has considered the verification, validation, and analysis of time averaged flow structures in meander bends with separation zones. Flow structures in bends with both inner and outer bank separation have been investigated. The chapter has demonstrated that numerical modelling can be applied to these bends even where highly complex grids are required using boundary fitted co-ordinates. Indeed, the combination of fieldwork for validation of a numerical model provides an extremely powerful means of investigating flows in these complex bends where field data cannot realistically provide adequate process representation.

The results indicate that the flow structures in bends with separation are significantly different from bends that are more classical, although notable similarities in flow structures do exist. In both inner and outer bank separation cases, the main downstream flow is contained within a streamtube of relatively high velocity that contains the classical curvature induced helical motion. However, the flow within the streamtube is characterised by an intense helical motion in the upper portions of the bend and this helical motion is rapidly dissipated in the downstream direction. In bends that are more classical, this helical motion is expected to extend into the entrance of the next bend. In both types of separation, the re-circulation zone is isolated from the main flow structure in the streamtube. In the inner bank separation cases, the re-circulation zone acts like a large point bar steering flow around the outer bank and in the outer bank case it acts like an outer bank boundary, particularly at the proximal end of flow reattachment where flow out of the separation zone impinges into the streamtube.

In both cases, large amounts of shear exist between the slowly re-circulating flow and the fast streamtube. However, the nature of this shear differs significantly between inner and outer bank separations. In outer bank separation cases shear is generated between the downwelling portion of the streamtube and the slower flow within the separation zone. In the inner bank separation case, this shear is along the upwelling edge of the streamtube. This results in more time-averaged deformation of the inner bank shear layer as upwelling flow at the bed is more dominant where flow is slower moving.

The issue of stage dependence was explored for one inner bank separation case, which was thought to be most sensitive to changes in discharge. The investigation revealed that, in the modelled bend, inner bank separation was maintained at high flow and that the main features of the flow were still present at bank full stage. Nevertheless, the size of the separation zone reduced slightly and with the velocity within the 'dead zone' increasing appreciably. The intensity of shear along the boundary also increased substantially, making it difficult to obtain a fully converged solution.

The modelling has permitted some insights into the factors responsible for the production of separation at these sites. The flow structure is produced by an interaction of streamline curvature, inflow distribution asymmetry, and topographic forcing with the presence of the re-circulation zone acting as a fourth factor once it is produced. The relative contribution of each of these factors is difficult to determine and requires numerical experiments similar to that of Hodskinson and Ferguson (1998) to be performed.

The re-circulation zones contain a significant volume of recirculating fluid. This significantly modifies the structure of flow through the bend. The patterns of bed shear stress are remarkably different from those expected in bends that are more classical. Regions of high bed shear follow the path of the streamtube through the bend with the large areas of low stress over the re-circulation zone acting as a sink for fine sediments. The zones also seem to have large residence times although this is likely to be mediated by turbulent transfers not modelled using time-averaged processes. Specific studies of flow mixing and dispersion effects of these complex bends are necessary (*e.g.* Boxall *et al.*, 2002; Hankin *et al.*, 2002) and techniques that allow study of instantaneous flow fields are also required.

During low flow, these re-circulation zones act as sink for fine sediments, although the high velocity within the re-circulation zone at bankfull flow in bend 37 indicates that in bends with inner bank separation they become sources of fine sediments during higher flow stages. The evacuation of sediment form the re-circulation zone at higher flows has significant implications for the maintenance of the separation zone and for the sediment dynamics of the system as a whole. As fine sediment is evacuated from the re-circulation zone, bar development is reduced and bed elevations remain lower through the separated region, maintaining the expansion in

channel width that is necessary for separation production. The movement of the bends through the study period has also been investigated and reveals that the migration patterns of these bends is significantly different from the classical bend migration model and that movements can be rapid. This finding of rapid migration rates is contrary to some earlier reports that bends with separation zones are stalled floodplain features. Movement in the inner bank separation case is upstream of the apex where flow impinges into the outer bank at a high angle. Movement in the outer bank case is through migration of the inner convex bank and the outer bank well beyond the bend apex. This indicates that the separation zones act to maintain themselves and are dynamic features of the fluvial system.

A conceptual model of the self-regulation of these bends has been developed which explains the formation of outer bank separation and suggests an interplay between separation at the inner and outer banks that effects the position of the streamtube through the bend. The position of the streamtube in the bend ultimately governs the areas of erosion and deposition in these bends. It was also suggested that because the flow structures through and out of bends with separation are significantly different to classical bends it explains the formation of irregular meanders trains, which often accompany the presence of separation. However, the nature of cause and effect between the two remain unclear and long-term monitoring of bends with separation zones is required.

This section has only considered the time averaged flow structure through the bends. The presence of a large amount of shear between the streamtube and the re-circulation zone in both cases will produce large coherent flow structures that are likely to be extremely important processes, not adequately represented by time-averaged techniques. The following chapter investigates these flow processes and attempts to model then using transient turbulence closure methods.

Chapter 6

Transient Flow Structures in Bends with Separation

6.1 INTRODUCTION

Based on field validated numerical modelling results, the previous chapter investigated and explained the time-averaged flow structures in meander bends where zones of flow separation were present. The modelling techniques used an RNG modified version of the κ-ε turbulence model to account for the effect of turbulence on the main flow field. In many situations, this is an acceptable treatment of turbulence and the κ-ε model is widely applied in modelling studies throughout many applications and disciplines. However, its applicability is limited in situations where there are intense shearing processes present. The boundary between the separation zone and the main downstream flow is a region of intense shear, which is known to produce large turbulent fluctuations. Such turbulent flow structures include the formation of Kelvin-Helmholtz instabilities in the shear layer (*e.g.* Leeder and Bridges, 1975; Kimura and Hosoda, 1997; Best and Roy, 1991; Sukhodolov and Rhoads, 2001), longer-term shear layer migration (*e.g.* Biron *et al.*, 1993b; Sukhodolov and Rhoads, 2001), and periodic upwelling and downwelling at certain positions in the channel (*e.g.* Bradbrook *et al.*, 1998). These unsteady flow structures will be important for the amount and timing of momentum transfers, flow mixing, dispersion, boundary shear stress and thus sediment entrainment and transport. Because of these large-scale coherent flow structures, intermittently each of these processes could be several orders of magnitude greater than the predicted time-average means. As a result, analysis of flow structure with time-averaged techniques can lead to inaccurate or incorrect interpretations and conclusions. It has been suggested that the nature of identified flow structures such as secondary circulation cells could be an artefact of averaging periodic or intermittent processes (Lane *et al.*, 2000), and that concentrations of a pollutant could periodically exceed computed time-averaged levels (Lane *et al.*, 1999c). Thus, there may be a need to

consider the time-variant flow structures in bends with separated flow, and examine how well the time-averaged numerical modelling results presented in chapter 5 represent these processes, particularly close to the shear layer and within the separation zone.

The shear layer is similar to plane mixing layers investigated in the engineering and fluid mechanics literature (*e.g.* Brown and Roshko, 1974). Mixing layers exhibit large, predominantly two-dimensional, vortex structures with vertical axes that are derived from the co-rotation, merging and propagation of Kelvin-Helmholtz instabilities as they are convected downstream and spread laterally (*e.g.* Winant and Browand, 1974; Rogers and Moser, 1992). Sukhodolov and Rhoads (2001) show that flow in a transverse shear layer in river channel confluences is quasi two-dimensional although they acknowledge that more work is required to fully investigate the nature of flow in this zone and to characterise the relationship between mixing processes and shear layer processes.

Thus, there is a need to examine the nature of these instantaneous flow processes and a requirement for measurement and modelling techniques that can identify and permit analysis of 3-D flow fields instantaneously and simultaneously from a large number of measurement locations throughout the flow. Moreover, although the modelling results presented in Chapter 5 are spatially rich, the results only address the time-averaged nature of the flow across the shear layer in these bends. The position and deformation of the shear layer through time due to shear-generated turbulence is thus un-quantified and unknown and the time-averaged modelling strategy employed may not adequately represent or indeed correctly account for important processes that are operating within these bends.

In order to address these issues, the nature of transient flow structures in two of the field bends examined in chapter 5, namely bends 17 and 25, are explored (6.3). The ability of the numerical model to reproduce these shear layer processes with a large eddy simulation (LES) turbulence scheme invoked is then examined (6.4). LES modelling of the flow in the natural bends (6.4.2) and in a simplified open channel double width expansion (6.4.3) is detailed. The assessment of the LES modelling results concerns the comparison of velocity time-series for modelled and observed points.

Analysis of signals or time-series data is an extremely complex area of research. Although conventional time series analysis methods, such as spectral analysis (fast-Fourier transform), are now well established, they are often inadequate for analysis of non-stationary signals that can have several scales of superimposed, intermittent, variability. This problem is of particular importance in analysing point turbulence data or when comparing two time series that are likely to have different scales of variability. This chapter introduces relatively new methods of time series analysis that can be used for investigation of the non-stationary signals in this research (6.2). The chapter ends with a brief conclusion on the ability and potential of the numerical model to simulate the transient flow structures in open channel flow problems (6.5)

6.2 TIME SERIES ANALYSIS METHODS

6.2.1 Conventional time series analysis

Conventional signal or time series analysis (spectral analysis) is generally based upon the Fourier transform, which can be used to produce a power spectra for given frequencies within the time series. Thus, the signal is broken down into constituent sinusoids of different frequencies that effectively transforms the view of the signal from time-based to frequency-based. For many signals, Fourier analysis is extremely useful because the signal's frequency content is of great importance. However, Fourier analysis has a serious drawback. In transforming to a frequency domain the time-dependent information is lost. This results in it being impossible to tell when a particular event took place. If the signal properties are stationary, and do not change much over time, this drawback is not very important. However, if the signal exhibits non-stationary or transitory characteristics, such as drift, trends, abrupt changes, and beginnings and ends of events, Fourier analysis is unable to place the events in time or even detect them in certain situations. Analysis methods such as the Short-Time Fourier Transform (*e.g.* Gabor, 1946) were developed to overcome some of these limitations. The STFT is a compromise between time- and frequency-based views of a signal and uses a window to compartmentalize the signal into small sections of time. Although the STFT provides some information about both when and at what frequencies a signal event occurs, the window size chosen is fixed and applied to all frequencies in the signal and thus only provides information of limited accuracy

(Kaiser, 1994). This inaccuracy is created by the aliasing of higher and lower frequency components that do not fall within the frequency range of the chosen window scale. Most signals require a more flexible approach, where the window size is adjusted depending on the scale of the feature analysed. This has lead to the development of a signal analysis technique called wavelet analysis.

6.2.2 Wavelet analysis

Wavelet analysis is a relatively new signal analysis technique that represents the next logical step to STFT: a windowing technique with variable-sized regions for different scales of variability (*e.g.* Farge, 1992). Wavelet analysis allows the use of long time intervals where low-frequency information is required and shorter regions where high-frequency information is required. It effectively analyses for all scales (frequencies) of flow variability for all times through time. The main advantage this approach affords is the ability to perform local analysis on the signal. The time or space-frequency localization permits study of features locally within the signal with a detail that matches the scale of the feature being analysed. Thus, wavelet analysis can indicate the occurrence and provide the location of discontinuities, abrupt changes, and the beginnings and ends of individual events through a signal.

The concepts behind wavelet transforms were formalized in the early 1980s in a series of papers by Morlet and their development and application proliferated throughout the 1990s. Wavelets are now used in diverse areas of application such as image processing and compression, speech recognition technology, fingerprint processing technology and areas of atmospheric physics. They have also been used to analyse turbulent flow signals in geophysics (*e.g.* Farge, 1992; Foufoula-Georgiou and Kumar, 1994). However, their application for understanding geomorphological processes has been disappointingly limited.

A wavelet is a wave of a given form of effectively limited duration that has an average value of zero. This wavelet is used to break up a signal into shifted and scaled versions of the original (or mother) wavelet. The wavelet is compared to a small section at the start of the original signal and a coefficient is calculated based on how closely correlated the wavelet is with this section of the signal. The higher the coefficient is, the more the similarity between the two. This wavelet is then shifted

along the length of the signal and a coefficient calculated for each time point. The wavelet is then stretched (scaled) and applied along the length of the signal series once more. This can be completed for a range of wavelet scales, from that equivalent to twice the sampling interval to a scale equivalent to half the length of the signal series. This produces a two-dimensional matrix of wavelet coefficients for different scales of wave through the signal and is called a continuous wavelet transform (CWT). A contour plot of the CWT coefficients, with position along the signal (time or space) on the x-axis and wavelet scale (frequency) on the y-axis provides a space or time-scale view of the signal, decomposing the variability of the signal through both time and scale. Alternatively, traces at specific scales along the signal can be plotted, indicating the power contained within the series at that particular scale through time. The quantitative relationship between wavelet scale and feature frequency depends on the wavelet transform that is applied and the sampling interval of the signal. A psudeo-frequency can be calculated for each scale (Meyer, 1993). Qualitatively, low scales correspond to the most compressed wavelets, highlighting rapidly changing details that correspond to high frequency events. Higher scales apply larger 'stretched' wavelets, which are compared to longer portions of the signal, and thus correspond to larger features that operate at lower frequencies.

Many types of wavelet base function and kernel form are available (*e.g.* Farge, 1992; Meyer, 1993). In the application used here a Mexican hat wavelet form is applied that is based on a derivative of Gaussian is applied. This type of wavelet is the standard choice in a range of applications and gives excellent time localization. Torrance and Compo (1998) state that the choice of wavelet should not significantly alter the qualitative nature of the results, although further work is required to ascertain the sensitivity of the results to the selected wavelet for analysis of open channel shear layer processes.

6.2.3 Wavelet analysis in turbulence interpretation and LES assessment

Because of the property of time-frequency localization, wavelets are an ideal technique for analysing turbulence signals (*e.g.* Farge, 1992). Turbulence signals are generally non-stationary and composed of several scales of superimposed variability, which can alter through time. Thus, wavelets can identify and separate out the scales

of this variability through the length of the signal, identifying where and when and at what scale the main variations in the signal occur.

LES time series will also contain non-stationarity elements. Thus, wavelets are also ideal for assessing at a point LES results. Moreover, the assessment and 'validation' of LES results is extremely difficult because LES involves a temporal cut-off, both of the smaller scales of variation as defined by grid spacing, as well as the larger scales where variability is generated at spatial scales that are greater than the bend scale. The empirical data will contain a whole range of variability related to aspects of the flow that the LES will not be simulating. Thus, measured flows are temporally rich but spatially poor whilst the LES results are spatially rich but temporally poor. As wavelet analysis separates the scales of variability, it can be used to investigate which scales of variability the LES is correctly simulating, which it is not simulating, and if and how this variation alters through time. Wavelets are thus an excellent method for assessment of LES results as it facilitates a resolution to the problems that the differences in the spatial and temporal richness of the two signals create.

6.3 OBSERVED TRANSIENT FLOWS

6.3.1 Introduction

This section concerns the nature of transient flow structures in two of the natural bends investigated in Chapter 5. This is achieved by performing time series analysis on velocity measurements at fixed points along transects through the shear layers. The primary aim of the data collection procedure was to provide a data set for an LES model assessment rather than to quantify fully the nature of the turbulent flow structure in the field situation. Nevertheless, the data provide some indication of the nature of turbulent fluctuations within these bends and permit some speculative points to be raised.

The methods applied in the field data collection (6.3.2) are outlined and the results of the time series analysis are presented (6.3.3) for both the inner bank separation case (bend 17) and the outer bank separation case (bend 25). A discussion of the results (6.3.4) includes an interpretation of the nature of the fluctuations monitored and consideration of the implications of the findings for the time-averaged modelling methodology employed in chapter 5. The section ends with a brief summary (6.3.5).

6.3.2 Data collection methods

Using an acoustic Doppler velocimeter (ADV), long time series of velocity were sampled along transects through both bends 17 and 25 (Figure 6.1). In bend 25, two transects were set up along the length of the shear layer and additional points were also sampled from within the dead zone (Figure 6.1a). In bend 17 the transect was placed across-stream, from the main flow in the streamtube towards the inner bank where flow begins to separate (Figure 6.1b). The ADV was rotated parallel with the transects in bend 25, and perpendicular to the transect in bend 17.

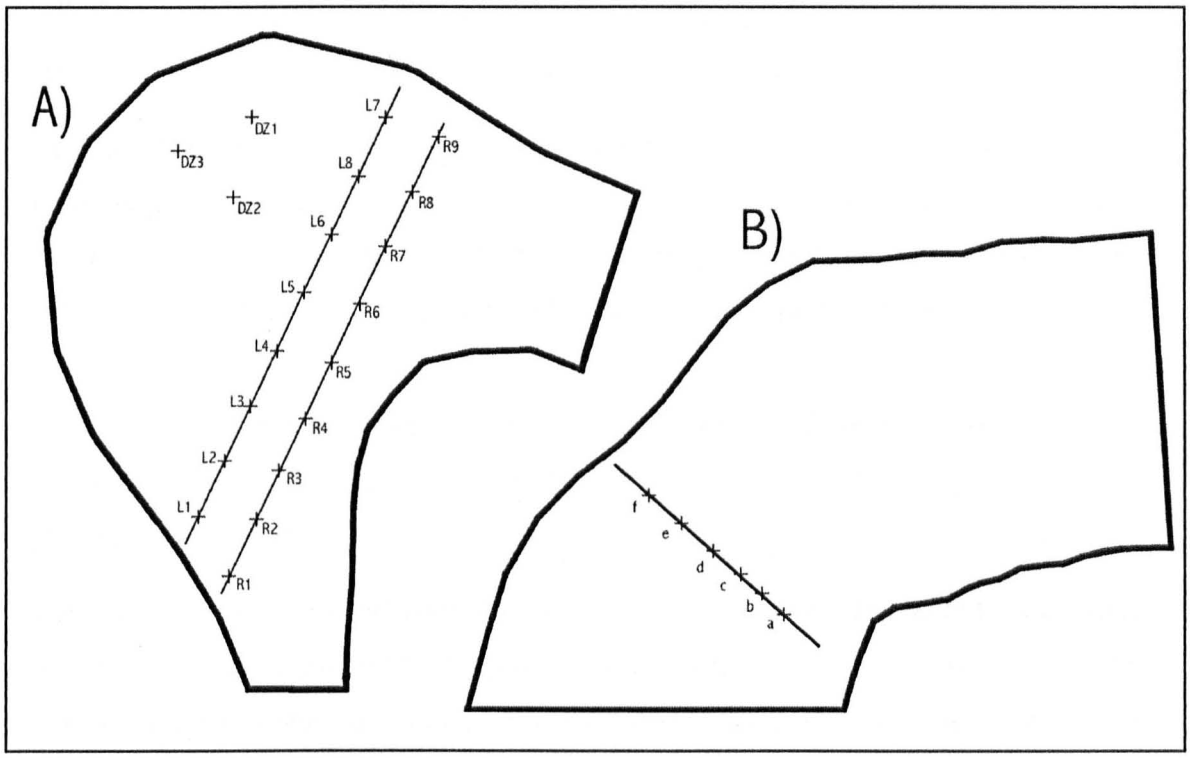

Figure 6.1: Locations of long time series points in (a) bend 25; and (b) bend 17.

At all points, velocity was sampled at 25 Hz for at least 90 seconds, although many were sampled for over 170 seconds, both of which provided dyadic series lengths that are suitable for time series analysis. Many of the series required filtering before time series analysis could be performed and the acceleration spike filter of Goring and Nikora (2002) was applied. This attempts to identify individual velocity readings in the time series that exhibit consecutive large and opposite changes in velocity direction and magnitude relative to adjacent velocity data. The differences are compared to a threshold acceleration that is independent of the units system.

Points that are filtered are replaced with weighted average values of surrounding 'clean' points. In all velocity series, fewer than 5% of sampled points were filtered and replaced.

6.3.3 Results

Figure 6.2 illustrates the nature of the shear layer variability present within bends with separation zones and a shear layer. The simultaneous deformation of the two ribbons qualitatively demonstrates the extent and amplitude of large coherent structures along the deforming shear layer in bend 25. Whilst collecting long time series data the ADV wading rod holder could identify the passage of large-scale structures, which simultaneously appeared on the notebook display.

The quantitative nature of the fluctuations of velocity in the shear layer is demonstrated in time-series taken in different parts of the bends (Figure 6.3; 6.4). For bend 25, the inflow to the bend is generally steady and consistently downstream (Figure 6.3a). Figure 6.3b demonstrates that the flow within the shear layer (point L4 Figure 6.1a) is dominated by large-scale fluctuations in all three velocity components, with a large amount of variance in each (Table 6.1). Several scales of variability are evident, with periods where different velocity components are in phase.

The various scales of flow structure evident in the traces of the velocity time-series (Figure 6.3b) are separated by wavelet analysis of the time series (Figure 6.4). The wavelet spectra (Figure 6.4) of the velocity components demonstrate the nature of the low frequency events at point L4. Through each of the three spectra, high wavelet coefficients (power) exist for two distinct frequencies contained between 10 and 100 second periods. The U1 (downstream) spectrum reveals a distinct variability of flow with a period of close to 20 seconds in the first 80 seconds of the signal. This variability exists together with a longer-term variation with a period close to 100 seconds. The shorter-term variation wanes after 90 seconds into the trace, although the longer-term variability remains. There is a large event close to 150 seconds encompassing a range of frequencies. The V1 (cross-stream) trace has events of similar periodicity, although the longer periodicity of 100 seconds is less pronounced. Two distinct areas of high wavelet power are evident centred close to

Figure 6.2: Sequential photographs of ribbons within the shear layer demonstrating large-scale coherent flow structures along the shear layer in bend 25 (looking upstream).

40 seconds and 150 seconds along the signal. The W1 spectrum confirms that the turbulence in this shear layer is three-dimensional, with the existence of similar periodicities. There are clear linkages between the three velocity components within the shear layer, with coincidence of high power during several periods throughout the trace. This indicates that the passage of large-scale horizontal shear layer events is associated with periodic upwelling and downwelling as the shear layer bulges. The wavelet spectra confirm that these fluctuations in velocity are not periodic features, but are highly intermittent with distinct periods of activity, particularly at 40 seconds and 150 seconds along the trace.

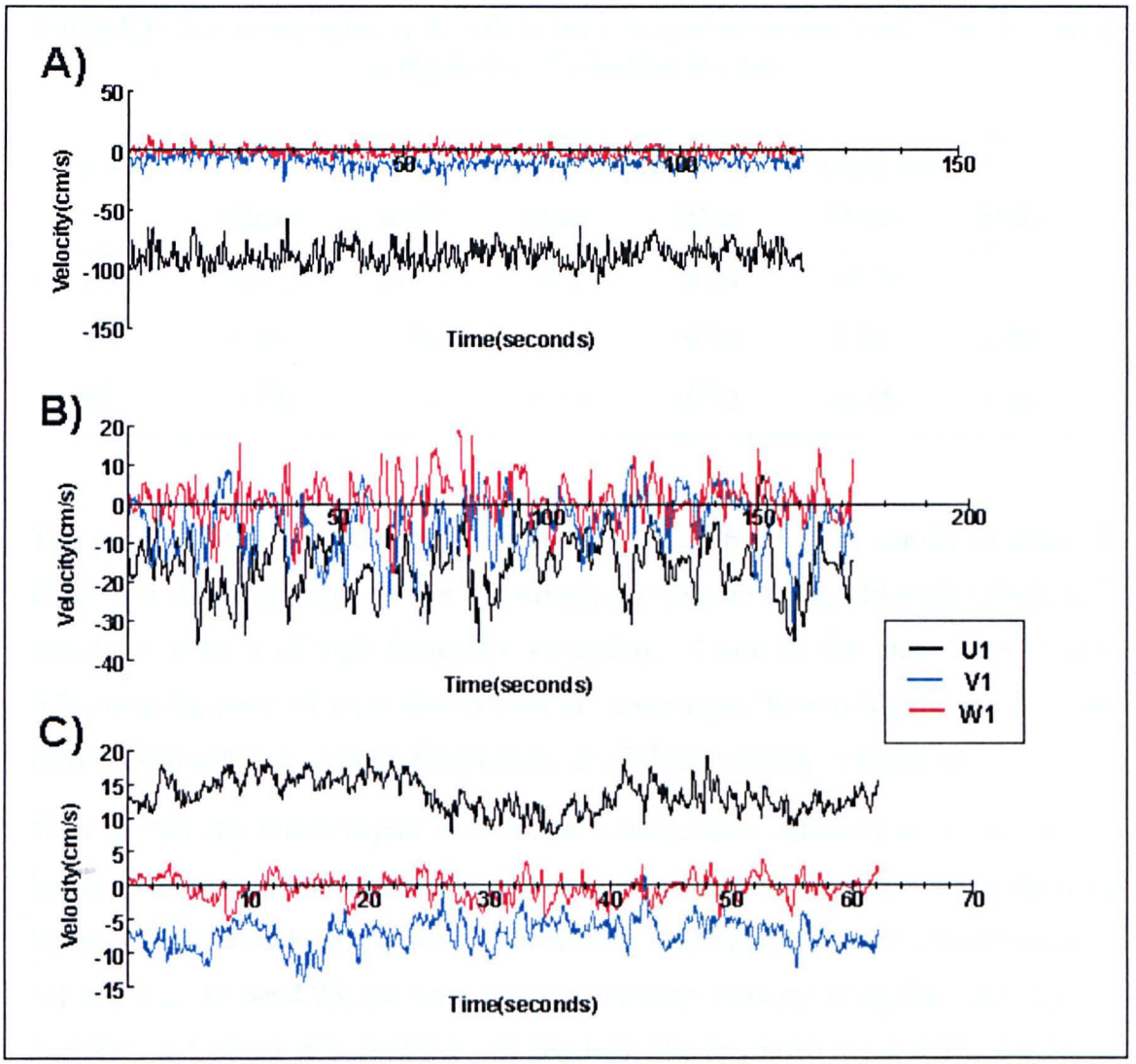

Figure 6.3: Examples of velocity time-series measured in bend 25 (a) at the bend inflow; (b) in the shear layer (point L4); and (c) in the dead zone (point DZ2). Note the variation in scales between the plots.

Flow within the large dead zone in bend 25 (point DZ2 Figure 6.1a) also exhibits low frequency variations in observed velocities (Figure 6.3c). The relatively short length of continuous, good-quality data with acceptable signal correlations, at the points within the dead zone prevents the use of wavelet analysis at these points. However, careful examination of Figure 6.3c reveals significant low frequency events. Once more, these variations occur both in phase and out of phase at different periods though the time-series. The variance within the dead zone is considerably less than at the location within the shear layer (Figure 6.3b; Table 6.1), particularly for the higher frequency variability close to 20 seconds.

Table 6.1: Summary velocity data from the three points within bend 25 as illustrated in Figure 6.3. Velocities in cm/s.

Point	Inflow		Shear layer (L4)		Dead Zone (DZ2)	
	Mean	RMS	Mean	RMS	Mean	RMS
U1	88.02	11.43	15.11	9.54	-13.36	2.37
V1	9.88	7.74	5.13	9.36	7.20	2.04
W1	-0.70	5.47	0.73	5.52	-0.45	1.60

The general pattern of unsteady flow present within bend 17 is similar to bend 25. Flow near the outer bank, within the streamtube (Figure 6.5a), although turbulent, is mainly composed of high frequency variability. Close to the inner bank (Figure 6.5c) near the point of separation within the shear layer, flow is highly turbulent and three-dimensional, with large fluctuations in all three velocity components.

Flow within the shear layers is however considerably different between the two bends. The time-averaged differences between the vertical velocities along the shear layers are indicated by the numerical modelling in chapter 5 are confirmed by Tables 6.1 and 6.2. In bend 25, the time-averaged vertical velocity along the shear layer is negative, indicating downwelling. In bend 17, the possative mean vertical velocity indicates weak upwelling. However, Figures 6.3b and 6.5c illustrates that there is considerable variability in the shear layer flows, with periods of upwelling and downwelling in both cases. There are differences in the amount of variability in the

flow between the two shear layers. The variability in the bend 25 shear layer (Figure 6.3b; point L4; Table 6.1) is much greater than in the shear layer in bend 17 (Figure 6.5c; point c; Table 6.2).

Table 6.2: Summary velocity data from the three points within bend 17 as illustrated in Figure 6.5. Velocities in cm/s.

Point	Near outer bank		Mid channel		Shear layer	
	Mean	RMS	Mean	RMS	Mean	RMS
U1	33.34	7.71	20.14	3.66	0.66	1.98
V1	16.15	6.51	5.67	3.64	0.85	1.68
W1	-3.13	4.04	2.38	3.25	0.10	1.82

6.3.4 Discussion

Shear layers are known to be highly unstable and are temporally variable at a range of spatial scales (Tritton, 1988). Even in simplified analogues, the nature of this instability is complex and it thus remains poorly understood in natural river channels. Only relatively recently have studies of flow dynamics in river channels been able to quantify and interpret the turbulent structures present in shear layers. For example, Sukhodolov and Rhoads (2001) have begun to disentangle the complexity of shear layer dynamics at river channel confluences.

The shear layer in bends with separation zones has been visually observed to exhibit large-scale flow variability. For example, both Leeder and Bridges (1975), in bends with inner bank separation, and Hickin (1978), in bends with outer bank separation, observed that the shear layer between the separation zone and the downstream flow periodically deformed into a series of spiral vortices that were sometimes advected into the separation zone. In relatively large bends, Hickin (1978) noted periodicities of 30 seconds to several minutes. In both bends investigated above, the shear layers exhibit significant amounts of movement through time. Analysis of the points close to the shear layer reveal that the turbulence is three-dimensional with a range of periodicities in each velocity component (Figure 6.4). This three-dimensionality is in contrast to the findings of Sukhodolov and Rhoads (2001) who found that the shear

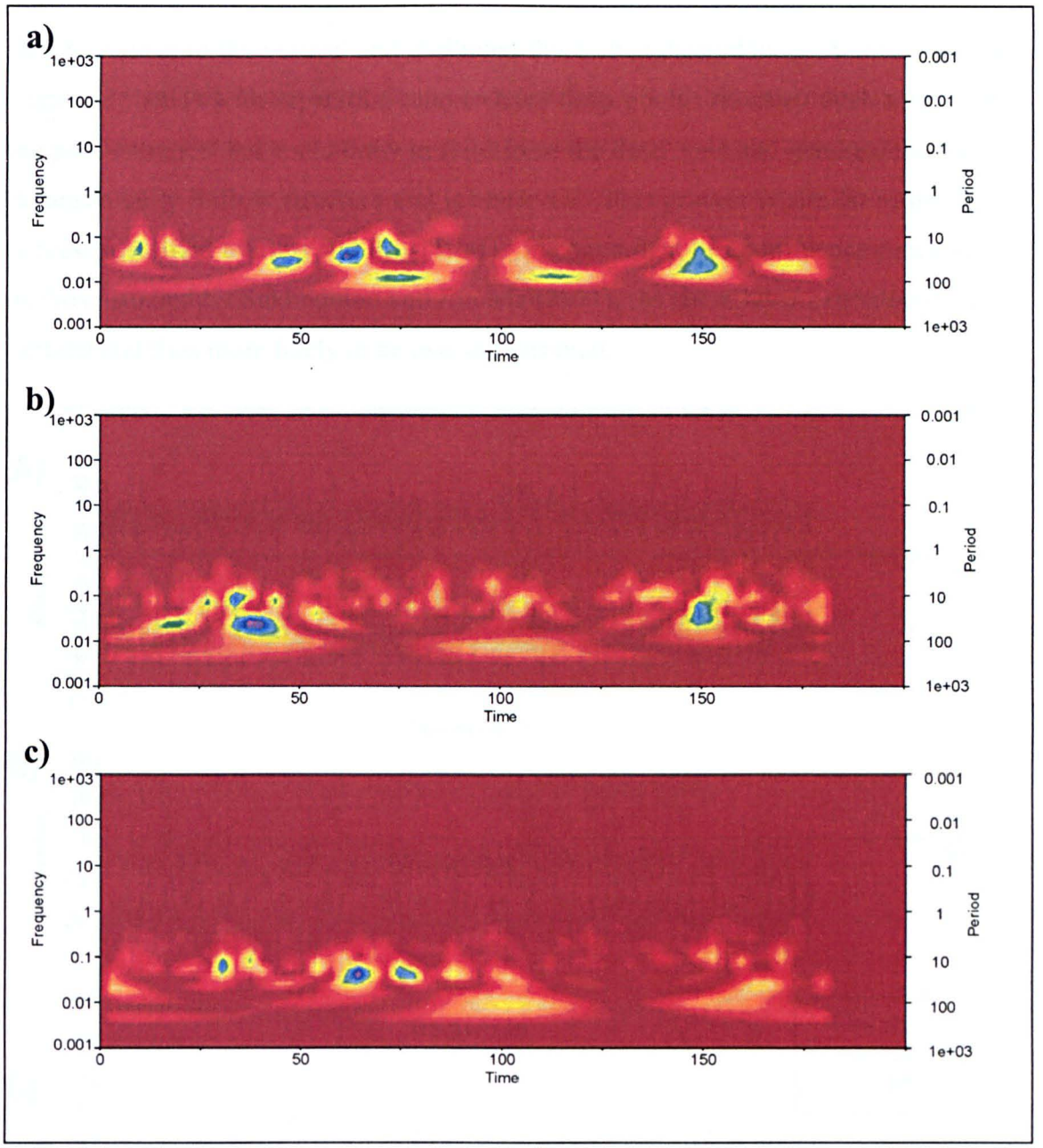

Figure 6.4: Wavelet spectra for velocity time series in the shear layer of bend 25 (point L4). (a) U1 downstream; (b) V1 cross-stream; and (c) W1 (vertical). Wavelet coefficients are contoured from red (low) through to blue (high).

layers in concordant river channel confluences are quasi two-dimensional at low frequencies, becoming three dimensional at smaller scales and higher frequencies. The three-dimensionality of shear layers in bends with separation and reversed flow zones could be explained by the tilting of the shear layer in these situations. This tilting has also been noted in discordant bed confluences (Biron *et al.*, 1996; McLelland *et al.*, 1996; De Serres *et al.*, 1999) where separation over avalanche faces can generate vertical motions within the shear layer (Best and Roy, 1991). Indeed, Bradbrook *et al.* (2000b), in a modelling study, noted periodic distortion of

the shear layer in the vertical and attributed this to bed discordance. As discussed in chapter 3, bends with separation tend to have deep pools and steep avalanche faces the pool entrance that could draw in fluid from the dead zone and generate the three-dimensionality in flow structure that is observed. This process is similar to the flow process identified by Best and Roy (1991). In concordant bed confluence cases, such as those studied by Sukhodolov and Rhoads (2001), the shear layer is predominantly vertical and thus more likely to be two-dimensional.

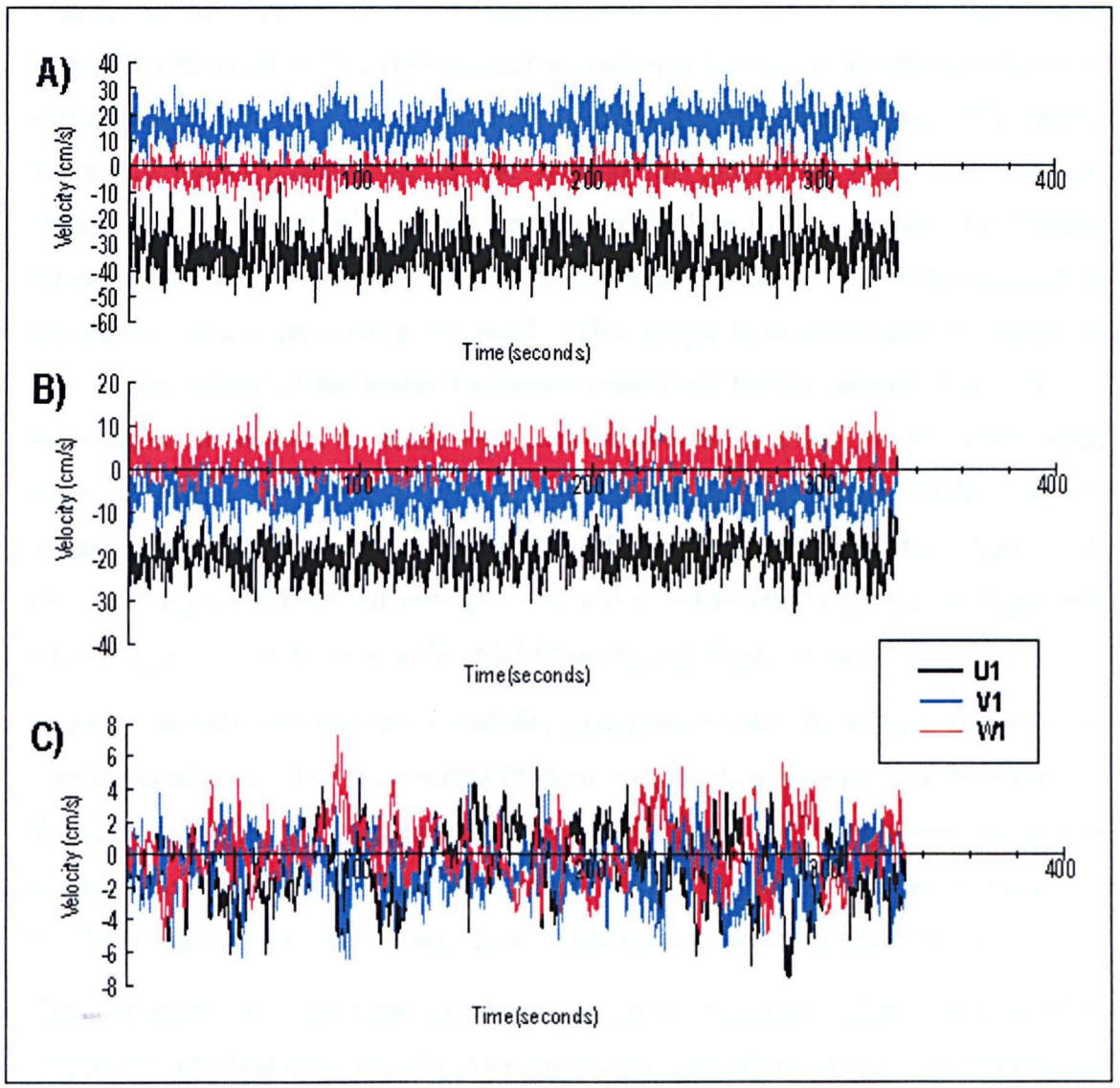

Figure 6.5: Examples of velocity time-series measured in bend 17 (a) near the outer bank in the streamtube (point f); (b) mid channel (point c); and (c) close to the separation point in the shear layer (point a). Note the variation in the scales.

The three-dimensionality of turbulence could also be explained by the strong vertical velocities that occur in the streamtube along the shear layer boundary. The time-averaged flow modelled in Chapter 5 indicated that upwelling from the streamtube

interacts with the shear layer in the inner bank case and downwelling in streamtube interacts with the shear layer in the outer bank case. The lateral shear combined with the interaction with the vertical motion from within the streamtube could generate the vertical instability required for the development and propagation of vertical components in the shear layer.

The time series (Figures 6.3 and 6.5) and wavelet spectra (Figure 6.4) indicate that there are several scales of superimposed variability in the velocity signals from within the shear layers. In shear layer of bend 25 (point L4), most of the wavelet power is contained within two distinct frequencies that seem to interact with each other at significant locations through the time series (Figure 6.4). The higher frequency events correspond to the passage of individual large scale Kelvin-Helmholtz type instabilities with a periodicity of close to 20 seconds. The longer-term periodicities, of close to 80 seconds, can be attributed to shifts in the position of the entire shear layer within the bend. This longer-term movement explains the intermittent nature of the higher frequency events and the movement of the velocity components in and out of phase with each other through time. As the whole shear layer migrates past the point sample, the relative position of the ADV sampling volume with respect to the passing Kelvin-Helmholtz type instabilities changes. If the shear layer migrated far enough, it would result in relatively quiescent periods, such as that observed between 90 and 140 seconds in Figure 6.4a.

Figure 6.3c indicates that the variability generated by the shear layer is convected into the dead zone. The trace seems to show periodicities associated with features of the scale matching the long-term migration of the shear layer. However, analysis of connections between the shear layer processes and the flow structures observed in the dead zone would require long-term, simultaneous, measurements at both.

The presence of such high variability of flow structure within the bends has important implications for the time-averaged modelling results presented and discussed in chapter 5. The quantification of time-averaged velocities in regions of significant shear-generated turbulence will average out the fluctuations and misrepresent or perhaps exclude some of the important processes occurring within the bends. Questions thus remain as to whether the time-averaged simulations capture the significant processes operating within the system, particularly with respect to flow mixing between the main flow and the dead zone.

6.3.5 Summary

The shear layers within natural meander bends with separation zones have large scale coherent flow structures of various scales. They are generated as the fast flowing fluid in the streamtube interacts with the slower moving fluid within the dead zone. This interaction generates instabilities that seem to have a three-dimensional structure. This three-dimensionality may result from a combination of the steep avalanche face into the pool and the intense helical flow within the streamtube.

However, the full quantification and understanding of the transient flow in and through these bends requires measurement and modelling techniques that can capture the instantaneous three-dimensional flow at many points within the domain of interest. Moreover, the differences between how significant the averaging process is when interpreting flow structures in these situations remains un-quantified. The following section details the use of LES to investigate the transient flow structures along shear layers where separation zones are present.

6.4 MODELLING TRANSIENT FLOW STRUCTURES

6.4.1 Introduction

The previous section detailed the existence and examined the nature of large-scale coherent turbulent fluctuations of shear layers present in natural bends with separation zones. However, the interpretation of flow structures from point velocity measurements through time is extremely difficult and often requires the use of more qualitative methods such as quadrant or octant analysis and flow visualization techniques (*e.g.* Roy and Buffin-Belanger, 2001). As discussed above, there is a need for measurement and/or modelling techniques that provide instantaneous values at many points in the flow field. Moreover, the time-averaged numerical modelling methods applied to examine the flow structures in bends 17 and 25 may not adequately represent the flow processes occurring within the bends. A numerical turbulence modelling technique called Large eddy simulation (LES) offers the possibility of simulating these temporal flow processes and permits a four dimensional investigation of the flow structure through the bends. LES thus permits the flow processes to be inferred directly, rather than implicitly through at-a-point flow structure techniques.

A full background to LES was provided in section 4.4.3. LES is a compromise between time-averaging all turbulence and directly simulating all turbulent fluctuations in the solution domain. Using the local grid spacing as a filter, LES only models the large-scale turbulent fluctuations with the smaller fluctuations accounted for by a sub-grid scale turbulence model. The main advantage of this approach is that it can be used in complex flows and at high Reynolds numbers where Direct Numerical Simulation (DNS) is impractical.

Although LES has been applied in various studies in the engineering literature, application to open channel flow problems have been a recent development. Application to specifically investigate the temporal nature of flow processes in open channels is only a very recent development. For example, Bradbrook *et al.* (2000b) found that LES could replicate some of the turbulence-generated periodicities empirically measured in a simple parallel confluence. They also applied LES to a natural confluence and found that the larger scale structures were reproduced. Nevertheless, in both applications small-scale but significant features were not reproduced by the model and poor correspondence was also noted in the frequency, timing, and amplitude of the larger turbulent fluctuations. Some of the problems in the numerical model assessment in Bradbrook *et al.* (2000b) could be due to their assessment being based upon the results of conventional time series analysis, which, as explained in section 6.2, is not ideally suited for the purpose.

With the importance of unsteady components in open channel flow established and the potential of LES in modelling some of the flow features highlighted, this section, using wavelet analysis, aims to investigate fully the extent to which LES can reproduce the significant unsteady components of the flow field.

6.4.2 Modelling transient flow structures in natural bends

Despite several attempts at running an LES model of the natural bends detailed above and modelled using RANS in Chapter 5, it consistently failed to converge on a solution. The main reasons attributed to this failure relate to the shortcomings of the Smagorinsky sub-grid scale model applied in PHOENICS. As described in section 4.3.3, this SGS model uses the average grid spacing as the filter length scale that discriminates between the larger and the smaller scales. The boundary fitted co-

ordinate grids used for both bends 17 and 25 are highly deformed and anisotropic in all three dimensions. As a result, the filter length scale that is applied in separate areas of the grid is unsuitable for the flow processes present and consequently produces a high level of numerical or false diffusion in the model solution.

Two separate developments are required to apply LES to such anisotropic meshes. Firstly, the development and inclusion of a higher order SGS model is required in PHOENICS, which is analogous to the development of two-equation turbulence models applied in RANS. Secondly, a method by which structured grids can be used with complex boundaries is required. Current work, under NERC grant (GR9/5059) is concentring on the second of these. This work is developing the use of a porosity (or partial solid cut-cell technique) algorithm that uses a structured cuboidal grid with the boundaries of the bed and the banks effectively blocked out from the flow. The initial results from this development look promising (Lane *et al.*, 2002).

6.4.3 Modelling transient flow structures in an open channel double width expansion

6.4.3.1 Introduction

To investigate the ability of LES to model transient flow structures in a shear layer produced at the boundary of fast downstream flow and a dead zone, a simple experiment was performed. The flow in an open channel flow double width expansion was measured experimentally and modelled numerically and attempts were made to investigate and optimise LES for application to open channel flow problems. This geometry was chosen as it contains many of the features of the natural bends investigated above: a sharp change in curvature (*i.e.* 90° in this case); a width expansion; and a shear layer between the main flow and a separation zone. In the lee of the width expansion, a reverse flow recirculation is present. The inflow expands, decelerates, and reattaches some distance downstream. Strong shear exists between the main flow and dead zone, which should provide a stern test of the LES model, whilst providing a relatively simple geometry for both a flume experiment and a numerical investigation. The objectives are to thoroughly validate LES by comparison to experimental results and to perform a detailed sensitivity analysis to investigate what factors are important in controlling the predictions made by the LES model. To this end, both the time-averaged flow structure and the instantaneous flow

fields will be analysed, with wavelet analyses applied to the experimental and modelled time series at a number of points.

Section 6.4.3.2 introduces the modelling set-up and the empirical methods employed to obtain validation data. The following section (6.4.3.3) details the results of both the time-averaged modelling using a κ-ε RNG turbulence model and the results using the LES turbulence model. Section 6.4.3.4 discusses the ability of the LES model to predicting the turbulent fluctuations present within the system and highlights the importance of considering the transient flow field in comparison with the time-averaged case. The section ends with a brief summary (6.4.4).

6.4.3.2 Methods

The experiment combined laboratory experiment with numerical modelling (CFD). Two measurement tools were used in the laboratory experiment: an acoustic Doppler velocimeter (ADV) and a particle image velocimeter (PIV). This experimental design provides a strong three-way validation between measurements and modelling approaches and permitted a more in-depth analysis of the flow structure present within the system.

In order to obtain the experimental data a flume experiment was set up in a 0.3 m wide, glass sided, water re-circulating flume in the School of Earth Sciences at the University of Leeds. A 2.5 m long and 0.15 m wide plywood block was assembled and placed into the flume to create a 90° flow expansion (Figure 6.6; Figure 6.7). At the upstream end, a gentle curve was constructed so the flow was slowly constricted into half the flume width. At the downstream end, the return was perpendicular to the channel, creating a doubling of the channel width. An inflow discharge of 0.01125 m^3/s was set, which produced an average inflow velocity at the expansion of 0.5 m/s. Basic hydraulic data of the experiment are provided in Table 6.3.

To obtain both time-averaged and time-dependent measurements of velocity, turbulent kinetic energy and vorticity, both the ADV (Kraus *et al.*, 1994; Lane *et al.*, 1998) and the PIV (Dantek, 2001) were used for 3-D point and 2-D area measurements respectively. A total of 62 ADV measurements were made (Figure 6.7). The ADV was mounted such that u-velocity is negative downstream (with subsequent correction so that further reference to u is positive downstream), v-

velocity is positive towards the left wall, and *w*-velocity is positive upwards. The ADV was held on a sliding mounting arm with orientation in *uv* accurate to about 0.5° and 0.25° in *w*. The location of the ADV sampling volume from the expansion point was determined for each point. Distance from the bed was measured by the instrument itself. Measurements were taken at two flow depths at 0.035 m and 0.095 m from the flume bed. This was performed for an inflow cross section 1 m upstream from the expansion, to check that the flow was fully developed after constriction, and for a series of eight cross sections downstream of the expansion. Each cross section had four measurement locations across the channel at 0.225, 0.15, 0.075, and 0.05 m from the right wall. For each location, the velocity was measured at 25 Hz for a period of at least 180 s. For twelve of the locations, time series over 420 s were measured. The quality of the data collected was consistently high, with correlations around 90% and signal to noise values in the region of 25 dB. Due to the presence of Doppler noise at high frequencies, the series were filtered before analysis and calculation of variance required for measures of turbulent kinetic energy (see Lane *et al.*, 1998 for details) and the instantaneous values where Doppler noise was high (spikes) were removed using the acceleration spike filter algorithm of Goring and Nikora (2002) introduced above.

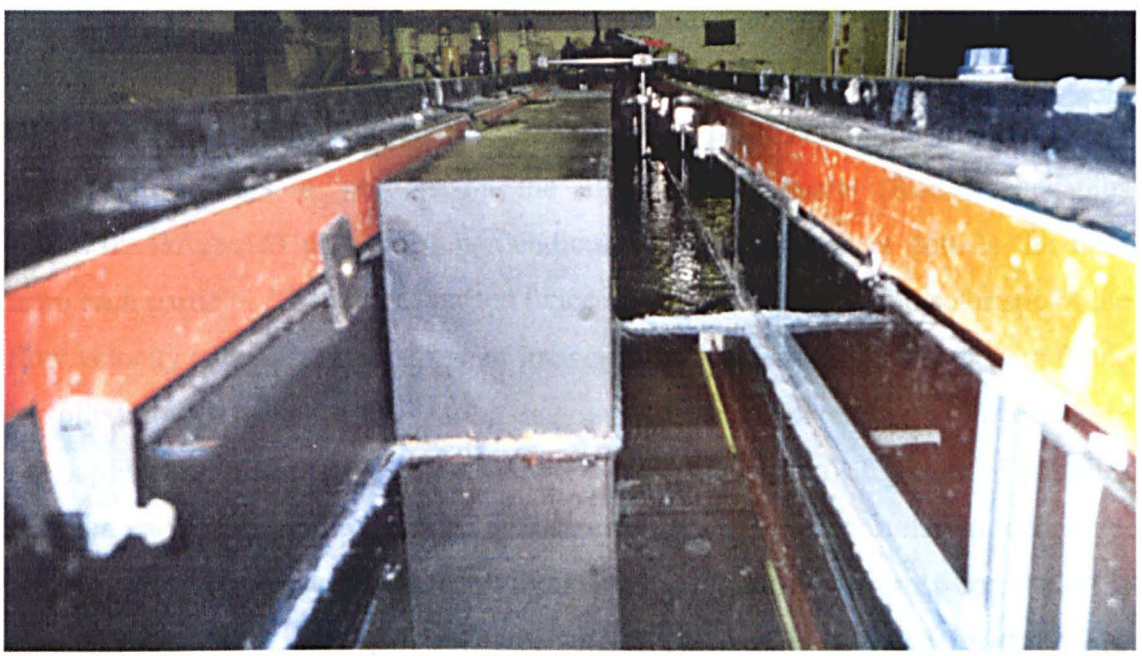

Figure 6.6: Photograph of the experimental set-up for the open channel double width expansion.

Table 6.3: Basic hydraulic data associated with the flume experiment.

Parameter	Experimental value
Inflow width (m)	0.15
Slope	0.0001
Flow depth (m)	0.15
Mean inflow velocity (m/s)	0.5
Discharge (m^3/s)	0.01125
Reynolds number	19,200
Froude number	0.412

To obtain a 2-D map of shear layer dynamics close to the point of expansion, the PIV was used. The PIV measurement region covers an area of approximately 0.2 m^2 (Figure 6.7), and was obtained for two flow depths: 0.035 m and 0.115 m from the bed for a period of 45 seconds at 15 Hz. The major advantage of PIV over ADV is that it is multi-point velocimeter with the ability to produce instantaneous 2-D flow fields at high spatial and temporal resolutions rather than single point 3D values at very high temporal resolutions. The measurement of instantaneous 2-D flow fields allows for a quantified visualisation of flow evolution, providing an effective method of flow field analysis, validation of numerical flow models and, more specifically, large eddy simulation methods. PIV flow measurements are obtained by seeding the flow with neutrally buoyant tracer particles and illuminating a plane of the flow field with a laser light sheet. The seeding material in the plane is illuminated by the laser sheet and scatters a portion of the light. A camera (Kodak Megaplus ES1.0/1kx1k/type16) positioned perpendicular to the laser sheet detects the light from each particle. The laser is pulsed twice at an interval that is characteristic of the flow velocity and the camera takes an image for each laser pulse. The camera frame is split into fixed size interrogation regions (16 by 16 pixels), that have a 50% overlap in each direction. For each region, the displacement of groups of particles between each of the paired images is measured using a cross-correlation technique, producing a velocity vector for each interrogation region. This cross-correlation is performed for each interrogation region and the process is repeated for each time interval over the length of the record, producing a vector map for each time interval. For each vector map, the region that the plywood box occupies is masked out and the vector values discarded. Range validation is also performed, which removes

spurious vectors and interpolates an average based on the values of the previous and next region. This process creates a series of vector maps, which trace particle motion through time and space. These maps can be analysed collectively as instantaneous flow fields, individual points can be extracted to provide a time series at a point, or all maps can be averaged through time to produce a time-averaged velocity map.

A numerical model of the same dimensions of the flume set-up was specified. A fully developed inflow velocity profile (see 4.5.2.2) using smooth boundaries was computed for a discharge of 0.01125 m^3/s. In the model, the inflow was simulated from 0.5 m upstream of the flow expansion and for 2.5 m downstream of the expansion. This was far enough downstream to ensure no negative dynamic pressures at the outlet. The boundaries were specified as smooth and the free surface approximation was applied. A time-averaged solution was obtained and was used to 'hot-start' the LES runs. LES runs were undertaken at a temporal discretisation of 10 Hz, which gives an average Courant number in the range of 1, which is acceptable for an implicit solution scheme. Three grid resolutions were used, with cuboidal grid cells in each run (Table 6.4). Both time-averaged and LES runs were conducted with each grid resolution, although the analysis of the modelled flow structure in each case is based upon the finest of the three. The following section details model verification and time-averaged velocity validation, before the transient modelling results using LES are considered.

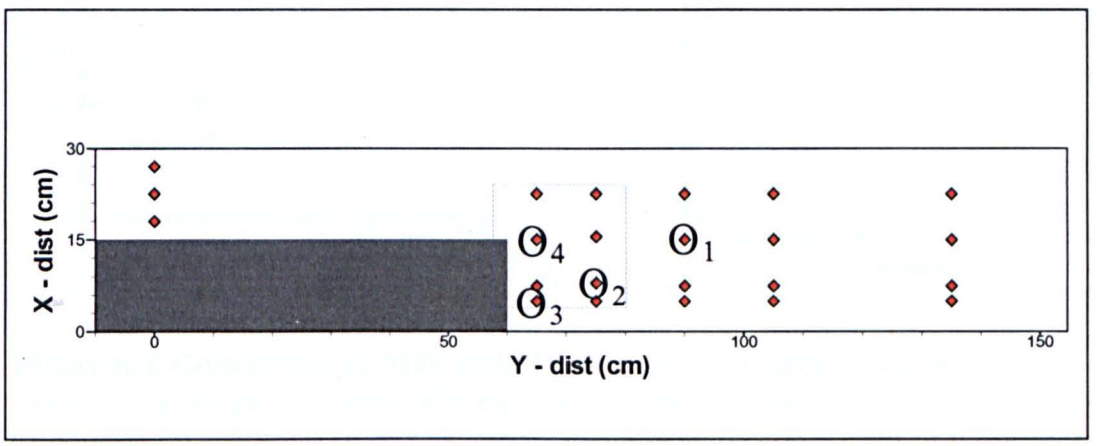

Figure 6.7: Planform geometry for the flume experiment and numerical simulation of the double width expansion. The post expansion channel was 0.3m wide, with the inflow half this. Location of the ADV sample points taken a several flow heights (diamonds) and the area observed by the PIV at 3.5 and 11.5 cm from the bed (square) are indicated. Circled points show those used for time series analysis.

6.4.3.3 *PIV and ADV comparison*

Before the measurements techniques are used for model assessment purposes, there is an interesting comparison to be made between the two measurement techniques themselves. Figure 6.8 shows the comparisons between the streamwise and cross-stream velocity and the streamwise and cross-stream turbulent intensity measured by the ADV and the PIV.

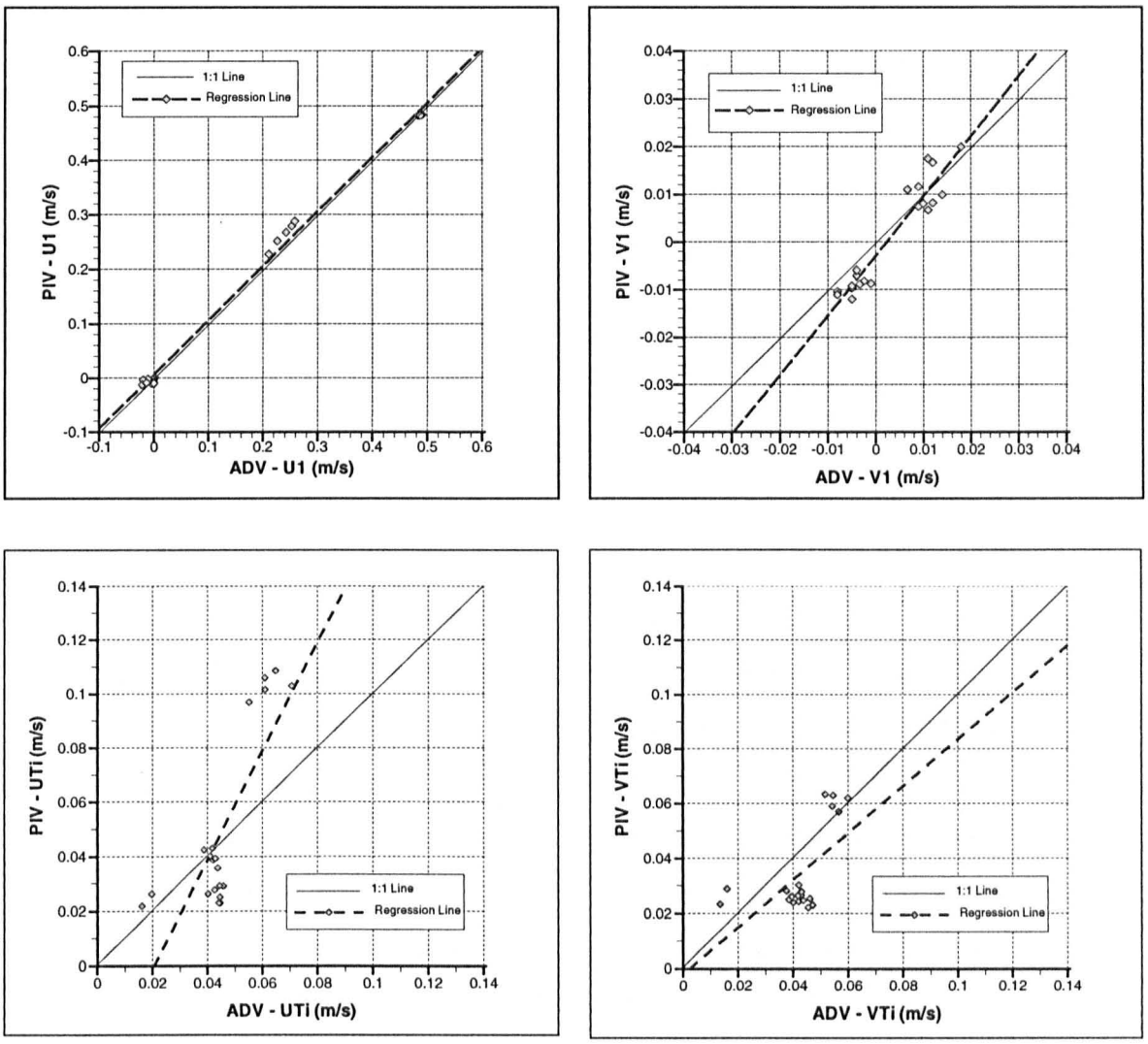

Figure 6.8: Comparison of ADV and PIV velocity measurements (a) stream-wise velocity (U1); (b) cross-stream velocity (V1); (c) stream-wise velocity component of turbulence intensity (UTi); and (d) cross-stream velocity component of turbulence intensity (VTi).

The streamwise velocity shows very close agreement with the regression line being very close to the 1:1 line. The cross-stream velocity comparison is also generally good with two clusters of points (from either side of the shear) clearly visible. The

comparisons of the turbulent intensities agree less well, particularly in the streamwise case where the PIV measurements are twice as high as the ADV. This could be explained by the different sampling volumes used in each measurement instrument and the different levels of spatial filtering applied in each technique. For example, the ADV volume is approximately 0.5 cm^3, whereas the PIV samples over 0.15 cm^2. The length of the PIV sampling period (~60 s) may also be too short to adequately capture the full range of turbulent processes present.

There is clearly a need for further investigations and comparisons of the two measurement techniques. Such an experiment is beyond the scope of this thesis and is left as an avenue for further research.

6.4.3.4 Model assessment: mean flow predictions

The confidence that can be placed in the interpretation of the simulated flow structures discussed above will depend upon model verification and validation with the empirical measurements.

For the purpose of verification, three different model grid resolutions were run (Table 6.4). In each run, the grid was kept cuboidal with an increase or decrease in resolution achieved through doubling or halving the number of cells in each direction. Table 6.5 shows the GCI results for three different grid resolutions. This indicates that both the mid- and the high-resolution results are acceptable in terms of spatial discreteisation, with low GCI percentages for all velocity components (4.6.2.1), particularly the planimetric velocities. However, as found for other studies, the turbulence parameters, particularly turbulent dissipation, are far from converged. This suggests that the lower resolution grids are not capable of correctly accounting for the turbulent processes operating within the system and this may have implications for the use of these models in analysing turbulent signals. In the model results, presented below the high-resolution grid is used.

Figures 6.9 and 6.10 show the time-averaged ADV and PIV data used for model assessment. As mentioned above both these techniques provide complementary but different character data. The ADV data is spatially poor but temporally rich, whereas the PIV is spatially rich but temporally poorer in terms of sample length (~60 s) and

resolution (10 Hz). The use of both for a full assessment provides a strong validation of the numerical model.

Table 6.4: The grid dimensions used for the GCI analysis

Mesh resolution	Number of cells in each direction			Grid size (mm)
	x	y	z	
Fine	640	64	32	4.6875
Mid	320	32	16	9.3750
Coarse	160	16	8	18.750

Table 6.5: GCI results for the open channel flow expansion (%)

Variable	Coarse-Mid	Mid-Fine
U1	2.35	2.00
V1	0.97	1.51
W1	5.39	1.10
tke	1.36	0.24
ep	10.47	21.72

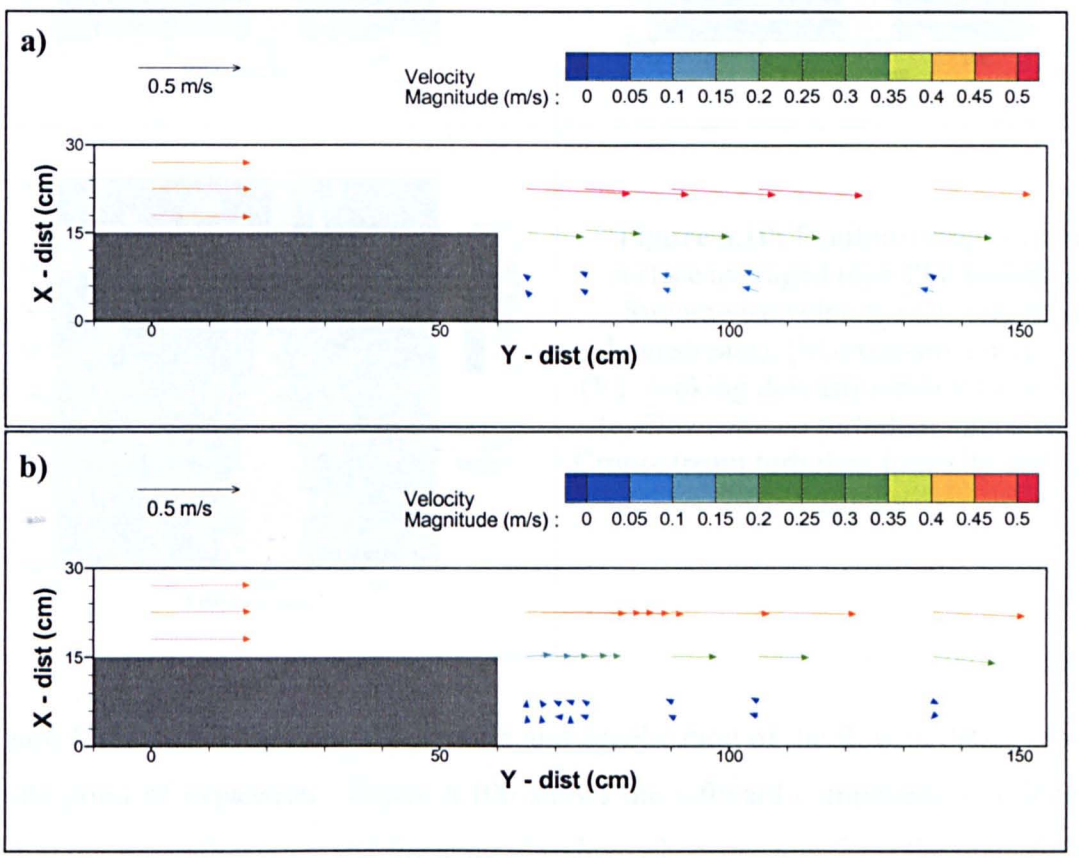

Figure 6.9: Planform map of mean vectors measured by the ADV (a) near surface; and (b) near bed.

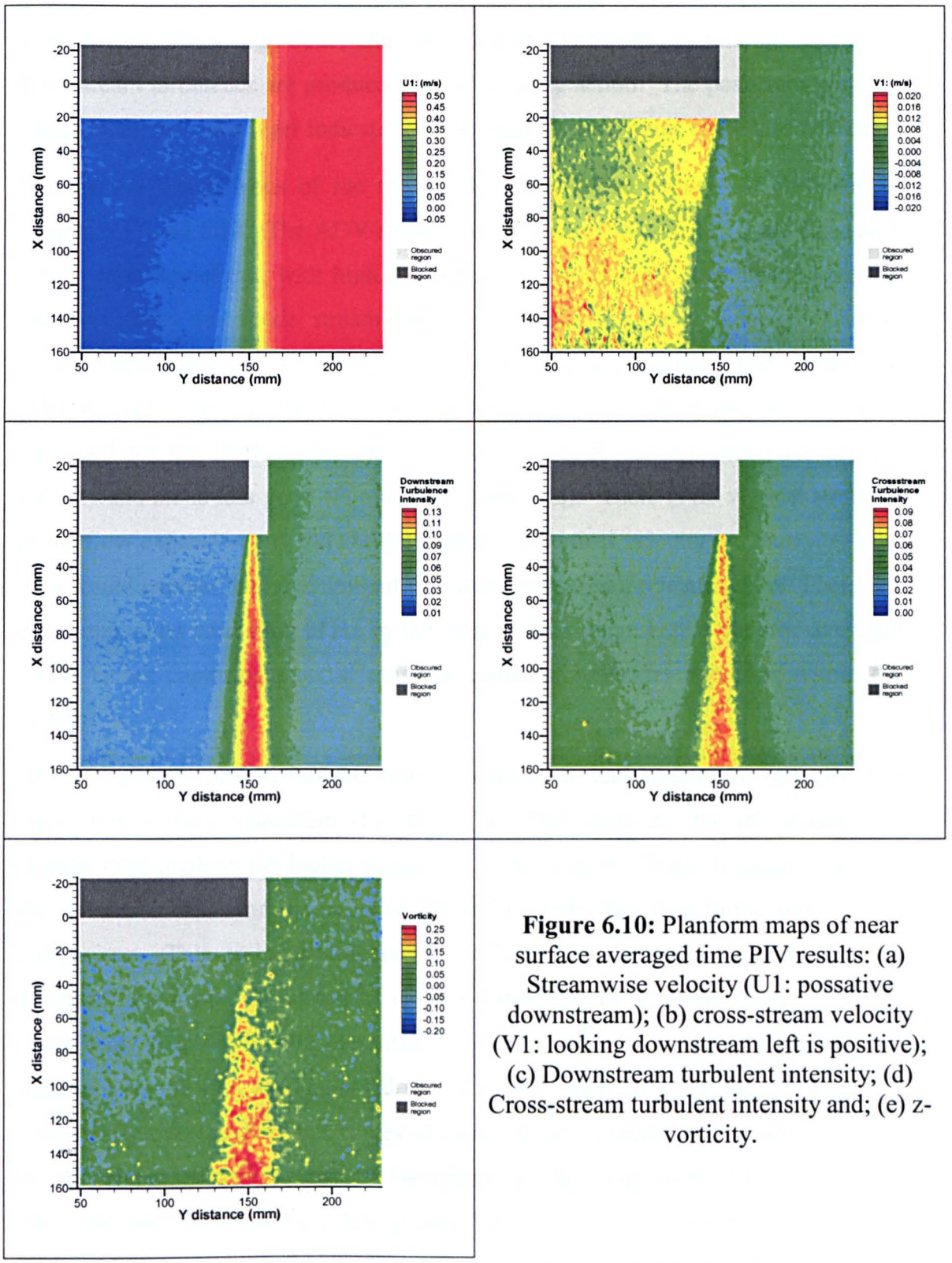

Figure 6.10: Planform maps of near surface averaged time PIV results: (a) Streamwise velocity (U1: possative downstream); (b) cross-stream velocity (V1: looking downstream left is positive); (c) Downstream turbulent intensity; (d) Cross-stream turbulent intensity and; (e) z-vorticity.

Figure 6.10a shows the lateral expansion and deceleration of the flow in detail, close to the point of expansion. Figure 6.10b shows the leftward component of velocity within the separation zone and the general rightwards expansion from the main flow, particularly along the shear layer boundary. The shear layer position and expansion

is highlighted by Figures 6.10c, d, and e. Figures 6.10c and d both show the shear layer in particularly high detail and indicate that significant amounts of lateral and downstream turbulence are produced by the shearing action. The positive *z*-vorticity values along the shear layer indicate that the shear layer contains clockwise vortices.

Quantitative comparisons of the measured and modelled results are presented in Figures 6.11 and 6.12. The ADV-model comparisons (Figure 6.11; Table 6.6) show a very close agreement, with high R^2 values and regression slopes close to the 1:1 line for velocity magnitude, streamwise velocity, and cross-stream velocity. There is a very slight tendency for over prediction of velocity magnitude and streamwise velocity, particularly in the main downstream flow. Following the familiar trend identified for the field studies presented in Chapter 5, the agreement for vertical velocity and *tke* is less good (Figure 6.11; Table 6.6). There is no vertical structure in the flow expansion and the absolute values of vertical velocity are thus very low. This would explain the large amount of scatter present in the relationship. There is a consistent under prediction of *tke* by the model. This suggests that the time-averaged model is not capturing the full range of turbulent processes operating within the system.

The PIV-model comparisons for velocity magnitude and streamwise velocity also show a very close agreement (Figure 6.12). They indicate that the model very slightly over predicts the higher velocities in the domain. There is larger scatter in the lower velocities and the negative streamwise velocities than in the ADV-model comparison. This probably reflects the smaller area over which the PIV samples, resulting in a higher likelihood of slight positioning errors across and close to the shear being manifest within the results. The comparison of cross-stream velocity measured by the PIV and predicted by the model, suggests some bias. The model consistently over predicts the values of cross-stream velocity, particularly for some of the higher positive values. Nevertheless, the general trends are correctly predicted, and there are very few points (~5 of 450) where the direction of flow differs between the two. *tke* is not calculated or compared for the PIV as it only measures velocity in two dimensions.

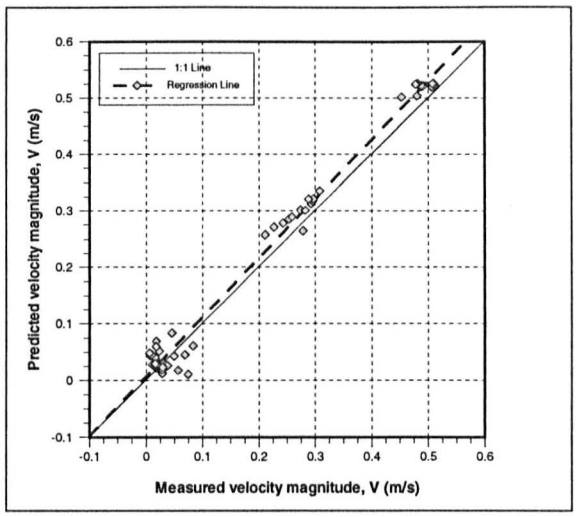

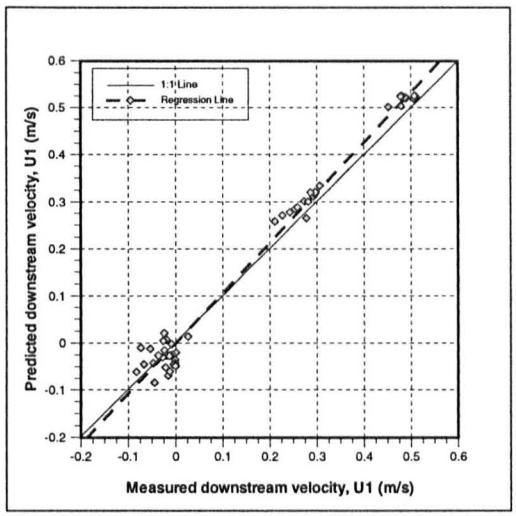

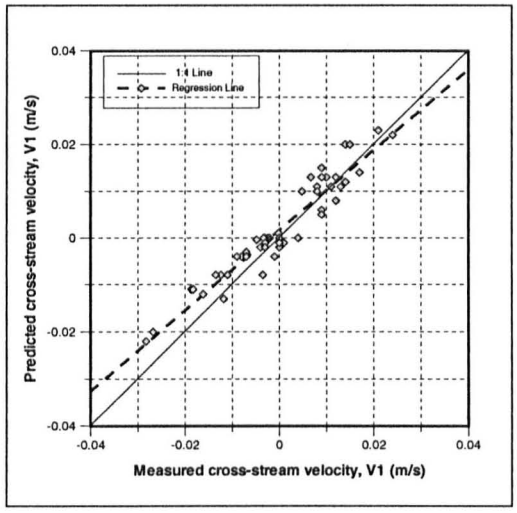

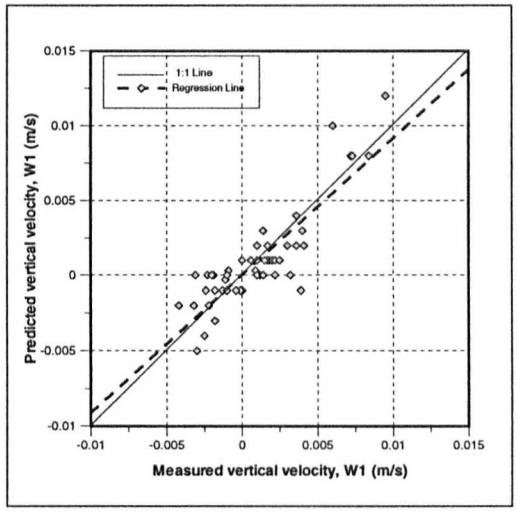

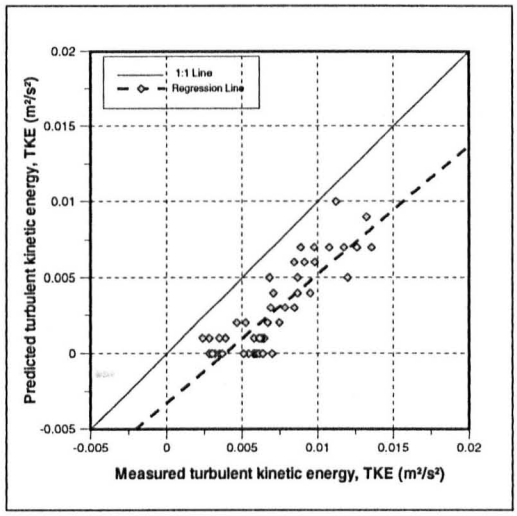

Figure 6.11: Scatter plots of time-averaged velocity (magnitude, streamwise, cross-stream and vertical) and turbulent kinetic energy model predictions against those observed using the ADV. Both the 1:1 line (solid) and the regression line (dashed) are shown.

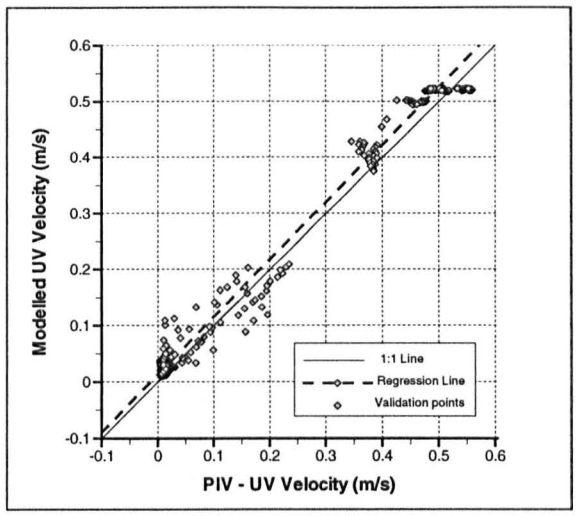

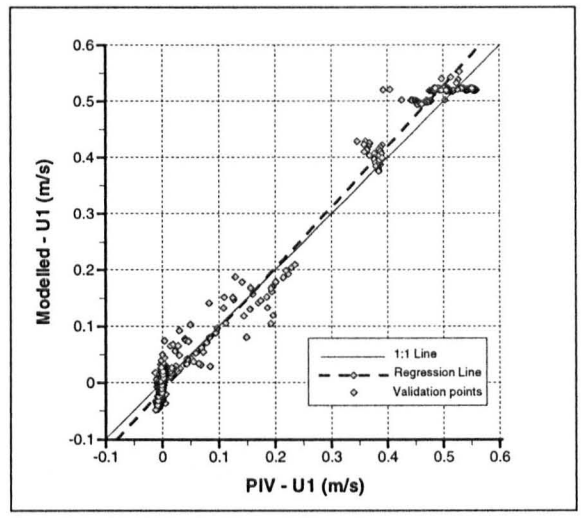

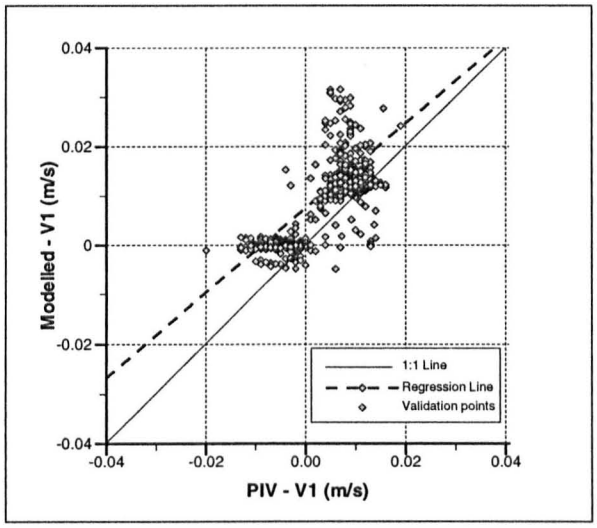

Figure 6.12: Scatter plots of time-averaged velocity (magnitude, streamwise, cross-stream) model predictions against those observed using the PIV. Both the 1:1 line is shown (solid) and the regression line (dashed).

Table 6.6: Regression results of ADV with the numerical model

Variable	Correlation Coefficient	R^2 (%)	Regression Equation
Velocity magnitude	0.993	98.7	$1.048x$ +7.7E-03
Downstream velocity	0.994	98.8	$1.068x$ –3.1E-04
Cross-stream velocity	0.955	91.2	$0.856x$ +1.7E-03
Vertical velocity	0.871	75.9	$0.914x$ +3.3E-05
Turbulent kinetic energy	0.861	74.0	$0.849x$ –3.3E-03

Overall, the numerical model is well validated against the two measurements techniques. Indeed the variance in the predicted and measured velocities is of the same order as that between the two measurement techniques. This highlights the fact that error exists in both the model predictions and the measurement technique

applied in any study and that differences between the two are not solely due to poor model performance.

6.4.3.5 Results: Time averaged flow structure

With suitable confidence in the numerical model attained, the flow structures within the expansion can be analysed in greater spatial detail than possible with the ADV and over a greater area than is possible using the PIV.

The flow structure is dominated by the rapid expansion in the flow field and the shear layer that is produced between the downstream flow and the reverse flow in the lee of the stepped width increase (Figure 6.13; 6.14; 6.15). The core of incoming fluid in the true left channel is fully developed and has an average velocity of 0.5 m/s. Post expansion, this flow decelerates and expands to occupy the greater channel width. The incoming core of faster velocity contracts, both at the bed and the surface (Figure 6.14). At 10 expansion widths downstream (x/h=10) the velocity in this downstream core reduces to approximately 0.3 m/s as the flow expands laterally to adjust to the increase in cross sectional area. This lateral spreading is indicated by Figure 6.16, where rightward components of velocity locally exceed 0.02 m/s mid-channel. Due to the smooth boundaries, flow at the surface and at the bed is similar, although the deceleration at the surface occurs at a slightly slower rate (Figure 6.15). The similarity in the planform flow structure indicates that the time-averaged shear layer is in a vertical plane (Figure 6.14; 6.15).

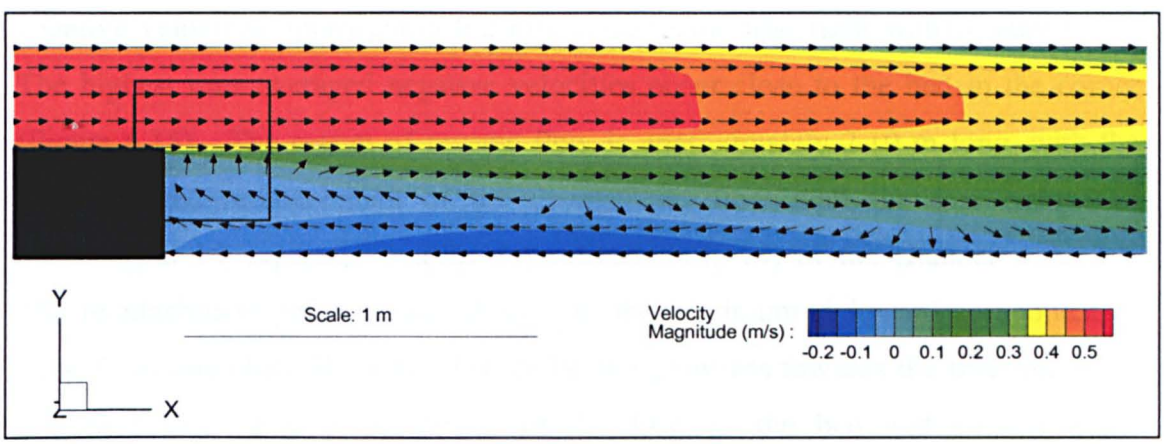

Figure 6.13: Time-averaged planform map of near surface velocity magnitude with superimposed unit vectors. PIV interrogation region is indicated by the box outline.

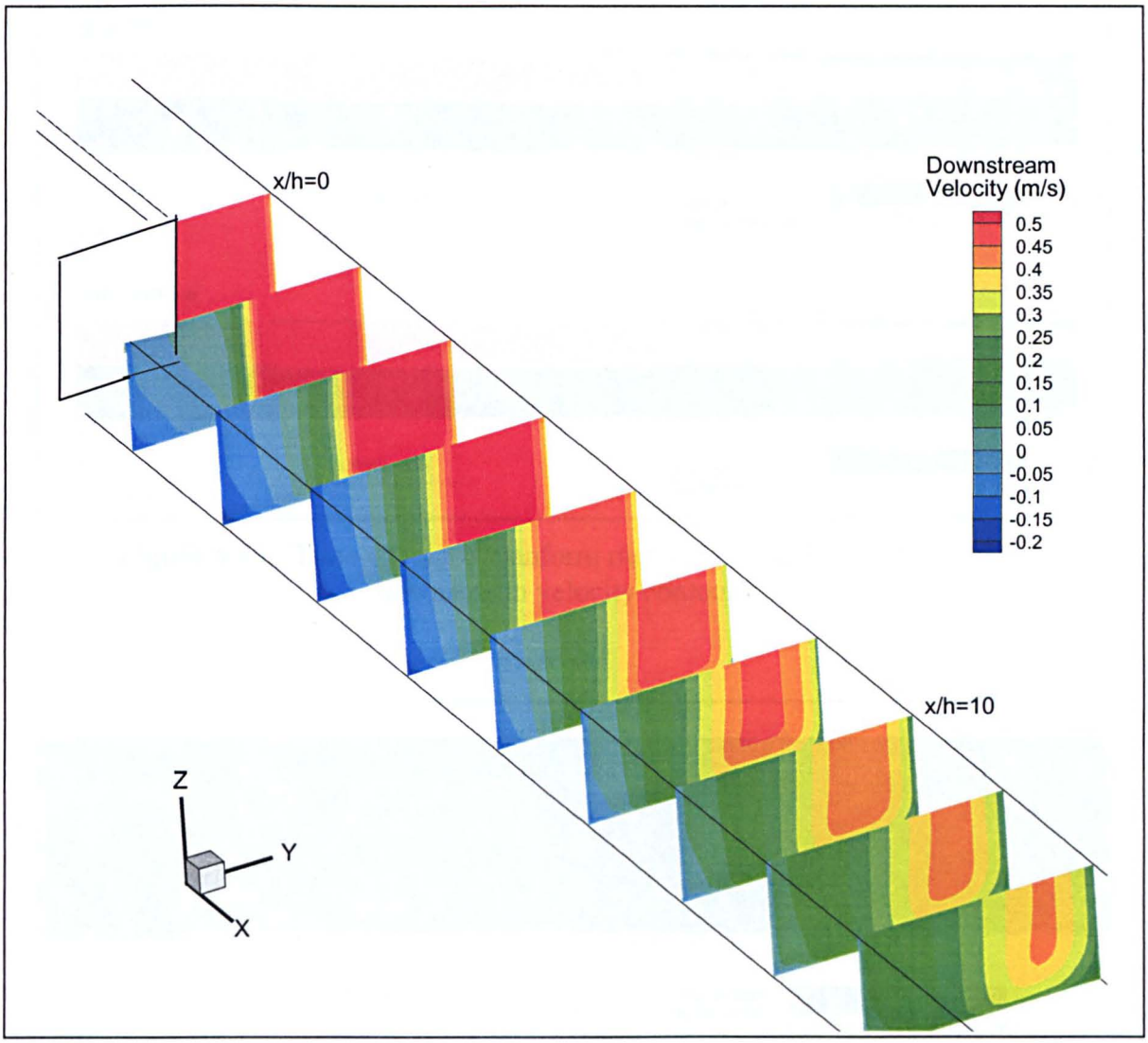

Figure 6.14: Downstream velocity contours at 10 equally spaced cross-sections down the domain from the expansion point.

In the step of the expansion, a region of reverse flow exists with time averaged negative velocities approaching 0.2 m/s close to the true right wall (Figure 6.13). The highest time-averaged negative velocities occur close to the bed in the corner (Figure 6.15). The region of reverse flow is approximately 2.10 m long, with the time-averaged re-attachment of the downstream flow with the true right wall occurring at 14 expansion widths downstream (x/h=14) of the channel widening. The re-attachment point occurs adjacent to the maximum rightward component of velocity in mid-channel, as the flow expands rightwards towards the true right wall (Figure 6.16). The re-attachment of the flow at the bed and surface occur concurrently.

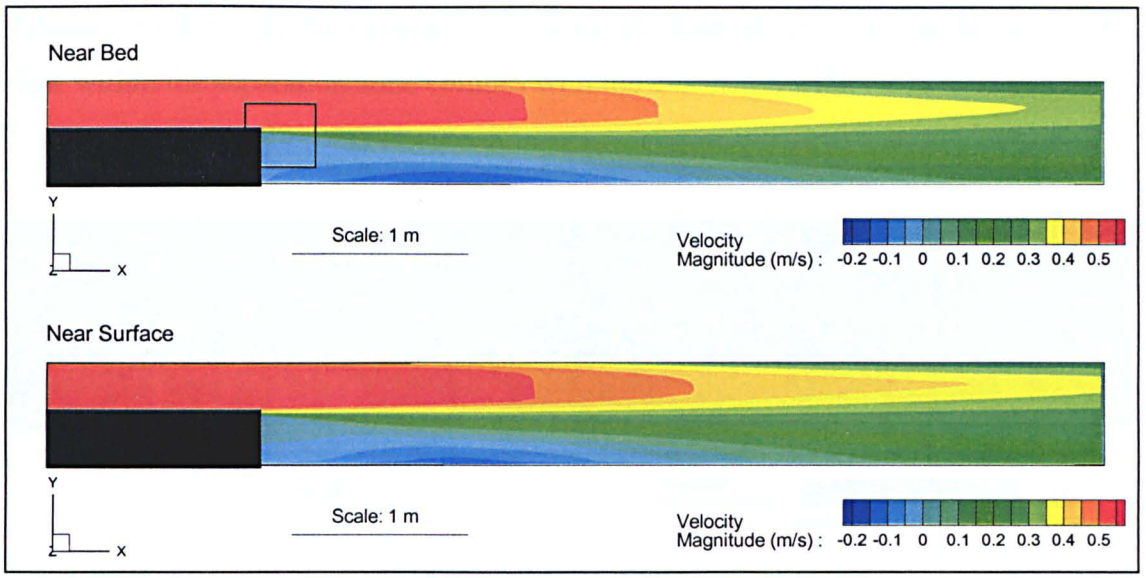

Figure 6.15: Time-averaged planform map of near surface and near bed downstream velocity contours.

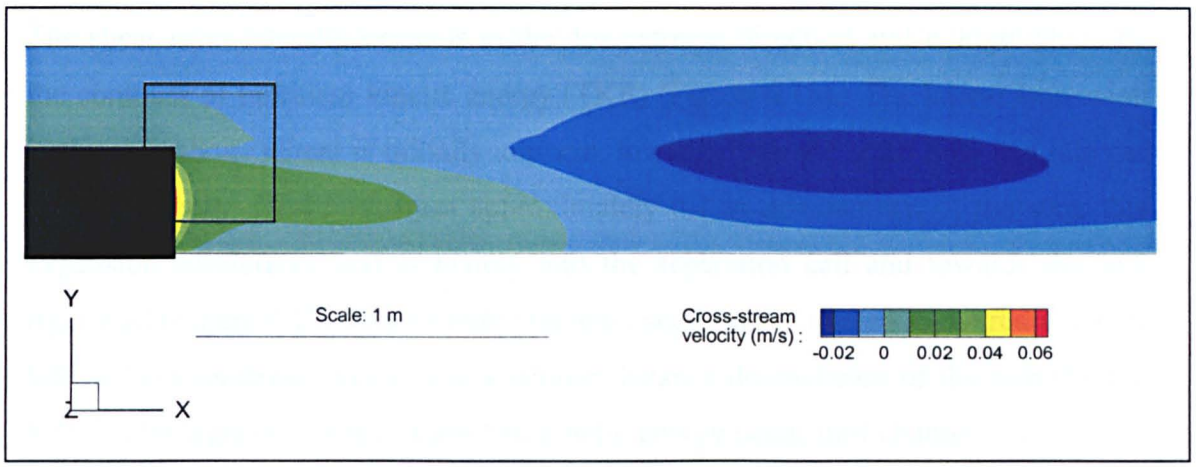

Figure 6.16: Time-averaged planform map of near surface cross-stream velocity contours.

The reverse flow within the separation zone begins to be forced towards the true left channel (Figure 6.13; 6.16), out of the separation zone and towards the main flow, from approximately 0.7 m downstream of the expansion. The leftward component of the upstream flow increases towards the expansion wall, where the maximum velocities approach 0.05 m/s in the lee of the step as the upstream flow collides with the expansion wall (Figure 6.16). The movement of this fluid out towards the shear layer and the main downstream flow completes the circuit of flow within the separation cell. Except for a small region adjacent to the expansion wall, the time-averaged vertical velocities are negligible throughout the domain (Figure 6.17).

Adjacent to the step, the vertical velocity locally exceeds 0.03 m/s as the upstream flow within the separation zone collides with the expansion wall.

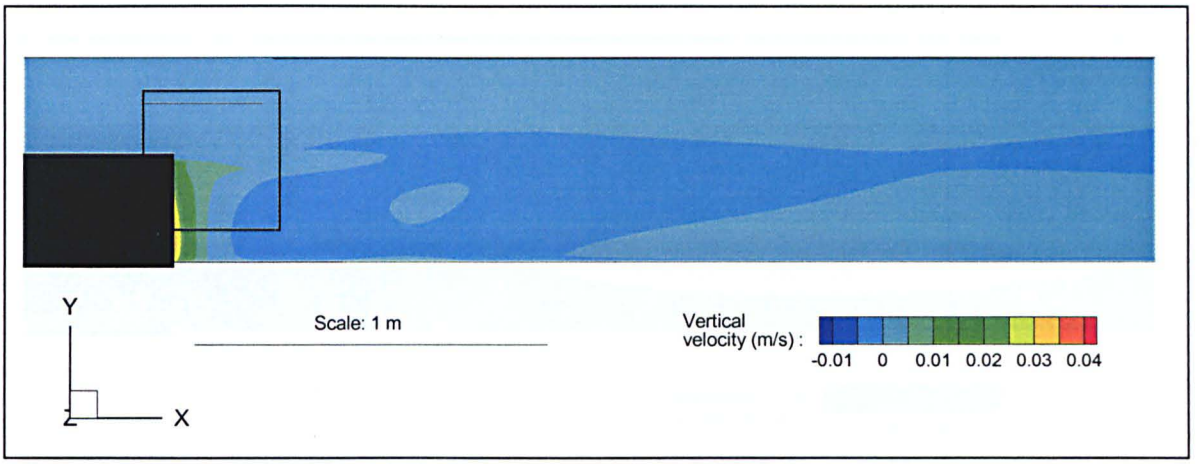

Figure 6.17: Time-averaged planform map of mid-height vertical velocity contours.

The shear layer laterally expands in the downstream direction and is highlighted by the contours of turbulent kinetic energy (TKE) (Figure 6.18). The lateral expansion in the shear layer extent is initially uniform, towards both the main flow and into the separation cell. However, from approximately 0.7 m downstream of the step, this expansion accelerates, and is mainly into the separation cell and towards the true right wall (Figure 6.18). This sudden increase seems to be related to the reduction of leftwards cross-stream velocity at a similar distance downstream of the step (Figure 6.16). The highest values of turbulent kinetic energy occur mid-channel, close to the region of highest rightward flow, further demonstrating the close relationship between cross-stream velocity and shear layer extent and intensity. This region of high TKE is adjacent to the time-averaged position of re-attachment to the true right wall and suggests that the position of re-attachment is certain to fluctuate though time.

6.4.3.6 Model assessment: Transient flow structures

For confidence to be placed in the transient flow structures simulated by the LES, comparison of model predictions with time series measurements is required. ADV time series at two points (Figure 6.7), one within the shear layer (point 1) and one within the dead zone (point 2), are used for this assessment process. Time series of

velocity were then extracted at the equivalent points in the LES results. The instantaneous maps produced by the PIV (*see* Figure 6.27) are also used for a qualitative comparison, close to the point of expansion.

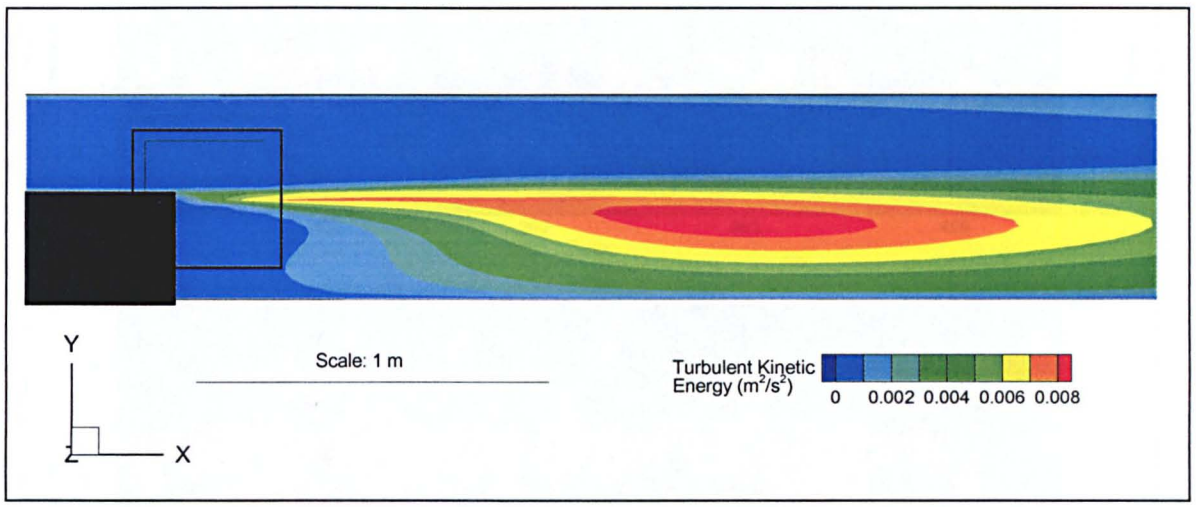

Figure 6.18: Time-averaged planform map of near surface turbulent kinetic energy contours.

To determine and compare what frequencies are present within the model predictions and the ADV measurements, wavelet analysis is applied to each velocity component at both points. Figures 6.19 and 6.20 show the wavelet spectra for the LES model at points 1 and 2 respectively and Figures 6.21 and 6.22 show the spectra for the ADV measurements at the same two points. Exact coincidence between the two spectra is not expected, given the higher frequencies of the ADV measurements. Good validation of the LES model will be represented by concurrence in the frequency and duration of events in both predictions and measurements.

Figure 6.19 indicates that the predicted streamwise flow within the shear layer two expansion widths downstream of the expansion has a dominant period close to 100 seconds, with events that last for approximately 50 seconds. This scale of event is also evident in both the cross-stream and vertical velocity spectra, although less relative power is contained in these velocity components. The cross-stream velocity spectra has significant amounts of spectral power contained in higher frequency events with a period varying between 1 and 10 seconds. Both the cross-stream and the vertical velocity components have a similar scale structure although it is less significant. At certain points through the time series, there are significant

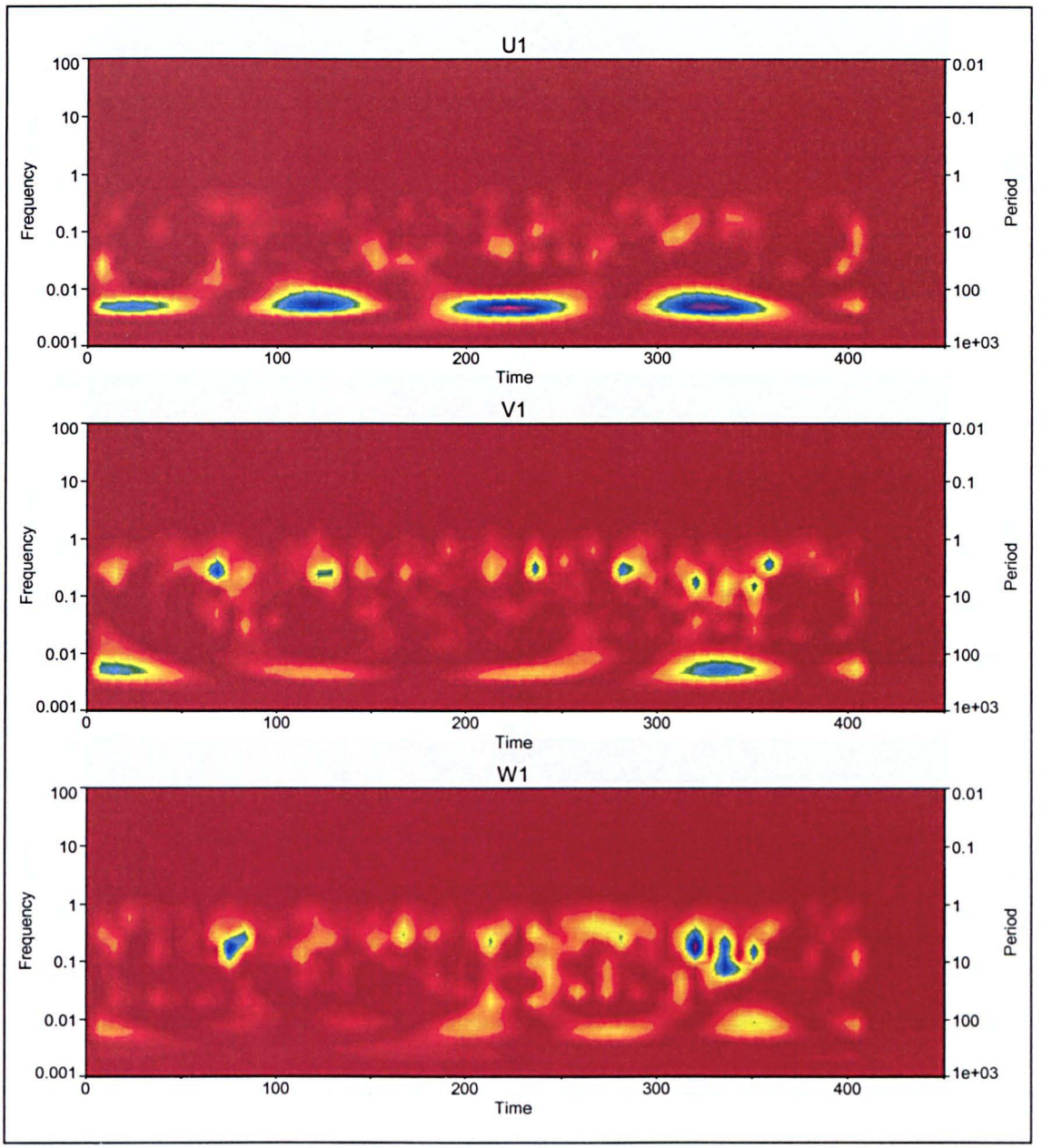

Figure 6.19: Wavelet coefficient spectra of model velocity predictions from within the shear layer mid-channel 2 x/h downstream of the expansion (point 1).

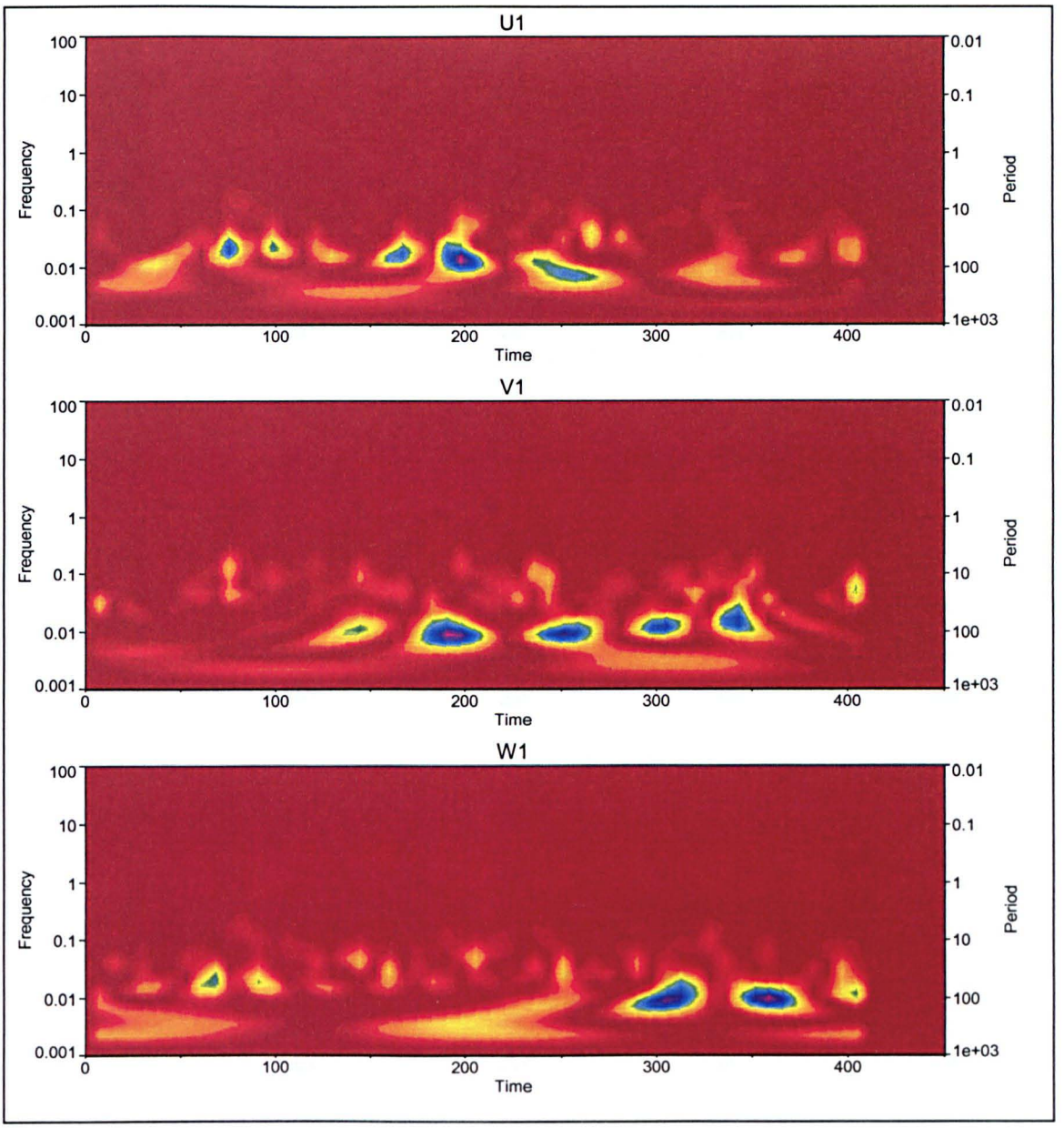

Figure 6.20: Wavelet coefficient spectra of model velocity predictions from within the dead zone 8 cm from the true right wall and 1 x/h downstream of the expansion (point 2).

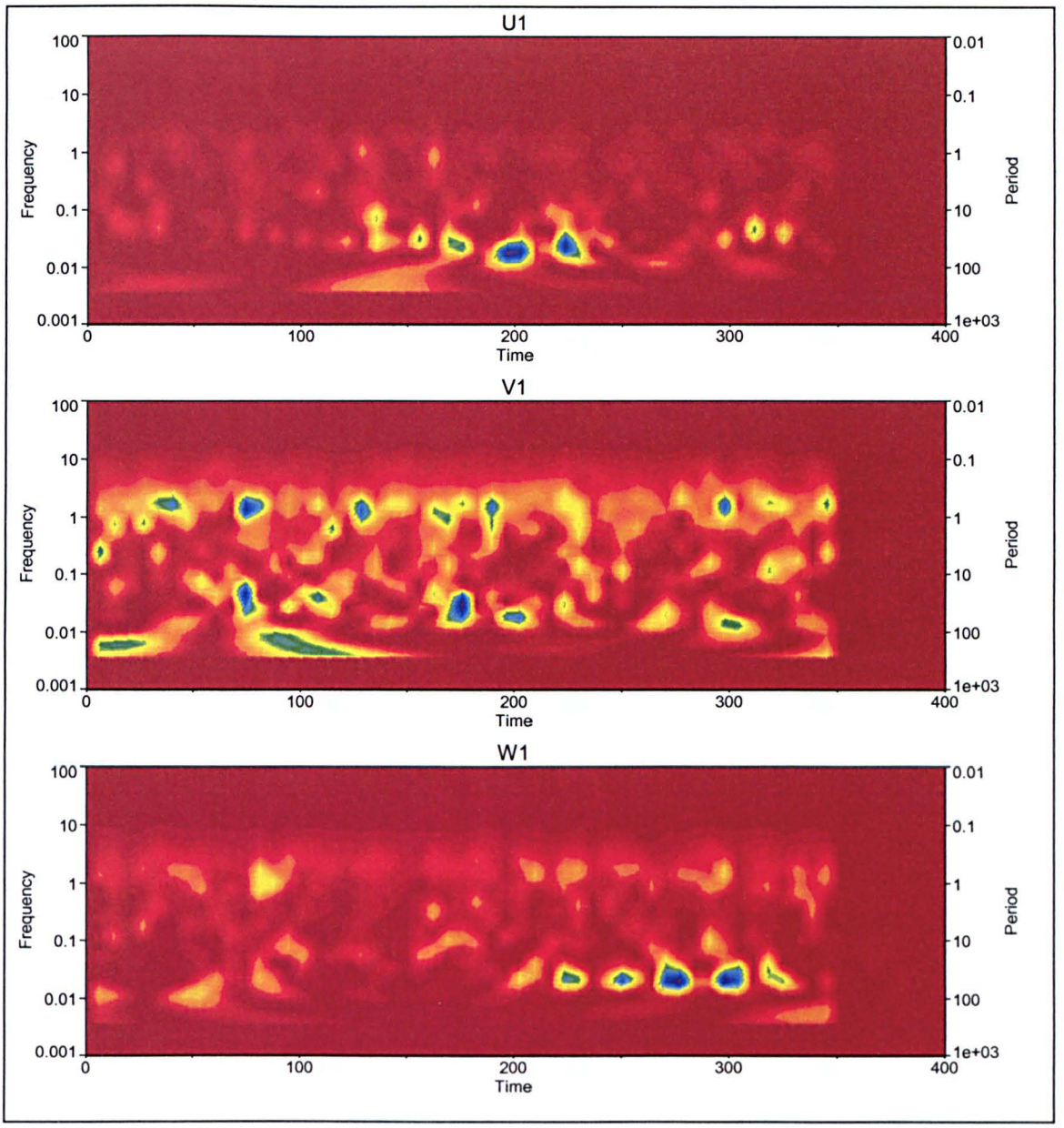

Figure 6.21: Wavelet coefficient spectra of ADV velocity measurements from within the shear layer mid-channel 2 x/h downstream of the expansion (point 1).

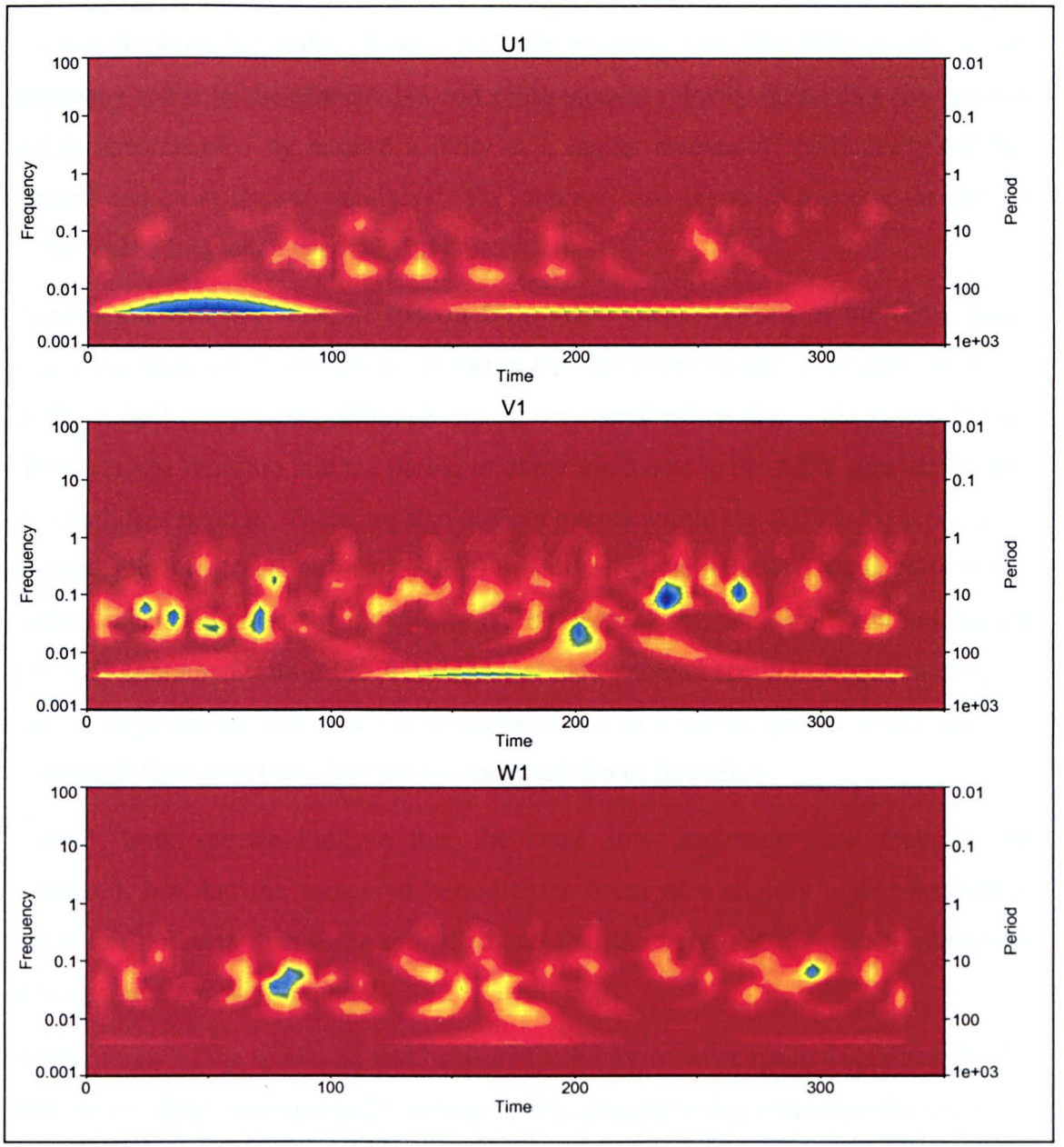

Figure 6.22: Wavelet coefficient spectra of ADV velocity measurements from within the dead zone, 8cm from the true right wall 1 x/h downstream of the expansion (point 2).

linkages between the scales of variation. For example, just after 300 seconds a low frequency event in the streamwise and cross-stream velocity dominates the spectra and is accompanied by intense activity at a higher frequency, particularly for the vertical and cross-stream velocities. This linkage also seems to increase the period of the higher frequency event slightly.

Comparison with the wavelet spectra from ADV measurements at the same point within the shear layer (Figure 6.21) shows that the lower frequency events predicted by the model are present, although the power contained at that scale is much less. Moreover, the duration and the period of event are lower in the ADV time series and are much less regular. There are also distinct events within the ADV time series with a period close to 1 second that the LES model fails to simulate. This is particularly evident when the cross-stream spectra are compared, where a significant amount of power is contained within the ADV cross-stream wavelet spectra. Figure 6.21 does contain large amounts of power in events with a 2 to 3 second period, which may be equivalent flow structures that have a predicted lower frequency.

Overall, both spectra indicate that the same low frequency flow features are simulated, but that the measured periodicities occur at a slightly higher frequency and lower duration than those modelled and that the very high frequency variations are not simulated within model.

Comparisons of the modelled and measured velocity wavelet spectra obtained for the point in the dead zone (point 2) show a similar pattern to that identified for the point within the shear layer (Figure 6.20, 6.22). Higher frequency events are not present within the dead zone and the flow is dominated by low frequency events in all three velocity components, with the model predicting a period close to 100 seconds and event duration of approximately 20 seconds. This corresponds to the pulsing of upstream flow that can be identified from the ADV measurements (Figure 6.23). Figure 6.23 also indicates this pulsing of flow is accompanied by out of phase movement of fluid toward the true left bank as flow is forced out of the dead zone. The wavelet spectra of the measured velocities show similar scales of feature for the cross-stream and streamwise velocity. As found for point 1, the periodicity of the measured feature is slightly higher than that modelled. There is a good match in both the period and duration of events for the vertical velocity within the dead zone. Once more the same trend is apparent with the event period predicted close to and slightly

above 100 seconds and the ADV measurements indicating a slightly higher frequency event and a slightly shorter duration.

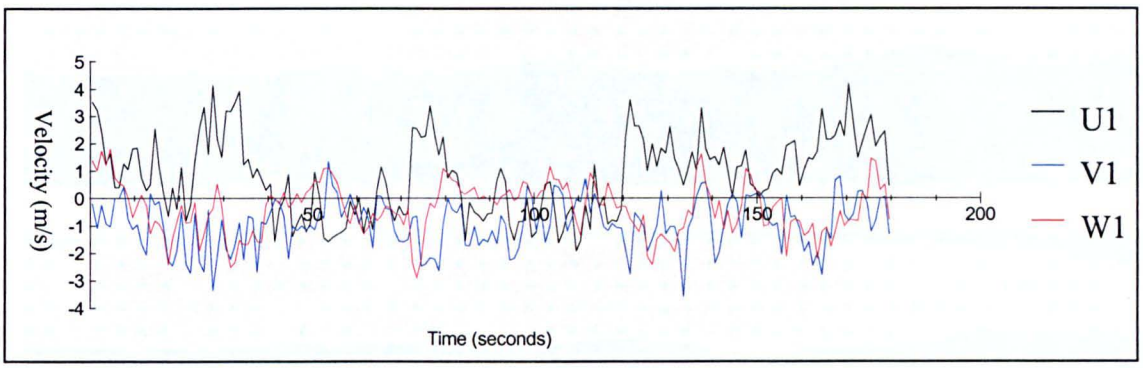

Figure 6.23: ADV velocity time series from within the dead zone close to the expansion wall (point 4)

6.4.3.7 Results: Transient flow structures

Despite there not being perfect agreement between the temporal scales of flow structure measured and predicted by the LES model, the results form the LES are of interest. This is because the simulations presented here are at a higher resolution than previous applications of LES to open channel flow and because the spatial richness of LES predictions the whole flow field can be visualized. This means that the flow structures can be inferred directly, rather than implicitly through techniques such as quadrant analysis.

The sequential plots of model predictions in Figure 6.24 and Videos 6.1 and 6.2 (see appendix 1) show that the shear layer is extremely dynamic and has a range of fluctuations at different scales. From a combination of the point wavelet analysis and the Videos of model predictions, dominant periods of about 3, 16 and 50 seconds are apparent. Small instabilities are initially generated close to the point of the expansion by the intense shear between the main downstream flow and the slow flow in the dead zone. These small Kelvin-Helmholtz type instabilities are advected downstream where they coalesce and are propagated, resulting in larger scale, lower frequency, vortex flow features further downstream. The mechanism for the coalescence is thought to be driven from co-rotation and merging as vortices of slightly differing scale are advected at slightly different rates. As the larger features

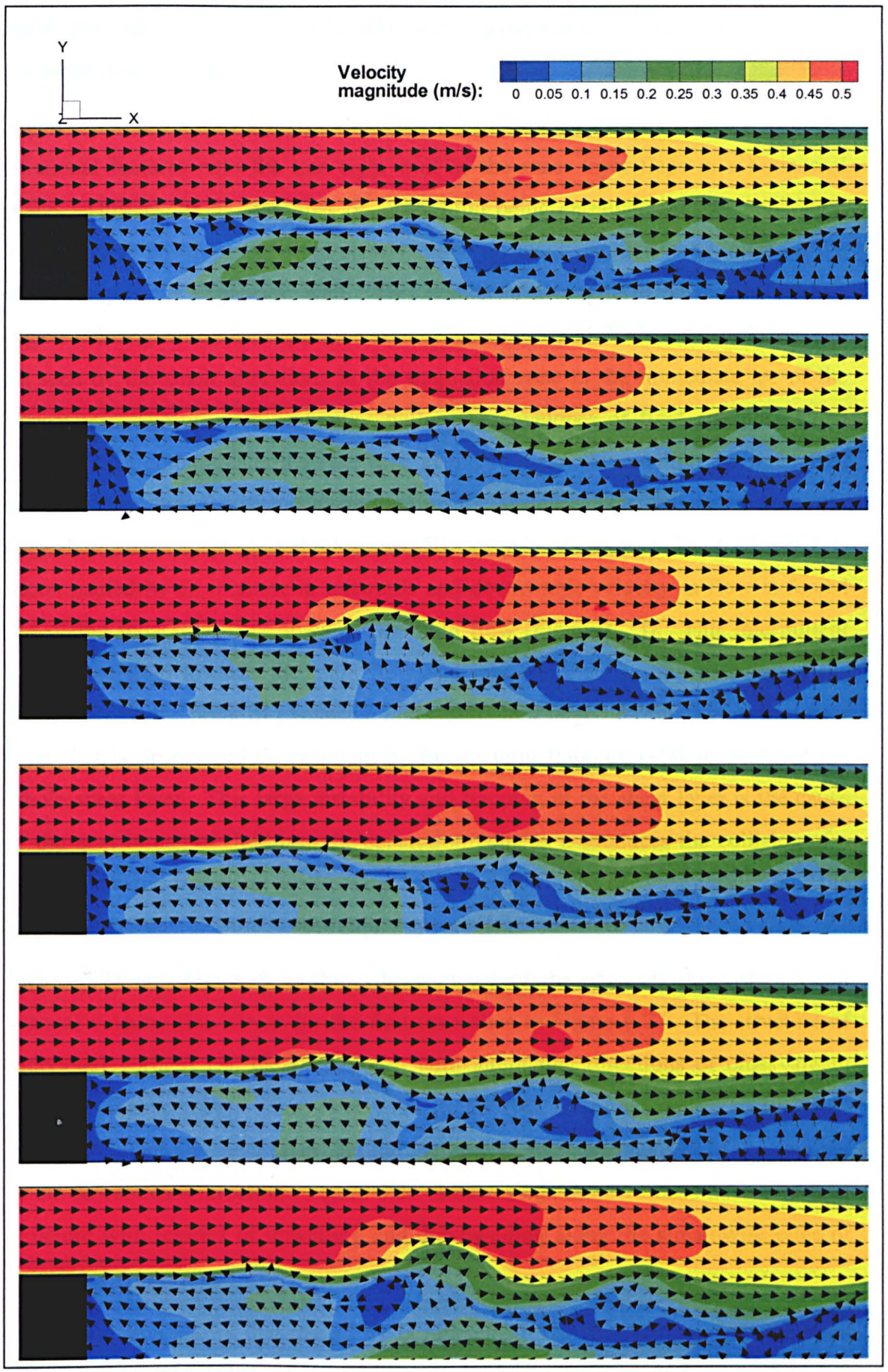

Figure 6.24: Planform contour maps of predicted velocity magnitude with unit vectors at and downstream of the width expansion. Maps are at 1-second intervals.

move downstream, they spread laterally and expand before breaking up as they are stretched downstream.

Figure 6.24 and Video 6.1 also show the intermittent impingement of these larger rotational features onto the true right wall as the shear layer flaps in a horizontal plane. This results in envelopes of faster fluid being entrained into the separation zone. These envelopes of fluid slowly move up the separation zone, close to the wall, towards the expansion wall. This results in a long-term pulsing of slightly higher velocity within the separation zone (Figures 6.23, 24; Videos 6.1, 6.2) that can be seen by the small alterations in the stagnation zone in the immediate lee of the expansion. The upstream velocities within the envelopes of fluid are close to an order of magnitude greater than the time-averaged mean value within the separation zone and are thus significant events within the system. This pulsing of upstream flow has an average period close to 50 seconds (Figures 6.22; 6.23) and is accompanied by an increase in leftwards and downwards velocity as flow is forced out of the separation zone towards the main flow (Figure 6.23). This intermittent ejection of fluid towards the main flow and into the shear layer will enhance the shear close to the point of expansion and results in a large deformation of the shear layer that is propagated downstream by longer term flapping (~50 seconds) of the whole shear layer. This large instability and flapping of the shear layer is the cause of the next inrush of fluid into the separation zone as it produces the collision of a vortex with the true right wall. This completes a circuit of instability within the system that dominates the lower frequency turbulent spectrum.

Figure 6.25 and Figure 6.26 show the contours of the unsteady cross-stream and vertical velocity flow fields for the first time slice in Figure 6.27. The structure of individual vortices can clearly be seen with alternating directions of cross-stream velocity (Figure 6.25). This clearly illustrates that rotational nature of the flow structures along the shear layer and the increase in size and intensity of the rotation in the downstream direction. Figure 6.26 indicates that these vortices have a vertical structure with regions of upwelling and downwelling along the streamwise edge of individual vortices.

This simulation shows that instability is inherent in the flow dynamics at the open channel flow expansion, even without the superimposition and interactions of fluctuations from upstream. Coalelescence of smaller Kelvin-Helmholtz features

into larger vortices are similar to those found in free shear layers (*e.g.* Winant and Browand, 1974; Rogers and Moser, 1992) and in the parallel confluence of Best and Roy (1991). Pulses of upstream flow within the dead zone result from the impingement of these larger vortices on the true right wall that interacts with the shear layer close to the expansion.

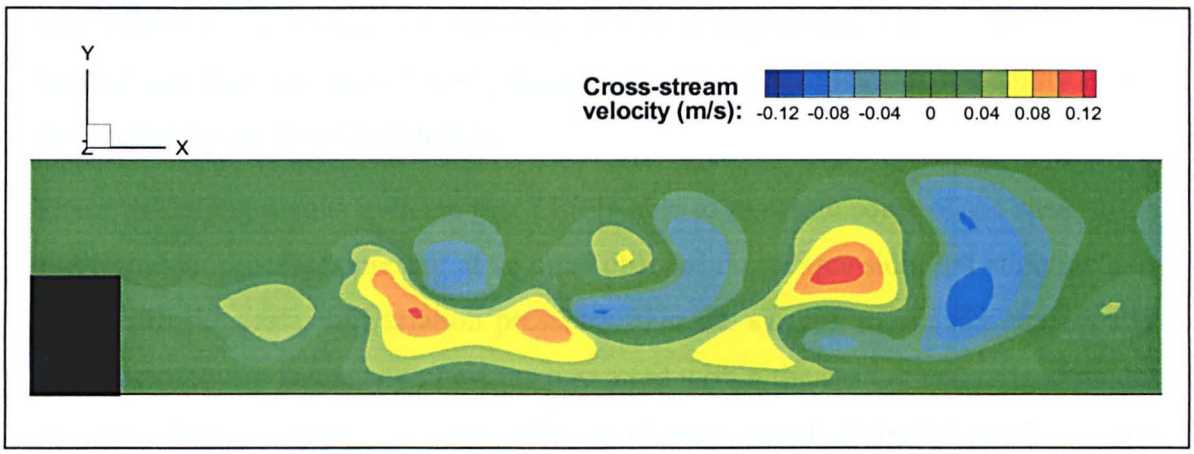

Figure 6.25: Planform contour maps of predicted cross-stream velocity at and downstream of the width expansion. At first time slice of figure 6.19.

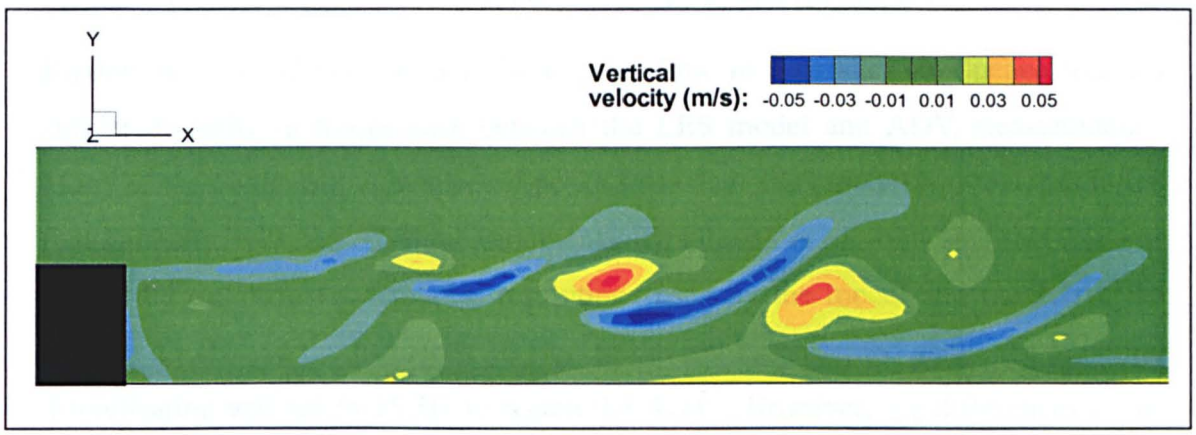

Figure 6.26: Planform contour maps of predicted vertical velocity at and downstream of the width expansion. At first time slice of figure 6.19.

6.4.3.8 Discussion

The flow structure in an open channel flow expansion is similar to standard flow investigated over a backwards-facing step. For a backward-facing step geometry Simpson (1989) identified two characteristic frequencies of large-scale turbulent

structures: (1) related to fluctuations of the reattachment point due to the shedding of Kelvin-Helmholtz instabilities from the horizontal shear over the step; (2) related to vertical flapping of the re-attaching shear layer. Driver *et al.* (1987) suggested that flapping is generated when a high momentum fluctuation moves far downstream before re-attaching which creates a reverse pressure gradient that results in a pulse of flow within the separation zone at a later time. This is similar to the flow investigated here, although the shear layer is far longer and re-attaches almost twice the distance downstream in the expansion case. The frequencies of variability in the flow structure are thus much lower.

These modelling results indicate that LES is able to re-create some of the shear layer and turbulent processes present at an open channel flow expansion, but is not able to capture all the scales of variation present within the system. The LES consistently under predicts the frequency of events measured within the system and fails to model the very high frequency events associated with small Kelvin-Helmsholz type instabilities. The two-dimensional time series maps produced by the PIV (Figure 6.27) show the generation and prorogation of small instabilities along the shear layer close to the point of expansion. This high frequency variation is also measured by the ADV (Figure 6.21) but is not simulated by the model (Figure 6.19).

Bradbrook *et al.* (2000b) in a LES study of flow in a parallel confluence found a similar disparity in frequencies between the LES model and ADV measurements. Many of the comparisons in spectral peaks from their LES model had matches in the first harmonic with the ADV measurements. Bradbrook *et al.* suggested that this was caused by the different temporal resolutions used by the model and the ADV, the latter at 25 Hz and the former at 10 Hz. In the results presented above the temporal discretisation was set to 25 Hz to match the ADV. However, the differences in the frequencies between the LES model and the ADV measurements remain, but are close to a factor of 1.4 (Figures 6.23, 6.24, 6.25, 6.26) rather than 2.0 as reported by Bradbrook *et al.* (2000b). The discrepancy between measured and modelled periodicities is lower here and could be explained by the grid resolution applied.

Figure 6.28 indicates the effect of spatial resolution on process representation within the model. This effect is two-fold and involves both the effect of spatial discreteisation itself on the solution and the effects of this imposed filter scale has on the temporal resolution due to scale-frequency interactions. The predicted time-

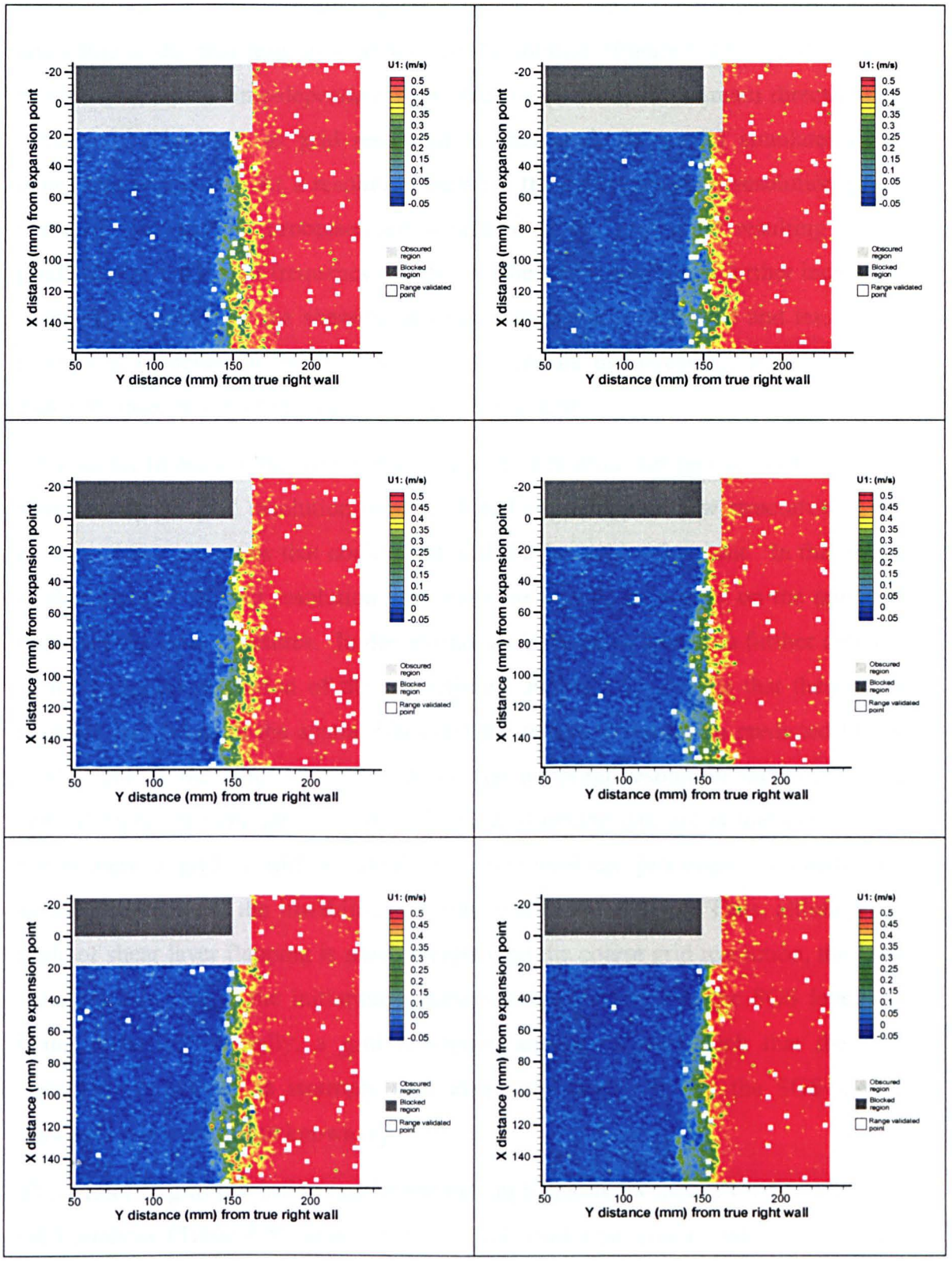

Figure 6.27: Streamwise velocity contour maps from the PIV time series (time sequence from top left to bottom right in columns at intervals of 0.066 seconds).

series of downstream velocity at point 1 within the domain is dramatically altered according to the grid resolution applied in the solution (Figure 6.28). At the coarse resolution grid, no time-dependant flow structures in the downstream direction are simulated. However, as grid resolution is increased, the model simulates time-dependent processes. At a resolution between the coarse and mid resolution grids, some of the shearing processes are simulated at the grid scale resulting in the prediction of the longer frequency events. As the grid resolution is further increased, increasing amounts of the shearing processes are directly simulated and less of the process is modelled at the SGS level. This results in increasing the amounts of higher frequency variations that are directly simulated.

This seems to answer the question posed by Hardy *et al.* (in press). In their study only the highest grid resolution used predicted any temporal flow structures. They envisaged two scenarios that could exist with further grid refinement. In the first, a further increase in grid resolution will make no significant impact on the temporal nature of the flow structures. In the second, an increase will cause a further increase in the temporal resolution of the predictions. Figure 6.28 reveals that there is an intrinsic link between the spatial filter and the temporal resolution predicted by the model and as the filter scale is reduced the temporal resolution increases. The critical aspect of simulating the periodic flow structures present is that the scale of the numerical grid should be adequate to represent the processes responsible for initial generation of the instabilities present within the system. Thus, although the scale of shear layer flapping is much greater than the coarse grid resolution, the large filter scale results in the initiation processes being modelled at the SGS level and being dispersed. Ideally, a grid resolution should be used such that the high frequency turbulence is isotropic and adequately dealt with by the SGS model. However this scale is not known *a priori.*

This effect of grid resolution has important implications for model verification. The GCI analysis (Table 6.5) shows that the mid resolution grid is independent when time-averaged results are considered. However, when time-dependant processes are considered this resolution is not sufficient to capture the range of flow processes present within the system. Thus verification of a numerical grid for RANS is an inadequate criterion for verification of a LES.

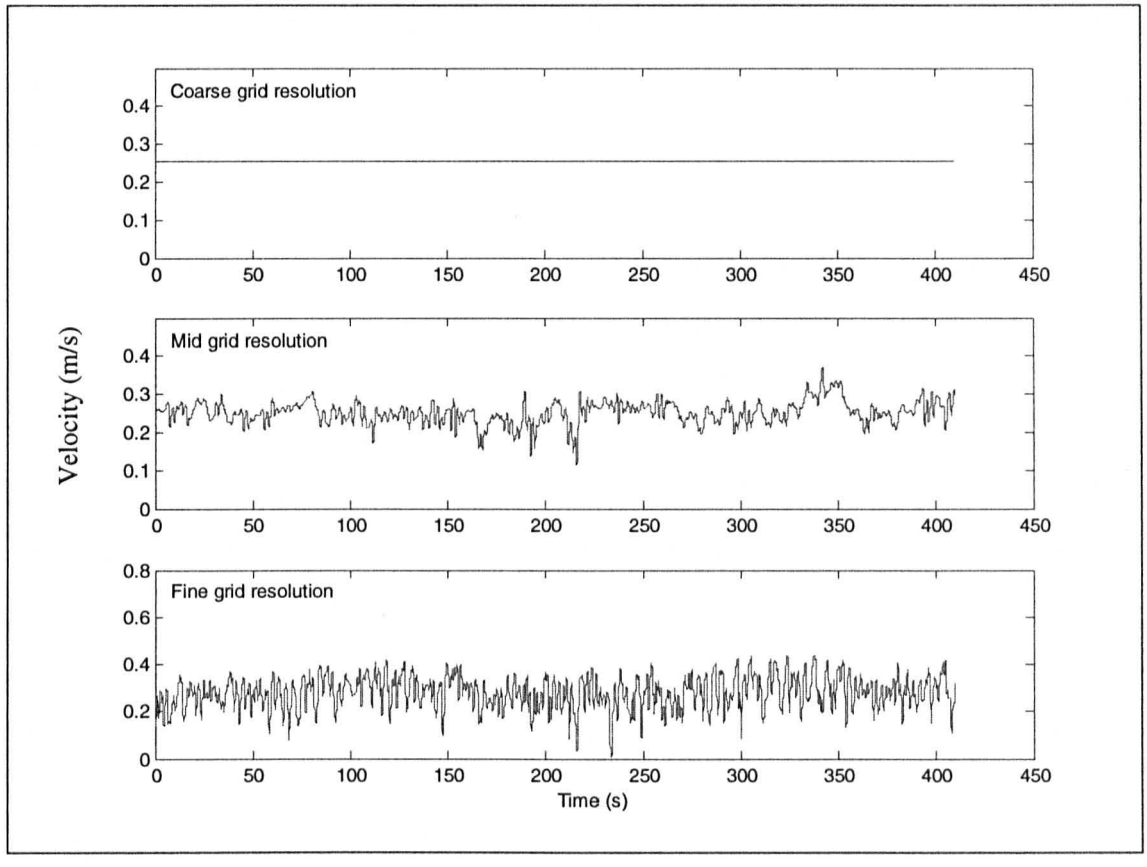

Figure 6.28: Time series of downstream velocity at a point within the shear layer (point 2) at three different grid resolutions.

Levels of turbulence within the system are very high with a range of superimposed scales of variation. In the RANS modelling, these are averaged out and the effect of this turbulence on the mean flow is modelled (Figure 6.8). In LES, the turbulence larger than the grid scale is solved directly and energy can be transferred up the turbulence scale resulting in the formation of channel-scale flow structures and fluctuations in velocity (Figure 6.24). The presence of large channel-scale fluctuations in flow, when shear layers are present, cautions against the interpretation of flow structure controls based entirely on mean flow fields. The averaging process can misrepresent the physical processes present within the system and result in explanation of incorrect controls on the mean flow structures analysed. Thus, the intermittent nature of the flow structures in such situations requires consideration before controls on flow structure can be adequately discussed (*e.g.* Lane *et al.*, 2000). Nevertheless, the RANS model does seem to be a good time-averages representation of the flow structure in this simile case, although whether this extends to natural

bends with separated flow, with the interaction of a curvature induced secondary flow structure within the streamtube, is unknown.

LES also offers the potential to investigate the mixing processes between the main streamwise flow and the dead zone. For example, Gaudet and Roy (1995) show how the passage of large-scale vortices in a confluence mixing layer can result in high magnitude variations in tracer concentration. LES could be used to predict the ranges of concentration that may occur at a point within the separated flow dead zone and be used to investigate residence times that are particularly important for the transport of pollutants through river systems (*e.g.* Hankin *et al.*, 2002). Potentially, the nature of the mixing process between and across the shear layer can also be investigated with LES techniques.

The variation in flow direction and strength produced by the shear layer processes has important implications for the prediction of bed shear stresses and fine sediment movement into and out of the dead zone. For example, Hickin (1978) suggested that the dispersion of vortices within the dead zone resulted in the deposition of the concave bank bench. Thus, LES has the potential to simulate and investigate this hypothesis.

6.4.4 Summary

This section has demonstrated the ability of LES to investigate periodic aspects of the flow field where flow separation and re-circulation are present. The model predicts the initiation and development of instabilities within the shear layer and the interaction between the dead zone and the impingement of vortices within the shear layer on the wall.

The under prediction in the flow fluctuation frequency is believed to be due to the effect of the spatial filter applied in the LES. A grid resolution study confirmed the linkage between filter scale and resolution of temporal predictions.

The results presented above indicate that consideration of transient flow structures when shear layers and dead zones are present is possible and necessary for complete understanding of the flow structures and their controls in such situations.

6.5 CHAPTER CONCLUSION

This chapter has demonstrated that transient flow structures exist in bends with separation zones. The velocity time series from within the shear layer in bends indicates that the shearing process results in a three-dimensional flow structure that is characteristically intermittent.

The potential of LES in predicting transient shear layer processes in a simple open channel flow expansion, which has some of the features of the natural bends, has been investigated. The model successfully predicts some of the longer-term variability of the shear layer and correctly simulates the pulsing of reverse flow up the dead zone. The sensitivity of the temporal predictions to the spatial discretisation is demonstrated, highlighting the need of a clearer verification process in LES applications more generally.

The LES model consistently failed to converge for a natural meander bend and this is related to the need to skew the numerical grid to the channel geometry and the failings of the SGS model applied in the LES routine. Thus, there is a need for development of both the SGS model and the way in which the channel geometry is represented in the numerical grid. Current work is focusing on the second of these, using a porosity algorithm to block out the channel boundaries on a structured cuboidal mesh.

Chapter 7

Summary, Conclusions and Further Research

7.1 INTRODUCTION

This chapter summarises the results of the thesis with respect to the main thesis aim and the five objectives outlined in Section 1.5.2. The following section (7.2) addresses each of the research objectives individually. Section 7.3 then considers the directions for future research arising from the work presented within this thesis.

7.2 SUMMARY AND CONCLUSIONS

7.2.1 Ascertain the frequency of occurrence of flow separation

The results of a reconnaissance survey (2.3) demonstrated that flow separation is widespread in the two small lowland rivers investigated (the River Dean and River Bollin, Cheshire, UK). The survey indicated that almost half of all bends exhibited flow separation at one or both banks. Inner- and outer-bank separation are almost equally common overall, although inner-bank separation is commoner than outer-bank separation along the larger River Bollin and the reverse is true of the River Dean. The size distributions of inner- and outer-bank separation zones were found to be skewed for both types of separation. Separation zones that extend over half the channel width are comparatively rare, occurring in about 10% of surveyed bends. Small inner bank separations were found to be relatively common, particularly along the River Bollin. This was attributed to the steering of the flow around the larger point-bars prevalent in the River Bollin.

7.2.2 Identify factors responsible for the formation of separation zones

The reconnaissance survey demonstrated that some simple parameters could explain the presence of separation zones in some bends. In both rivers, the factors that seem

to influence the occurrence and size of inner-bank separation zones are increases in bend angle of turn, main flow impingement angle onto the outer bank and point-bar existence and size. Factors that seem to influence the occurrence and size of outer-bank separation are increases in main flow impingement angle, outer-bank strength, and bend angle of turn. However, although the factors investigated in the reconnaissance survey were statistically significant, they only explained low amounts of variance, highlighting their inadequacy in the detail required for a full understanding of flow separation in bends.

Therefore, a more detailed field study of a subset of twenty-two bends was performed. Building on the results of the reconnaissance survey, this more detailed investigation identified that the bend curvature is a significant factor in the development of separation in bends. However, it also found that breaks in bankline curvature are perhaps more crucial to separation production, especially in terms of position of separation within the bend. The width and depth ratios were also found to be significant factors: in both, the degree of expansion towards the apex was positively correlated with separation occurrence and size. However, due to the covariant nature of variables considered, these relationships were difficult to disentangle. The occurrence of sharp breaks in bankline curvature was found to be more likely in sharper bends and the depth ratio was correlated with bend tightness. Although the reconnaissance survey found that the impingement angle of the main flow at the outer bank was important in generating separation, the more detailed investigation identified that it is the distribution of velocity and notably asymmetry at the bend entrance rather than the flow direction that was important in producing separation in bends. When bend inflow is skewed towards the outer bank, inner bank separation is more likely and when the main inflow is close to the inner bank, outer bank separation is more likely. The nature of impingement at the outer bank was therefore found to be governed more by the bend curvature and the inflow momentum rather than actual inflow deviation across the riffle.

7.2.3 Quantify the three-dimensional flow structure in meander bends with separated flow and evaluate the ability of the numerical model in simulating the observed flow structures

A combination of field case study monitoring and computational fluid dynamics (CFD) modelling of individual bends was employed to investigate the time-averaged flow structure in three natural river bends with flow separation. Two of the bends had an inner-bank recirculation eddy (one small, one large), and the third had a large outer-bank eddy. It was found that, with careful consideration of grid construction, the numerical modelling approach could be applied to these bends, even where highly complex grids were required using boundary fitted co-ordinates. All the models were successfully verified and validated using clearly defined and structured procedures. The combination of fieldwork for validation of a numerical model provided an extremely powerful means of investigating flows in these complex bends where field data cannot realistically provide adequate process representation.

The modelling results indicate that the flow structures in bends with separation are significantly different from more 'classical' meander bends where curvature-induced helical circulation occupies most or all of the channel width. In both inner and outer bank separation cases, fast downstream flow with a helical circulation was present, but it is restricted to a streamtube occupying less than half the channel width, near the opposite bank to the one with the zone of flow separation. The flow within the streamtube is characterised by an intense helical motion in proximal portions of the bend, but both velocity magnitude and strength of helical circulation decrease distally past the apex, and the secondary circulation disappears before the exit of the bend. This is contrary to bends that are more classical, where this helical motion usually extends beyond the bend exit, often into the entrance of the next bend. In bends with separation, the fastest flow is progressively below the water surface, becoming close to the bed in the bend with the large inner-bank recirculation. In both types of separation, the dead zone is somewhat isolated from the main flow structure in the streamtube. In the inner bank separation cases, the dead zone acts like a large point bar steering flow around the outer bank. In the outer bank case, it acts like an outer bank boundary, particularly at the proximal end of flow reattachment where return flow out of the separation zone impinges into the streamtube. In both inner and outer bank separation, the recirculation extends further

across the channel at the surface than the bed; this was attributed to the different orientations of near-surface and near-bed velocity in the streamtube of downstream flow.

In both cases, large amounts of shear exist between the slowly recirculating flow and the fast downstream streamtube. However, the time-averaged nature of this shear was found to differ significantly between inner and outer bank separations. In outer bank separation cases, shear is generated between the downwelling portion of the streamtube and the slower flow within the separation zone. In the inner bank separation case, this shear is along the upwelling edge of the streamtube. This results in deformation of the time-averaged inner bank shear layer into an S-shaped feature, as upwelling flow at the bed of the streamtube is dominant where flow is slower moving within the dead zone. The recirculation eddy is similar to what occurs in a sudden channel expansion, with a near-vertical axis shear layer and the strongest reverse flow close to the separated bank.

Mixing between downstream and separation zone is driven by fluid escaping from the decelerating streamtube into the downstream end of the recirculation eddy beyond the apex of the bend. Re-entrainment of fluid from the dead zone is through an interaction of the return flow with the vertical motion within the streamtube helix. However, field observations and analysis indicated the presence of large-scale turbulent structures along the shear layer, which are advected into the dead zone. Kelvin-Helmholtz type vortices were also observed shedding from the shear layer. Therefore, the transient shear layer processes play an important role and are key to understanding the nature of mixing in these bends.

7.2.4 Assess the ability of LES in modelling periodic aspects of the flow field

As mentioned above the presence of a large amount of shear between the streamtube and the dead zone produces large coherent flow structures that are likely to be extremely important processes within these bends. An attempt was made to model these processes numerically using Large Eddy Simulation. However, models of the bend geometries could not converge on a solution. This was due to the highly anisotropic nature of the numerical grid and the limitations of the spatial filter based sub-grid scale model in such situations.

However, the potential of LES in predicting transient shear layer processes in a simple open channel flow expansion was demonstrated and assessed. This geometry has some of the main flow and form features of the natural bends with separation zones, including a sharp change in curvature, a width expansion, a shear layer, and a recirculation zone. A particle image velocimeter and an acoustic Doppler velocimeter were used to obtain empirical flume data with which to assess the numerical model. Wavelet analysis was applied both to validate the numerical model and to investigate the nature of the transient flow structures within the domain. Wavelet analysis revealed that the model was able to successfully predict some of the longer frequency variability of the shear layer and correctly simulate the pulsing of reverse flow up the dead zone. However, the model did not simulate the higher frequency variations and the model consistently under predicted the frequencies of all the longer period events. The sensitivity of the temporal predictions to the spatial discretisation was demonstrated, perhaps explaining this under prediction. The grid sensitivity also highlighted a need of a clearer verification process in LES applications more generally, as verification of a time-averaged grid is not an adequate criterion for an LES solution.

7.2.5 Explore flow structures generated by different combinations of boundary conditions and flow stages, and consider the geomorphological implications of the modelling results.

The issue of stage dependence was explored for one inner bank separation case, which was thought to be most sensitive to changes in discharge. The investigation revealed that, in bend 37, inner bank separation was maintained at high flow and that the main features were still present at bankfull stage, including a large recirculation eddy with an outer-bank helix wrapped around it. However, the size of the separation zone reduced slightly. The strength of both the outer-bank helix and the inner-bank recirculation significantly increased, reflecting the stable interaction between the two features over a range of discharges. The intensity of shear along the boundary also increased substantially, making it difficult to obtain a fully converged solution.

The dead zones contain a significant volume of recirculating fluid. This modifies the structure of flow through the bend. The patterns of bed shear stress are remarkably different from those expected in bends that are more classical. Regions of high bed shear follow the path of the streamtube through the bend with the large areas of low stress over the dead zone acting as a sink for fine sediments. During low flow, the dead zones act as a sink for fine sediments, although the predictions of high velocity within the dead zone at bankfull flow in bend 37 indicates that in bends with inner bank separation they become sources of fine sediments during higher flow stages. The evacuation of sediment from the dead zone at higher flows has significant implications for the maintenance of the separation zone and for the sediment dynamics of the system as a whole. As fine sediment is evacuated from the dead zone, bar development is reduced and bed elevations remain lower through the separated region, maintaining the expansion in channel width that is necessary for separation production.

The movement of the bends through the study period has also been investigated and reveals that the migration patterns of these bends is considerably different from the classical bend migration model and that movements can be rapid. This finding of rapid migration rates is contrary to some earlier reports that bends with separation zones are stalled floodplain features. Movement in the inner bank separation case is upstream of the apex where flow impinges into the outer bank at a high angle. Movement in the outer bank case is through migration of the inner convex bank and the outer bank well beyond the bend apex. This indicates that the separation zones act to maintain themselves and are dynamic features of the fluvial system.

A conceptual model of the self-regulation of these bends has been developed which explains the formation of outer bank separation from an inner bank case and suggests an interplay between separation at the inner and outer banks that affects the position of the streamtube through the bend. The position of the streamtube in the bend ultimately governs the areas of erosion and deposition in these bends. It was also suggested that because the flow structures through and out of bends with separation are significantly different to classical bends it explains the formation of irregular meander trains, which often accompany the presence of separation.

7.3 FURTHER RESEARCH

There are many avenues for further research arising from the findings of this thesis. This section briefly describes a few possibilities for future research objectives, which will enhance the understating of these complex bends.

7.3.1 Long-term bend development

Long-term monitoring of the bends is required. There is a need to understand how these bends develop and alter over a longer period of time. Aerial photographs could be used to investigate the longer-term development of individual bends that currently have large-scale separation. This should be combined with continued detailed surveying in the three intensive study bends to produce further digital elevation models through time, providing a detailed picture of how these bends develop and migrate within the river system.

7.3.2 Stage dependence

In the work presented above the sensitivity of separation size and extent was examined numerically for one bend with a large inner bank separation. However, the generalisations that can be made from this study are undetermined. An extension to the reconnaissance survey detailed in Chapter 2 to higher flow events would provide some information on the generality of separation maintenance across a fuller range of discharges. A sub-reach of the channel could be surveyed at different flow levels to ascertain whether the changes modelled in bend 37 are representative of bends with inner bank separation.

7.3.3 Mixing processes and dispersion

The mixing between the main flow and the dead zone is still poorly understood. A field study, combined with numerical experiments where a tracer is inserted into the flow, could be used to investigate and quantify the amount, nature, and timing of mixing between the main flow and the dead zone. The results of this work would provide information on the importance of these separated flow zones to longitudinal

dispersion through river reaches and could be used to better parameterise aggregated dead zone models.

7.3.4 Numerical model development

7.3.4.1 Large eddy simulation of natural river bends

To use LES in natural channels with a complex geometry, developments are required on two main fronts: 1) enhancement of the performance of the sub-grid scale model analogous to the developments in standard time-averaged turbulence models and 2) developments to incorporate topography of the bend within a structured grid. Progress on the second of these is underway with an ongoing NERC funded project (Lane and Hardy, 2002). The boundary fitted co-ordinates used to represent the channel are often highly distorted, have high aspect ratios and are sometimes heavily skewed to the main flow direction. These cause significant problems in attaining a converged solution, especially when LES is used. Current work is developing the use of a new porosity algorithm (Lane and Hardy, 2002) for geometric representation of the bed and banks within an isotropic grid that is regular in both Cartesian and computational space. This algorithm minimises the numerical diffusion associated with fitting boundary co-ordinates to complex geometries. As the algorithm allows retention of structured numerical grids it will permit the use of the simple, Smagorinsky (1963) spatial filter-based Large Eddy Simulation to simulate the time dependence of 3D flows in complex channel geometries. Thus, the nature of the interactions of the shear layer dynamics with the separation zone can be modelled and analysed numerically, providing spatially rich flow field predictions through time. Future work will concentrate on applying the porosity algorithm to the bends investigated in this thesis.

7.3.4.2 Coupling sediment transport to 3D hydraulics

Numerical modelling of sediment transport is now a widespread activity within geomorphology (*e.g.* Hoey and Ferguson, 1994; Bridge, 1992). Most sediment transport routines are driven by simple hydraulics, sometimes 2D although typically 1D. The importance of the three-dimensional flow structure in meander bends with separation zones has been demonstrated and suggests that a 3D routine will be

required to investigate the development of these bends. The development of such a model will have the capability of investigating the form-process feedback in natural channel flows, and will be a significant development in reach-scale channel investigations.

References

Ackers P, Charlton FG. 1970. Dimensional analysis of alluvial channels with reference to meander length. *Journal of Hydraulic Research* 8: 287-316

Alford JJ, Baumann RH, Lewis AJ. 1982. Circular meander pools. *Earth Surface Processes and Landforms* 7: 183-8

Allen JRL. 1985. *Principles of physical sedimentology.* London: Allen & Unwin

Almquist CW, Holley ER. 1985. *Transverse mixing in meandering laboratory channels with rectangular and naturally varying cross sections.* Report of the CRWR 205, the University of Texas.

Anderson DA, Tanehill JC, Pletcher RH. 1984. *Computational Fluid Dynamics and Heat Transfer.* New York: Hemisphere Publishing

Andrle R. 1994. Flow Structure and Development of Circular Meander Pools. *Geomorphology* 9: 261-70

ASCE Task Committee on Turbulence Models in Hydraulic Computations. 1988. Turbulence modelling of surface water flow and transport. *J. Hydr. Engrg.*, ASCE, 114: 970–1073

Ashmore PE, Ferguson RI, Prestegaard KL, Ashworth PJ, Paola C. 1992. Secondary Flow in Anabranch Confluences of a Braided, Gravel- Bed Stream. *Earth Surface Processes and Landforms* 17: 299-311

Ashworth PJ, Bennett SJ, McLelland SJ, Best JL, eds. 1996. *Coherent Flow Structures in Open Channels.* Chichester: Wiley

Ashworth PJ, Ferguson RI. 1986. Interrelationships of Channel Processes, Changes and Sediments in a Proglacial Braided River. *Geografiska Annaler Series A-Physical Geography* 68: 361-71

Bagnold RA. 1960. Some aspects of the shape of river meanders. *USGS Professional Paper* 282E

Bates PD, Anderson MG, Hervouet J-M, Hawkes JC. 1997. Investigating the behaviour of two-dimensional finite element models of compound channel flow. *Earth Surface Processes and Landforms* 22: 3-18

Bates PD, Lane SN, eds. 1998. Special Issue: High-resolution flow modelling. *Hydrological Processes* 12 (8)

Bathurst JC, Thorne CR, Hey RD. 1979. Secondary flow and shear stress at river bends. *Journal of the Hydraulics Division, ASCE* 105: 1277-95

Bathurst JC, Thorne CR, Hey RD. 1977. Direct measurements of secondary currents in river bends. *Nature* 269: 504-06.

Begin ZB. 1981. Stream curvature and bank erosion: A model based on the momentum equation. *Journal of Geology* 89: 497-504

Bernard RS, Schneider ML. 1992. *Depth-averaged numerical modelling for curved channels*, US Army Corps Engineers, Vicksburg, Mississippi

Best JL, Roy AG. 1991. Mixing-Layer Distortion At the Confluence of Channels of Different Depth. *Nature* 350: 411-3

Beven KJ. 1989. Changing ideas in hydrology - the case of physically-based models. *Journal of Hydrology* 105: 157-72

Beven KJ. 1992. Future of distributed modelling. *Hydrological Processes* 6: 253-4

Beven KJ, Binley A. 1992. The future of distributed models: model calibration and uncertainty predictions. *Hydrological Processes* 6: 279-98

Bhowmik NG. 1982. Shear stress distribution and secondary currents in straight open channels. In *Gravel bed rivers*, ed. RD Hey, JC Bathurst, CR Thorne, pp. 31-55. Chichester: Wiley

Biedenharn DS, Combs PG, Hill GJ, Pinkard CF, Pinkston CB. 1989. Relationship between channel migration and radius of curvature on the Red River. In *Sediment Transport Modelling*, ed. SS Wong, pp. 536-41: American Society of Civil Engineers

Biron P, Boy AG, Best JL. 1996. Turbulent flow structure at concordant and discordant open-channel confluences. *Experiments in Fluids* 21: 437-46

Biron P, De Serres B, Roy AG, Best JL. 1993b. Shear layer turbulence at an unequal depth channel confluence. In *Turbulence: Perspectives on Flow and Sediment Transport*, ed. NJ Clifford, JR French, J Hardisty. Chichester: Wiley

Biron P, Roy AG, Best JL, Boyer CJ. 1993a. Bed Morphology and Sedimentology At the Confluence of Unequal Depth Channels. *Geomorphology* 8: 115-29

Biron PM, Richer A, Kirkbride AD, Roy AG, Han S. in press. Spatial patterns of water surface topography at a river confluence. *Earth Surface Processes and Landforms*:

Blanckaert K, Graf WH. 2001. Mean flow and turbulence in open-channel bend. *Journal of Hydraulic Engineering-ASCE* 127: 835-47

Bluck BJ. 1971. Sedimentation in the meandering river Endrick. *Scottish Journal of Geology* 7: 93-138

Boussinesq J. 1877. Essai sur la theorie des eaux courantes. *Memoires presentes par diver savants a l'Academie des Sciences, Paris.*

Booker DJ, Sear DA, Payne AJ. 2001. Modelling three-dimensional flow structures and patterns of boundary shear stress in a natural pool-riffle sequence. *Earth Surface Processes and Landforms* 26: 553-79.

Boxall J, Guymer I, Marion A. 2002. Locating outfalls on meandering channels to optimise transverse mixing. *Journal of the chartered institution of water and environmental management* 16: 194-8.

Bradbrook KF, Biron PM, Lane SN, Richards KS, Roy AG. 1998. Investigation of controls on secondary circulation in a simple confluence geometry using a three-dimensional numerical model. *Hydrological Processes* 12: 1371-96

Bradbrook KF, Lane SN, Richards KS. 2000a. Numerical simulation of three-dimensional, time-averaged flow structure at river channel confluences. *Water Resources Research* 36: 2731-46

Bradbrook KF, Lane SN, Richards KS, Biron PM, Roy AG. 2000b. Large Eddy Simulation of periodic flow characteristics at river channel confluences. *Journal of Hydraulic Research* 38: 207-15

Bradbrook KF, Lane SN, Richards KS, Biron PM, Roy AG. 2001. Role of bed discordance at asymmetrical river confluences. *Journal of Hydraulic Engineering-ASCE* 127: 351-68

Bray DI. 1980. Evaluation of effective boundary roughness for gravel-bed rivers. *Canadian Journal of Civil Engineering* 7: 392-7

Brice JC. 1974. Evolution of meander loops. *Geological Society of America Bulletin* 85: 581-6

Bridge JS. 1977. Flow, bed topography, grain size, and sedimentary structure in open channel bends: A three-dimensional model. *Earth Surface Processes* 2: 401-16

Bridge JS. 1984. Flow and sedimentary processes in river bends: comparison of field data and theory. In *River Meandering: Proceedings of the Conference Rivers '83*, ed. M Elliot, pp. 857-72. New York: ASCE

Bridge JS. 1992. A Revised Model For Water-Flow, Sediment Transport, Bed Topography and Grain-Size Sorting in Natural River Bends. *Water Resources Research* 28: 999-1013

Bridge JS. 1993. The interaction between channel geometry, water flow, sediment transport and deposition in braided rivers. In *Braided rivers, Special*

publication 75, ed. JL Best, CS Bristow, pp. 13-75. London: Geological Society

Bridge JS, Gabel SL. 1992. Flow and Sediment Dynamics in a Low Sinuosity, Braided River - Calamus River, Nebraska Sandhills. *Sedimentology* 39: 125-42

Bridge JS, Jarvis J. 1976. Flow and sedimentary processes in the meandering river South Esk, Glen Clova, Scotland. *Earth Surface Processes* 1: 303-36

Bridge JS, Jarvis J. 1982. The dynamics of a river bend: a study in flow and sedimentary processes. *Sedimentology* 29: 499-541

Brown GL, Roshko A. 1974. On density effects and large structure in turbulent mixing layers. *Journal of Fluid Mechanics* 64: 775-816

Buffin-Belanger T, Roy AG, Kirkbride AD. 2000a. On large-scale flow structures in a gravel-bed river. *Geomorphology* 32: 417-35

Buffin-Belanger T, Roy AG, Kirkbride AD. 2000b. On the integration of turbulent flow structures within the dynamics of a gravel-bed river reach. *Geographie Physique Et Quaternaire* 54: 105-17

Burge LM, Smith DG. 1999. Confined meandering river eddy accretions: sedimentology, channel geometry and depositional processes. *Special Publication of the International Association of Sedimentologists* 28: 113-30

Carey WC. 1969. Formation of flood plain lands. *Journal of the Hydraulics Division, ASCE* 95: 981-94

Carling PA, Orr HG, Glaister MS. 1994. Preliminary observations and significance of dead zone flow strycture for solute and fine particle dynamics. In *Mixing and Transport in the Environment*, ed. KJ Beven, PC Chatwin, JH Millbank. Chichester: Wiley

Carling PA, Wood N. 1994. Simulation of flow over pool-riffle topography: A consideration of the velocity reversal hypothesis. *Earth Surface Processes and Landforms* 19: 319-32

Carson MA. 1986. Characteristics of High-Energy Meandering Rivers - the Canterbury Plains, New-Zealand. *Geological Society of America Bulletin* 97: 886-95

Carson MA, Lapointe MF. 1983. The Inherent Asymmetry of River Meander Planform. *Journal of Geology* 91: 41-55

Casulli V, Stelling GS. 1998. Numerical simulation of three-dimensional quasi-hydrostatic free surface flows. *Journal of Hydraulic Engineering-ASCE* 124: 678-86

Chen G, Shen HW. 1984. River curvature-width ratio effect on shear stress. In *River Meandering: Proceedings of the Conference Rivers '83*, ed. M Elliot, pp. 687-99. New York: ACSE

Chollet JP, Lesieur M. 1981. Parameterisation of small scales of three-dimensional isotropic turbulence utilising spectral closures. *Journal of Atmospheric Science* 38: 2747-57

Church M, Mark DM. 1980. On size and scale in geomorphology. *Progress in Physical Geography* 4: 342-90

Clifford NJ, Richards KS, Robert A. 1992a. The Influence of Microform Bed Roughness Elements On Flow and Sediment Transport in Gravel Bed Rivers - Comment. *Earth Surface Processes and Landforms* 17: 529-34

Clifford NJ, Robert A, Richards KS. 1992b. Estimation of Flow Resistance in Gravel-Bedded Rivers - a Physical Explanation of the Multiplier of Roughness Length. *Earth Surface Processes and Landforms* 17: 111-26

Correia LRP, Krishnappan G, Graf WH. 1992. Fully coupled unsteady mobile boundary flow model. *Journal of Hydraulic Engineering-ASCE* 118: 476-94

Dantec Dynamics Inc. 2001. An overview of the FlowMap systems. www.dantecmt.com/PIV/System/Index.html.

De Serres B, Roy AG, Biron P, Best JL. 1999. Three-dimensional flow structure at a river channel confluence with discordant beds. *Geomorphology* 26: 313-35

De Vriend HJ, Geldof HJ. 1983. Main flow velocity in short river bends. *Journal of Hydraulic Engineering-ASCE* 109: 991-1011

Deardorff JW. 1970. Convective velocity and temperature scales for the unstable planetary boundary layer and Rayleigh convection. *Journal of the Atmospheric Sciences* 27: 1211-3

Deardorff JW. 1973. The use of subgrid transport equations in a three-dimensional model of atmospheric turbulence. *Journal of Fluids Engineering-Transactions of the Asme* 95: 429-38

Demuren AO. 1993. A numerical model for flow in meandering channels with a natural bed topography. *Water Resources Research* 29: 1269-77

Dietrich WE. 1987. Mechanics of flow and sediment transport in river bends. In *River channels: environment and process*, ed. KS Richards, pp. 179-227. Oxford: Blackwell

Dietrich WE, Smith JD. 1983. Influence of the point bar on flow through curved channels. *Water Resources Research* 19: 1173-92

Dietrich WE, Smith JD. 1984. Bed-Load Transport in a River Meander. *Water Resources Research* 20: 1355-80

Dietrich WE, Whiting PJ. 1989. Boundary shear stress and sediment transport in river meanders of sand and gravel. In *River Meandering, American Geophysical Union monograph 12*, ed. S Ikeda, G Parker, pp. 1-50. Washington D.C. AGU

Dury GH. 1955. Bend width and wave-length in meandering valleys. *Nature* 176

Einstein HA, Harder JA. 1954. Velocity distribution and boundary layer at channel bends. *Transactions of the American Geophysical Union* 35: 114-20

Einstein HA, Shen HW. 1964. A study of meandering in straight and alluvial channels. *Journal of Geophysical Research* 69: 5239-346

Engelund F. 1974. Flow and bed topography in channel bends. *Journal of Hydraulic Engineering-ASCE* 100: 1631-48

Farge M. 1992. Wavelet transforms and their applications to turbulence. *Annual Review of Fluid Mechanics* 24: 395-457

Ferguson R. 1979. River meanders: regular or random? In *Statistical applications in the spatial sciences*, ed. N Wrigley, pp. 229-41. London: Pion

Ferguson R, Hoey T, Wathen S, Werritty A. 1996. Field evidence for rapid downstream fining of river gravels through selective transport. *Geology* 24: 179-82

Ferguson RI. 1973. Channel pattern and sediment type. *Area* 5: 38-41

Ferguson RI. 1976. Disturbed periodic model for river meanders. *Earth Surface Processes* 1: 337-47

Ferguson RI. 1987. Accuracy and Precision of Methods For Estimating River Loads. *Earth Surface Processes and Landforms* 12: 95-104

Ferguson RI. 1981. Channel form and channel changes. In *British rivers*, ed. Lewin J, p90-125, Allen and Unwin.

Ferro V, Baiamonte G. 1994. Flow velocity profiles in gravel bed rivers. *Journal of Hydraulic Engineering-ASCE* 120: 60-80

Ferziger JH, Peric M. 1997. *Computational Methods for Fluid Dynamics*. Berlin: Springer

Fisk HN. 1944. *Geological investigation of the alluvial valley of the Lower Mississippi River*. Vicksburg, Mississippi

Foufoula-Georgiou F, Kumar P, eds. 1994. *Wavelets (Volume 4) and its applications in Geophysics*. San Diego: Academic Press

Friedkin JF. 1945. *A laboratory study of the meandering of alluvial rivers*, US Waterways Experiment Station, Vicksburg, Mississippi

Friedrich R, Arnal M, Unger F. 1991. Large eddy simulation of turbulence in engineering applications. *Applied Scientific Research* 48: 437-45

Furbish DJ. 1988. River-Bend Curvature and Migration - How Are They Related. *Geology* 16: 752-5

Furbish DJ. 1991. Spatial Autoregressive Structure in Meander Evolution. *Geological Society of America Bulletin* 103: 1576-89

Fureby C, Tabor G, Weller HG, Gosman AD. 1997. A comparative study of subgrid-scale models in homogeneous isotropic turbulence. *Physics and Fluids A* 9: 1416-29

Gabor D. 1946. Theory of Communications. *Journal of the institute of electrical engineering* 93: 429-457

Gagliano, SM, and Howard, PC. 1983. The neck cut-off oxbow lake cycle along the lower Mississippi River. In *River Meandering: Proceedings of the Conference Rivers '83*, ed. CM Elliott, pp. 885-94. New York: American Society of Civil Engineers

Gaudet HJ, Roy AG. 1995. Effect of bed morphology on flow mixing length at river confluences. *Nature* 373: 138-9

Geldof HJ, De Vriend HJ. 1993. Distribution of main flow velocity in alternating river bends. *Special Publication of the International Association of Sedimentologists* 6: 85-95

Germano M. 1992. Turbulence - the Filtering Approach. *Journal of Fluid Mechanics* 238: 325-36

Gessler D, Hall B, Spasojevic M, Holly F, Poutaheri H, Raphelt N. 1999. Application of 3D mobile bed, hydrodynamic model. *Journal of Hydraulic Engineering-ASCE* 125: 737-49

Goring DG, Nikora VI. 2002. Despiking Acoustic Doppler Velocimeter Data. *Journal of Hydraulic Engineering-ASCE* 128: 737-49

Grass AJ. 1971. Structural features of turbulent flow over smooth and rough boundaries. *Journal of Fluid Mechanics* 50: 233-55

Grass AJ, Mansour-Tehrani M. 1996. Generalised scaling of coherent bursting structures in the near wall region of turbulent flow over smooth and rough boundaries. In *Coherent Flow Structures in Open Channels*, ed. PJ

Ashworth, SJ Bennett, JL Best, SJ McLelland, pp. 41-62. Chichester: Wiley

Guymer I. 1998. Longitudinal dispersion in sinuous channels with changes in shape. *Journal of Hydraulic Engineering-ASCE*: 124: 33-40

Hankin BG, Hardy R, Kettle H, Beven KJ. 2001. Using CFD in a GLUE framework to model the flow and dispersion characteristics of a natural fluvial dead zone. *Earth Surface Processes and Landforms* 26: 667-87

Hankin BG, Holland MJ, Beven KJ, Carling PA. 2002. Computational fluid dynamics modelling of flow and energy fluxes for a natural fluvial dead zone. *Journal of Hydraulic Research* 40: 389-401

Hardy R, Lane SN, Ferguson R, Parsons DR. in press. Assessing the credibility of a series of computational fluid dynamic simulations of open channel flow. *Hydrological Processes*:

Hartel C, Kleiser L. 1997. Galilean invariance and filtering dependence of near-wall grid-scale/sub-grid-scale interactions in large-eddy simulation. *Physics of Fluids* 9: 473-5.

Hasegawa K, Yamaoka I. 1984. Phase shifts of pools and their depths in meander bends. In *River Meandering: Proceedings of the Conference Rivers '83*, ed. CM Elliott, pp. 885-94. New York: American Society of Civil Engineers

Hattingh J, Rust IC. 1993. Flood Transport and Deposition of Tracer Heavy Minerals in a Gravel-Bed Meander Bend Channel. *Journal of Sedimentary Petrology* 63: 828-34

Haworth DC, Tahry EL, Huebler SH. 1993. A global approach to error estimation and physical diagnostics in mutli-dimensional computational fluid dynamics. *International Journal for Numerical Methods in Fluids* 17: 75-97

Hey RD. 1976. Geometry of river meanders. *Nature* 262: 482-4

Hey RD, Thorne CR. 1975. Secondary flow in river channels. *Area* 7: 191-5

Hickin EJ. 1974. The development of meanders in natural river channels. *American Journal of Science* 274: 414-42

Hickin EJ. 1977. Hydraulic factors controlling channel migration. In *Research in fluvial systems, Proceedings of the 5th Guelph geomorphology symposium*, ed. R Davidson-Arnott, W Nickling, pp. 59-72. Norwich: Geobooks

Hickin EJ. 1978. Mean flow structure in meanders of the Squamish River, British Columbia. *Canadian Journal of Earth Sciences* 15

Hickin EJ. 1979. Concave bank benches on the Squamish River, British Columbia. *Canadian Journal of Earth Sciences* 16: 200-3

Hickin EJ. 1986. Concave bank benches in the flood plains of the Muskwa and Fort Nelson Rivers, British Columbia. *The Canadian Geographer* 30: 111-22

Hickin EJ, Nanson GC. 1975. The character of channel migration on the Beatton River, North-east British Columbia, Canada. *Geological Society of America Bulletin* 86: 487-94

Hirt CW, Nichols BD. 1981. Volume of Fluid (VOF) method for the dynamics of free boundaries. *Journal of Computational Physics*: 201-25

Hodskinson A. 1996. Computational fluid dynamics as a tool for investigating separated flow in river bends. *Earth Surface Processes and Landforms* 21: 993-1000

Hodskinson A. 1997. *Flow structure and geomorphology of non-classical meander bends*. PhD Thesis, University of Sheffield, Sheffield

Hodskinson A, Ferguson RI. 1998. Numerical modelling of separated flow in river bends: Model testing and experimental investigation of geometric controls on the extent of flow separation at the concave bank. *Hydrological Processes* 12: 1323-38

Hoey TB, Ferguson R. 1994. Numerical-Simulation of Downstream Fining By Selective Transport in Gravel-Bed Rivers - Model Development and Illustration. *Water Resources Research* 30: 2251-60

Hooke JM. 1987. Lateral Migration Rates of River Bends - Discussion. *Journal of Hydraulic Engineering-ASCE* 113: 915-8

Hooke JM. 1995. River channel adjustment to meander cutoffs on the River Bollin and River Dane, northwest England. *Geomorphology* 14: 235-53

Hooke JM. 1997. Styles of channel changes. In *Applied fluvial geomorphology for river engineering and management*, ed. CR Thorne, RD Hey, MD Newson. Chichester: Wiley

Hooke JM, Harvey AM. 1983. Meander changes in relation to bend morphology and secondary flows. In *Modern and ancient fluvial systems*, ed. JD Collinson, J Lewin, pp. 121-32: Special Publication of the International Association of Sedimentologists

Hooke JM, Harvey AM, Miller SY, Redmond CE. 1990. The Chronology and Stratigraphy of the Alluvial Terraces of the River Dane Valley, Cheshire, N W England. *Earth Surface Processes and Landforms* 15: 717-37

Hooke RlB. 1975. Distribution of sediment transport and shear stress in a meander bend. *Journal of Geology* 83: 543-65

Howes S, Anderson MG. 1988. Computer simulation in geomorphology. In *Modelling Geomorphological Systems*, ed. MG Anderson, pp. 421-40. Chichester: Wiley

Huang J, Weber LJ, Lai YG. 2002. Three-dimensional numerical study of flows in open-channel junctions. *Journal of Hydraulic Engineering-ASCE* 128: 268-80

Ikeda S. 1984. Flow and bed topography in channels with alternate bars. In *River Meandering: Proceedings of the Conference Rivers '83*, ed. CM Elliott, pp. 733-46. New York: American Society of Civil Engineers

Ikeda S. 1985. Bed topography in bends of sand-silt rivers. *Journal of Hydraulic Engineering-ASCE* 111: 1397-411

Ikeda S. 1989. Sediment transport and sorting at bends. In *River Meandering*, ed. S Ikeda, pp. 103-25: American Geophysical Union Monograph

Ikeda S, Parker G, Sawai K. 1981. Bend theory of river meanders. Part 1. Linear development. *Journal of Fluid Mechanics* 112: 363-77

Ippen AT, Drinker PA. 1962. Boundary shear stress in curved trapezoidal channels. *Journal of the Hydraulics Division, ASCE* 88: 143-79

Issa RI. 1986. Solution of the implicitly discretised fluid flow equations by operator splitting. *Journal of Computational Physics* 62: 66-82

Jackson RG. 1975. Velocity-bedform-texture patterns of meander bends in the lower Wabash River, Illinois and Indiana. *Geological Society of America Bulletin* 86: 1511-22

Jackson RG. 1976. Depositional model of point bars in the lower Wabash River. *Journal of Sedimentary Petrology* 46: 579-94

Jia YF, Wang SSY. 1999. Numerical model for channel flow and morphological change studies. *Journal of Hydraulic Engineering-ASCE* 125: 924-33

Johannesson H, Parker G. 1989a. Linear theory of river meanders. In *River Meandering, American Geophysical Union monograph 12*, ed. G Parker, pp. 181-213. Washington D.C. AGU

Johannesson H, Parker G. 1989b. Secondary flow in mildly sinuous channels. *Journal of Hydraulic Engineering-ASCE* 115: 289-308

Johannesson H, Parker G. 1989c. Velocity Redistribution in Meandering Rivers. *Journal of Hydraulic Engineering-ASCE* 115: 1019-39

Jordan SA, Ragab SA. 1998. A large-eddy simulation of the near wake of a circular cylinder. *Journal of Fluids Engineering-Transactions of the Asme* 120: 243-52

Kaiser G. 1994. *A Friendly Guide to Wavelets*: Birkhauser

Keulegan G. H. (1938) Laws of turbulent flow in open channels. *Journal of Research, National Bureau of Standards* 21: 707-41.

Kimura I, Hosoda T. 1997. Fundamental properties of flows in open channels with dead zone. *Journal of Hydraulic Engineering-ASCE* 123: 98-107

Knighton DK. 1970. *Changes in channel morphology and hydrology, River Bollin-Dean, Cheshire*. Ph.D. thesis. University of Manchester, Manchester

Knighton DK. 1975. Variations in at-a-station hydraulic geometry. *American Journal of Science* 275: 186-218

Kolmogorov AN. 1942. Equations of turbulent motion of an incompressible fluis. *Akad. Nank. SSR., Seriafizichesda* 1-2: 56-8

Kosovic B. 1997. Subgrid-scale modelling for the large-eddy simulation of high-Reynolds-number boundary layers. *Journal of Fluid Mechanics* 336: 151-82

Kraus NC, Lohrmann A, Cabrera R. 1994. New acoustic meter for measuring 3D laboratory flows. *Journal of Hydraulic Engineering-ASCE* 120: 406-12

Lane SN. 1998a. Hydraulic modelling in hydrology and geomorphology: A review of high resolution approaches. *Hydrological Processes* 12: 1131-50

Lane SN. 1998b. The use of digital terrain modelling in the understanding of dynamic river channel systems. In *Landform Monitoring, Modelling and Analysis*, ed. SN Lane, KS Richards, JH Chandler, pp. 311-42. Chichester: Wiley

Lane SN, Biron PM, Bradbrook KF, Butler JB, Chandler JH, et al. 1998. Three-dimensional measurement of river channel flow processes using acoustic Doppler velocimetry. *Earth Surface Processes and Landforms* 23: 1247-67

Lane SN, Bradbrook KF, Caudwell SWB, Richards KS. 1999c. Mixing processes at river confluences: Field informed numerical modelling. In *Environmental Hydraulics*, ed. JHW Lee, AW Jayawardena, ZY Wang, pp. 345-50. Rotterdam: A.A. Balkema

Lane SN, Bradbrook KF, Richards KS, Biron PA, Roy AG. 1999a. The application of computational fluid dynamics to natural river channels: three-dimensional versus two-dimensional approaches. *Geomorphology* 29: 1-20

Lane SN, Bradbrook KF, Richards KS, Biron PM, Roy AG. 1999b. Time-averaged flow structure in the central region of a stream confluence: A discussion. *Earth Surface Processes and Landforms* 24: 361-7

Lane SN, Bradbrook KF, Richards KS, Biron PM, Roy AG. 2000. Secondary circulation cells in river channel confluences: measurement artefacts or coherent flow structures? *Hydrological Processes* 14: 2047-71

Lane SN, Chandler JH, Richards KS. 1994a. Developments in Monitoring and Modeling Small-Scale River Bed Topography. *Earth Surface Processes and Landforms* 19: 349-68

Lane SN, Hardy R, Elliott L, Ingham DB. 2002. High-resolution numerical modelling of three-dimensional flows over complex river bed topography. *Hydrological Processes* 16: 2261-72

Lane SN, Hardy RJ, Keylock CJ, Elliott L, Ingham DB, Ferguson RI, Parsons DR. in press. The implications of complex river bed structure for numerical modelling and the identification of channel-scale flow structures.

Lane SN, Richards KS. 1997. Linking river channel form and process: Time, space and causality revisited. *Earth Surface Processes and Landforms* 22: 249-60

Lane SN, Richards KS. 1998. High resolution, two-dimensional spatial modelling of flow processes in a multi-thread channel. *Hydrological Processes* 12: 1279-98

Lane SN, Richards KS. 2001. The validation of hydrodynamic models: some critical perspectives. In *Model validation: Perspectives in hydrological science*, ed. MG Anderson, PD Bates, pp. 414-38. Chichester: Wiley

Lane SN, Richards KS, Chandler JH. 1994b. Application of Distributed Sensitivity Analysis to a Model of Turbulent Open-Channel Flow in a Natural River Channel. *Proceedings of the Royal Society of London Series a-Mathematical Physical and Engineering Sciences* 447: 49-63

Lane SN, Richards KS, Chandler JH. 1995. Within-reach spatial patterns of process and channel adjustment. In *River Geomorphology*, ed. EJ Hickin, pp. 105-30. Chichester: Wiley

Lapointe MF, Carson MA. 1986. Migration patterns of an asymmetric meandering river: The Rouge River, Quebec. *Water Resources Research* 22

Launder BE, Spalding DB. 1972. *Lectures in mathematical models of turbulence.* New York: Academic Press

Launder BE, Spalding DB. 1974. The numerical computation of turbulent flows. *Computer Methods in Applied Mechanics and Engineering* 3: 269-89

Lawless M, Robert A. 2001. Three-dimensional flow structure around small-scale bedforms in a simulated gravel-bed environment. *Earth Surface Processes and Landforms* 26: 507-22

Le H, Moin P, Kim J. 1997. Direct numerical simulation of tubulent flow over a backward facing step. *Journal of Fluid Mechanics* 330: 349-74

Leeder MR, Bridges PH. 1975. Flow separation in meander bends. *Nature* 253: 338-9

Leith CE. 1990. Stochastic backscatter in a subgrid-scale model: Plane shear mixing layer. *Physics and Fluids A* 2: 297-9

Leliavsky S. 1955. *An Introduction to Fluvial Dynamics*. London: Constable

Leonard A. 1974. Energy cascade in large-eddy simulations of turbulent fluid flows. *Advances in Geophysics* 18: 237

Leopold LB, Maddock T. 1953. The hydraulic geometry of stream channels and some physiographic implications. *USGS Professional Paper* 252-D

Leopold LB, Wolman MG. 1960. River Meanders. *Bulletin of the Geological Society of America* 71: 769-94

Leschziner MA, Rodi W. 1979. Calculation of strongly curved open channel flow. *Journal of Hydraulic Engineering-ASCE* 105: 1297-314

Lesieur M, Comte P, Lamballais E, Metais O, Silvestrini G. 1997. Large-eddy simulations of shear flows. *Journal of Engineering Mathematics* 32: 195-215

Lewin J. 1978. Meander development and floodplain sedimentation: a case study from mid-Wales. *Geological Journal* 13: 25-36

Lewin J, Brindle BJ. 1977. Confined meanders. In *River Channel Changes*, ed. KJ Gregory. Chichester: John Wiley and Sons Ltd.

Li CW, Wang JH. 2000. Large eddy simulation of free surface shallow-water flow. *International Journal for Numerical Methods in Fluids* 34: 31-46

Lien FS, Leschziner MA. 1994. Application of an RNG turbulence model to flow over a backwards-facing step. *Computers and Fluids* 23: 983-1004

Lien HC, Hsieh TY, Yang JC, Yeh KC. 1999. Bend-flow simulation using 2D depth-advanced model. *Journal of Hydraulic Engineering-ASCE* 125: 1097-108

Lilly DK. 1966. On the application of the eddy viscosity concept in the inertial sub-range of turbulence. *NCAR Manuscript* 123

Lilly DK. 1967. *The representation of small scale turbulence in numerical simulation experiments.* Presented at IBM Scientific Computing Symposium on Environmental Science

Lu X, Dalton C, Zhang J. 1997. Application of large eddy simulation to flow past a circular cylinder. *Journal of Offshore Mechanics and Arctic Engineering-Transactions of the Asme* 119: 219-25

Ma L, Ashworth PJ, Best JL, Elliott L, Ingham DB, Whitcombe LJ. 2002. Computational fluid dynamics and the physical modelling of an upland urban river. *Geomorphology* 44: 375-91

Manhart M. 1998. Vortex shedding from a hemisphere in a turbulent boundary layer. *Theoretical Computational Fluid Dynamics* 12: 1-28

Markham AJ, Thorne CR. 1992. Geomorphology of gravel-bed river bends. In *Dynamics of Gravel-bed rivers*, ed. P Billi, RD Hey, CR Thorne, P Tacconi, pp. 433-50. Chichester: Wiley

McLelland SJ, Ashworth PJ, Best JL. 1996. The origins and development of coherent flow structures at channel junctions. In *Coherent Flow structures in Open Channels*, ed. PJ Ashworth, SJ Bennett, JL Best, SJ McLelland, pp. 491-517. Chichester: Wiley

McLelland SJ, Nicholas AP. 2000. A new method for evaluating errors in high-frequency ADV measurements. *Hydrological Processes* 14: 351-66

Meneveau C, Katz J. 2000. Scale-invariance and turbulence models for large-eddy simulation. *Annual Review of Fluid Mechanics* 32: 1-32

Meselhe EA, Odgaard AJ. 1998. 3D numerical flow model for fish diversion studies at Wanapum Dam. *Journal of Hydraulic Engineering-ASCE* 124: 1203-14

Meyer Y. 1993. *Wavelets: algorithms and applications*. Philadelphia: SIAM

Murray AB, Paola C. 1994. A cellular model of braided rivers. *Nature* 371: 54-7

Naot D, Nezu I, Nakagawa H. 1993. Hydrodynamic behaviour of compound rectangular open channels. *Journal of Hydraulic Engineering-ASCE* 119: 390-408

Nelson JM, Smith JD. 1989a. Evolution and stability of erodiable channel beds. In *River Meandering, American Geophysical Union water resources monograph 12*, ed. S Ikeda, G Parker. Washington D.C. AGU

Nelson JM, Smith JD. 1989b. Flow in meandering channels with natural topography. In *River Meandering, American Geophysical Union water resources monograph 12*, ed. S Ikeda, G Parker. Washington D.C. AGU

Nezu I, Nakagawa H. 1993. *Turbulence in open channel flows*. Rotterdam: A.A. Balkema

Nezu I, Tominaga A, Nakagawa H. 1993. Field-Measurements of Secondary Currents in Straight Rivers. *Journal of Hydraulic Engineering-ASCE* 119: 598-614

Nicholas AP, Smith GHS. 1999. Numerical simulation of three-dimensional flow hydraulics in a braided channel. *Hydrological Processes* 13: 913-29

Niekerk A, Vogel KR, Slingerland RL, Bridge JS. 1992. Routing of heterogeneous sediment over mobile bed; model development. *Journal of Hydraulic Engineering-ASCE* 118: 246-262

Nikuradse J. 1952. Laws for flows in pipes. *VDI Forschungsheft (English translation NACA Technical Memorandum No. 1292 from 1933)*

Odgaard AJ. 1986a. Meander flow model, I, Development. *Journal of Hydraulic Engineering-ASCE* 112: 1117-36

Odgaard AJ. 1986b. Meander flow model, II, Applications. *Journal of Hydraulic Engineering-ASCE* 112: 1137-50

Odgaard AJ. 1987. Stream bank erosion along two rivers in Iowa. *Water Resources Research* 23: 1225-36

Odgaard AJ. 1989a. River meander model, I, Development. *Journal of Hydraulic Engineering-ASCE* 115: 1451-64

Odgaard AJ. 1989b. River meander model, II, Applications. *Journal of Hydraulic Engineering-ASCE* 115: 1451-64

Odgaard AJ, Bergs MA. 1988. Flow processes in a curved alluvial channel. *Water Resources Research* 24: 45-56

Onishi Y. 1972. *Effects of meandering on sediment discharges and friction factors of alluvial streams*. Unpublished thesis. University of Iowa

Oreskes N, Shrader-Frechette K, Belitz K. 1994. Verification, validation and confirmation of numerical models in the earth sciences. *Science* 263: 641-6

Osman AM, Thorne CR. 1988. River bank stability analysis. I. Theory. *Journal of Hydraulic Engineering-ASCE* 114: 134-50

Ouillon S, Dartus D. 1997. Three-dimensional computation of flow around a groyne. *Journal of Hydraulic Engineering-ASCE* 123: 962-72

Page KJ, Nanson GC. 1982. Concave-bank benches and associated floodplain formation. *Earth Surface Processes and Landforms* 7: 529-43

Paice C. 1990. *Hydraulic control of river bank erosion: An environmental approach.* University of East Anglia, Norwich

Pantankar SV. 1980. *Numerical Heat Transfer and Fluid Flow.* New York: Hemispere Publishing

Pantankar SV, Spalding DB. 1972. A calculation procedure for heat, mass and momentum transport in three-dimensional parabolic flows. *International Journal of Heat and Mass Transfer* 15: 1782

Parker G, Diplas P, Akiyama J. 1983. Meander bends of high amplitude. *Journal of Hydraulic Engineering-ASCE* 109: 1323-37

Phillips JD. 1992. Non-linear dynamical systems in geomorphology: Revolution or evolution. *Geomorphology* 5: 219-29

Piomelli U, Moin P, Ferziger JH. 1988. Model consistency in large eddy simulation of turbulent channel flows. *Physics and Fluids* 31: 1884-91

Pope SB. 2000. *Turbulent Flows*, Cambridge University Press

Prandtl L. 1925. Lieber die ausgebildete Turbulenz. *A. Angew. Math. Mech.* 5: 136-9

Prandtl L. 1945. Uber ein neues Formelsystem fur die ausgebildete Turbulenze. Translated 1953. *Jet Propulsion Laboratory Publication* 13

Prandtl L. 1952. *Essentials of Fluid Dynamics.* London: Blackie & Sons

Reid JB. 1984. Artificially induced concave bank deposition as a means of floodplain erosion control. In *River Meandering: Proceedings of the Conference Rivers '83*, ed. CM Elliott, pp. 295-304. New York: American Society of Civil Engineers

Reynolds CS. 2000. Hydroecology of river plankton: the role of variability in channel flow. *Hydrological Processes* 14: 3119-32

Reynolds O. 1985. On the dynamical theory of incompressible viscous fluids and the determination criterion. *Philosophical Transactions of the Royal Society 186A*: 123-64.

Rhoads BL. 1996. Mean structure of transport-effective flows at an asymmetrical confluence when the main stream is dominant. In *Coherent Flow Structures in Open Channels*, ed. PJ Ashworth, SJ Bennett, JL Best, SJ McLelland, pp. 459-90. Chichester: Wiley

Rhoads BL, Kenworthy ST. 1995. Flow Structure At an Asymmetrical Stream Confluence. *Geomorphology* 11: 273-93

Rhoads BL, Kenworthy ST. 1998. Time-averaged flow structure in the central region of a stream confluence. *Earth Surface Processes and Landforms* 23: 171-91

Rhoads BL, Kenworthy ST. 1999. On secondary circulation, helical motion and Rozovskii-based analysis of time-averaged two-dimensional velocity fields at confluences. *Earth Surface Processes and Landforms* 24: 369-75

Rhoads BL, Sukhodolov AN. 2001. Field investigation of three-dimensional flow structure at stream confluences: 1. Thermal mixing and time-averaged velocities. *Water Resources Research* 37: 2393-410

Richards KS. 1978. Simulation of flow geometry in a riffle-pool stream. *Earth Surface Processes* 3

Richards KS. 1996. Samples and cases: Generalisation and explanation in geomorphology. In *The scientific basis of geomorphology*, ed. BL Rhoads, CE Thorne, pp. 171-90: Elsevier

Roache PJ. 1976. *Computational fluid dynamics.* Albuquerque, New Mexico: Hermosa

Roache PJ. 1994. Perspective: a method for uniform reporting of grid refinement studies. *Journal of Fluids Engineering-Transactions of the Asme* 116: 405-13

Roache PJ. 1997. Quantification on uncertainty in computational fluid dynamics. *Annual Review of Fluid Mechanics* 29: 123-60

Roache PJ. 1998. Verification of codes and calculations. *American Institute for Aeronautics and Astronautics* 36: 696-702

Rodi W. 1980. *Turbulence Models and their Application in Hydraulics.* Delft: International Association of Hydraulic Research

Rodi W. 1993. *Turbulence Models and their Application in Hydraulics.* Rotterdam: A.A. Balkema

Rodi W, Ferziger JH, Breuer M, Pourquie M. 1997. Status of large eddy simulation: Results of a workshop. *Journal of Fluids Engineering-Transactions of the Asme* 119: 248-61

Rogallo RS, Moin P. 1984. Numerical simulation of turbulent flows. *Annual Review of Fluid Mechanics* 16: 99-137

Rogers MM, Moser RD. 1992. The three-dimensional evolution of a plane mixing layer: The Kelvin-Helmholtz rollup. *Journal of Fluid Mechanics* 183-226

Rohrer. 1984. Effects of flow and bank materials on meander migration in alluvial rivers. In *River Meandering: Proceedings of the Conference Rivers '83*, ed. CM Elliott, pp. 770-82. New York: American Society of Civil Engineers

Roy AG, Buffin-Belanger T. 2001. Advances in the study of turbulent flow structures in gravel bed rivers. In *Gravel-Bed Rivers V*, ed. P Mosley: New Zealand Hydrological Society

Rozovskii IL. 1957. *Flow of water in bends of open channels, Academy of Sciences of the Ukrainian SSR, Kiev (translated from Russian by the Isreal Program for Scientific Translations, Jerusalem, 1961).* 233 pp.

Rubin DM, McDonald RR. 1995. Non-periodic eddy pulsations. *Water Resources Research*: 1595-605

Rubin DM, Schmidt JC, Moore JN. 1990. Origin, structure and evolution of a reattachment bar, Colorado River, Grand Canyon, Arizona. *Journal of Sedimentary Petrology* 60: 982-91

Sagaut P. 1996. Simulations of separated flows with subgrid models. *Recherche Aerospatiale* 1: 51-63

Schlichting H. 1955. *Boundary Layer Theory.* New York: McGraw-Hill

Schlichting H. 1979. *Boundary-Layer Theory.* New York: McGraw-Hill

Schmidt JC. 1990. Recirculating flow and sedimentation in the Colorado River in Grand Canyon, Arizona. *Journal of Geology* 98: 709-24

Schmidt JC, Rubin DM, Ikeda h. 1993. Flume simulation of recirculating flow and sedimentation. *Water Resources Research* 29: 2925-39

Schumann U. 1975. Subgrid scale model for finite difference simulations of turbulent flows in plane channels and annuli. *Journal of Computational Physics* 18: 376-404

Schumm SA. 1977. *The fluvial system.* New York: Wiley

Schumm SA, Lichty RW. 1965. Time, space and causality in geomorphology. *American Journal of Science* 263: 110-9

Scotti A, Meneveau C, Lilly DK. 1993. Generalised Smagorinsky model for anisotropic grids. *Physics and Fluids A* 5: 2306-8

Shi J, Thomas TG, Williams JJR. 1999. Development of a large-eddy simulation open channel code. *International Journal of Numerical Methods for Heat & Fluid Flow* 9: 6-17

Silveira Neto A, Grand D, Metais O, Lesieur M. 1991. Large eddy simualtion of the turbulent flow in the downstream region of a backward facing step. *Physical Review* 66: 2320-3

Simpson GG. 1963. Historical science. In *The Fabric of Geology*, ed. CC Albritton, pp. 24-48. Stanford: Freeman, Copper & Co.

Smagorinsky J. 1963. General circulation experiments with primitive equations. 1. The basic experiment. *Monthly Weather Review* 91: 99-164

Smith JD, McClean SR. 1984. A model for meandering streams. *Water Resources Research* 20: 1301-15

Spalding DB. 1972. A novel finite difference formulation for differential expressions involving both first and second derivatives. *International Journal of Numerical Methods in Engineering* 4: 551-66

Spalding DB. 1985. The computation of flow around ships with allowance for free surface and density gradient effects. *Proceedings of the First Intercontinental Symposium on Maritime Simulation.*

Spalding DB. 2001. X-Cell: a new algorithm for fluid-flow simulation. www.cham.co.uk/phoenics/d_polis.

Speziale CG. 1991. Analytical methods for the development of Reynolds stress closures in turbulence. *Annual Review of Fluid Mechanics* 23: 107-57

Speziale CG. 1998. Turbulence modelling for time-dependent RANS and VLES: A review. *American Institute of Aeronautics and Astronautics* 36: 173-84

Strahler AN. 1950. Equilibrium theory of erosional slopes approached by frequency distribution analysis. *American Journal of Science* 248: 673-96 & 800-14

Strahler AN. 1952. Dynamic basis of geomorphology. *Bulletin of the Geological Society of America* 63: 923-38

Sukhodolov AN, Rhoads BL. 2001. Field investigation of three-dimensional flow structure at stream confluences 2. Turbulence. *Water Resources Research* 37: 2411-24

Sun T, Meakin P, Jossang T, Schwarz K. 1996. A simulation model for meandering rivers. *Water Resources Research* 32: 2937-54

Taylor G, Crook KAW, Woodyer KD. 1971, Upstream-dipping foreset cross stratification: origin and implications for palaeoslope analysis. *Journal of Sedimentary Petrology* 41, 578-581.

Thomas TG, Williams JJR. 1995a. Large Eddy Simulation of a symmetrical trapezoidal channel at a Reynolds number of 430, 000. *Journal of Hydraulic Research* 33: 825-42

Thomas TG, Williams JJR. 1995b. Large Eddy Simulation of turbulent flow in an asymmetric compound channel. *Journal of Hydraulic Research* 33: 27-41

Thompson A. 1986. Secondary flows and the pool-riffle unit: a case study of the processes of meander development. *Earth Surface Processes and Landforms* 11: 631-41

Thorne CE, Welford MR. 1994. The equilibrium concept in geomorphology. *Annals of the Association of American Geographers* 84: 666-96

Thorne CR. 1982. Processes and mechanisms of river bank erosion. In *Gravel-Bed Rivers*, ed. RD Hey, JC Bathurst, CR Thorne, pp. 227-59. Chichester: Wiley

Thorne CR. 1992. Bend scour and bank erosion on the meandering Red River, Louisianna. In *Lowland Floodplain Rivers - Geomorphological Perspectives*, ed. PA Carling, G Petts, pp. 95-115. Chichester: Wiley

Thorne CR, Lewin J. 1979. Bank processes, bed amterial movement and planform development in a meandering river. In *Adjustments of the Fluvial System*, ed. DD Rhodes, GP Williams, pp. 117-37. Dubuque, Iowa: Kendal/Hunt

Thorne CR, Tovey NK. 1981. Stability of composite river banks. *Earth Surface Processes and Landforms* 6: 469-84

Thorne CR, Zevenbergen LW, Pitlick JC, Rais S, Bradley JB, Julian PY. 1985. Direct measurement of secondary currents in a meandering sand-bed river. *Nature* 316: 746-7

Tipping E, Woof C, Clarke K. 1993. Deposition and Resuspension of Fine Particles in a Riverine Dead Zone. *Hydrological Processes* 7: 263-77

Thomson J. 1876. On the origins and winding of rivers in alluvial plains. *Proceedings of the Royal Society of London* 25: 5-8.

Torrence C, Compo GP. 1998. A practical guide to wavelet analysis. *Bulletin of the American Meteorological Society* 79: 61-78

Tritton DJ. 1988. *Physical Fluid Dynamics*. Oxford: Oxford Science Publications

Usunoff E, Carrera J, Mousavi SF. 1992. An approach to the design of experiments for discriminating among alternative conceptual models. *Advances in Water Resources* 15: 199-214

van Alphen JSLJ, Bloks PM, Hoekstra P. 1984. Flow and Grain-Size Pattern in a Sharply Curved River Bend. *Earth Surface Processes and Landforms* 9: 513-22

van Doormal JP, Raithby DG. 1984. Enhancements of the SIMPLE method for predicting incompressible fluid flows. *Numerical Heat Transfer* 7: 147-63

Versteeg HK, Malalasekera W. 1995. *An Introduction to Computational Fluid Dynamics*. Harlow: Longman

Vreman B, Geurts B, Kuerten H. 1997. Large eddy simulation of the turbulent mixing layer. *Journal of Fluid Mechanics* 339: 357-90

Waterson NP. 1994. Validation of convection discretisation schemes. In *VKI Dip. Rep.*, pp. 1-33. Rhode-Saint-Genese, Belgium: Von Karmen Institute for Fluid Dynamics

Weber LJ, Schumate ED, Mawer N. 2001. Experiments on Flow at a 90 Degree Open Channel Junction. *Journal of Hydraulic Engineering-ASCE* 127: 340-50

Whiting PJ. 1997. The effect of stage on flow and components of the local force balance. *Earth Surface Processes and Landforms* 22: 517-30

Whiting PJ, Dietrich WE. 1993a. Experimental Studies of Bed Topography and Flow Patterns in Large-Amplitude Meanders .1. Observations. *Water Resources Research* 29: 3605-14

Whiting PJ, Dietrich WE. 1993b. Experimental Studies of Bed Topography and Flow Patterns in Large-Amplitude Meanders .2. Mechanisms. *Water Resources Research* 29: 3615-22

Wilson IG. 1973. Equilibrium cross sections of meandering and braided rivers. *Nature* 241: 393-4

Winant CD, Browand FK. 1974. Vortex pairing: The mechanism of turbulent mixing layer growth at moderate Reynolds numbers. *Journal of Fluid Mechanics* 63: 237-55

Woodyer KD, Taylor G, Crook KAW. 1979. Depositional processes along a very low-gradient, suspended-load stream: the Bawrwon River, New South Wales. *Sedimentary Geology* 22: 97-120

Wu W, Rodi W, Wenka T. 2000. 3D numerical modelling of flow and sediment transport in open channels. *Journal of Hydraulic Engineering-ASCE* 126: 4-15

Yakhot V, Orszag SA. 1986. Renormalization group analysis of turbulence. *Journal of Scientific Computing* 1: 536-51

Yakhot V, Orszag SA, Thangham S, Gatshi TB, Speziale CG. 1992. Development of a turbulence model for shear flow by a double expansion technique. *Physics and Fluids A* 4: 1510-20

Yalin M. 1992. *River Mechanics*. New York: Pergamon

Yamaoka I, Hasegawa K. 1984. Effects of bends and alternate bars on meander evolution. In *River Meandering: Proceedings of the Conference Rivers '83*, ed. CM Elliott, pp. 783-93. New York: American Society of Civil Engineers

Ye J, McCorquodale JA. 1998. Simulation of curved and open channel flows by 3D hydrodynamic model. *Journal of Hydraulic Engineering-ASCE* 124: 687-98

Younis BA. 1992. *Is turbulence modelling of any use?* Presented at IAHR Conference, Institution of Civil Engineers, London

Zedler EA, Street RL. 2001. Large-eddy simulation of sediment transport: Currents over ripples. *Journal of Hydraulic Engineering-ASCE* 127: 444-52

Appendix

The Compact Disc in the back cover contains three .AVI files of the flow in the expansion experiment detailed in Chapter 6.

- The first (6.1.AVI) is a video of sequential plots of contoured near surface vectors predicted by the numerical model.
- The second (6.2.AVI) is a video of sequential plots of contoured near bed vectors predicted by the numerical model.
- The third (6.3.AVI) has a video of sequential contour plots obtained by the PIV for the area close to the width expansion point.

All files should run from the CD drive with any type of media player, such as: Windows media player; Quick Time Player; Real Player; Adobe Film; etc.